

# **Manganese biogeochemistry in the sunlit ocean**

Dissertation  
zur Erlangung des Doktorgrades  
der Mathematisch-Naturwissenschaftlichen Fakultät  
der Christian-Albrechts-Universität  
zu Kiel

vorgelegt von  
**Dipl.-Chem. Kathrin Wuttig**

Kiel 2013



Referent: Prof. Dr. Arne Körtzinger  
Korreferent: Prof. Dr. Peter L. Croot

Tag der mündlichen Prüfung: 16.Mai 2013

Zum Druck genehmigt: Kiel, den 16.Mai 2013

gez. Prof Dr. Wolfgang J. Duschl, Dekan



Die vorliegende Arbeit wurde am GEOMAR Helmholtz-Zentrum für Ozeanforschung Kiel an der Christian-Albrechts-Universität zu Kiel von November 2009 bis April 2013 unter der Anleitung von Prof. Dr. Peter L. Croot durchgeführt.



*So eine Arbeit wird eigentlich nie fertig.  
Man muß sie für fertig erklären,  
wenn man nach Zeit und Umständen  
das Möglichste getan hat.  
Johann Wolfgang von Goethe, aus Italienisch Reise, 1787*





## THIS THESIS COMPRISES THE FOLLOWING MANUSCRIPTS:

- 1. Manuscript 1:** K. Wuttig, M. I. Heller and P. L. Croot, "Pathways of  $O_2^-$  decay in the Tropical Atlantic." *Environmental Science and Technology*, submitted, 2013.

**Contribution:** Kathrin Wuttig took the samples together with Maija I. Heller. They performed superoxide and hydrogen peroxide measurements. Kathrin Wuttig measured manganese, evaluated the data and wrote the paper. Peter L. Croot and Maija I. Heller helped evaluating the data and assisted with input and revision of the manuscript.
- 2. Manuscript 2:** K. Wuttig, M. I. Heller and P. L. Croot, "Reactivity of inorganic Mn and Mn Desferrioxamine B with  $O_2$ ,  $O_2^-$  and  $H_2O_2$  in seawater." *Environmental Science and Technology*, submitted, 2013.

**Contribution:** Kathrin Wuttig took the samples together with Maija I. Heller and they performed superoxide and hydrogen peroxide measurements on M83/1 and MSM17/4. Additional experiments were designed and performed by the authors at GEOMAR, PML and on M90 by Kathrin Wuttig and Peter L. Croot. Kathrin Wuttig measured manganese and evaluated the data. Peter L. Croot and Maija I. Heller helped evaluating the data. All three authors wrote the manuscript together.
- 3. Manuscript 3:** K. Wuttig, T. Wagener, D. Booge, P. Streu and P. L. Croot, "Contrasting behavior of cadmium, iron and manganese in the Eastern Tropical Atlantic." manuscript 2013 for submission to *Global Biogeochemical Cycles*.

**Contribution:** Kathrin Wuttig took the samples together with Thibaut Wagener, measured manganese together with Dennis Booge, evaluated the data and wrote the paper. Peter L. Croot and Thibaut Wagener assisted with input to the manuscript and revision. Peter Streu provided the total trace metal data.
- 4. Manuscript 4:** K. Wuttig, T. Wagener, M. Bressac, A. Damshäuser, P. Streu, C. Guieu and P. L. Croot (2012), "Impacts of dust deposition on dissolved trace metal concentrations (Mn, Al and Fe)." in press, *Biogeosciences*, 2013.

X

**Contribution:** Kathrin Wuttig took the samples together with the other DUNE-2 participants, measured manganese on site, evaluated the data and wrote the paper. Thibaut Wagener, Matthieu Bressac, Anna Dammshäuser, Peter Streu, Cécile Guieu and Peter L. Croot assisted with input to the manuscript and revision. Peter Streu provided the total trace metal data, Anna Dammshäuser the aluminium and Matthieu Bressac and Thibaut Wagener the iron data.

In addition I have contributed to the following manuscripts, publications and book chapters:

1. K. Bluhm, P. L. Croot, K. Wuttig, and K. Lochte (2010), "Transformation of iodate to iodide in marine phytoplankton driven by cell senescence." *Aquatic Biology* 11(1): 1-15.
2. P. L. Croot, M. I. Heller, C. Schlosser and K. Wuttig (2011), "Utilizing Radioisotopes for Trace Metal Speciation Measurements in Seawater." *Radioisotopes - Applications in Physical Sciences*. N. Singh, InTech: 247-278.
3. P. L. Croot, P. Streu, F. Malien and K. Wuttig, "Trace Metal Distributions across the Peruvian Oxygen Minimum Zone." manuscript 2013 for submission to *Global Biogeochemical Cycles*.
4. P. L. Croot, M.I. Heller, P. Streu and K. Wuttig, "Impacts of ocean deoxygenation on trace metal biogeochemical cycles." manuscript, 2013.
5. P. Pondaven and DUNE-Team, "Response of a microbial food web to atmospheric dust deposition: results from a theoretical model applied to mesocosm experiments in the Mediterranean Sea." manuscript for special issue *Biogeosciences (BG)*, 2013.

## TABLE OF CONTENTS

1	SUMMARY.....	3
2	ZUSAMMENFASSUNG .....	6
3	GENERAL INTRODUCTION.....	11
3.1	Oceanic Manganese (Mn) distribution, sources and sinks.....	11
3.2	Mn speciation and photochemical processes .....	17
3.3	Low O <sub>2</sub> conditions and the influence on Mn.....	19
3.4	Study Areas .....	21
3.4.1	Eastern Tropical Atlantic (ETA) .....	22
3.4.2	Eastern Tropical Pacific (ETP) .....	24
3.4.3	North Western Mediterranean .....	27
3.5	Thesis outline .....	28
4	MATERIAL AND METHODS.....	33
4.1.1	Reagents and bottles .....	33
4.2	Sample collection.....	33
4.2.1	CTD-sampling .....	34
4.2.2	GoFlo-sampling .....	34
4.2.3	Sampling with a Teflon™ pump.....	35
4.3	Chemical analysis.....	36
4.3.1	Total dissolved trace metal analysis.....	36
4.3.2	Dissolved manganese (Mn) analysis.....	37
4.3.3	Hydrogen peroxide (H <sub>2</sub> O <sub>2</sub> ) analysis.....	39
4.3.4	Superoxide (O <sub>2</sub> <sup>-</sup> ) analysis and experiments.....	39
5	MANUSCRIPTS .....	43
	MANUSCRIPT 1 .....	45
	MANUSCRIPT 2 .....	83
	MANUSCRIPT 3 .....	123
	MANUSCRIPT 4 .....	151
5	FINAL CONCLUSIONS AND FUTURE PERSPECTIVES .....	175
6	REFERENCES.....	182
7	ABBREVIATIONS .....	190
	DANKSAGUNG.....	192
	CURRICULUM VITAE.....	195
	EIDESSTATTLICHE ERKLÄRUNG .....	199



# SUMMARY



## 1 SUMMARY

The trace metal manganese (Mn) plays a significant role in seawater as it is bio-essential for phytoplankton. Mn plays a critical role as a redox center in Photosystem II (PSII) during the conversion of water to oxygen in photosynthesis. It is also essential in other redox related enzymatic processes; in particular Mn is important as the active metal center in superoxide dismutase (SOD) which provides intracellular protection against oxidative stress due to photochemically produced superoxide ( $O_2^-$ ). Mn exists in seawater in three redox states: soluble and prevalent Mn(II), insoluble Mn(III) and Mn(IV)-oxides. In the euphotic zone the biogeochemical cycling of Mn is strongly influenced by reactive oxygen species (ROS). The highly reactive and short-lived superoxide ( $O_2^-$ ) and hydrogen peroxide ( $H_2O_2$ ) can both act as oxidants and reductants, and they play a key role in the Mn processes in seawater. For example the dominant Mn sources to the open ocean are the Mn-oxides which are present in atmospheric dust which are reduced to soluble Mn(II) by photochemically produced  $H_2O_2$ . While these processes have been crudely identified, the dominant reactions and mechanisms of Mn and ROS in seawater are poorly understood. This lack of knowledge demands investigations into the *in-situ* dissolution processes of Mn from dust and into studying the exact reaction mechanisms between Mn and ROS in the euphotic zone.

This thesis comprises four manuscripts. Manuscripts 1 and 2 (Wuttig *et al.*, subm., 2013a; Wuttig *et al.*, subm., 2013b) focus on the cycling and reaction mechanisms of Mn and ROS. Manuscript 3 (Wuttig *et al.*, in prep., 2013) addresses differences in the input and distribution of cadmium (Cd), iron (Fe) and Mn in the Eastern Tropical Atlantic Ocean off Cape Verde, and manuscript 4 (Wuttig *et al.*, 2013) describes Mn cycling after dust additions in a trace metal clean mesocosm experiment in the Mediterranean Sea.

This study has conclusively shown that Mn and organic matter are the dominant sinks for  $O_2^-$  in the Eastern Tropical North Atlantic (manuscripts 1; Wuttig *et al.*, subm., 2013a). Mn dominates this decay especially in the surface waters which are influenced by high atmospheric dust deposition and near the sediment/water interface due to Mn sediment resuspension. This contrasts with current knowledge based on findings from the Mn poor Southern Ocean where copper (Cu) was shown to be the major sink.

In manuscript 2 it is demonstrated that  $O_2^-$  decays by reaction with inorganic Mn(II) in seawater following a first order loss rate which appears to involve a catalytic reaction involving the Mn(II)/ $MnO_2^+$  couple, in which  $MnO_2^+$  is a manganous superoxide complex (Wuttig *et al.*, subm., 2013a). Thus in sunlit and oxygenated waters Mn(III) is unlikely to be found in significant concentrations when strong Mn(III) binding ligands are not present. In other studies Mn(III) was found under anoxic conditions in the presence of unknown strong

Mn(III) binding ligands. Therefore, in contrast to the Mn(II)/MnO<sub>2</sub><sup>+</sup> pair, Mn(III) cannot act as a SOD in the oxygenated surface ocean.

In the Eastern Tropical North Atlantic Ocean atmospheric dust is the main source of Mn to surface waters (manuscript 3; Wuttig *et al.*, in prep., 2013). However this study provides clear evidence that equatorial upwelling and sediment resuspension are important Mn sources in this region. In contrast to findings from the Eastern Tropical Pacific, where unexpected high surface concentrations were observed, no secondary Mn(II) maximum was found in the Eastern Tropical North Atlantic Ocean. This could have been introduced by a combination of lateral transport of Mn rich waters from the coastal margins and reduction of Mn-oxides.

While Aeolian sources were predominantly influencing Mn and also Fe cycling in the Eastern Tropical Atlantic, Cd was not controlled by dust deposition (manuscript 3; Wuttig *et al.*, in prep., 2013). These biologically relevant elements exhibited contrasting distribution patterns. For Fe and Mn, atmospheric depositions masked a classical nutrient type profile, while Cd was very depleted at the surface and concentrations steadily increased with depth. Cd was highly correlated to Phosphate (hereafter referred to as P). The Cd/P ratio was mainly controlled by P with elevated concentrations at depth resulting in strongly differing ratios in surface and subsurface layers of 16.6 pmol/ μmol and 237 pmol/ μmol, respectively.

The complex photochemical processes during the dissolution of Mn dust are also subject of manuscript 4. This paper describes a mesocosm project in the Mediterranean with two consecutive additions of evapocondensed dust conducted. The data also show that the dissolution and loss rates of Mn were comparable during both seedings. The calculated fractional solubilities for the first and the second dust addition were 41 ± 9 % and 27 ± 19 %, respectively.

The results presented in this thesis have significantly improved our understanding of Mn distribution and especially cycling in the euphotic zone. An insight into the mechanisms between Mn and ROS and into the dissolution processes from dust is given.



# ZUSAMMENFASSUNG

## 2 ZUSAMMENFASSUNG

Das Spurenelement Mangan (Mn) ist von zentraler Bedeutung im Meer, da es ein essenzieller Mikronährstoff für Phytoplankton ist. Es spielt eine wichtige Rolle im Photosystem II (PSII) bei der Sauerstoffbildung aus Wasser in der Photosynthese. Des Weiteren ist Mn wichtig für weitere enzymatische Redoxprozesse, insbesondere als aktives Metallzentrum in Superoxiddismutase (SOD), welche als intrazelluläre Schutzmechanismen vor oxidativem Stress durch photochemisch produziertes Superoxid ( $O_2^-$ ) fungieren. Im Meerwasser kommt Mn in drei Oxidationsstufen vor: in erster Linie als lösliches Mn(II), als unlösliches Mn(III) und als Mn(IV)-Oxide. Der biogeochemische Kreislauf von Mn im lichtdurchfluteten Ozean ist signifikant durch reaktive Sauerstoffspezies (ROS) beeinflusst. Hierbei können das stark reaktive und kurzlebige Superoxid ( $O_2^-$ ) und seine Tochterprodukt Wasserstoffperoxid ( $H_2O_2$ ) gleichermaßen eine oxidierende als auch eine reduzierende Wirkung haben und spielen somit eine Schlüsselrolle für Mn Prozesse im Meerwasser. Im offenen Ozean beispielsweise ist atmosphärischer Staub die Haupteintragsquelle für Mn und das in oxidierte Form vorliegende Mn im Staub kann durch photochemisch gebildetes  $H_2O_2$  reduziert und als Mn(II) im Wasser gelöst werden. Obwohl die groben Zusammenhänge dieser Prozesse bekannt sind, sind die Hauptreaktionen und Mechanismen des Zusammenspiels von Mn und ROS im Meerwasser kaum verstanden.

Die Dissertation umfasst vier Manuskripte. Manuskripte 1 (Wuttig *et al.*, subm., 2013a) und 2 (Wuttig *et al.*, subm., 2013b) konzentrieren sich auf Kreisläufe und Reaktionsmechanismen von Mn und ROS. Manuskript 3 beschreibt die Unterschiede zwischen den Eintragsprozessen und der Verteilung von Cd, Fe und Mn im östlichen tropischen Atlantik nahe den Kapverdischen Inseln (Wuttig *et al.*, in prep., 2013). Manuskript 4 (Wuttig *et al.*, 2013) widmet sich der Untersuchung des Mn Kreislaufs in Folge der wiederholten Staubzugabe in das oligotrophe Oberflächenwasser von spurenmittel-sauberen Mesokosmen im Mittelmeer.

Im Gegensatz zu früheren Beobachtungen im Südpolarmeer, konnte in dieser Studie klar gezeigt werden, dass im östlichen tropischen Atlantik Mn und organische Substanzen als vorwiegende Senken für  $O_2^-$  darstellen (Manuskript 1; Wuttig *et al.*, subm., 2013a). Mn dominiert diesen Zerfall besonders im Oberflächenwasser, welches stark durch atmosphärischen Staubfluss beeinflusst ist, und nahe dem Meeresboden durch die Resuspension aus dem Sediment.

Zudem konnte gezeigt werden, dass der Abbau von  $O_2^-$  durch Reaktion mit anorganischem Mn(II) in Seewasser einer Zerfallsrate erster Ordnung folgt (Manuskript 2, Wuttig *et al.*, subm., 2013b). Diese scheint eine katalytische Reaktion des Mn(II)/ $MnO_2^+$  Paares zu beinhalten, wobei  $MnO_2^+$  der Superoxidkomplex ist. Des Weiteren ist es in der euphotischen

und sauerstoffreichen Zone unwahrscheinlich, nennenswerte Mn(III) Konzentrationen aufzufinden, welche ohne starke Mn(III) bindende Liganden nur unter anoxischen Bedingungen erwartet werden. Somit kann Mn(III) im Gegensatz zum Mn(II)/MnO<sub>2</sub><sup>+</sup> Paar im sauerstoffreichen Oberflächenwasser nicht als SOD agieren.

Atmosphärischer Staub ist die Haupteintragsquelle von Mn im Oberflächenwasser des östlichen tropischen Atlantiks (Manuskript 3; Wuttig *et al.*, in prep., 2013). Jedoch wurden in dieser Region zusätzlich auch Einträge von Mn durch äquatorialen Auftrieb und Resuspension aus dem Sediment beobachtet. Zusätzlich wurde hier kein sekundäres Mn(II) Maximum gefunden, welches bei gleichen Untersuchungen im östlichen tropischen Pazifik in 200 m Tiefe der Fall war und vermutlich durch eine Kombination aus Einträgen durch atmosphärischen Staub und laterale Transportprozesse verursacht wurde.

Während atmosphärische Quellen dominierend den Mn und Fe Kreislauf beeinflussen, sind Cd Konzentrationen im tropischen Atlantik nicht durch Staubeintrag kontrolliert (Manuskript 3; Wuttig *et al.*, in prep., 2013). Generell zeigten diese Spurenelemente unterschiedliche Verteilungsmuster. Während die für biologisch relevante Elemente zu erwartenden typischen nährstoffähnlichen Tiefenprofile durch den atmosphärischen Eintrag von Fe und Mn überlagert wurden, waren die Cd Konzentrationen im Oberflächenwasser sehr niedrig und nahmen mit der Tiefe zu. Das Cd/P Verhältnis wurde dabei in erster Linie durch die in der Tiefe erhöhten P Konzentrationen bestimmt und wies dort ein Cd/P Verhältnis von 237 pmol/µmol gegenüber 16.6 pmol/µmol im Oberflächenwasser aus.

Auch im Manuskript 4 (Wuttig *et al.*, 2013), welches sich mit der Löslichkeit und dem Kreislauf von Mn nach zwei Zugaben prozessierten Staubs während eines Mesokosmen Projektes im Mittelmeer beschäftigt, spielen die komplexen photochemischen Experimente eine zentrale Rolle. Hinzukommend zeigen die Daten, dass die Mn Löslichkeits- und Verlustraten nach den beiden Staubbzugaben vergleichbar sind. Die anteilige Löslichkeit von Mn aus dem Staubmaterial betrug  $41 \pm 9 \%$  für die erste Staubbzugabe und  $27 \pm 19 \%$  für die zweite Staubbzugabe.



**3**

**GENERAL**

**INTRODUCTION**



### 3 GENERAL INTRODUCTION

The central focus of this thesis is on manganese (Mn), its concentration, its sources (e.g. atmospheric input) and sinks and its relevance other biogeochemical cycles in seawater. The thesis examines in detail the behavior of Mn with key reactive oxygen species (ROS) including superoxide ( $O_2^-$ ) and hydrogen peroxide ( $H_2O_2$ ) in the oligotrophic Eastern Tropical Atlantic (ETA) Ocean. This general introduction describes the present knowledge for the sources and sinks of Mn, its global oceanic distribution, biogeochemical processes and photochemical reactions. This thesis encompasses studies of Mn chemistry in a wide range of oceanic environments, from the surface ocean, the euphotic zone and in oxygen minimum zones. Basic descriptions of the physical, chemical and biological oceanography for each of the study areas is presented here as background information. Finally, the objectives of this thesis, including an outline of the five manuscripts incorporated here and their relevance to this thesis are presented.

#### 3.1 Oceanic Manganese (Mn) distribution, sources and sinks

Mn is the twelfth most abundant element in the Earth's crust (Wedepohl, 1995) whereas in open ocean Mn concentrations are in the low nanomolar range of  $0.08 - 5 \text{ nmol L}^{-1}$  (Bruland and Lohan, 2003). A compilation of published Mn surface distributions in the Atlantic ocean

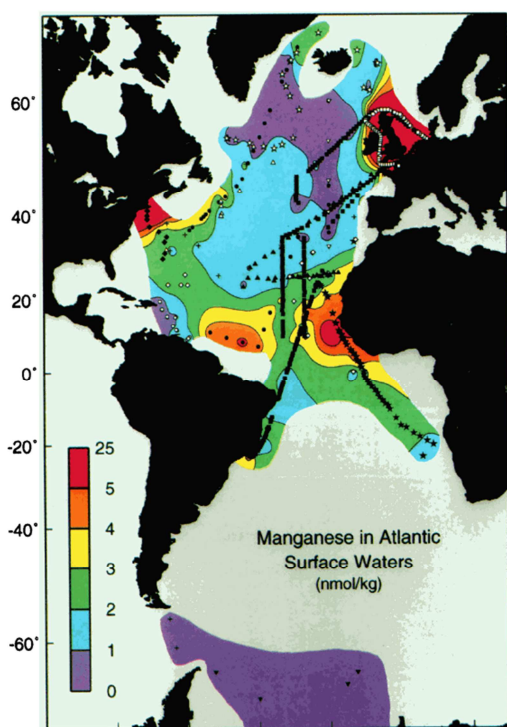


**Fig. 3.1. Mn distribution in the surface waters (0 - 30 m) of the Atlantic Ocean as collected by Shiller (1997).**

were mapped by Shiller (1997) and clearly illustrate the impact of atmospheric sources (i.e. Saharan dust) and continental land runoff as visualized in Fig. 3.1. The concentrations in the surface can range from as low as  $0.04 \text{ nmol L}^{-1}$  in the Southern Ocean (Middag *et al.*, 2011a) to  $4.8 \text{ nmol L}^{-1}$  (Pohl *et al.*, 2011) or even  $7.3 \text{ nmol L}^{-1}$  in the ETA (Chester and Stoner, 1974), and up to  $18.4 \text{ nmol L}^{-1}$  on the European shelf (Kremling, 1983). The high concentrations observed are close to continental margins and their runoff, whereas the levels in the Mn tongue in the ETA coincide with the area of the high Saharan dust input which can be observed in Fig. 3.2. Based on three model studies (Ginoux *et al.*, 2001; Mahowald and Luo, 2003; Tegen *et al.*, 2004) Jickells (1995) calculated and plotted a global map with the annual global dust inputs. In this figure the Mn tongue correlates

with the dust deposition over this oligotrophic region. Mn is prevalent in crustal dust and the supply of atmospheric dust input to the surface ocean has been argued to be the dominant input pathway for Mn (Duce *et al.*, 1991). A study published this year shows the importance of long distance transport of Saharan dust particles which can act as cloud condensation nuclei as far field as over the Western USA (Creamean *et al.*, 2013). Dust is not only a source of Mn, but of a number of important macronutrients (e.g. phosphate ( $\text{PO}_4^{3-}$ )) and micronutrients (e.g. Fe) (Jickells, 1995). In addition dust supplies a number of potential lithogenic tracers to the ocean. Two of these tracers are Al and Ti. Al is suggested to be mainly dissolved from Saharan dust in regions strongly influenced by wet deposition and it is scavenged onto biogenic particles, whereas the contrasting Ti distribution in the surface waters seems to be rather reflecting the annual dust deposition not the precipitation. Therefore Al and Ti can be used as dust tracers but on different time scales. Al is suggested to reflect the seasonal changes in the dust deposition and has a residence time of months to years which is  $\sim 10$  times longer for Ti which is suggested to show longer time scales (Damshäuser *et al.*, 2011).

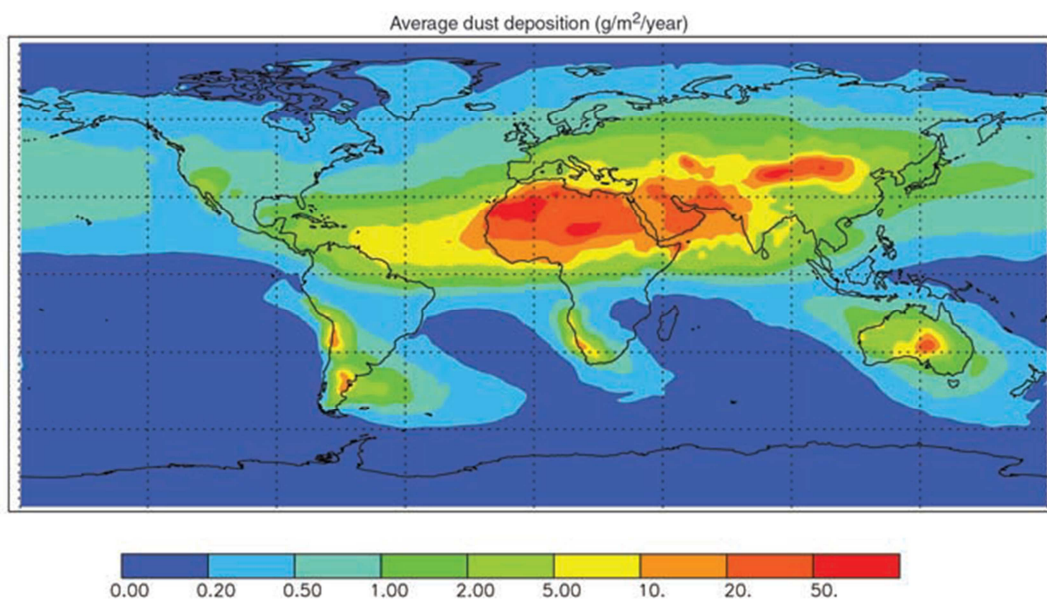


**Fig. 3.2:** Average annual global surface dust deposition (Jickells *et al.*, 2005). The model calculations are based on three studies (Ginoux *et al.*, 2001; Mahowald and Luo, 2003; Tegen *et al.*, 2004).

Not only the amount of dust is important for the dissolution from dust, but also a number of other factors, e.g. the origin and type of the dust (Baker *et al.*, 2006), the type of deposition (wet or dry) (Pohl *et al.*, 2011), the repetition of the dust input (Wuttig *et al.*, 2013) and the microbial processes and photoreduction of Mn-oxides in seawater which can be a major contributor to the Mn surface maximum in the ocean (Sunda and Huntsman, 1994).



The Mn concentration in seawater is strongly influenced by its sources which, apart from the atmospheric sources (Baker *et al.*, 2006), also include lateral transport from continental margins (Martin and Knauer, 1983), upwelling (Johnson *et al.*, 1992; Lewis and Luther III, 2000; Martin and Knauer, 1984) and reducing sediments (suboxic or anoxic) (Johnson *et al.*, 1992; Pakhomova and Yakushev, 2011). In coastal sediments as a result to MnO<sub>2</sub> reduction by biota organic matter can be remineralized (Canfield *et al.*, 1993). Other important pathways are fluvial input (Aguilar-Islas and Bruland, 2006; Elderfield, 1976) and hydrothermal vents (Klinkhammer *et al.*, 1985; Klinkhammer and Bender, 1980; Middag *et al.*, 2011b).

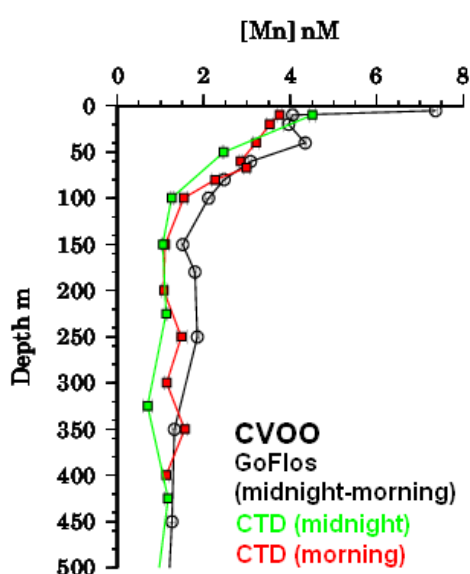


Fig. 3.3. Three dissolved Mn depth profiles from CVOO in the ETA. The samples have been taken at different times of one day (on M83/1) and with different sampling devices: black circles with GoFlo bottles (3 casts from midnight to morning), green squares (midnight) and red squares (morning) with the CTD.

In Fig. 3.3 three typical Mn depth profiles, sampled at the Cape Verdean Ocean Observatory (now: CVOO, former: TENATSO) time series station between midnight and morning are shown. Mn is usually described as having a scavenged-type distribution in seawater (Bruland and Lohan, 2003; Nozaki, 1997). The deep distribution of Mn in seawater is uniformly low ranging from  $\sim 0.1 - 0.2 \text{ nmol L}^{-1}$  (Landing and Bruland, 1980; Middag *et al.*, 2011a) with the exception of areas with additional input pathways occurring. Mn concentrations are highest close to the sources, e.g. in the surface, due to atmospheric dust deposition or continental land runoff as shown in Fig. 3.1. Scavenged elements show strong interactions with particles in seawater (Landing and Bruland, 1980; Middag *et al.*, 2011a; Statham *et al.*, 1998) and are removed with depth. Due to the depletion with depth, the deep Mn concentrations are usually in the range of

$0.1 - 0.2 \text{ nmol L}^{-1}$ . Another typical attribute of scavenged elements is their relatively short residence time in seawater (about 100 – 1000 yr) in contrast to elements that show nutrient-type distribution (Bruland and Lohan, 2003). Residence time for Mn in the deep ocean is thought to be approximately 400 yr in the ETA (Statham *et al.*, 1998). The range in the surface water is significantly shorter with an estimation of 1 to 74 yr with shorter residence times in areas of high dust deposition (Jickells, 1995; Jickells *et al.*, 1994; Jickells, 1999; Landing and Bruland, 1987). In some cases Mn is thought to belong to the category of hybrid-type behavior as it can be controlled by recycling and scavenging processes. In the photic zone soluble Mn(II) can be photooxidized to insoluble Mn(III)- and especially Mn(IV)-oxides, -oxyhydroxides and hydroxides and is then lost from the water column as the soluble

dissolved Mn(II) species is not strongly complexed by sinking particles (Sunda and Huntsman, 1987; Sunda and Huntsman, 1988; Yeats and Strain, 1990). Scavenging is a ubiquitous trace metal process in seawater (Turekian, 1977). This process can be influenced e.g. by carbon dioxide ( $\text{CO}_2$ ), oxygen ( $\text{O}_2$ ) and reactive oxygen species (ROS) (Tebo *et al.*, 2007). In sunlit waters photo-produced ROS play an important role in the recycling of Mn(II) as shown in Fig. 3.4 for hydrogen peroxide ( $\text{H}_2\text{O}_2$ ) and superoxide ( $\text{O}_2^-$ ). In the euphotic zone insoluble  $\text{MnO}_2$  can be reduced by  $\text{H}_2\text{O}_2$  to form dissolved Mn(II) (Sunda and Huntsman, 1988; Sunda and Huntsman, 1990; Sunda and Huntsman, 1994; Sunda and Kieber, 1994). In the presence of organics this reaction can be accelerated due to an enhanced  $\text{H}_2\text{O}_2$  production or complexation (Matsunaga *et al.*, 1995).

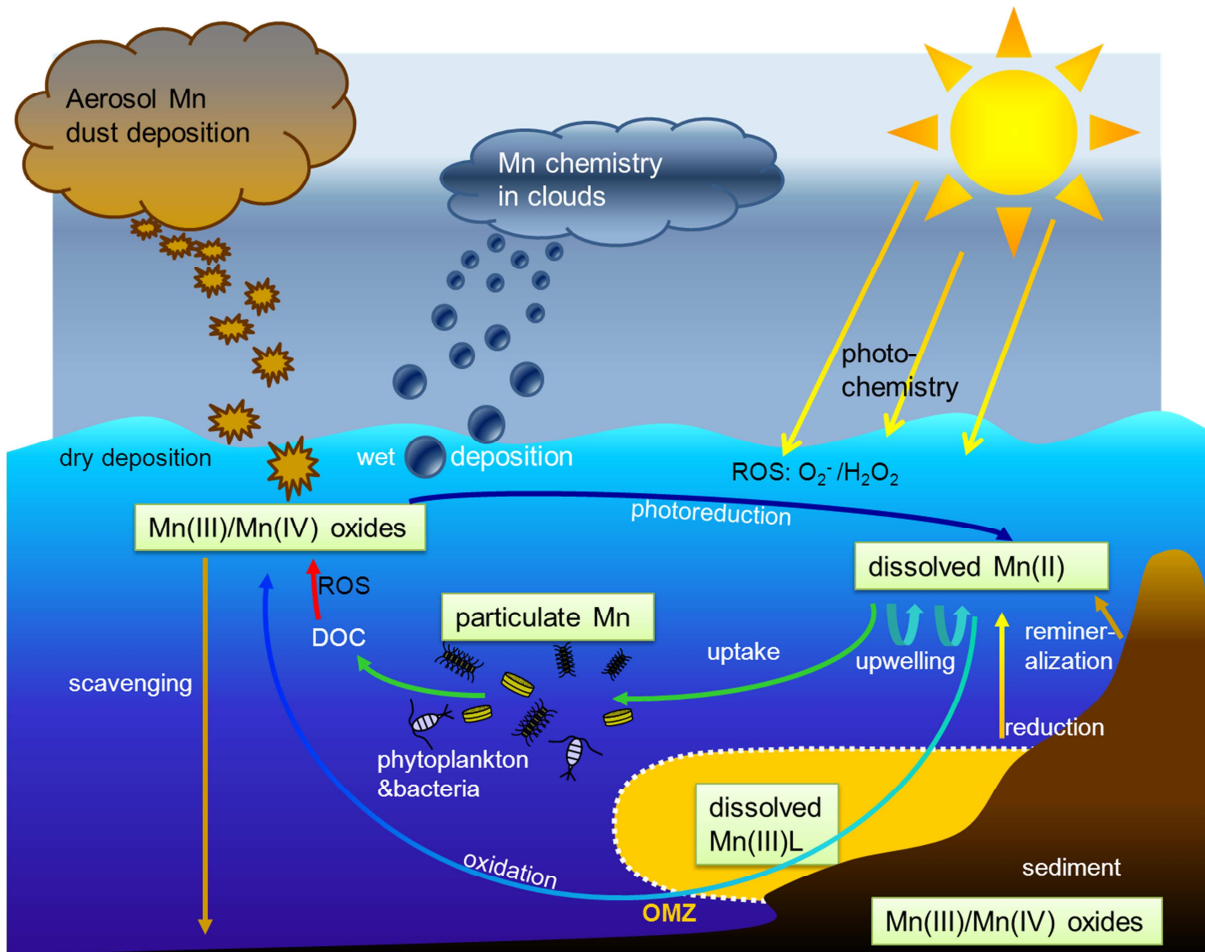
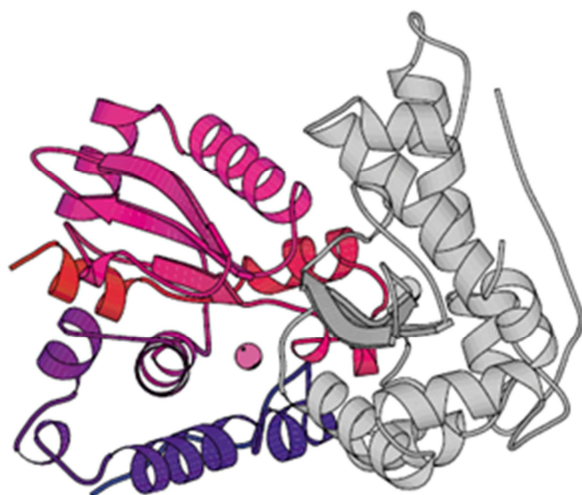


Fig. 3.4: The Mn cycle in seawater.

In experiments with an excess of Mn(II), a catalytic decay of  $O_2^-$  was observed and a cycle between Mn(II) and Mn(III) proposed by Hansard *et al.* (2011). This implies that inorganic Mn(II) could be an important sink for  $O_2^-$  in seawater which could play an important role in sunlit waters in the biological protection against the cell damage by  $O_2^-$ .

This means that Mn is not only controlled by particle scavenging and its different input pathways, but Mn can also be controlled biologically as it is a vital micronutrient for phytoplankton (Bruland and Lohan, 2003). Abiotic Mn(II) oxidation, e.g. by  $O_2$  at pH close to 8 (Morgan, 2005; von Langen *et al.*, 1997), is slow compared to biological Mn(II) oxidation processes (Emerson *et al.*, 1982).

The second important sink in seawater is the biological utilization by phytoplankton. It is important to distinguish between internal and external uptake. These are two different mechanisms. The first one is biological and means uptake before oxidation and the second one is vice versa oxidation before uptake which is surface-adsorbed (Nakabayashi *et al.*, 2002). The Mn requirement of the species depend on the environmental conditions as estuarine species have been shown to have a higher Mn requirement than species in metal impoverished areas (Brand *et al.*, 1983), where e.g. diatoms can be Mn limited (Sunda and Huntsman, 1983) or some diatom species can be colimited by Mn and Fe (Peers and Price, 2004). A complicating factor here is also that Mn and the potentially toxic copper (Cu) share the same uptake mechanisms and that Cu is thermodynamically favored, though strong organically complexed by natural ligands.



**Fig. 3.5: Mn-SOD monomer with folded protein strings and Mn as the active cofactor shown as a magenta ball (Miller, 2004).**

Microbiological oxidation of Mn(II) to Mn(IV) is thought to be driven by bacteria and fungi (and in particular by multicopper oxidase (MCOs) (Webb *et al.*, 2005)). The simplest member of the MCO-family are laccases and MCOs are capable of catalyzing the four-electron reduction of  $O_2$  at their trinuclear center to water ( $H_2O$ ) (Bento *et al.*, 2005). Also MCOs have been shown to oxidize Mn(II) in two one-step electron transfer processes in marine *Bacillus* sp. whereas the first reaction is the rate limiting step (Webb *et al.*, 2005).

Mn plays a key role in biological processes, especially in the Photosystem II (PSII) in one of the most significant reactions (Parkhill *et al.*, 2001) in the 4 electron light energy using conversion of  $H_2O$  to  $O_2$  (McEvoy and Brudvig, 2006). PSII is positioned in the thylakoid membranes of cyanobacteria and its catalytic activity is located on a  $Mn_4Ca$  cluster (Brudvig,

2008). Mn also play an important role in a number of redox enzymes as the active metal center such as in catalase or in superoxide dismutase (SOD) (Wolfe-Simon *et al.*, 2006). Mn-SOD shown as a monomer in Fig. 3.5 (Miller, 2004) can also occur as dimer or tetramers (Wintjens *et al.*, 2004).

The functionality of SODs is to protect cells from intracellular oxidative stress. As the reactive oxygen species (ROS) superoxide radical ( $O_2^-$ ) is very short-lived reactive and can damage the cell. SODs catalyze the reaction 1:

(reaction equation 1)

$O_2^-$  is the intermediate product in the redox cycle of oxygen ( $O_2$ ) and  $H_2O_2$  (Fig. 3.6).

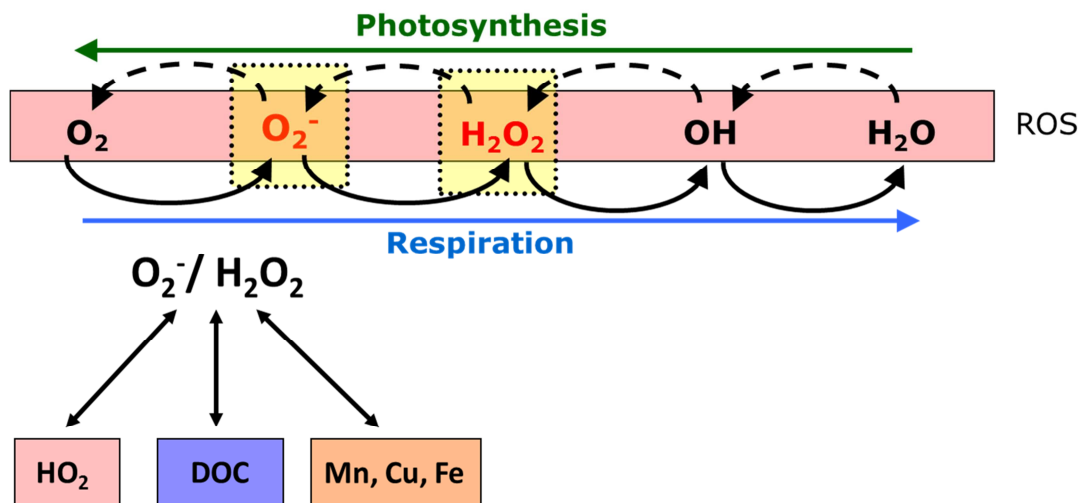


Fig. 3.6: The redox pathways of the different reactive oxygen species (ROS) such as superoxide ( $O_2^-$ ) and hydrogen peroxide ( $H_2O_2$ ). There are three different types of decay reactions of  $O_2^-$  to  $H_2O_2$ . In pink the self-dismutation reaction. In blue the reaction with dissolved organic carbon (DOC) and in orange the metal catalyzed (by manganese (Mn), copper (Cu) or iron (Fe)) destruction of  $O_2^-$ .

Three types of SODs are known (1) Cu/Zn-SODs, (2) Ni-SODs and (3) Fe/Mn-SODs (Miller, 2004). The Fe/Mn-SODs are divided into SODs that are specific either for just Fe or Mn or that function with both metals which is called cambialistic behavior (Miller, 2004). The different types of SODs are found in different marine organisms. While Fe-SODs are widely distributed in Archaea (Wolfe-Simon *et al.*, 2005), the Mn-SOD gene, *sodA*, was rather often found in bacteria (Li *et al.*, 2002) and eukaryotes (Fridovich, 1995) especially in some marine diatoms (Peers and Price, 2004; Wolfe-Simon *et al.*, 2006). Mn can be especially important for marine diatoms under low Fe conditions as they respond to the oxidative stress induced by the missing Fe with an upregulation of the SOD which requires more Mn (Peers and Price, 2004). Growth rates of marine phytoplankton cultures are reduced as a result to low

levels of free Mn(II) (Brand *et al.*, 1983; Sunda and Huntsman, 1986), but this has not been yet shown for species in ambient seawater (Peers and Price, 2004). In a culture of *Thalassiosira oceanica* Sunda and Huntsman (1986) showed that the growth was not limited by Mn(II) concentrations down to 0.6 nmol L<sup>-1</sup>, but *Thalassiosira pseudonia* was limited below 1.7 nmol L<sup>-1</sup>. The difference is that *T. oceanica* can accumulate Mn intracellularly. When the authors added Cu to their culture, the growth rate and the intracellular accumulation decreased as a result to the favored Cu instead of Mn uptake.

In the case of Mn-SOD the active redox pair is Mn(II)/Mn(III) (Hansard *et al.*, 2011) and both species can react quickly with O<sub>2</sub><sup>-</sup> leading to a catalytic decay. Not only inorganic Mn(II) can act as a Mn-SODs but also naturally produced Mn porphyrins (Batinic-Haberle *et al.*, 2010).

### 3.2 Mn speciation and photochemical processes

Mn is a bioactive metal with a complex chemistry in seawater. Mn exists in three main oxidation states: Mn(II), Mn(III) and Mn(IV). In oxygenated seawater and at high pH the thermodynamically favored species Mn(IV) is not the dominant species. In O<sub>2</sub>-free seawater and at low pH the thermodynamically favored species would be Mn(II) (Tebo *et al.*, 2007). Most of the Mn in seawater exists as the soluble Mn(II) which is the oxidation state taken up by biota (Tebo *et al.*, 2007). Mn(II) can persist in oxygenated waters partially due to its slow reaction kinetics (Huntsman and Sunda, 1980), but an important factor are the photochemical reactions especially with ROS. In contrast to the speciation of other trace metals, such as Fe and Cu, dissolved Mn(II) is not thought to be organically complexed (Sunda, 1984). In seawater it exists mainly as the free aquo ion, MnCl<sup>+</sup>, and to a smaller extent as sulfate and carbonate complexes (Byrne, 1988).

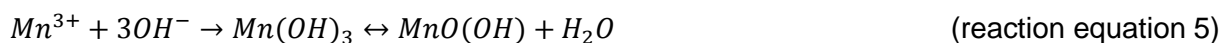
A number of reactions can influence the natural cycle of Mn (Fig. 3.4). Mn(II) can be oxidized by O<sub>2</sub> to Mn(III) or Mn(IV) via one-electron transfer reactions (Luther III, 2005; Luther III, 2010), though this process is very slow (Morgan, 2005; von Langen *et al.*, 1997), but it can be accelerated by particle surfaces (Morgan, 2005; Yeats and Strain, 1990), via microbial processes (Sunda and Huntsman, 1987; Tebo and Emerson, 1986; Tebo *et al.*, 2005) or via photo-oxidation due to humic substances in seawater (Nico *et al.*, 2002):



Jacobsen *et al.* (1997) observed these two reaction equilibria (3 and 4) are affected most by the transient aquo Mn(II)-oxy, MnO<sub>2</sub><sup>+</sup>, complex. In reaction 3 the forward reaction was determined to be significantly faster than the back reaction -3. In reaction 4 both reactions are similarly fast. The decay reactions of MnO<sub>2</sub><sup>+</sup> are described in the following reactions:



The higher oxidation states of Mn are poorly soluble and while dissolved Mn(III) and Mn(IV) organic species are possible, there is no strong evidence for their existence in oxygenated seawater and are thought to be negligible (Roitz and Bruland, 1997). Under these conditions Mn(III) is easily hydrolyzed and precipitated as Mn(III) oxides. Thus dissolved Mn(III) can be only determined under special conditions like in suboxic zones in the presence of ligands that stabilize Mn(III) (Trouwborst *et al.*, 2006).



Additionally the thermodynamically unstable Mn(III) disproportionates rapidly into Mn(IV) oxides and Mn(II) (Kostka *et al.*, 1995; Nealson *et al.*, 1988; Stumm and Morgan, 1996). Mn(III) is only stabilized in the presence of strong ligands such as pyrophosphate (Barnese *et al.*, 2008; Klewicki and Morgan, 1998; Kostka *et al.*, 1995), citrate (Barnese *et al.*, 2012) or oxalate (Hatakka, 1994; Stone, 1987; Xyla *et al.*, 1992). Often EDTA, CDTA or DTPA are used as artificial Mn(III)-ligands (e.g. Stein *et al.*, 1979), but the strong oxidizing Mn(III) can oxidize the ligand.

Mn(II) and  $O_2^-$  are in equilibrium with the transient  $MnO_2^+$  in pyrophosphate and phosphate (Barnese *et al.*, 2008; Cabelli and Bielski, 1984a; Cabelli and Bielski, 1984b) as shown in the reactions 3 and -3. Barnese *et al.* (2008) postulated that the strong Mn(III) complexing ligands stabilize the Mn(III):



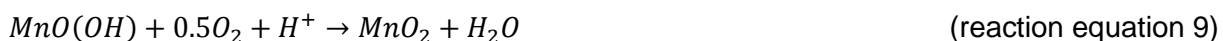
In environments with only weak Mn(III) ligands, the transient  $MnO_2^+$  does not decay to Mn(III). In a disproportionation of  $MnO_2^+$  second-order kinetics are followed instead (Barnese *et al.*, 2008; Jacobsen *et al.*, 1997):



At lower pH, the reaction velocity is increased and below pH 2 the reaction becomes first-order (Jacobsen *et al.*, 1997):



Mn(II) can also be a minor part of the insoluble Mn(III)/(IV) oxides. As  $MnO_x$  the Mn can be lost from the water column and brought into sedimentation (Post, 1999) (Fig. 3.4). Mn(III) oxides can be further oxidized to form particulate  $MnO_2$ :



In the sunlit waters a Mn diel cycle has been postulated as Mn can be reduced and oxidized and the dissolution and formation of particles is strongly influenced by photochemical and microbial processes (Sunda and Huntsman, 1990). Organic matter can complex Mn(II) or lead to photo-produced  $H_2O_2$  (Bertino and Zepp, 1991; Matsunaga *et al.*, 1995). This can enhance the effect that particulate  $MnO_2$  can be reduced by  $H_2O_2$  to soluble Mn(II) in the euphotic zone (Sunda and Huntsman, 1988; Sunda and Huntsman, 1990; Sunda and Huntsman, 1994; Sunda and Kieber, 1994):



As seen in the reaction schematics presented above, there are numerous dual redox-reactions of Mn and ROS as in the case of Mn and  $H_2O_2$ :



Mn(III)O(OH) is oxidized above pH 8 (equation 11) whereas Mn(IV) $O_2$  is reduced below pH 8 (equation 12) (Kanungo *et al.*, 1981). This shows that the dissolution rate is pH-sensitive and that the dissolution processes of  $MnO_2$  depend on the structure of the particulates as MnO(OH) is thought to be on the surface and in the lattice of  $MnO_2$ .

There are also a number of redox processes with other trace metals or reducing or oxidizing species like  $HS^-$ , which will be discussed in more detail in section 3.3.

### 3.3 Low $O_2$ conditions and the influence on Mn

In tropical oceans low  $O_2$  conditions can be observed in vast areas. These oxygen minimum zones (OMZs) differ in their  $O_2$  content, as  $O_2$  concentrations in the southern Pacific OMZ are for example significantly lower than  $O_2$  concentrations in the northern Atlantic OMZ (Karstensen *et al.*, 2008). These OMZs and their properties are described in detail in section 3.4.1 and 3.4.2. Nonetheless it is important to note here that the  $O_2$ -deficient waters are

expanding worldwide.  $O_2$  concentrations are decreasing in the layer between 300 to 700 m depth and consequences for the ecosystems have to be expected (Stramma *et al.*, 2008).

The  $O_2$  concentration in seawater can affect numerous biogeochemical processes including the whole redox chain and the Mn cycle. In Fig. 3.7 the redox chain for a number of important redox-sensitive elements in suboxic ( $<5 \mu\text{mol L}^{-1}$ ) seawater is shown (Rue *et al.*, 1997). Under these conditions the first ones to be reduced completely are iodate ( $\text{IO}_3^-$ ) to iodide ( $\text{I}^-$ ) and particulate  $\text{MnO}_2$  to soluble  $\text{Mn(II)}$ .

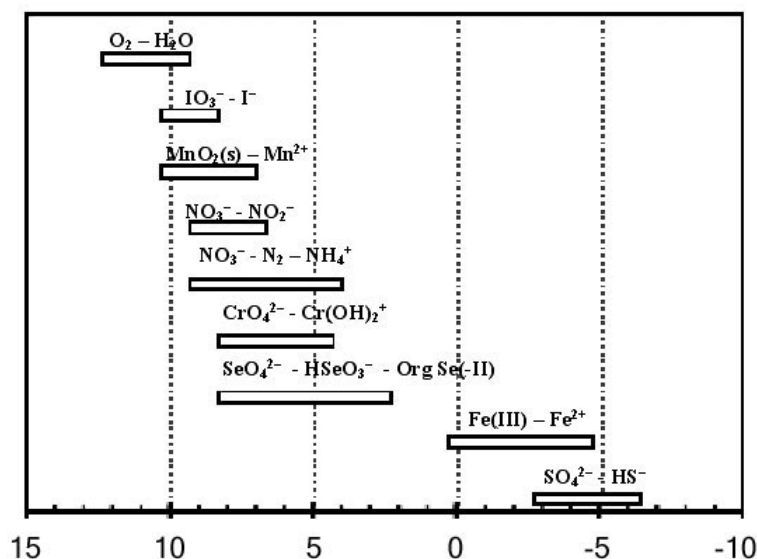


Fig. 3.7: Redox chain with calculated redox potentials pE predicted for seawater at pH 7.5 (Rue *et al.*, 1997) and modified after (Stumm and Morgan, 1996).

With its three oxidation states in seawater and due to its rapid reactions by bacteria and photochemical processes, Mn can serve as a catalyst in seawater. It can be a one-electron-transfer system and help shaping the  $O_2$ -poor regions and their gradients. In the Pacific Ocean both, dissolved  $\text{Mn(II)}$  and  $O_2$  are enriched in the surface waters and decrease with depth (left Fig. 3.8 by Johnson *et al.*, 1992). Between 500 and

1000 m, the seawater is  $O_2$ -deficient whereas the  $\text{Mn(II)}$  concentration is enhanced to a secondary Mn peak. And finally both elements increase close to the bottom (bottom depth at 2000 m).

The observation of a secondary  $\text{Mn(II)}$  maximum can be observed under suboxic conditions (Johnson *et al.*, 1992; Lewis and Luther III, 2000) due to the reduction of  $\text{MnO}_2$  as a result of its high redox potential. The reaction occurring under the anoxic conditions is:



Lewis and Luther III (2000) and Johnson *et al.* (1992) found high fluxes from the continental margins in the secondary  $\text{Mn(II)}$  maximum and observed a more pronounced and shallower secondary  $\text{Mn(II)}$  peak in the Pacific OMZ than in the Atlantic. The  $\text{Mn(II)}$  concentrations were increased when the  $O_2$  concentrations were depleted below  $2 \mu\text{mol L}^{-1}$  (right side of Fig. 3.8 by Lewis and Luther III (2000)).



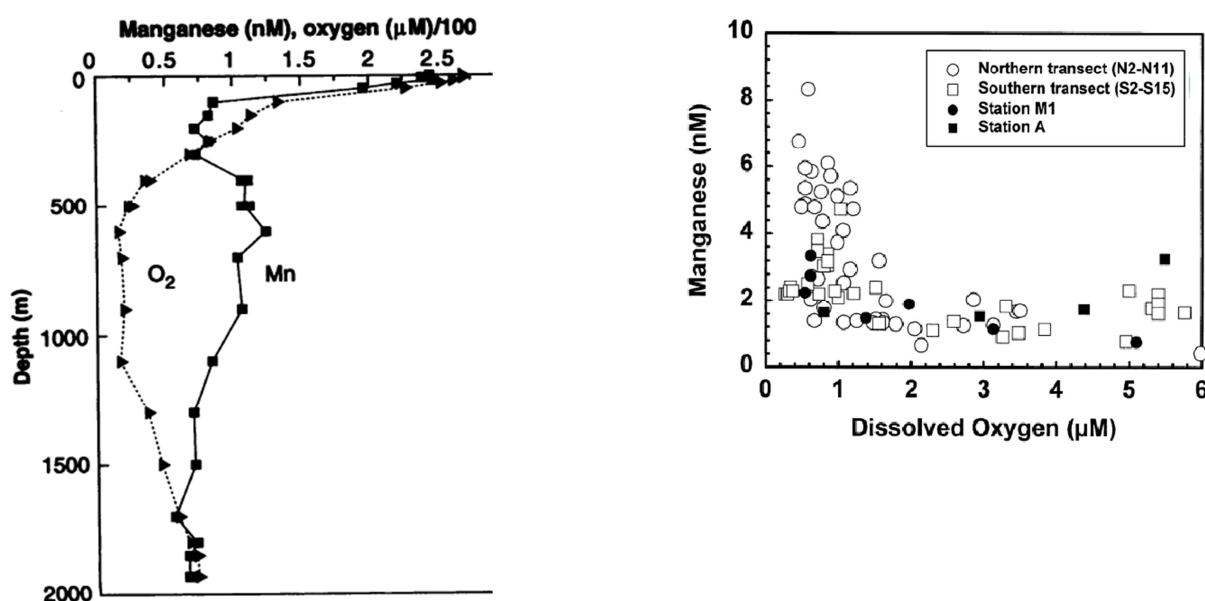


Fig. 3.8: On the left Mn and O<sub>2</sub> depth profiles in the Pacific OMZ (Johnson *et al.*, 1992). On the right Mn(II) versus O<sub>2</sub> from the upper 2000 m of the Arabian Sea. Enhanced Mn(II) concentrations are correlated with O<sub>2</sub> levels < 2 μmol L<sup>-1</sup> and in the euphotic zone > 150 μmol L<sup>-1</sup> (Lewis and Luther III, 2000).

In two regions with extreme O<sub>2</sub>-deficiency, the Chesapeake Bay and the Black Sea, Trouwborst *et al.* (2006) measured soluble Mn(III) instead of soluble Mn(II). They used cathodic stripping voltammetry (CSV) to detect Mn(III) as the known desferrioxamine-B (DEF-B) complex. Bacteria produce the Fe(III)-binding ligand, DEF-B. The 1:1 complex Mn(III)DEF-B exhibits SOD activity (Faulkner *et al.*, 1994). Trouwborst *et al.* (2006) observed 5 μmol L<sup>-1</sup> soluble Mn(III) by this technique in the suboxic zone of the Black Sea which contributes up to 100% of the total dissolved Mn pool. Two different pathways result in this amount of soluble Mn(III) in the suboxic zone which is indicated to be stabilized by unknown natural ligands. At the top of the OMZ Mn(II) is thought to be oxidized and at the bottom Mn(IV)O<sub>2</sub> reduced.

### 3.4 Study Areas

In this thesis data from three different regions, the Eastern Tropical Atlantic (three cruises: M80/1, M83/1 and MSM17/4), the Eastern South Pacific Ocean (M77/4) and Mediterranean Sea (DUNE-2) are used to show the processes governing the Mn cycling in the sunlit oceans.

### 3.4.1 Eastern Tropical Atlantic (ETA)

The Eastern Tropical Atlantic (ETA) Ocean (the sampled area is shown in the red square in Fig. 3.9) is a key area to observe global changes to the ocean environment. This region has some very dominant and strongly influencing features, primarily it is strongly influenced by the deposition of atmospheric dust (Fig. 3.2 (Jickells, 1995)) and second, because of the

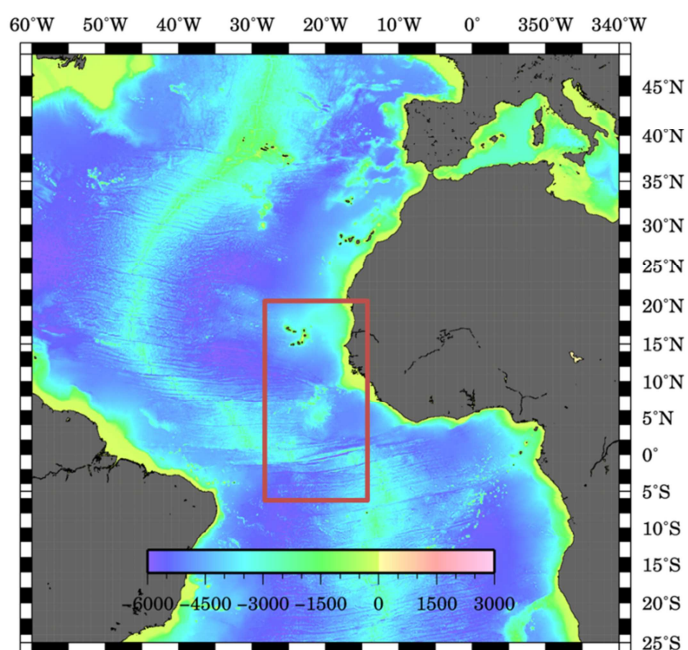


Fig. 3.9: Three cruises (M80/1, M83/1 and MSM17/4) were conducted in the ETA in the region of the red square.

presence of an expansive oxygen minimum zone (OMZ) between 100 and 700 m depth with its core around 400 m (Karstensen *et al.*, 2008). As shown by Duce *et al.* (1991) the input of desert dust can have severe impacts on the concentrations of micro- and macronutrients and thus the growth of biota, their capability of CO<sub>2</sub>- and N<sub>2</sub>-fixation and the influence of climate relevant greenhouse gases. Desert dust can enter the surface ocean via wet or dry deposition. Depending on the trace metal one or the other type can dominate the input. Dry deposition can introduce high amounts of Mn and Fe, for example close to the Cape Verdean Islands. However, in regions with strong precipitation such as the Inter Tropical Convergence Zone (ITCZ), wet deposition is the dominant source of trace metals. Here, surface Mn concentrations up to 4.8 nmol L<sup>-1</sup> were observed by Pohl *et al.* (2011). In the ITCZ tropical trade winds cluster and it is a band of high rainfall >2000 mm yr<sup>-1</sup> (Tchernia, 1980). The position of this band varies seasonally. During the northern summer and autumn it precipitates north of the equator (~10°N) while during northern winter and spring it is located nearly on the equator (Sultan and Janicot, 2000). As precipitation and dust deposition vary heavily over the ETA, the influence of dry and wet deposition does as well. The ITCZ was observed to induce high levels of H<sub>2</sub>O<sub>2</sub> to the surface ocean and H<sub>2</sub>O<sub>2</sub> was shown to have a remarkable influence on the speciation of trace metals (Croot *et al.*, 2004). As ROS and Mn have been shown to be related and this influences the speciation of Mn and therefore its bioavailability for marine phytoplankton, the location of the ITCZ plays an important role in the biogeochemical cycling of Mn (Sunda and Huntsman, 1988).

This OMZ in this oceanic region is usually not suboxic with oxygen ( $O_2$ ) values not lower than  $40 \mu\text{mol kg}^{-1}$  (Karstensen *et al.*, 2008). But recently  $O_2$  values below this threshold and an deoxygenation rate of  $\sim 0.5 \mu\text{mol kg}^{-1} \text{yr}^{-1}$  have been measured (Stramma *et al.*, 2009). This deoxygenation might have severe impacts on the delicate ecosystems and the high primary productivity coastal upwelling regions of the ETA (Stramma *et al.*, 2008; Stramma *et al.*, 2010b) (Fig. 3.9). Upwelling is an important supply pathway of macro- and micronutrients like phosphate ( $\text{PO}_4^{3-}$ ) and cadmium (Cd) to the surface waters (Van Der Loeff *et al.*, 1997). This permanent relatively weak upwelling region is part of the North Equatorial Current (NEC), the North Equatorial Countercurrent (NECC) and the North Equatorial Undercurrent (NEUC) and it coincides with the OMZ (Siedler *et al.*, 1992).

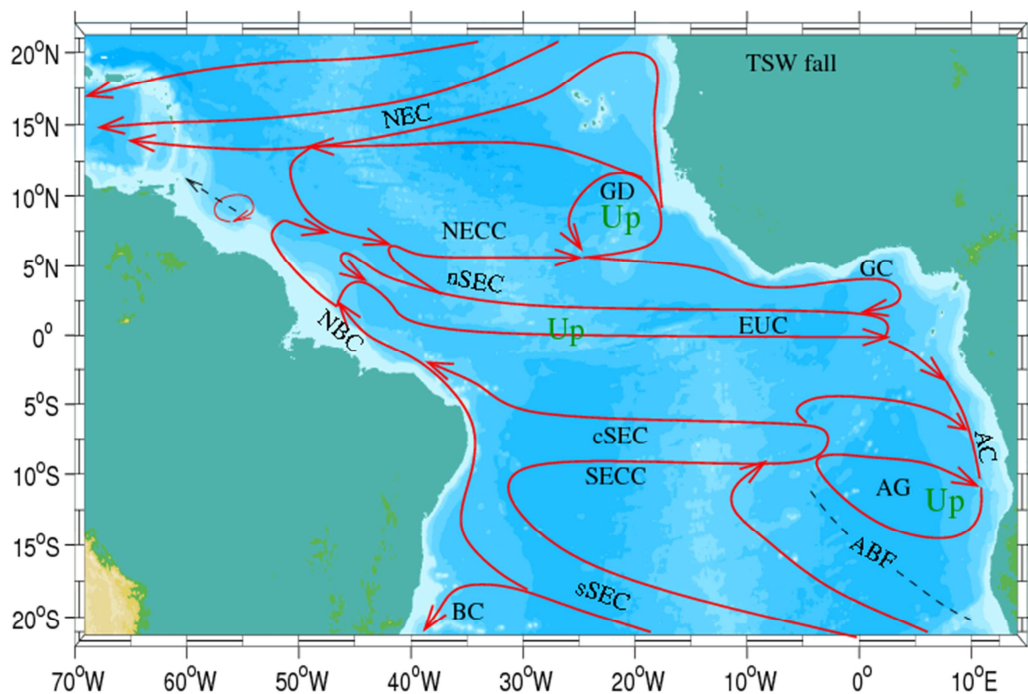


Fig. 3.10: The main currents for the upper 100 m of the Tropical Surface Water layer (TSW) (Stramma *et al.*, 2003). Abbreviations are as follows: North Equatorial Current (NEC), the Guinea Dome (GD), the North Equatorial Countercurrent (NECC), the Guinea Current (GC), the South Equatorial Current (SEC) with the northern (nSEC), equatorial (eSEC), central (cSEC) and southern branches (sSEC), the Equatorial Undercurrent (EUC), the North Brazil Current (NBC), the Angola Gyre (AG), the Angola Current (AC), the Angola Dome (AD), the South Equatorial Undercurrent (SEUC), the South Equatorial Countercurrent (SECC) and the Brazil Current (BC). The general upwelling areas are marked as green "Up".

In Fig. 3.10 the predominant currents in the Tropical Surface Water (TSW) are shown. It is the mixed, near surface layer ( $\sim 0 - 100 \text{ m}$ ) with temperatures about  $27^\circ\text{C}$ . The TSW is separated from the waters below by a sharp thermocline in which  $10^\circ\text{C}$  over the next  $50 \text{ m}$  are lost (Stramma *et al.*, 2003; Stramma and Schott, 1999). It is important to note that in this region zonal jets and counter current bands of smaller meridional and vertical extent play an important role in the transport of water masses to this region and with it macro- and

micronutrients. The South Equatorial Current (SEC) is the main water supply pathway to the tropical Atlantic and it consists of two westward flowing branches, the northern (nSEC) and the eastern (eSEC). These two parts of the SEC heckle the Equatorial Undercurrent (EUC) (Schott *et al.*, 2003 and Brandt *et al.*, 2006). On the Meteor cruise M80/1 (which will be discussed in manuscript 3 in details) the eastward flowing EUC was an ostentatious feature observed on the equator and its core was allocated at 60 – 80 m depths (Brandt *et al.*, 2011). The EUC also has two more important branches, the NEUC and the Southern Equatorial Undercurrent (SEUC) (Stramma *et al.*, 2003).

### 3.4.2 Eastern Tropical Pacific (ETP)

The dominant feature in the Eastern Tropical Pacific (ETP) is its OMZ which is pictured in Fig. 3.11 (Stramma *et al.*, 2010a).

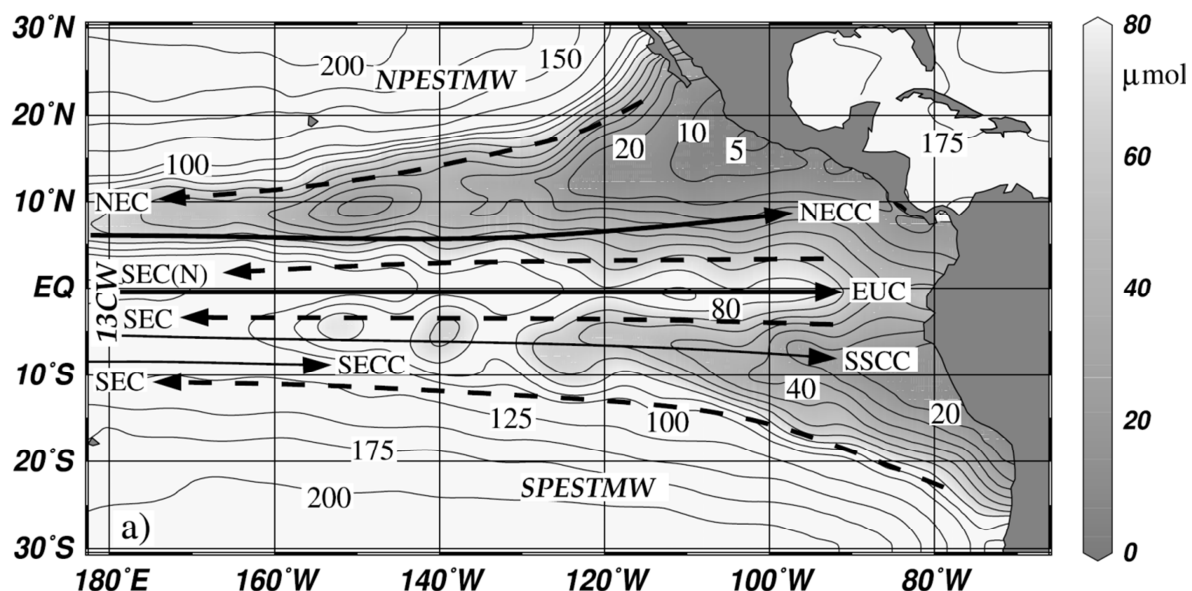
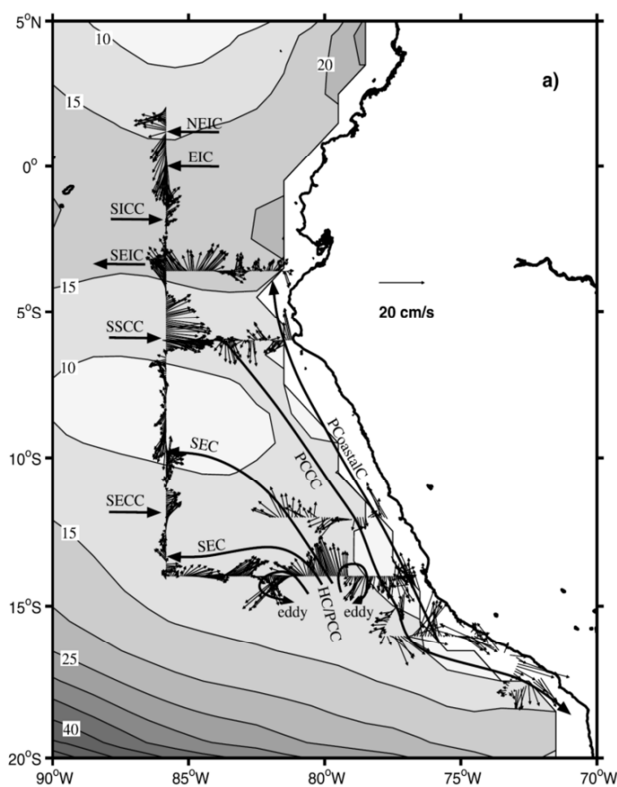


Fig. 3.11: Eastern Tropical Pacific  $O_2$  concentrations at a salinity of  $26.3 \text{ kg m}^{-3}$  between 150 - 300 m and showing the near surface currents (Stramma *et al.*, 2010a). Abbreviations are as follows: North Equatorial Current (NEC), the North Equatorial Countercurrent (NECC), the South Equatorial Current (SEC) with the northern (SEC(N)) branch, the Equatorial Undercurrent (EUC), the Northern and Southern Subsurface Countercurrents (NSCC and SSSC) and the South Equatorial Countercurrent (SECC).

The core of the OMZ is between 300 and 500 m at  $10^\circ\text{S}$  where  $O_2$  concentrations are below  $4.5 \mu\text{mol kg}^{-1}$  and can even reach less than  $1 \mu\text{mol kg}^{-1}$  (Karstensen *et al.*, 2008). Fuenzalida *et al.* (2009) showed that the OMZ ( $<20 \mu\text{mol kg}^{-1}$ ) has huge extensions 1000 km off the coast of Peru from  $5$  to  $13^\circ\text{S}$  and with a thickness of more than 600 m. The large extensions are due to ocean circulation and to oxygen utilization in the OMZ (Karstensen *et al.*, 2008). The suboxia is formed by the distinct remineralization in the coastal Peruvian upwelling accompanied by a missing  $O_2$  supply from adjacent waters (Czeschel *et al.*, 2011).



**Fig. 3.12. Horizontal distribution of the dissolved  $O_2$  concentration and the main zonal currents at 400 m depth taken on M77/4 (manuscript 4) (Czeschel *et al.*, 2011).**

The main supply of  $O_2$  to the OMZ of the ETP is by oxygen-rich zonal tropical currents (Stramma *et al.*, 2010a). In Fig. 3.12 the  $O_2$  concentration (M77/4) of this region is shown together with the main currents (Czeschel *et al.*, 2011).  $O_2$  is supplied by the EUC, Northern and Southern Subsurface Countercurrents (NSCC and SSCC) and the Northern and Southern Intermediate Countercurrents (NICC and SICC) (Stramma *et al.*, 2010a). Over the last 34 yr the  $O_2$  concentration decreased by  $\sim 0.5 - 0.8 \mu\text{mol kg}^{-1} \text{yr}^{-1}$  in this region (Czeschel *et al.*, 2012). The shallow Peruvian coastal upwelling is climate relevant as it allows significant concentrations of greenhouse gases to be emitted to the atmosphere (Paulmier *et al.*, 2008). Also the concentration of  $O_2$

can have severe influences on the speciation of trace metals and their half-life times as, for example, in the case of Fe. Croot *et al.* (subm.) showed that the short-lived species Fe(II) can be stabilized in the permanent Peruvian OMZ and high Fe(II) fluxes from the sediments into the water column were observed. The relationship of the  $\text{Mn(IV)O}_2$  - Mn(II) couple to the  $O_2$  -  $H_2O$  couple is illustrated in Fig. 3.7 (Rue *et al.*, 1997). In contrast to the Peruvian OMZ, in the OMZ of the Arabian Sea two Mn maxima were found. The upper one was observed in the core of the OMZ coinciding with the secondary nitrite maximum and the deeper Mn maximum ( $\sim 600$  m) due to horizontal fluxes from reducing sediments (Lewis and Luther III, 2000). In the ETP this phenomenon has not been investigated yet.

Immediately prior to, and during, this PhD thesis I took part in two research expeditions to the Eastern Tropical Pacific, M77-4 (Feb 2009) and M90 (Nov 2012), in conjunction with the SFB754. The cruisetrack (M77/4) in the ETP is shown with its GoFlo sampling stations in Fig 3.13.

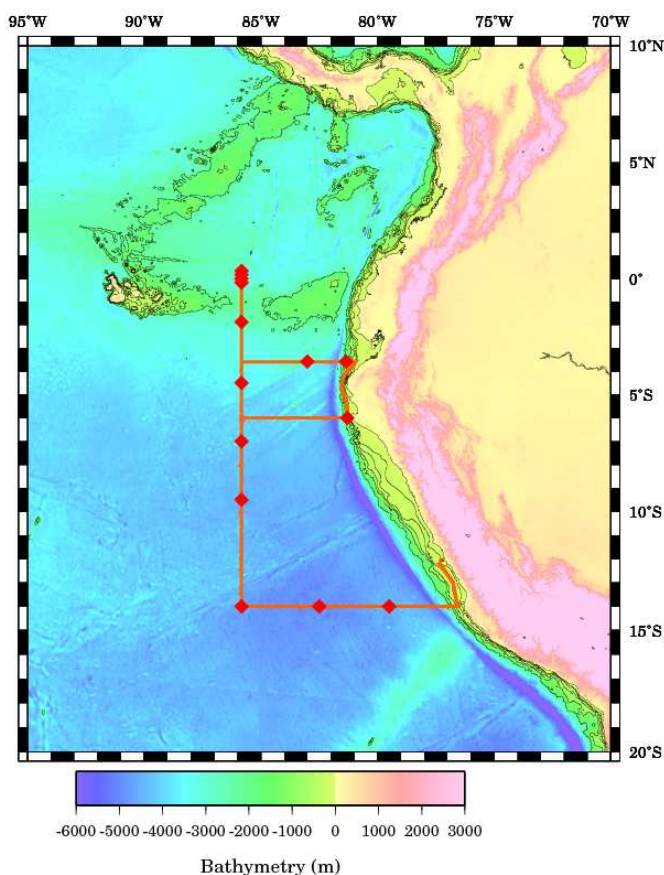


**Fig. 3.13: Cruise track in the Eastern Tropical Pacific (ETP) with the cruise track of M77/4 and its 15 GoFlo stations.**

The analysis of samples from M77-4 was undertaken during this thesis work and formed the initial stages of the optimization of the Mn-FIA method. The results of all the trace metal work performed during M77/4 are currently in preparation for publication (Croot *et al.*, in prep.). The Mn data are shown in Fig. 3.14 for comparison with the work conducted in the ETA presented in manuscripts 1-3. Surprisingly high concentrations of dissolved Mn were found offshore along 88° 50' W and appear to be related to the passage of eddies from the coast to the open ocean that are elevated in Mn. Dust deposition to the ocean from the trade wind transport of material from coastal Peru/Chile or the altiplano (Andean Plateau) also appears to be a factor. However, no strong supporting satellite evidence could be found due to the cloudiness of this region. A secondary Mn maximum was found at 200 m at 14°S coincident with the secondary  $\text{NO}_2^-$  maximum. Sea surface height anomalies (AVISO) indicate eddy presence at the time and place of sampling, which may explain the high  $\text{NO}_2^-$  and Mn at depth as these features are unlikely to have formed in the open ocean in the absence of a high DOM flux. Data from the M90 cruise are currently being analysed at the time of writing.

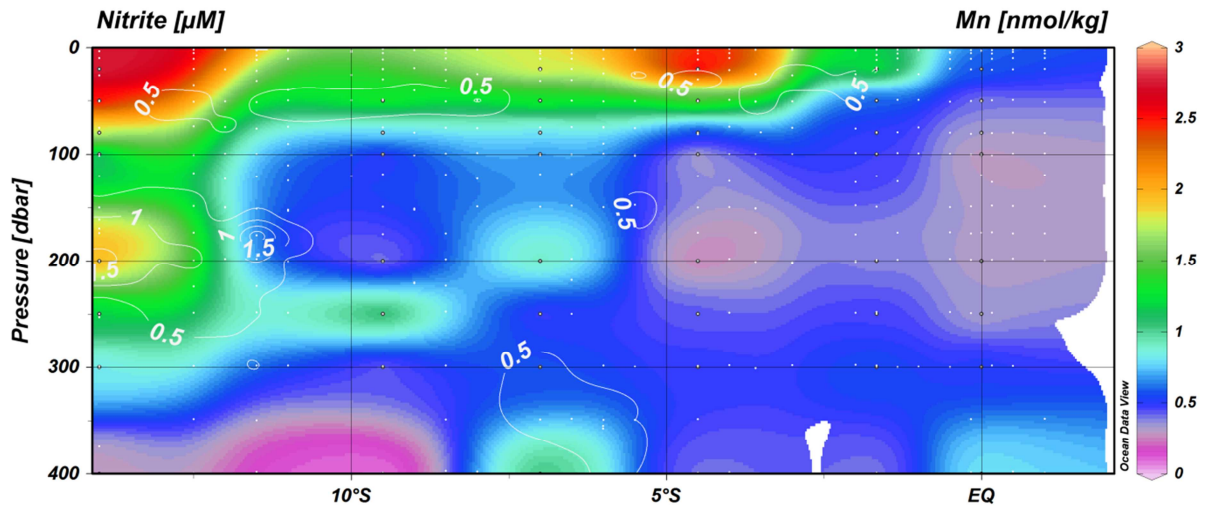


Fig. 3.14: Distribution of dissolved Mn (colours) and  $\text{NO}_2^-$  (white contours) along  $88^\circ 50' \text{ W}$  during M77-4 (Croot *et al.* in preparation).

### 3.4.3 North Western Mediterranean

The North Western Mediterranean between the Southern Coast of France and the isles of Corsica is called the Ligurian Sea. The predominant current is the Ligurian current. This cyclonic Western-Corsican Current which flows along the Western Coast of Corsica (Barth *et al.*, 2005) isolates the coast of the island from more productive waters in the middle of the Ligurian Sea (Guieu *et al.*, 2010). In summer it is a typical marine oligotrophic region with a chlorophyll-*a* content of less than  $0.1 \text{ mg m}^{-3}$  (Carr *et al.*, 2006). It can be also described as a low nutrient, low chlorophyll (LNLC) region. On the 1<sup>st</sup> July 2010, when the DUNE-2 (a **D**Ust experiment in a low **N**utrient, low chlorophyll (LNLC) **E**cosystem) experiment was started, Giovagnetti *et al.* (2012) determined a typical oligotrophic chlorophyll-*a* content of  $0.02 - 0.03 \text{ mg m}^{-3}$ . This feature can also be clearly seen in the MODIS satellite picture of this initial day in Fig. 3.15. In summer often strong thermal stratifications occur and the capture of water masses in mesocosms as shown in Fig. 4.2 simulates this naturally occurring process (Bressac *et al.*, in prep.).

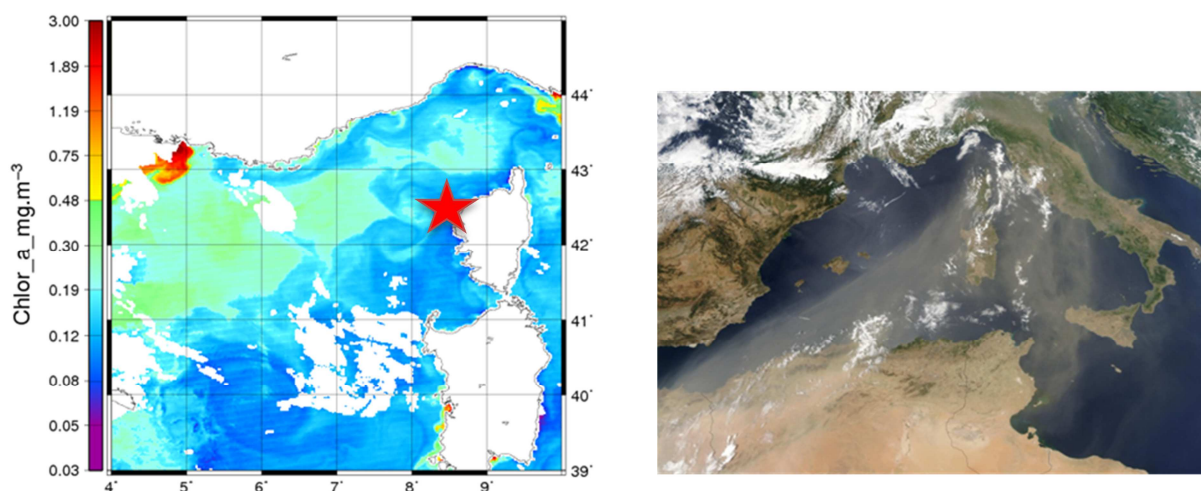


Fig. 3.15: On the left Aqua MODIS satellite image showing the chlorophyll-a distribution in the Ligurian Sea at the start of the DUNE-2 experiment (site marked with a red star at 42.374°N, 8.554°E) on the 1<sup>st</sup> July 2010 (Guieu *et al.*, in prep.) and on the right satellite image from space over the Western Mediterranean showing dust particles being transported (NASA-EO, 2011).

A second important influence in this region is the input of Saharan dust (Fig. 3.15). Nutrient release from desert dust can lead to a subsequent increase of biota in this LNLC region (Bonnet *et al.*, 2005; Herut *et al.*, 2005). On the coast of Corsica over a ten year period, an annual mean flux of 12.5 g m<sup>-2</sup> of dust has been recorded (Loye-Pilot and Martin, 1996). But during dust storms depositions of more than 22 g m<sup>-2</sup> have been observed (Bonnet and Guieu, 2006; Ternon *et al.*, 2010).

### 3.5 Thesis outline

Our understanding of the processes of Mn in the sunlit Tropical oceans is poor. The key processes that dominate in the eutrophic zone and their reaction velocities and importance are not clear. Not only the Mn concentration, but also the Mn speciation can be influenced by a number of factors. In the Tropical oceans atmospheric dust deposition is a main source of Mn to the surface. Previous research has identified the photochemically produced ROS especially O<sub>2</sub><sup>-</sup> and H<sub>2</sub>O<sub>2</sub> to have a major influence on the redox switch of Mn (Hansel and Francis, 2006; Sunda and Huntsman, 1988; Sunda and Huntsman, 1990). O<sub>2</sub><sup>-</sup> and its daughter product H<sub>2</sub>O<sub>2</sub> can both act as an oxidant and as a reductant of trace metals like Mn and their cycling. But the role and importance of the ROS in the ocean is only now starting to become clearer. Their mechanisms and critical kinetic rates and fluxes still need a lot of research, especially with different trace metals and organic species that can be present in seawater. In manuscript 1 I investigated the pathways of the O<sub>2</sub><sup>-</sup> decay in the Tropical Atlantic Ocean.



Recent research on the species Mn(III) found out that Mn(III) cannot only be particulate but also in high concentrations as the soluble species under suboxic condition (Dellwig *et al.*, 2011; Trouwborst *et al.*, 2006). As the O<sub>2</sub>-deficient areas are expanding in the Eastern Tropical oceans, this can have severe implications on the bioavailability of Mn. Mn(III) can be stabilized by the siderophore DEF-B and this complex can be influenced by the ROS, O<sub>2</sub><sup>-</sup> and H<sub>2</sub>O<sub>2</sub>, and by O<sub>2</sub>. I present these reaction pathways and the redox cycles in manuscript 2.

One of the goals of this thesis was to set up a method for Mn(II) determination that can be used at sea and is less time consuming than graphite furnace atomic absorption (ETAAS). Therefore, I refined the method by Aguilar-Islas *et al.* (2006) for a higher sample measuring capacity and enhanced the sensitivity significantly. I applied this method on a number of cruises and also on stored samples. Some of the obtained results are presented in a number of manuscripts (3, 4 and 5).

In manuscript 3, I investigated the different behavior of the three biologically relevant trace metals Cd, Fe and Mn on a transect under the Saharan dust plume and in the northeastern Atlantic OMZ. It can be clearly seen that these three metals are influenced by different input pathways.

In manuscript 4, I present the results of two consecutive artificial dust deposition events to mesocosms situated in an oligotrophic area (DUNE-2 experiment). The dissolution and loss rates and fractional solubility of Mn were determined. The key micronutrient Fe and the amount of it being complexed by Fe-binding ligands were investigated. The data were compared to the results for the lithogenic tracer Al.



4

**M**ATERIAL

AND

**M**METHODS



## 4 MATERIAL AND METHODS

### 4.1.1 Reagents and bottles

Due to the low concentrations of trace metals present in seawater, necessary precautions were taken to avoid contamination. All analytical work at sea was performed in an overpressurized ISO class 5 clean container, inside of which analysts wore the appropriate clean room apparel: overalls with hood (Tyvek), shoes (Abeba) and plastic gloves (Carl Roth). On land, the sample processing and analysis steps were performed in HEPA filtered laminar flow benches inside class 100 clean rooms. All manipulations were performed in class 100-laminar flow benches. All reagents that were used were of highest purity available (Fischer Scientific and Sigma-Aldrich) and were prepared using ultrapure ( $18 \text{ M}\Omega \text{ cm}^{-1}$  resistivity) water (MQ water) from a Milli-Q purification system (Millipore). Sub-boiled quartz-distilled hydrochloric acid (hereafter Q-HCl) and sub-boiled quartz-distilled nitric acid (hereafter Q-HNO<sub>3</sub>) were made by single distillation from 25 % HCl and from 65 % HNO<sub>3</sub>. All plasticware and bottles (low density high polyethylene (LDPE) and Polytetrafluoroethylene (PTFE)) used for seawater samples were cleaned according to the trace metal clean procedures (Bruland *et al.*, 1979; Cutter *et al.*, 2010) and then protected by double bags (Minigrip™).

### 4.2 Sample collection

Samples were collected during four ocean going expeditions and one mesocosm project. The latter was deployed in the Northwestern Mediterranean in the framework of the DUNE-2 project in June 2010. Samples were taken in-line with a Teflon™ pumping system as described in 4.1.3 and the results are published in manuscript 4 (Wuttig *et al.*, 2013).

On four cruises samples were taken with two types of hydrocasts: (1) the CTD rosette system and (2) the GoFlo-sampling devices. Work in the home laboratory in Kiel was performed in a clean room, inside of which analysts wore the appropriate clean room apparel.

This work in the ETA was performed using the German research vessels Maria S. Merian (MSM17/4, March/April 2011) on the Mauretanian shelf and Meteor (M80/1, October/November 2009 and M83/1, October/November 2010) and findings are shown in manuscript 1-3 (Wuttig *et al.*, *subm.*, 2013a; Wuttig *et al.*, *subm.*, 2013b; Wuttig *et al.*, *in prep.*, 2013). On the two Meteor cruises (M80/1 and M83/1) the Cape Verdean Ocean Observatory (CVOO) time series station was occupied.

For the work in the Pacific (ETP) sampling was also performed on board of the research vessel Meteor (M77/4, January/February 2009) and results are shown in manuscript 4 (Croot *et al.*, *in prep.*).

### 4.2.1 CTD-sampling

Samples for salinity, oxygen, macronutrients, chlorophyll-a and pigment measurements were obtained from two Seabird SBE 9 plus CTD rosette systems (Fig. 4.1) with one Digiquartz™ pressure and one chlorophyll-a sensor and double sensor packages for temperature, conductivity and oxygen (Brandt *et al.*, 2011). The discrete samples for oxygen, macronutrients and chlorophyll-a were unfiltered and analyzed using standard protocols (Grasshoff *et al.*, 1983). The oxygen and chlorophyll-a data were used for calibration of the relevant sensors. Samples for hydrogen peroxide (H<sub>2</sub>O<sub>2</sub>) and Fe(II) were also sampled from the CTD rosette into clean brown low density high polyethylene (LDPE) bottles. As Fe(II) species have a very short half live time, they are much less prone to contamination than other Fe species and can be sampled with less precautions. Samples for dissolved Mn and chromophoric dissolved organic matter (CDOM) were obtained from the CTD to achieve a higher resolution of sampling achieved by purely using the GoFlo-bottles. Both Mn and



**Fig. 4.1:** In the left corner the CTD rosette and on the Kevlar rope a GoFlo bottle attached coming out of the water (Foto: M. Dunker).

CDOM were sampled and then filtered with 0.2 µm filters (Sartorius Filtropur S 831826001) and Teflon syringes under a class 100-laminar flow bench. Discrete samples for Mn were further processed as described below (4.2.2).

### 4.2.2 GoFlo-sampling

Seawater samples were collected at 6 - 15 GoFlo stations per expedition. Each GoFlo station consisted of 1 - 3 casts with usually 4 GoFlo bottles each. One GoFlo bottle attached to a Kevlar line can be seen in Fig. 4.1. Samples were obtained from the upper water column (0 –

400 or max. 800 m depending on the cruise) using modified Teflon coated PVC General Oceanics (Miami, FL, USA) GoFlo bottles of 8 L in which the original drain cock was replaced by a Teflon stop cock. These bottles were deployed on a Kevlar line from the side of the ship. Immediately upon recovery of the GoFlo bottles, they were brought into the clean container and instantly unfiltered samples taken for H<sub>2</sub>O<sub>2</sub> and Fe(II) analysis. Then samples were filtered in-line through 0.2 µm filter cartridges (Sartorius Sartobran filter capsule 5231307H5) by N<sub>2</sub> overpressure into acid cleaned and three times rinsed bottles and then protected by double bags (Minigrip™). The filtered samples for dissolved trace metal analysis were directly acidified after the filtration with 3 mL 6 mol L<sup>-1</sup> quartz distilled hydro chloric acid (Q-HCl) per L to pH < 2 and for dMn 570 µL 6 mol L<sup>-1</sup> Q-HCl per 0.1 L to pH 1.7 under a class 100-laminar flow bench. Sample processing and analysis steps were performed under

HEPA filtered air on laminar flow benches inside a class 5 clean room in Kiel. For CDOM and superoxide ( $O_2^-$ ), the samples were stored in the dark at 4°C prior to analysis.

### 4.2.3 Sampling with a Teflon™ pump

In each of the six DUNE-2 mesocosms flexible reinforced PVC tubings were installed at 0.1, 5, and 10 m depth. Additionally in two dust seeded mesocosms (D1 and D2) three supplementary tubings were installed at 2.5, 7.5 and 12.5 m depth. Sampling was performed with a Teflon™ diaphragm pumping system as shown in Fig. 4.2. For dissolved trace metals, samples were filtered inline through 0.2 µm filter cartridges (Sartorius Sartobran filter capsule 5231307H5, Germany). The samples were stored in the dark prior to processing under HEPA filtered air on laminar flow benches.

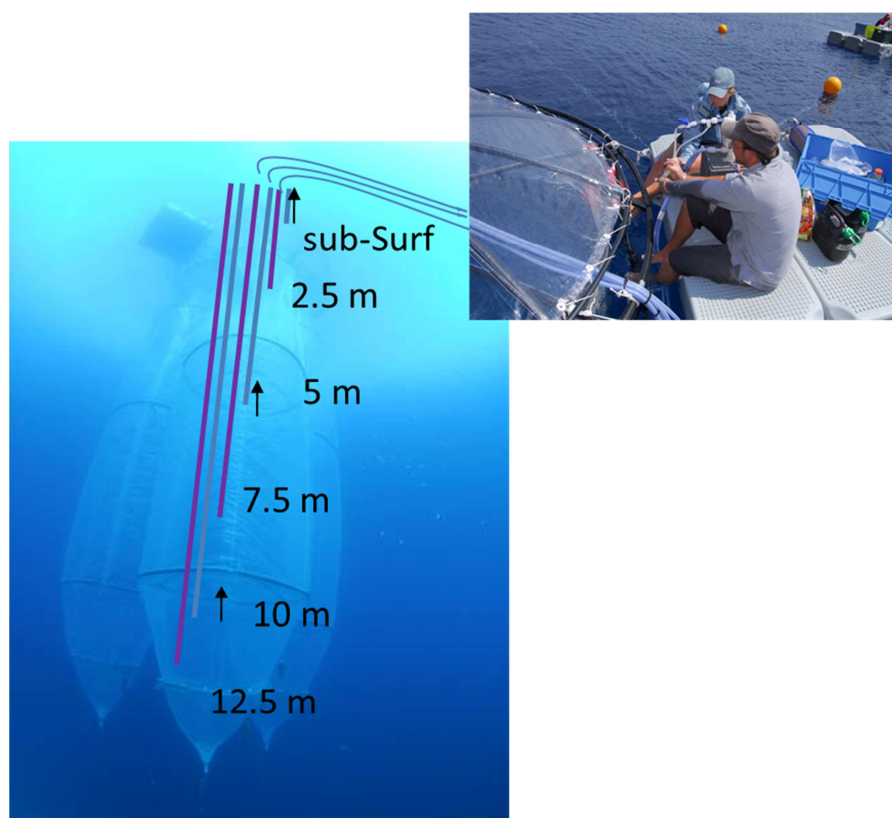


Fig. 4.2: Sampling of the DUNE-2 mesocosms with 6 sampling depths and inline filtration (photo D. Luquet).

## 4.3 Chemical analysis

### 4.3.1 Total dissolved trace metal analysis

The filtered samples for dissolved trace metal analysis were directly acidified with Q-HCl to  $\text{pH} < 2$  under a class 100-laminar flow bench. Precisely this means that to 1 L of  $0.2 \mu\text{m}$  filtered seawater in clean LDPE bottles 2 – 3 mL Q-HCl were added to adjust the pH. The bottles were double bagged and the sample processing and analysis steps were performed in laminar flow benches inside the class 100 clean room in the chemical oceanography department at GEOMAR in Kiel. Dissolved total trace metal (cadmium (Cd), cobalt (Co), copper (Cu), iron (Fe), nickel (Ni), lead (Pb) and zinc (Zn)) concentrations were determined using the graphite furnace atomic absorption (ETAAS, Perkin-Elmer Model 4100ZL) method after pre-concentration by simultaneous dithiocarbamate-freon extraction from seawater (100-250 g) (Danielsson *et al.*, 1978; Grasshoff *et al.*, 1983). The samples were not UV irradiated prior to analysis as recent work has shown that this is important for determining total Co concentrations (Milne *et al.*, 2010; Shelley *et al.*, 2010). The accuracy of the method was evaluated by measuring SAFe and GEOTRACES intercalibration samples. Our SAFe data in Table 1 are close to the average consensus (Bruland, 2011).

The precision for replicate analysis was between 3 - 5% at the concentrations found in this study. The procedural (analytical) blank was  $0.041 \pm 0.024(\sigma_{bl}) \text{ nmol L}^{-1}$  (Fe) and  $<1 \text{ pmol L}^{-1}$  (Cu).

**Table 1: SAFe comparison data of our data and the consensus values (Bruland, 2011).**

dissolved trace metal	SAFe Reference Sample	Our data ( $\text{nmol L}^{-1}$ ) <sup>(a)</sup>	Consensus values ( $\text{nmol L}^{-1}$ ) <sup>(b)</sup>
Cu	S	$0.395 \pm 0.025$	$0.52 \pm 0.05$
	D2	$2.22 \pm 0.23$	$2.28 \pm 0.15$
Fe	S	$0.112 \pm 0.013$	$0.093 \pm 0.008$
	D2	$0.829 \pm 0.127$	$0.933 \pm 0.023$
Mn	D2	$0.42 \pm 0.05$	$0.35 \pm 0.06$

(a) The errors presented with our data in this table correspond to the standard deviation as 95 % confidential intervall. Our data ( $n = 4$ ) was measured between January 2009 and March 2013.

(b) Note that in contrast to our data the errors presented with the consensus values in this table correspond to the standard deviation ( $1 \sigma$ ).



### 4.3.2 Dissolved manganese (Mn) analysis

Samples for dissolved Mn were analyzed using two different analytical approaches. The existing method used in the laboratory is solvent extraction using oxine, which is very labour intensive and cannot be used at sea. Equipment and software for the second method, Flow injection analysis (FIA) with spectrophotometric detection, was constructed and developed during this thesis (manuscripts 3 and 5).

For the Mn analysis by graphite furnace atomic absorption (ETAAS, Perkin-Elmer Model 4100ZL) after solvent extraction modified after Klinkhammer (1980), 200 g of filtered and acidified seawater were extracted with 8-hydroxyquinoline in distilled chloroform as Mn-oxinates, back-extracted with 3 mol L<sup>-1</sup> Q-HNO<sub>3</sub> and then analyzed with ETAAS. SAFE reference seawater D2 was determined as 0.42 ± 0.05 nmol L<sup>-1</sup> (consensus value 0.35 ± 0.06 nmol L<sup>-1</sup>) as shown in Table 1 and these Mn values for the validation are given in appendix. As explained above, the ETAAS method is very time consuming and not applicable at sea. As we were only able to analyze a certain number of samples in the given time frame by this method we primarily used it to demonstrate the comparability of the results of the FIA method.

For the flow injection method we collected 0.2 µm filtered seawater samples off the GoFlo bottles and off the CTD rosette system. The samples were acidified to pH 1.7 with Q- HCl under a class 100-laminar flow bench on board or in the case of the DUNE-2 project on site. Prior to analysis the acidified samples were equilibrated for at least 1 h. Then they were analyzed spectrophotometrically using a slightly modified flow-injection analysis system (FIA) modelled after Aguilar-Islas *et al.* (2006) as shown in Fig. 4.3. This Mn-FIA was built and developed further during the course of this thesis. We used one 8-channel peristaltic pump (Rainin), two electrically actuated 6-port valves, one electrically actuated 10-port sample valve (all VICI, Valco Instruments), one dry bath (Fisher) kept at 35 °C and a variable wavelength spectrophotometer (USB-4000, Ocean Optics, Inc.) with an internal Ocean-Optics light-source and a 1 cm quartz flow-through cell (100-QS, 10.00 mm, Hellma GmbH & Co. KG). The flow rates were identical with those described by Aguilar-Islas *et al.* (2006). The filtered and acidified seawater samples were preconditioned for 30 s by flushing with 0.05 mol L<sup>-1</sup> ammonium borate rinse solution on a pre-concentration column (GLOBAL-FIA) filled with Toyopearl AF-Chelate-650M resin. The timing parameters were for preconditioning, loading, rinse and elution of the column were 30, 120 - 180, 30, 180 s. This setup was used for DUNE-2 (Wuttig *et al.*, 2013). For the low Mn concentrations in the open ocean, the optical part was improved to enhance the sensitivity of the measurements and improve the detections limit. The variable wavelength spectrophotometer (USB-4000, Ocean Optics, Inc.) was coupled with the help of optical fibres (QP400-025-SR) to an external UV/VIS-light source (Micropak DT-Mini-2GS, Ocean Optics, Inc.) and to a 10 cm Liquid



**Fig. 4.3: Photo of the Mn flow-injection analysis system (Mn-FIA).**

Waveguide Capillary Cell (LWCC-2010, World Precision Instruments, Inc.) which replaced the 1 cm quartz flow-through cell (100-QS, 10.00 mm, Hellma GmbH & Co. KG) and the internal light source. The electrically actuated 10-port sample valve was replaced by an electrically actuated 26-port sample valve (all VICI, Valco Instruments) for a higher and continuous throughput of samples.

Calibration curves were determined daily by the addition of standards (0 - 10 nmol L<sup>-1</sup>) produced by serial dilution of a 1000 ppm Mn(II) standard (Fluka) into 0.2 µm filtered Mn depleted seawater of the corresponding region.

Samples, standard additions and blanks were measured in triplicates or quadruplicates. Analytical precision (expressed as percent relative standard deviation  $\sigma$ ) was typically <8 %. The

accuracy of the analytical procedure was evaluated by daily measurements of SAFe intercalibration samples S (consensus value  $0.79 \pm 0.06$  nmol L<sup>-1</sup> with the FIA methods yielding systematically slightly lower values than the ETAAS/ICP-MS methods) and D2 (consensus value  $0.35 \pm 0.06$  nmol L<sup>-1</sup>). This worked well in open ocean regions as the natural occurring Mn concentrations were in the same range as the intercalibration samples. The Mn concentrations in the Mediterranean DUNE-2 project were much higher than the concentrations in the SAFe standard (initially  $3.4 \pm 0.6$  nmol L<sup>-1</sup> versus <1 nmol L<sup>-1</sup>). This led to lower precision for the SAFe samples using our system optimized for Mediterranean surface waters. SAFe values determined in Corsica were as follows:  $0.85 \pm 0.14$  nmol L<sup>-1</sup> (S) and  $0.35 \pm 0.09$  nmol L<sup>-1</sup> (D2) of Mn (n = 8) (consensus values are  $0.79 \pm 0.06$  nmol L<sup>-1</sup> and  $0.35 \pm 0.06$  nmol L<sup>-1</sup> respectively) (Bruland, 2011). We used a large volume of secondary standard (0.2 µm filtered Mediterranean seawater (t0, sampled outside the mesocosms, 5 m)) throughout the DUNE-2 work as the seawater in which standard additions were prepared. The complete Mn-FIA measurements over the course of the work in Corsica resulted in a value of  $3.60 \pm 0.30$  nmol L<sup>-1</sup>, which was in good agreement with values measured by ETAAS in Kiel:  $3.55 \pm 0.08$  nmol L<sup>-1</sup>. The detection limit (3  $\sigma$  of the blank) for the Mn flow injection system used here was estimated in the lab in Kiel by repeated measurements of very low Mn Antarctic seawater (<0.2 nmol L<sup>-1</sup>; collected during ANTXXIV-3) at 150 pmol L<sup>-1</sup>. The use of a low Mn or Mn free seawater is preferred to running MQ blanks, as the MQ systems both in Corsica and in Kiel were contaminated with Mn due to problems with the ion-exchange units of the systems employed there.

The comparability of samples determined for Mn, which were taken of the GoFlo bottles and of the Niskin bottles attached to the CTD rosette system was tested. The metal parts in the Niskin bottles did not contaminate the samples for Mn.

### 4.3.3 Hydrogen peroxide (H<sub>2</sub>O<sub>2</sub>) analysis

Discrete samples for the redox sensitive species hydrogen peroxide (H<sub>2</sub>O<sub>2</sub>) and Fe(II) were collected in brown 125 mL LDPE bottles by a sample procedure similar to that used in sampling for dissolved oxygen (O<sub>2</sub>). The bottles were rinsed three times with seawater and then the sample was taken from the Niskin or GoFlo bottle with the help of acid cleaned tubing after flushing all the bubbles in the tubing. The filled bottles were immediately brought to the lab and analyzed within 1 – 2 h of collection. We used a flow injection chemiluminescence (FIA-CL) method which was recently developed in our group. With this method the two short-lived species H<sub>2</sub>O<sub>2</sub> and Fe(II) can be detected alternately. For H<sub>2</sub>O<sub>2</sub> the methodology was further developed after Yuan and Shiller (1999) and Croot *et al.* (2004). For Fe(II) the method, as described in Croot and Laan (2002), was combined with the H<sub>2</sub>O<sub>2</sub> method in the FIA. Both the H<sub>2</sub>O<sub>2</sub> and the Fe(II) method rely on the chemiluminescence reagent luminol, but differ slightly in the reagent cocktails used. For measuring both species, the reagents are injected alternately to the seawater sample stream allowing alternating detection in the same FIA.

Samples were analyzed 3 to 4 times: typical precision was 2 – 3 % through the concentration range 0.5 – 100 nmol L<sup>-1</sup>, the detection limit (3  $\sigma$ ) was typically 0.2 nmol L<sup>-1</sup>.

### 4.3.4 Superoxide (O<sub>2</sub><sup>-</sup>) analysis and experiments

An aliquot of 60 mL of clean seawater was transferred directly into a PTFE bottle. Diethylenetriaminepentaacetic acid (DTPA), Cu (0.79, 1.58 nmol L<sup>-1</sup>), Mn (1, 2 nmol L<sup>-1</sup>), or Fe (0.90, 1.79 nmol L<sup>-1</sup>) were added and samples were equilibrated overnight. Unamended samples were also incubated similarly and measured as blanks. In some experiments, Mn(III)-acetate in Ethanol (1, 2 nmol L<sup>-1</sup>) or Mn(III)-Desferioxamine B (Mn(III)DEF-B) (1, 2 nmol L<sup>-1</sup> or 1, 2  $\mu$ mol L<sup>-1</sup>) was added to the aliquot directly before the measurement as described in Wuttig *et al.* (subm., 2013b). The sampling and experimental set up is shown in Fig. 4.4. The next morning 10 mL of the prepared seawater aliquots were pipetted accurately into 60 mL PTFE bottles. The O<sub>2</sub><sup>-</sup> source was added either (1) 20  $\mu$ L of KO<sub>2</sub> directly when the measurement was started or (2) 20  $\mu$ L of the thermal source bis(4-carboxybenzyl)hyponitrite (SOTS) in dimethyl sulfoxide (DMSO) was added to all the aliquots at the same time and they were measured repetitively. SOTS decays exponentially at constant temperature allowing determination of the O<sub>2</sub><sup>-</sup> production rate (Heller and Croot, 2010a). O<sub>2</sub><sup>-</sup> was

measured by chemiluminescence of the Cypridina luciferin analog, 2-methyl-6-(p-methoxyphenyl)-3,7-dihydroimidazol[1,2- $\alpha$ ]pyrazin-3-one (MCLA) (Heller and Croot, 2010a).

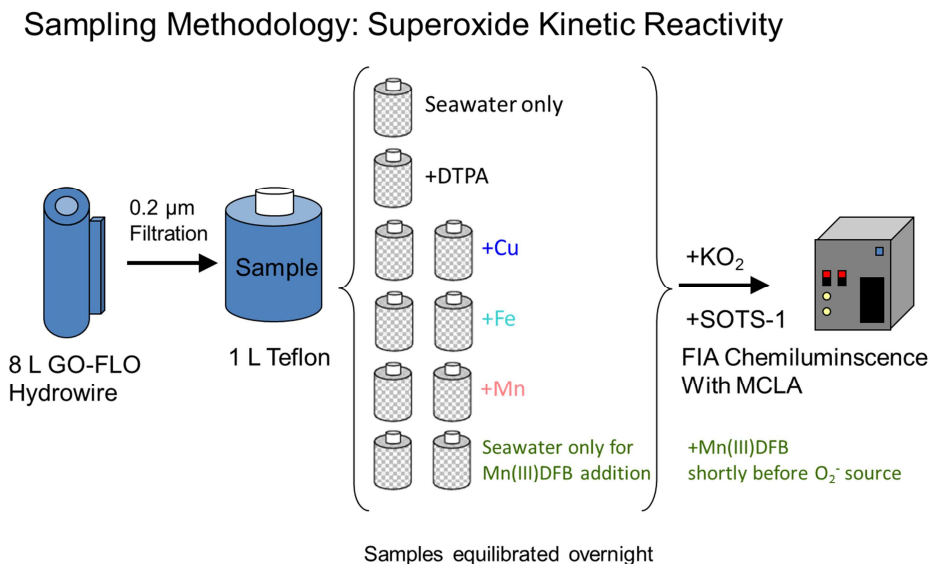


**Fig. 4.4:** The sampling methodology is shown with samples from the GoFlo-bottles filtered into 1 L Teflon bottles and the split up into 60 mL aliquots in Teflon bottles and spikes with different metals or DTPA and equilibrated over night. Directly before starting the measurement, the short-lived Mn(III)DFB was added to the corresponding aliquot. To every aliquot a superoxide source was added when the measurement was started.

The procedures were adapted according to earlier work (Heller and Croot, 2010a; Heller and Croot, 2010b; Heller and Croot, 2010c; Heller and Croot, 2011). Decay rates were similarly assessed using earlier procedures (Heller and Croot, 2010c; Heller and Croot, 2011). We applied the same terminology for the measured decay rates for  $O_2^-$  as used in previous works:  $k_{SW}$  ( $s^{-1}$ ) reaction in unamended seawater,  $k_{DTPA}$  ( $s^{-1}$ ) reaction in seawater with DTPA,  $k_M$  ( $M^{-1} s^{-1}$ ) metal (Cu, Fe and Mn) reaction rate constant in seawater calculated from regression analysis of the observed first order decay rates,  $k_{obs}$  ( $s^{-1}$ ), from the metal addition experiments. The rate of reaction with organic matter is assumed to be equal to the reaction in the presence of DTPA,  $k_{org} = k_{DTPA}$ . The calculation of  $O_2^-$  decay rate ( $k_{SW}$ ) in seawater from analysis is explained in detail in the manuscripts 1 and 2 (Wuttig *et al.*, *subm.*, 2013a; Wuttig *et al.*, *subm.*, 2013b).





**5**

# **M**ANUSCRIPTS





# MANUSCRIPT 1

Pathways of Superoxide ( $O_2^-$ )  
decay in the Eastern Tropical North  
Atlantic



# Pathways of Superoxide ( $O_2^-$ ) decay in the Eastern Tropical North Atlantic

Kathrin Wuttig<sup>1</sup>, Maija I Heller<sup>1,2</sup>, Peter L Croot<sup>1,3,\*</sup>

<sup>1</sup>GEOMAR Helmholtz Centre for Ocean Research Kiel, Marine Biogeochemistry, Düsternbrooker Weg 20, 24105 Kiel, Germany.

<sup>2</sup>University of Southern California, Department of Biological Sciences, Marine Environmental Biology, Los Angeles, United States of America.

<sup>3</sup>Earth and Ocean Sciences, School of Natural Sciences, National University of Ireland, Galway (NUIG), Galway, Ireland.

\*Corresponding Author

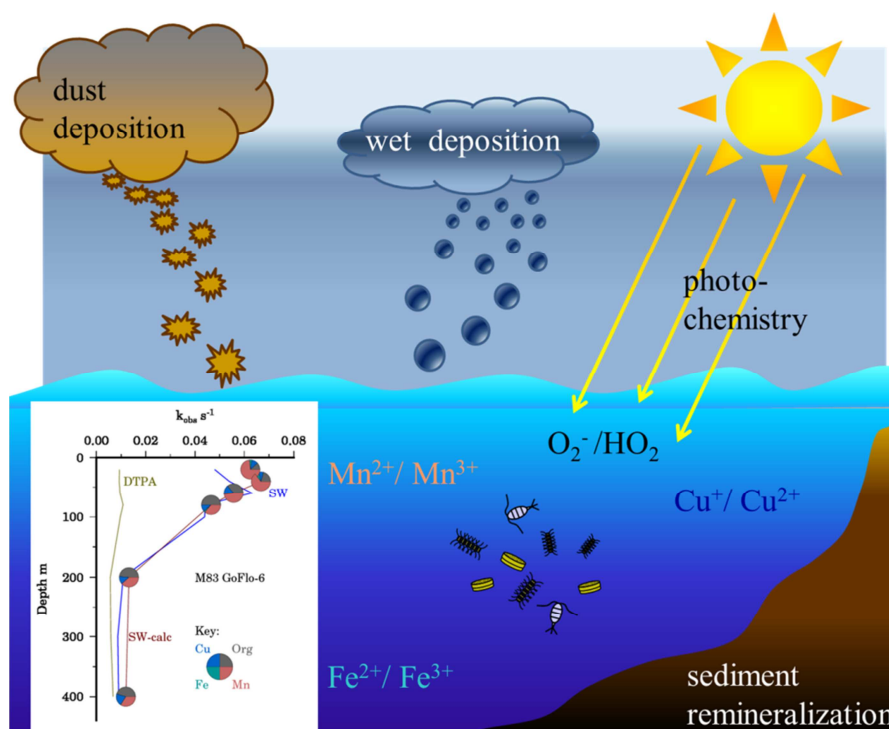
Draft only – do not cite unless prior permission from the authors.

Manuscript submitted to *Environmental Science and Technology*

This version 16 April 2013

## ABSTRACT

Superoxide ( $O_2^-$ : IUPAC name dioxide ( $\bullet 1^-$ )) is an important transient reactive oxygen species (ROS) in the ocean formed as an intermediate in the redox transformation of oxygen ( $O_2$ ) into hydrogen peroxide ( $H_2O_2$ ) and vice versa. This highly reactive and very short-lived radical anion can be produced both via photochemical and biological processes in the ocean. In this paper we examine the decomposition rate of  $O_2^-$  throughout the water column, using new data collected in the Eastern Tropical North Atlantic (ETNA) Ocean. For this approach we applied a semi factorial experimental design, to identify and quantify the pathways of the major identified sinks in the ocean. In this work we occupied 6 stations, 2 on the West African continental shelf and 4 open ocean stations, including the CVOO time series site adjacent to Cape Verde. Our results indicate that in the surface ocean, impacted by Saharan aerosols and sediment resuspension, the main decay pathways for superoxide is via reactions with Mn(II) and organic matter.



**Abstract Figure:** Trace metal and reactive oxygen species cycling in the sunlit tropical waters of the Eastern Tropical North Atlantic showing the influence on each other. This influence can be photochemistry, dust depositions and sediment remineralization. In this depth profile on the left hand side the observed loss rate of  $O_2^-$ ,  $k_{obs}$ , at the GOFLO-Station 6 (open ocean) is shown. The reaction with organic matter,  $k_{org}$ , is assumed to be equal to the measured reaction when DTPA is added,  $k_{DTPA}$  (beige line).  $k_{SW}$  is the reaction measured in unamended seawater (blue line).  $k_{SW-calc}$  is the calculated reaction with seawater (red line). With the help of the pie-charts the contribution from Organic matter, Cu, Fe and Mn on  $k_{SW-calc}$  is shown as explained for Figure 2.

## 1. INTRODUCTION

The short lived superoxide ( $O_2^-$ ) radical is the intermediate reaction product in the formation of hydrogen peroxide ( $H_2O_2$ ) from oxygen ( $O_2$ ) and is an important species in its own right in the redox cycling of metal ions and organic matter in the ocean<sup>1-8</sup>. In the sunlit surface ocean  $O_2^-$  is predominantly produced via  $O_2$  reactions during the photo-oxidation of coloured dissolved organic matter (CDOM)<sup>9</sup>.  $O_2^-$  may also be produced in the water column via metabolic processes in phytoplankton and bacteria<sup>10-13</sup>. Other sources of  $O_2^-$  in seawater may be significant below the euphotic zone and these may include the oxidation of reduced thiols and hydroquinones/semi-quinones derived from lysis or breakage of bacteria and phytoplankton cells<sup>7, 8</sup>. There have been a few attempts to directly measure  $O_2^-$  production rates in open ocean seawater, with a single study published on photoproduction<sup>9</sup>. More recent work has examined non-photochemical production<sup>13-15</sup> utilizing the reaction between  $O_2^-$  and 2-methyl-6-(p-methoxyphenyl)-3,7-dihydroimidazol[1,2- $\alpha$ ]pyrazin-3-one (MCLA) to produce chemiluminescence<sup>16</sup>.

For some metals, redox pairs exist (e.g. Cu(II)/Cu(I), Fe(II)/Fe(III) and Mn(II)/Mn(III)), where both species react rapidly with  $O_2^-$  leading to a catalytic cycle for superoxide decay<sup>2, 5, 6</sup>. These metals form the redox centre for enzymes such as catalases, peroxidases and superoxide dismutases (SODs) that are present in organisms to catalyse the dismutation of  $O_2^-$  and protect the cell from damage.

Previous work on  $O_2^-$  reactivity in filtered seawater has shown that reactions with organically complexed copper (Cu) are the dominant decay pathway<sup>2, 6</sup>. Hence reactions of iron (Fe) with  $O_2^-$  appear to be a smaller sink for  $O_2^-$ <sup>6, 17</sup> but may be significant for the formation of Fe(II) in seawater<sup>18, 19</sup> by reduction of inorganic or organically complexed Fe. More recently Mn was identified as a potential sink for  $O_2^-$  in surface waters<sup>5</sup>. CDOM may also be a significant sink for  $O_2^-$  in natural waters<sup>8, 20</sup>. A schematic summarizing the different pathways for superoxide decay is shown in Figure S1.

The aim of the present work was to determine and quantify the pathways of  $O_2^-$  decay in the upper water column of the Eastern Tropical North Atlantic (ETNA). We examine here the role of natural organic matter and the complexes of Cu, Fe, and manganese (Mn) in open ocean seawater to act as sinks for  $O_2^-$  by relating the decay rate of  $O_2^-$  to the metal concentrations and speciation. In the present work the concentration of  $O_2^-$  in the experimental treatments was followed by a chemiluminescence technique using MCLA after additions of potassium superoxide ( $KO_2$ ) as described previously<sup>6-8, 17</sup>.

## 2. EXPERIMENTAL SECTION

Complete descriptions of the experimental methods can be found in the supplementary information (SI) accompanying this manuscript.

### Materials and Chemicals:

Due to the low concentrations of the trace metals present in seawater, all laboratory work was performed in a trace metal clean chemistry laboratory under ISO Class 5 conditions. For shipboard work a specially designed containerized clean room (Clean Modules UK) belonging to the GEOMAR was employed.

The reagents were prepared as for our earlier works on  $O_2^-$  reactivity in seawater, a complete description is provided in the SI accompanying this manuscript. All chemicals that were used in this study were of ultrapure grade unless noted. Ultrapure (UP) water (resistivity  $>18.2 \text{ M}\Omega \text{ cm}^{-1}$ ) was obtained in the laboratory and in the ship going clean container via a Millipore Synergy 185 system that was fed by an Elix-3 (Millipore) reverse osmosis system connected to the mains supply. All plasticware and bottles (low density high polyethylene (LDPE) and Polytetrafluoroethylene (PTFE)) were extensively cleaned according to the GEOTRACES trace metal clean protocols<sup>21</sup>.

**Field Sample collection.** Seawater samples were collected at 6 GoFlo-Stations occupied during the Meteor M83/1 expedition in the ETNA (Table S1 and Figure S2).

### Procedure to Determine Superoxide reactivity in Seawater:

An aliquot of 60 mL of clean seawater was transferred directly into a PTFE bottle. This aliquot was either left unamended or diethylenetriaminepentaacetic acid (DTPA), Cu (0.79, 1.58 nM), Mn (1.00, 2.00 nM), or Fe (0.90, 1.79 nM) was added and equilibrated overnight. The next morning 10 mL of the prepared seawater aliquots were pipetted accurately into 60 mL PTFE bottles. 20  $\mu\text{L}$  of  $KO_2$  were added directly when the measurement was started. The procedures were adapted accordingly to our earlier work<sup>6-8, 17</sup>. Decay rates (Table S4) were similarly assessed using our earlier procedures<sup>6, 17</sup>. In this work we use the same terminology for the measured decay rates for  $O_2^-$  as used in our previous works:  $k_{\text{SW}}$  ( $\text{s}^{-1}$ ) reaction in unamended seawater,  $k_{\text{DTPA}}$  ( $\text{s}^{-1}$ ) reaction in seawater with DTPA,  $k_{\text{M}}$  ( $\text{M}^{-1} \text{s}^{-1}$ ) metal (Cu, Fe and Mn) reaction rate constant in seawater calculated from regression analysis of the observed first order decay rates,  $k_{\text{obs}}$  ( $\text{s}^{-1}$ ), from the metal addition experiments. The rate of reaction with organic matter is assumed to be equal to the reaction in the presence of DTPA,  $k_{\text{org}} = k_{\text{DTPA}}$ .

### Calculation of superoxide decay rate $k_{sw}$ in seawater from analysis:

The measured values of the decay rate  $k_{obs}$  from each experiment were combined using the following formula including all the experimental parameters:

$$k_{obs} = k_{org} + k_{Cu}[Cu] + k_{Fe}[Fe] + k_{Mn}[Mn] \quad (\text{Equation 1})$$

- (1) There are a number of assumptions inherent in this approach:
- (2) That the response of the system is simply a linear combination of the organic and metal species involved. That there are no synergistic effects (e.g. Cu(I) reduces Fe(III)).
- (3) That all the metal species are made inert by complexation with DTPA.
- (4) That the self-dismutation reaction can be ignored.
- (5) That there are no other species involved in the dismutation of  $O_2^-$  in seawater.
- (6) That the value of the metal reaction rate with  $O_2^-$ ,  $k_M$ , represents a catalytic reaction where the metal is cycled between the reduced and oxidized states via reaction with  $O_2^-$  such that the overall reaction rate is  $k_M = 2k_{red}k_{ox}/(k_{red}+k_{ox})$ , where  $k_{red}$  is the reaction rate of the reduced species with  $O_2^-$  and  $k_{ox}$  is the reaction rate of the oxidized species with  $O_2^-$ .

Equation 1 was solved by combining the data from the 8 independent experiments, the measured dissolved metal concentrations and solved for the 4 unknowns using the least squares multiple regression analysis tool in Excel<sup>TM</sup>. Individual metal addition experiments were also solved using single factor regression analysis as previously made. Figure 1 shows the 4 possible cases considered for the decay of  $O_2^-$  in seawater for the metal addition experiments.

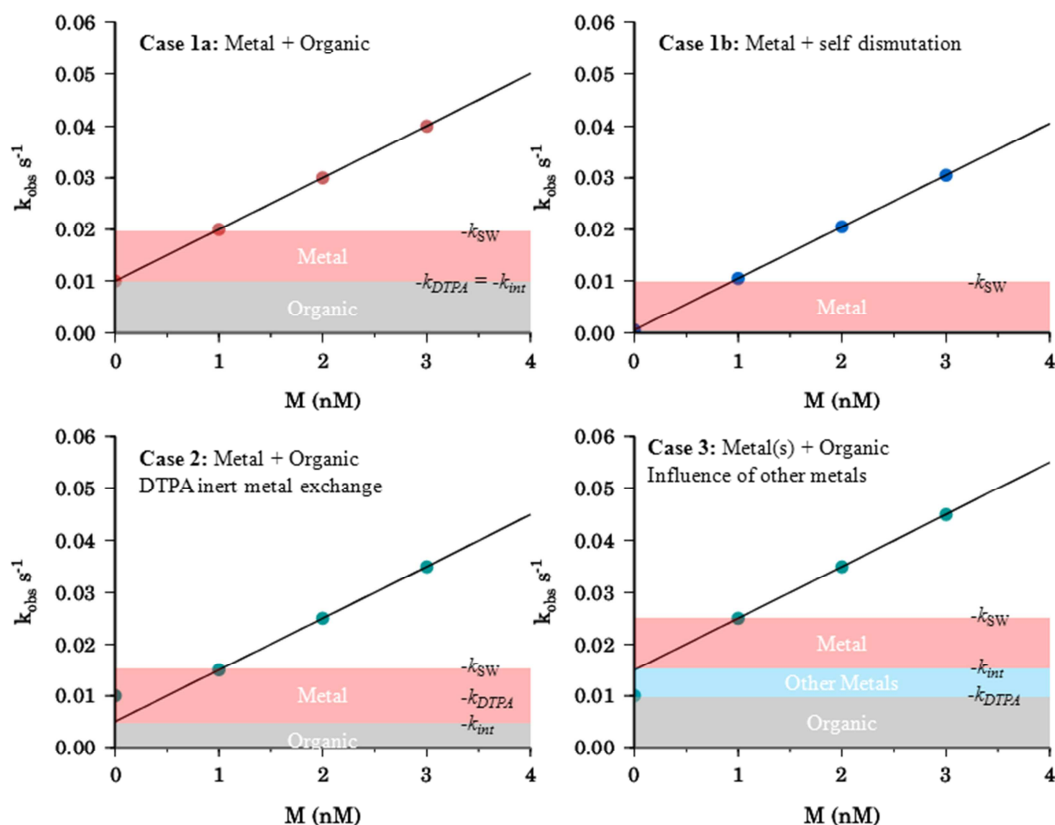


Figure 1: 4 different cases of the catalysed disproportionation of  $\text{O}_2^-$  in seawater.

All four cases are shown in the same way: the observed  $\text{O}_2^-$  loss rate in the presence of DTPA ( $k_{\text{DTPA}}$ ) is assumed to be at zero concentration, the observed rate in unamended seawater,  $k_{\text{SW}}$ , at its natural metal concentrations (measured by graphite furnace atomic absorption (ETAAS)) and seawater with two increasing metal ( $M$ ) additions (nM). Case 1a represents a scenario when there is a linear response for the metal additions and the intercept,  $k_{\text{int}}$ , is equivalent to  $k_{\text{DTPA}}$  indicating that the reaction in seawater can be described solely by a single metal and the organic reaction ( $k_{\text{org}}$ ). Case 1b is a special case related to case 1a in which there is no apparent organic reaction ( $k_{\text{org}} = 0$ ) and the self-dismutation reaction becomes significant. A further possibility is Case 2, where the intercept of the individual metal additions results in a value below  $k_{\text{DTPA}}$ , this represents a situation where some of the metal is inert to exchange with DTPA. The final possible scenario (Case 3) considered is where multiple metals contribute to the signal and the intercept for the single metal titration lies above the value for  $k_{\text{DTPA}}$ . Based on our previous work in the Southern Ocean we expected that most of our data would fit Case 3.



### 3. RESULTS

The locations of the Go-Flo sampling stations in the ETNA are shown in Figure S2 and listed in Table S1. In this paper we will focus on 3 stations: station 3 on the Mauritanian shelf and stations 4 and 6 in the open ocean. Stations 3 and 6 are located in upwelling zones, on the Mauritanian shelf and the equator respectively. For a full description of the study sites the reviewer is referred to other recent works on this region<sup>22, 23</sup>. There were distinct differences in the phytoplankton communities between the upwelling zones with the picoplankton *Prochlorococcus* dominating the biomass (~80 % of total chlorophyll *a* in the upper 60 m) at station 6, while it was almost completely absent at station 3 on the Mauritanian shelf which had high concentrations of diatoms and haptophytes in the mixed layer (Taxonomic chlorophyll data courtesy of Jasmin Franz, GEOMAR). Station 4 also had high concentrations of *Prochlorococcus* present throughout the euphotic zone (~60 % of total chlorophyll *a* in upper 60 m) and a distinct chlorophyll maximum was found at 50 m. The cyanobacterium *Synechococcus* was present in the upper part of the water column at station 3 but was found only in low concentrations at stations 4 and 6.

The dissolved metal concentrations (Table S2) were similar to concentrations and distributions observed in the ETNA previously<sup>24-26</sup>. Cu increased monotonically with depth at most stations and concentrations ranged from 0.5 to 1 nM with the highest values found at station 3 near the Mauritanian shelf. Fe concentrations increased with depth throughout the water column at all stations though at stations 4 and 6 the profiles showed a distinct minimum in the vicinity of the chlorophyll maximum. Highest concentrations of Fe were found in the bottom waters at station 3, consistent with the input of resuspended sediment at that location as has been observed recently for particulate Fe along this shelf region<sup>27</sup>. Dissolved Mn concentrations were elevated in the mixed layer of the ETNA with maxima of 2 – 3 nM due to atmospheric Saharan dust inputs and upwelling as has been observed previously<sup>25</sup>. For open ocean stations Mn decreased rapidly in the euphotic zone to deep values of 0.3 nM as found in earlier studies<sup>26</sup>.

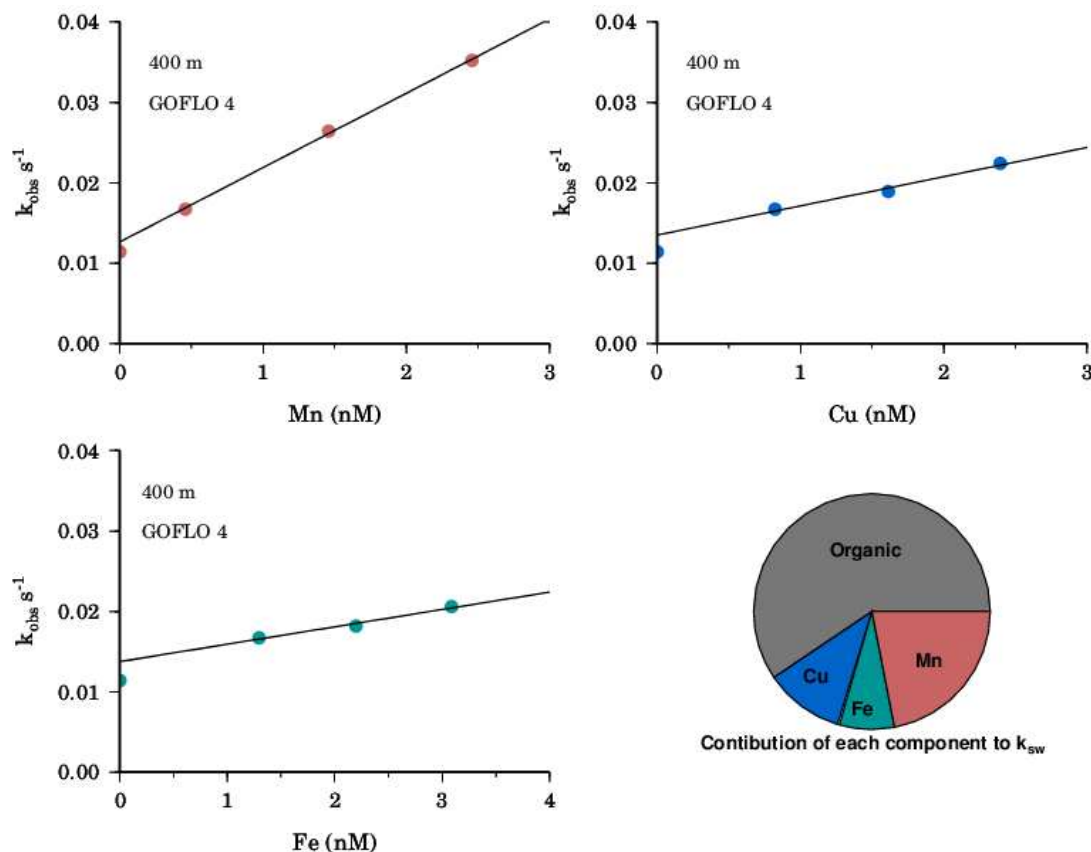


Figure 2: Example of the contribution of the organic matter (grey) and the three trace metals to  $k_{sw}$  with data from GOFLO-Station4, 400m (Pie-Chart). The contribution of Mn (red), Cu (blue) and Fe (green) is assessed via titration which is shown separately as x-y-plots for each metal.

Figure 2 shows an example of data from 400 m at station 4 of the individual metal additions and the resulting estimation, by multiple regression displayed as a pie chart of the contribution of organic matter and Fe, Cu and Mn towards the decay rate of  $O_2^-$ . In this example it can be seen that all 3 metals contribute to the loss, but Mn to a greater extent than Fe and Cu and this example is analogous to Case 3 as shown in Figure 1. In general, most data could be described by Case 3, suggesting more than one metal played a role in the decay of  $O_2^-$ . For some samples from surface waters with high Mn concentrations the data could not be statistically distinguished from Case 1. We observed a few examples of Case 2 data that were statistically significant (i.e.  $k_{int} < k_{DTPA}$ ) for Mn in the upper water 100 m at station 3 on the Mauritanian shelf and in the open ocean at station 4 at 60 m. In general the Mn additions were almost always linear in line with the lack of apparent organic complexation<sup>28</sup> (i.e. no complexation) while the Fe and Cu are almost always complexed and therefore the additions may not always be linear and easy to interpret. The full dataset for this work is found in Tables S3.

In Figure 3-5 it is demonstrated that at each depth of the GoFlo-Stations 3, 4 and 6 the contributors to the decay of  $O_2^-$  and therefore their slices of the pie vary depending on depth and location.

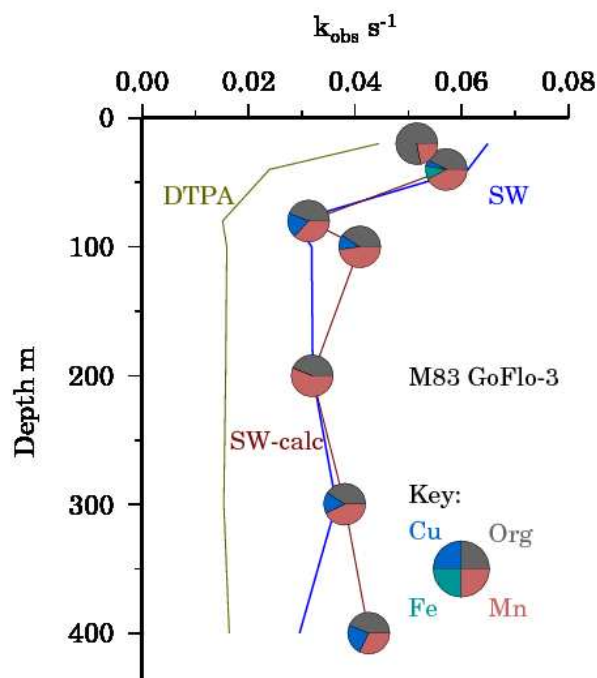


Figure 3: In this depth profile of observed loss rate of  $O_2^-$ ,  $k_{obs}$ , at the GOFLO-Station 3. The reaction with organic matter,  $k_{org}$ , is assumed to be equal to the measured reaction when DTPA is added,  $k_{DTPA}$  (beige line).  $k_{SW}$  is the reaction measured in unamended seawater (blue line).  $k_{SW-calc}$  is the calculated reaction with seawater (red line). With the help of the pie-charts the contribution from Organic matter, Cu, Fe and Mn on  $k_{SW-calc}$  is shown as explained for Figure 2.

The calculated (red) rates,  $k_{SW-calc}$ , coincide well with the measured rate,  $k_{SW}$  (blue). In the open ocean Mn clearly dominates the reaction in the euphotic zone (Figures 4 and 5) in contrast to the shelf (GoFlo-Station 3) where organic material is the main contributor throughout the whole water column, but most pronounced in the surface, where also high rates for  $k_{DTPA}$  were observed. At the offshore stations the  $k_{DTPA}$  rates varied little with depth, indicating a relatively constant contribution from organic matter to the decomposition of  $O_2^-$ .

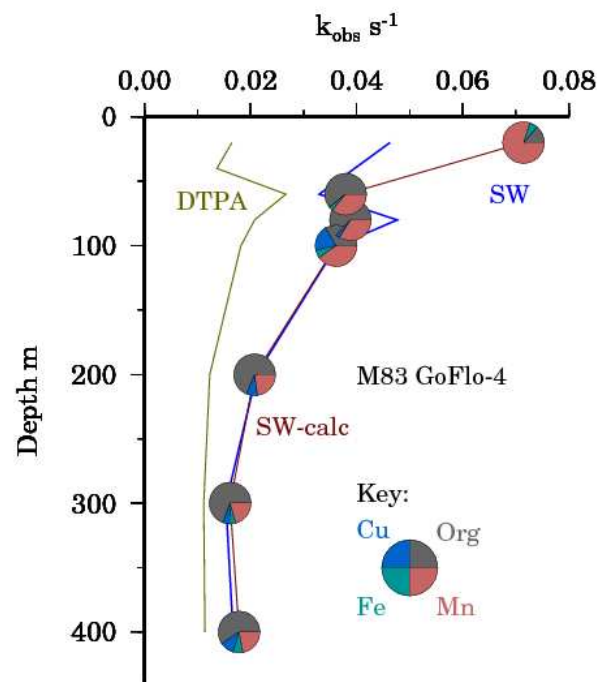


Figure 4. Contribution from Organic matter, Cu, Fe and Mn at GOFLO-Station 4 and plotted in the same way as Figure 3.

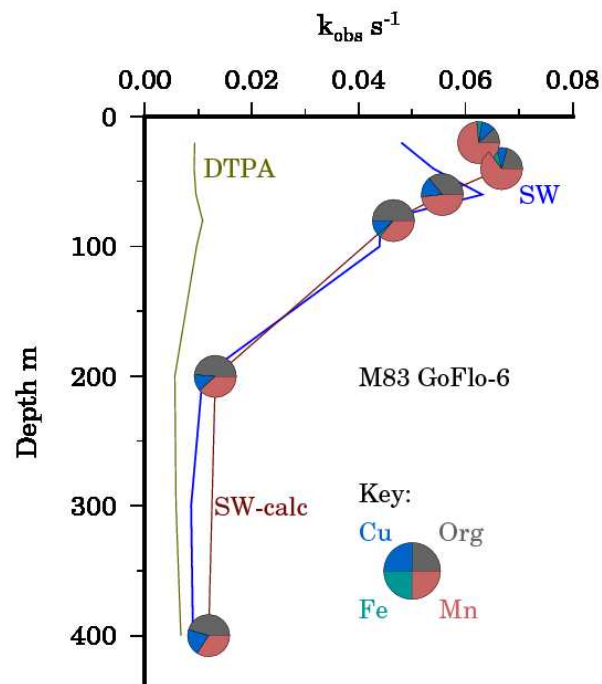


Figure 5. Contribution from Organic matter, Cu, Fe and Mn at GOFLO-Station 6 and plotted in the same way as Figure 3.

## 4. DISCUSSION

### **O<sub>2</sub><sup>-</sup> reactions with Cu and Fe**

In our previous work in the Southern Ocean<sup>6</sup> and in the Tropical Atlantic near Cape Verde<sup>17</sup> we had observed that Cu was a major pathway for O<sub>2</sub><sup>-</sup> decomposition. In the present work we find that the Cu pathway in the ETNA was somewhat reduced in comparison with lower values of  $k_{\text{Cu}}$  than observed previously (Table S5). A possible explanation for these results is differences in Cu complexation in these waters, as it has been shown that strong Cu binding ligands are produced by both *Synechococcus* and *Prochlorococcus*<sup>29</sup> and appear to be mostly effluxed from the cell in response to Cu stress<sup>30</sup>. Other eukaryotic phytoplankton also produce Cu binding ligands in response to Cu stress but these ligands are typically weaker Cu complexing agents<sup>31</sup>. The reactivity of O<sub>2</sub><sup>-</sup> with the Cu in the Cu complexes produced by *Synechococcus* in culture has been determined,  $k_{\text{Cu}} = 5 \pm 3 \times 10^7 \text{ M}^{-1} \text{ s}^{-1}$ <sup>2</sup>. There are no reported values for  $k_{\text{Cu}}$  for Cu binding ligands produced by other phytoplankton species. Throughout our study, *Prochlorococcus* was the dominant phytoplankton, thus one possible explanation is that the Cu complex produced by *Prochlorococcus* reacts more slowly with O<sub>2</sub><sup>-</sup>, though this remains to be proved.

In this study the O<sub>2</sub><sup>-</sup> decay pathway with Fe was a minor component throughout the study area in agreement with our previous work in the ETNA close to Cape Verde<sup>17</sup> and in the Southern Ocean<sup>6</sup>. It appears that much of the Fe present is relatively inert to reaction with O<sub>2</sub><sup>-</sup> and may exist as soluble or colloidal organic complexes<sup>17,32</sup>. Recent work suggests that the slow kinetics of exchange of Fe in thermodynamically weak Fe binding ligands helps to maintain soluble Fe in this region<sup>33</sup>.

It is now apparent that the O<sub>2</sub><sup>-</sup> reactivity of a complex is not simply related to the conditional or thermodynamic binding strength of the complex. For example the Cu complex of 1,4,8,11-Tetraazacyclotetradecane (Cyclam) ( $\log K_{\text{Cu}} = 27.2$ ) is thermodynamically strong and essentially inert to exchange in seawater<sup>34</sup>, but SOD active, because it has free sites for water exchange<sup>35</sup>. Measurement of the rate of exchange of fluoride (<sup>19</sup>F) with SODs has shown strong correlations with their O<sub>2</sub><sup>-</sup> reaction rates<sup>36,37</sup>. These findings have been suggested as evidence for an inner sphere second-order mechanism where ligand exchange is the rate limiting step and the dissociation of the complex is not required<sup>38</sup>. Thus it is clear that specific data on the O<sub>2</sub><sup>-</sup> reactivity of Cu and Fe complexes produced in seawater by bacteria and phytoplankton are required to help interpret field data of this type.

### **Mn reactivity with O<sub>2</sub><sup>-</sup> in seawater**

Mn speciation in seawater contrasts with that of Fe and Cu as there is no apparent organic complexation<sup>28</sup> and it exists mainly as the free aquo ion, MnCl<sup>+</sup> and to a smaller extent as

sulphate and carbonate complexes<sup>39</sup>. Mn is similar to Fe in that the higher oxidation states are poorly soluble, however there is no strong evidence for organic forms of Mn(III) or Mn(IV). The abiotic oxidation of Mn(II) by O<sub>2</sub> is slow<sup>40, 41</sup> but the rate is enhanced on particle surfaces<sup>40, 42</sup> and via microbial processes<sup>43</sup>. Assuming no organic complexation of Mn(II), it would be inferred that  $k_{\text{Mn}}$  would not vary with depth as there are only minor changes in pH, chloride or carbonate concentrations. This is indeed what we observed (Table S4) with no significant variation in  $k_{\text{Mn}}$  apparent with depth and a mean value of  $\log k_{\text{Mn}} = 7.29 \pm 0.26$  ( $n = 35$ ). For more details on the proposed mechanism for the Mn reactions with O<sub>2</sub><sup>-</sup> in seawater the reader is referred to the companion paper to this work<sup>44</sup>.

### **O<sub>2</sub><sup>-</sup> loss rates in the presence of DTPA: organic or non-exchangeable SODs**

At stations in regions of high primary productivity (Stations 2, 3 and 6) elevated values for  $k_{\text{DTPA}}$  were found in the euphotic zone and may represent increases in fresh reactive organic matter produced by phytoplankton exudation or zooplankton grazing. However measurements of bulk CDOM absorbance and fluorescence showed no direct correlation between  $k_{\text{DTPA}}$  and CDOM as seen previously in oligotrophic waters at CVOO<sup>8</sup>. In that work, quinones were identified as the most likely functional group to explain the vertical distribution of  $k_{\text{DTPA}}$ . In the following we explore the possibility that  $k_{\text{DTPA}}$  includes inert metal complexes that can act as SODs.

SODs catalyse the dismutation reaction of O<sub>2</sub><sup>-</sup> radicals to H<sub>2</sub>O<sub>2</sub> and O<sub>2</sub>. These different metalloproteins are grouped by their central redox-active metal cofactor into three major families: Cu/Zn-, Mn- or Fe-SOD (specific for either or, or some can use both = cambialistic) and Ni-SOD<sup>45</sup>. SODs fulfil an important role as a primary defence mechanism against oxidative stress and are found in most cells in the cytosol, chloroplasts and mitochondria depending on the type of SOD. A review of SOD usage by algae<sup>46</sup> indicated that Fe-SODs are prevalent in Archaea, which include some cambialistic SODs. The Mn-SOD gene, *sodA*, is more widely distributed in the bacteria and eukaryote in particular some marine diatoms<sup>47</sup>. Cu/Zn-SODs appear to be mostly absent in eukaryotic algae<sup>48</sup> but are found in the periplasm of  $\alpha$ ,  $\beta$ , and  $\gamma$  proteobacteria<sup>46</sup>. In the marine environment, recent work has shown that Ni-SODs are the sole SOD found in the cyanobacteria *Prochlorococcus* and in some open ocean *Synechococcus* species<sup>49</sup>.

Extracellular SODs are known to be produced by higher organisms in the terrestrial environment<sup>50</sup> but there is no data on marine organisms. There is however evidence for the presence of dissolved catalase or peroxidase in seawater, as experiments with filtered seawater (0.4  $\mu\text{m}$ ) indicate a continual loss of H<sub>2</sub>O<sub>2</sub> in the dark<sup>15</sup>. Ultrafiltration experiments suggest that the decomposition of H<sub>2</sub>O<sub>2</sub> is predominantly by colloidal species

(1 kDa < x < 0.4  $\mu$ m)<sup>51</sup>; thus specific SODs from bacteria and phytoplankton may be present in the dissolved phase through direct excretion, zooplankton grazing or viral lysis.

The question then arises, can natural SODs contribute to the high values for  $k_{\text{DTPA}}$  found in the euphotic zone (Figures 3-5), and can they exchange their metal content with DTPA? Unfortunately there is very little data about the binding strength of the metal centres in SODs. It is common practice in biological studies to add EDTA at a concentration of 0.1 mM immediately prior to experiments using Cu/Zn-SOD to bind extraneous Cu. It is reported that EDTA has no influence on the observed  $\text{O}_2^-$  decay rate<sup>52</sup>, though these experiments are too short to allow the Cu in the SOD to come into equilibrium with EDTA. Some data does exist for the Cu/Zn-SOD binding strength for bovine erythrocyte SOD  $\text{Cu}_2\text{Zn}_2\text{-SOD}^2$ , which contains two identical subunits. For Cu there was a strong pH dependence with  $\log K_1 = 15.6$  and  $\log K_2 = 14.1$  at pH 7 (0.2 M phosphate buffer) and the solutions took several days to come into equilibrium with 2-pyridinecarboxylate<sup>53</sup>. A further study examining the inhibition of human erythrocyte Cu/Zn found that DTPA and EDTA were able to strongly inhibit this SOD and suggested a chelator with a  $\log K_1$  between 12.6 and 13.8 is required to remove Cu from the enzyme<sup>54</sup>. We could find no relevant data on the binding strength of Mn- or Fe-SODs. There have been a few studies on the use of EDTA to remove metals from organic ligands in seawater. EDTA was used in combination with XAD-2 resin<sup>55</sup> or electro dialysis<sup>56</sup> to determine the binding strength of natural Cu and Zn complexes in seawater. Kinetic experiments indicated that equilibrium was achieved in less than 24 hours under the experimental conditions employed, though it is not clear if 100 % recovery was achieved<sup>55,56</sup>. In our work, Case 2 above would result from incomplete exchange with DTPA, and we only observed this in the specific case of Mn and this could suggest the existence of Mn-SODs in the dissolved phase. Thus it appears that DTPA removes the bulk of metals from the natural organic complexes but further work is required to verify this for SODs from the marine environment.

### **Involvement of other metals as SODS in solution**

Ni-SODs are present in *Synechococcus* and *Prochlorococcus*<sup>49</sup>, the predominant picoplankton found in the ETNA<sup>22</sup>. Thus there is the possibility that Ni-SODs may be released to the dissolved phase via grazing or viral lysis, the stability of extracellular Ni-SODs in seawater is not known at present however. During M83/1 dissolved Nickel (Ni) concentrations ranged from 2 to 6 nM (Table S3) in the water column. The only study published on Ni speciation in the open ocean suggests that only 10 - 20 % of the dissolved Ni is present as strong organic complexes, with the rest present as weak organic or inorganic species<sup>57</sup>. Thus potentially 0.2 to 1.2 nM of Ni may have been present as Ni organic complexes some of which may have been Ni-SODs or other extracellular Ni enzymes or

transport ligands<sup>58</sup>. However the slow exchange kinetics of Ni<sup>59</sup> makes it difficult to determine the true degree of organic complexation in seawater as most approaches measuring its speciation are most likely of shorter duration than that required to reach equilibrium. In relation to the present work, as the inorganic form of Ni(II) is apparently in excess in seawater and by itself it does not react rapidly with  $O_2^-$ , it would be expected that metal addition experiments with inorganic Ni(II) would not influence  $k_{SW}$ . Thus the question of whether Ni-SODs are present in solution is still open and further work on this is needed.

Cobalt (Co) when incorporated into Vitamin B<sub>12</sub> - cob(II)alamin – has been identified as a functional SOD<sup>60</sup> however dissolved cobalt (all forms) is only present at 40 to 100 pM in the Atlantic Ocean<sup>61</sup>. If all the Co were B<sub>12</sub> it would only be a minor contributor to  $k_{SW}$  ( $k_{Co} = 10^7 \text{ M}^{-1} \text{ s}^{-1} \times 10^{-10} \text{ M} = 10^{-3} \text{ s}^{-1}$ ). Most other trace metals lack a suitable redox pair for reaction with  $O_2^-$  (e.g. Cd and Zn) or their reactivity (e.g. Mo and V) with  $O_2^-$  is sluggish<sup>62</sup>.

The present work strongly indicates that reaction with dissolved Mn(II) can be a significant pathway for  $O_2^-$  decay in the surface ocean of regions impacted by terrestrial runoff or atmospheric deposition.



## ACKNOWLEDGMENTS

The officers and crew of the research vessel Meteor are gratefully acknowledged for their help in performing sampling at sea. This work was supported by the efforts of Peter Streu, Mirja Dunker and Dörte Nitschkowski (all GEOMAR) in the laboratory in Kiel. Special thanks are due to Jasmin Franz (GEOMAR) for providing the HPLC data. This work is a contribution of the Collaborative Research Centre 754 "Climate - Biogeochemistry Interactions in the Tropical Ocean" ([www.sfb754.de](http://www.sfb754.de)), which is supported by the Deutsche Forschungsgemeinschaft (DFG). K. W.'s participation was financially supported by a grant, awarded to P. L. C., from the DFG (CR145/17-1). Financial support for M. I. H. was provided by the BMBF Verbundprojekt SOPRAN2 (IG03) and this forms part of the German contribution to SOLAS (Surface Ocean Lower Atmosphere Studies).

### Supporting Information Available

Full details of Station Locations and the experimental setup and related analysis methods are supplied as supplementary information. The cruise track and stations locations (Figure S2), experimental set up and design (Figure S4) are also provided. An example of the signal data from the FeLume was shown in Heller and Croot, 2010c<sup>63</sup>. This information is available free of charge via the Internet at <http://pubs.acs.org>.

## REFERENCES

1. Voelker, B. M.; Sedlak, D. L., Iron reduction by photoproduct superoxide in seawater. *Marine Chemistry* **1995**, *50*, 93-102.
2. Voelker, B. M.; Sedlak, D. L.; Zafiriou, O. C., Chemistry of Superoxide Radical in Seawater: Reactions with Organic Cu Complexes. *Environmental Science and Technology* **2000**, *34*, 1036-1042.
3. Zafiriou, O. C.; Voelker, B. M.; Sedlak, D. L., Chemistry of the superoxide radical ( $O_2^-$ ) in seawater: Reactions with inorganic copper complexes. *Journal of Physical Chemistry A* **1998**, *102*, (28), 5693-5700.
4. Rose, A. L.; Waite, D., Role of superoxide in the photochemical reduction of iron in seawater. *Geochimica Et Cosmochimica Acta* **2006**, *70*, (15), 3869-3882.
5. Hansard, S. P.; Easter, H. D.; Voelker, B. M., Rapid Reaction of Nanomolar Mn(II) with Superoxide Radical in Seawater and Simulated Freshwater. *Environmental Science & Technology* **2011**, *45*, (7), 2811-2817.
6. Heller, M. I.; Croot, P. L., Superoxide Decay Kinetics in the Southern Ocean. *Environmental Science & Technology* **2010**, *44*, (1), 191-196 DOI: 10.1021/es901766r.
7. Heller, M. I.; Croot, P. L., Application of a Superoxide ( $O_2^-$ ) thermal source (SOTS-1) for the determination and calibration of  $O_2^-$  fluxes in seawater. *Analytica Chimica Acta* **2010**, *667*, 1-13.
8. Heller, M. I.; Croot, P. L., Kinetics of superoxide reactions with dissolved organic matter in tropical Atlantic surface waters near Cape Verde (TENATSO). *J. Geophys. Res.* **2010**, *115*, (C12), C12038.

9. Micinski, E.; Ball, L. A.; Zafiriou, O. C., Photochemical Oxygen Activation - Superoxide Radical Detection and Production-Rates in the Eastern Caribbean. *J. Geophys. Res.-Oceans* **1993**, *98*, (C2), 2299-2306.
10. Marshall, J.-A.; Hovenden, M.; Oda, T.; Hallegraeff, G. M., Photosynthesis does influence superoxide production in the ichthyotoxic alga *Chattonella marina* (Raphidophyceae). *J. Plankton Res.* **2002**, *24*, (11), 1231-1236.
11. Kim, D.; Oda, T.; Ishimatsu, A.; Muramatsu, T., Galacturonic acid-induced Increase of Superoxide Production in Red Tide Phytoplankton *Chattonella marina* and *Heterosigma akashiwo*. *Biosci. Biotechnol. Biochem.* **2000**, *64*, 911-914.
12. Rose, A. L.; Godrant, A.; Furnas, M.; Waite, T. D., Dynamics of nonphotochemical superoxide production and decay in the Great Barrier Reef lagoon. *Limnol. Oceanogr.* **2010**, *55*, (4), 1521-1536.
13. Rose, A. L.; Webb, E. A.; Waite, T. D.; Moffett, J. W., Measurement and Implications of Nonphotochemically Generated Superoxide in the Equatorial Pacific Ocean. *Environ. Sci. Technol.* **2008**, *42*, (7), 2387-2393.
14. Hansard, S. P.; Vermilyea, A. W.; Voelker, B. M., Measurements of superoxide radical concentration and decay kinetics in the Gulf of Alaska. *Deep-Sea Res. Part I-Oceanogr. Res. Pap.* **2010**, *57*, (9), 1111-1119.
15. Vermilyea, A. W.; Hansard, S. P.; Voelker, B. M., Dark production of hydrogen peroxide in the Gulf of Alaska. *Limnol. Oceanogr.* **2010**, *55*, 580-588.
16. Nakano, M.; Sugioka, K.; Ushijima, Y.; Goto, T., Chemiluminescence probe with Cypridina luciferin analog, 2-methyl-6-phenyl-3,7-dihydroimidazo[1,2-a]pyrazin-3-one, for estimating the ability of human granulocytes to generate O<sub>2</sub>. *Analytical Biochemistry* **1986**, *159*, (2), 363-369.
17. Heller, M. I.; Croot, P. L., Superoxide decay as a probe for speciation changes during dust dissolution in Tropical Atlantic surface waters near Cape Verde. *Marine Chemistry* **2011**, *126*, (1-4), 37-55.
18. Croot, P. L.; Laan, P.; Nishioka, J.; Strass, V.; Cisewski, B.; Boye, M.; Timmermans, K.; Bellerby, R.; Goldson, L.; de Baar, H. J. W., Spatial and Temporal distribution of Fe(II) and H<sub>2</sub>O<sub>2</sub> during EISENEX, an open ocean mesoscale iron enrichment. *Marine Chemistry* **2005**, *95*, 65-88.
19. Fujii, M.; Ito, H.; Rose, A. L.; Waite, T. D.; Omura, T., Superoxide-mediated Fe(II) formation from organically complexed Fe(III) in coastal waters. *Geochimica Et Cosmochimica Acta* **2008**, *72*, (24), 6079-6089.
20. Goldstone, J. V.; Voelker, B. M., Chemistry of Superoxide Radical in Seawater: CDOM Associated Sink of Superoxide in Coastal Waters. *Environmental Science and Technology* **2000**, *34*, 1043-1048.
21. Cutter, G. A.; Andersson, P.; Codispoti, L.; Croot, P. L.; Francois, R.; Lohan, M.; Obata, H.; Rutgers van der Loeff, M. Sampling and Sample-handling Protocols for GEOTRACES Cruises. <http://www.geotraces.org/libraries/documents/Intercalibration/Cookbook.pdf>
22. Tarran, G. A.; Heywood, J. L.; Zubkov, M. V., Latitudinal changes in the standing stocks of nano- and picoeukaryotic phytoplankton in the Atlantic Ocean. *Deep Sea Research Part II: Topical Studies in Oceanography* **2006**, *53*, (14-16), 1516-1529.
23. Heller, M. I.; Gaiero, D.; Croot, P. L., Basin scale survey of marine humic fluorescence in the Atlantic: relationship to iron solubility. *Global Biogeochem. Cycles* **2012**, doi:10.1029/2012GB004427, in press. .
24. Croot, P. L.; Streu, P.; Baker, A. R., Short residence time for iron in surface seawater impacted by atmospheric dry deposition from Saharan dust events. *Geophysical Research Letters* **2004**, *31*, L23S08, doi:10.1029/2004GL020153.
25. Pohl, C.; Croot, P. L.; Hennings, U.; Daberkow, T.; Budeus, G.; Loeff, M. R. v. d., Synoptic transects on the distribution of trace elements (Hg, Pb, Cd, Cu, Ni, Zn, Co, Mn, Fe, and Al) in surface waters of the Northern- and Southern East Atlantic. *Journal of Marine Systems* **2011**, *84*, (1-2), 28-41.

26. Statham, P. J.; Yeats, P. A.; Landing, W. M., Manganese in the eastern Atlantic Ocean: processes influencing deep and surface water distributions. *Marine Chemistry* **1998**, *61*, (1-2), 55-68.
27. Lam, P. J.; Ohnemus, D. C.; Marcus, M. A., The speciation of marine particulate iron adjacent to active and passive continental margins. *Geochimica et Cosmochimica Acta* **2012**, *80*, (0), 108-124.
28. Sunda, W. G., Measurement of manganese, zinc and cadmium complexation in seawater using Chelex ion exchange equilibria. *Marine Chemistry* **1984**, *14*, (4), 365-378.
29. Moffett, J. W.; Brand, L. E., Production of strong, extracellular Cu chelators by marine cyanobacteria in response to Cu stress. *Limnol. Oceanogr.* **1996**, *41*, 388-395.
30. Croot, P. L.; Karlson, B.; van Elteren, J. T.; Kroon, J. J., Uptake and efflux of <sup>64</sup>Cu by the marine cyanobacterium *Synechococcus* (WH7803). *Limnol. Oceanogr.* **2003**, *48*, 179-188.
31. Croot, P. L.; Moffett, J. W.; Brand, L., Production of extracellular Cu complexing ligands by eucaryotic phytoplankton in response to Cu stress. *Limnol. Oceanogr.* **2000**, *45*, 619-627.
32. Fujii, M.; Rose, A. L.; Waite, T. D.; Omura, T., Superoxide-mediated dissolution of amorphous ferric oxyhydroxide in seawater. *Environmental Science & Technology* **2006**, *40*, (3), 880-887.
33. Croot, P. L.; Heller, M. I., The importance of kinetics and redox in the biogeochemical cycling of iron in the surface ocean. *Frontiers in Microbiology* **2012**, *3*.
34. Croot, P. L.; Moffett, J. W.; Luther, G. W., Polarographic determination of half-wave potentials for copper-organic complexes in seawater. *Marine Chemistry* **1999**, *67*, (3-4), 219-232.
35. Kimura, E.; Sakonaka, A.; Nakamoto, M., Superoxide dismutase activity of macrocyclic polyamine complexes. *Biochimica et Biophysica Acta (BBA) - General Subjects* **1981**, *678*, (2), 172-179.
36. Viglino, P.; Rigo, A.; Stevanato, R.; Ranieri, G. A.; Rotilio, G.; Calabrese, L., The binding of fluoride ion to bovine cuprozinc superoxide dismutase as studied by <sup>19</sup>F magnetic relaxation. *Journal of Magnetic Resonance (1969)* **1979**, *34*, (2), 265-274.
37. Summers, J. S.; Baker, J. B.; Meyerstein, D.; Mizrahi, A.; Zilbermann, I.; Cohen, H.; Wilson, C. M.; Jones, J. R., Measured Rates of Fluoride/Metal Association Correlate with Rates of Superoxide/Metal Reactions for FeIII(EDTA)(H<sub>2</sub>O)- and Related Complexes. *Journal of the American Chemical Society* **2008**, *130*, (5), 1727-1734.
38. Graf, E.; Mahoney, J. R.; Bryant, R. G.; Eaton, J. W., Iron-catalyzed hydroxyl radical formation. Stringent requirement for free iron coordination site. *J. Biol. Chem.* **1984**, *259*, (6), 3620-4.
39. Byrne, R. H., Seawater trace metal speciation. *Applied Geochemistry* **1988**, *3*, (1), 85.
40. Morgan, J. J., Kinetics of reaction between O<sub>2</sub> and Mn(II) species in aqueous solutions. *Geochim. Cosmochim. Acta* **2005**, *69*, (1), 35-48.
41. von Langen, P. J.; Johnson, K. S.; Coale, K. H.; Elrod, V. A., Oxidation kinetics of manganese (II) in seawater at nanomolar concentrations. *Geochimica Et Cosmochimica Acta* **1997**, *61*, (23), 4945-4954.
42. Yeats, P. A.; Strain, P. M., The oxidation of manganese in seawater: Rate constants based on field data. *Estuarine, Coastal and Shelf Science* **1990**, *31*, (1), 11-24.
43. Tebo, B. M.; Johnson, H. A.; McCarthy, J. K.; Templeton, A. S., Geomicrobiology of manganese(II) oxidation. *Trends in Microbiology* **2005**, *13*, (9), 421-428.
44. Wuttig, K.; Heller, M. I.; Croot, P. L., Reactivity of Mn(II/III)-Desferrioxamine B with O<sub>2</sub>, O<sub>2</sub><sup>-</sup> and H<sub>2</sub>O<sub>2</sub> in seawater. *submitted to Environmental Sciences and Technology* **2013**.
45. Miller, A.-F., Superoxide dismutases: active sites that save, but a protein that kills. *Current Opinion in Chemical Biology* **2004**, *8*, (2), 162-168.
46. Wolfe-Simon, F.; Grzebyk, D.; Schofield, O.; Falkowski, P. G., The role and evolution of superoxide dismutases in algae. *Journal Of Phycology* **2005**, *41*, (3), 453-465.

47. Wolfe-Simon, F.; Starovoytov, V.; Reinfelder, J. R.; Schofield, O.; Falkowski, P. G., Localization and role of manganese superoxide dismutase in a marine diatom. *Plant Physiology* **2006**, *142*, (4), 1701-1709.
48. Asada, K.; Kanematsu, S.; Uchida, K., Superoxide dismutases in photosynthetic organisms: Absence of the cuprozinc enzyme in eukaryotic algae. *Archives of Biochemistry and Biophysics* **1977**, *179*, (1), 243.
49. Dupont, C. L.; Neupane, K.; Shearer, J.; Palenik, B., Diversity, function and evolution of genes coding for putative Ni-containing superoxide dismutases. *Environmental Microbiology* **2008**, *10*, (7), 1831-1843.
50. Fridovich, I., Superoxide Radical And Superoxide Dismutases. *Annual Review Of Biochemistry* **1995**, *64*, 97-112.
51. Yuan, J.; Shiller, A. M., The distribution of hydrogen peroxide in the southern and central Atlantic ocean. *Deep-Sea Research II* **2001**, *48*, 2947-2970.
52. Goldstein, S.; Fridovich, I.; Czapski, G., Kinetic properties of Cu,Zn-superoxide dismutase as a function of metal content—Order restored. *Free Radical Biology and Medicine* **2006**, *41*, (6), 937-941.
53. Hirose, J.; Ohhira, T.; Hirata, H.; Kidani, Y., The pH dependence of apparent binding constants between apo-superoxide dismutase and cupric ions. *Archives of Biochemistry and Biophysics* **1982**, *218*, (1), 179-186.
54. Kelner, M. J.; Bagnell, R.; Hale, B.; Alexander, N. M., Inactivation of intracellular copper-zinc superoxide dismutase by copper chelating agents without glutathione depletion and methemoglobin formation. *Free Radical Biology and Medicine* **1989**, *6*, (4), 355-360.
55. Hirose, K.; Dokiya, Y.; Sugimura, Y., Determination of conditional stability constants of organic copper and zinc complexes dissolved in seawater using ligand exchange method with EDTA. *Marine Chemistry* **1982**, *11*, (4), 343-354.
56. Midorikawa, T.; Tanoue, E.; Sugimura, Y., Determination of complexing ability of natural ligands in seawater for various metal ions using ion selective electrodes. *Analytical Chemistry* **1990**, *62*, (17), 1737-1746.
57. Achterberg, E. P.; Van Den Berg, C. M. G., Chemical speciation of chromium and nickel in the western Mediterranean. *Deep Sea Research Part II: Topical Studies in Oceanography* **1997**, *44*, (3-4), 693.
58. Dupont, C. L.; Buck, K. N.; Palenik, B.; Barbeau, K., Nickel utilization in phytoplankton assemblages from contrasting oceanic regimes. *Deep Sea Research Part I: Oceanographic Research Papers* **2010**, *57*, (4), 553-566.
59. Hudson, R. J. M.; Morel, F. M. M., Trace metal transport by marine microorganisms: implications of metal coordination kinetics. *Deep-Sea Research* **1993**, *40*, 129-150.
60. Suarez-Moreira, E.; Yun, J.; Birch, C. S.; Williams, J. H. H.; McCaddon, A.; Brasch, N. E., Vitamin B12 and Redox Homeostasis: Cob(II)alamin Reacts with Superoxide at Rates Approaching Superoxide Dismutase (SOD). *Journal of the American Chemical Society* **2009**, *131*, (42), 15078-15079.
61. Saito, M. A.; Moffett, J. W., Temporal and spatial variability of cobalt in the Atlantic Ocean. *Geochim. Cosmochim. Acta* **2002**, *66*, (11), 1943-1953.
62. Bielski, B. H. J.; Cabelli, D. E.; Arudi, R. L.; Ross, A. B., Reactivity Of HO<sub>2</sub>/O<sub>2</sub><sup>-</sup> Radicals In Aqueous-Solution. *Journal Of Physical And Chemical Reference Data* **1985**, *14*, (4), 1041-1100.
63. Heller, M. I.; Croot, P. L., Superoxide Decay Kinetics in the Southern Ocean. *Environ. Sci. Technol.* **2010**, *44*, (1), 191-196.



## Supplementary Information

To accompany the manuscript entitled

# Pathways of Superoxide ( $O_2^-$ ) decay in the Tropical Atlantic

Kathrin Wuttig, Maija I. Heller and Peter L. Croot

Comprising:

27 Pages

6 Tables

4 Figures

## Supplementary Information:

A schematic summarizing the different pathways for  $O_2^-$  decay as described in the paper is shown in Figure S 1.

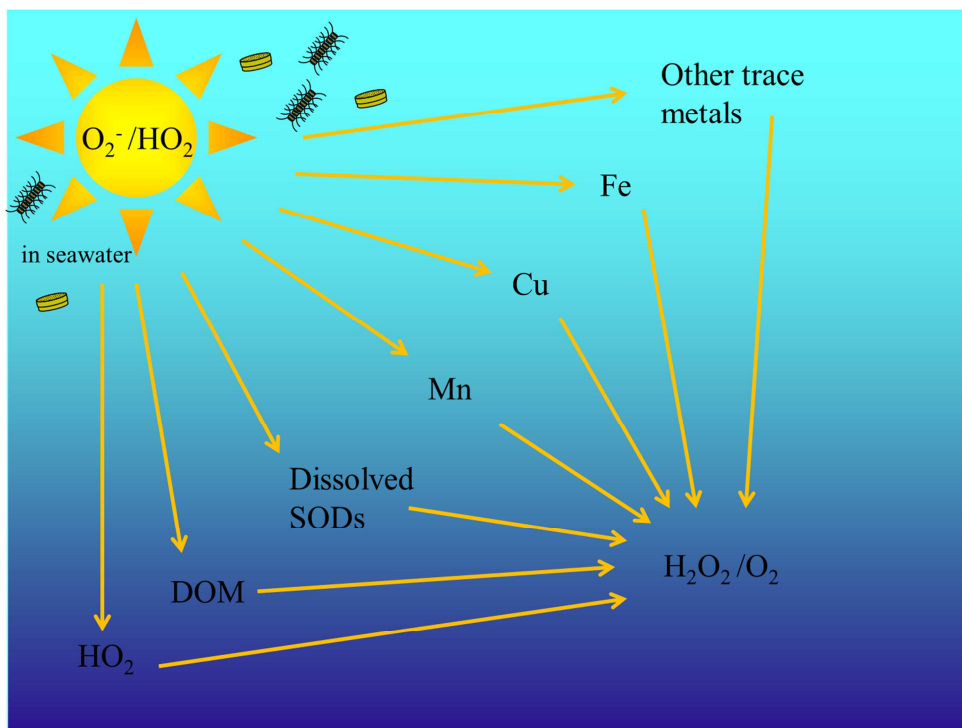


Figure S 1: Schematic of the different decay pathways for  $O_2^-$  decay in the ocean.  $O_2^-$  is biologically and photo produced.

### Seawater sampling

**Sampling Stations.** The location of the sampling GoFlo-Stations in the Eastern Tropical North Atlantic (ETNA) used in this study can be found in Table S 1 and Figure S 2.

Table S 1. Location of the 6 sampled GoFlo-Stations on M83/1.

Station	Date dd.mm.yy	Time (UTC)	Latitude	Longitude	Depth (m)
GOFLO1 ME831/769-1	17.10.10	23:15	17°39.01' N	24° 15.01' W	3593.7
GOFLO2 ME831/798-1	22.10.10	06:18	12°30.06' N	17° 37.36' W	649.9
GOFLO3 ME831/831-1	26.10.10	07:00	09°59.99' N	16° 59.98' W	444.0
GOFLO4 ME831/861-1	30.10.10	09:48	07°59.96' N	25° 29.98' W	4923.8
GOFLO5 ME831/881-1	03.11.10	09:13	10°00.06' N	24° 59.99' W	5475.1
GOFLO6 ME831/912-1	08.11.10	06:46	01°57.94' N	23° 00.06' W	4263.0

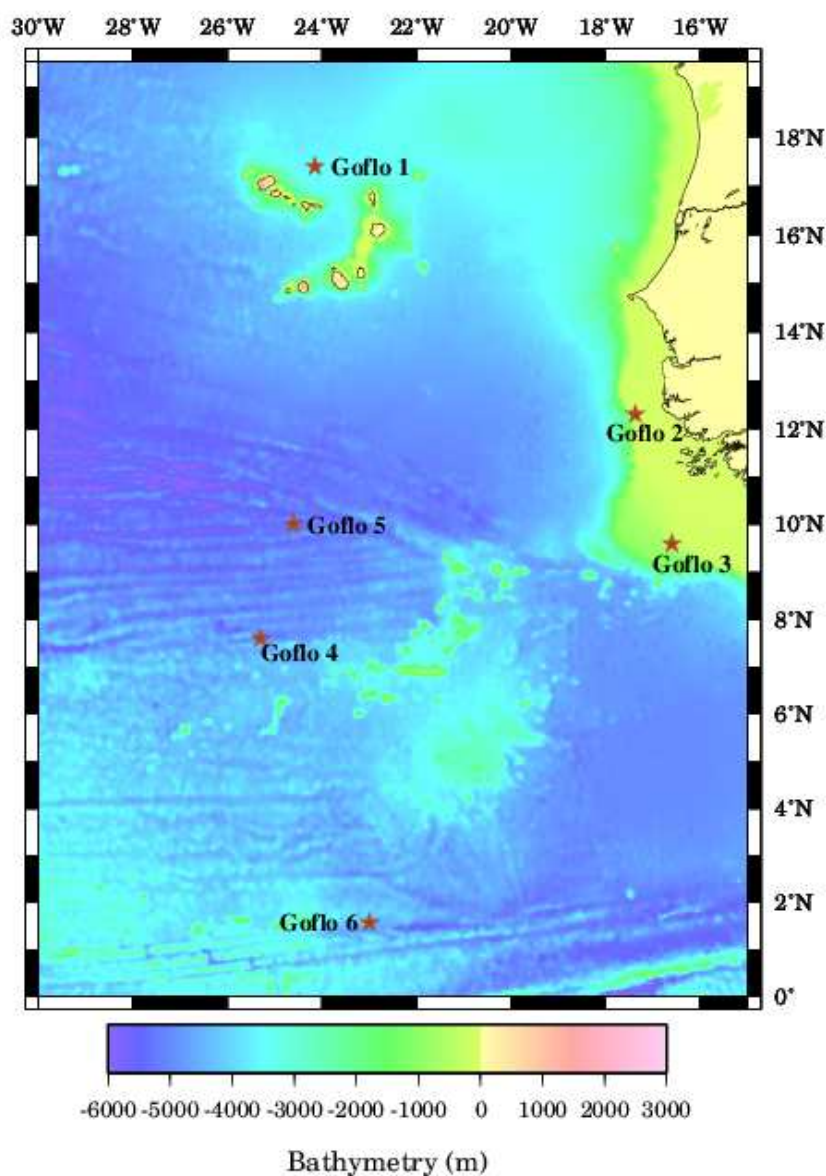


Figure S 2. Map showing the location of the 6 GoFlo sampling stations in this work (M83/1).

**Water Sampling.** All analytical work at sea was performed in an over-pressurized ISO class 5 clean container, inside of which analysts wore the appropriate clean room apparel, overalls with hood (Tyvek), shoes (Abeba) and plastic gloves (Carl Roth). Seawater samples in this work were obtained from the whole water column using modified Teflon coated PVC General Oceanics (Miami, FL, USA) GoFlo bottles of 8 L in which the original drain cock was replaced by a Teflon stop cock. These bottles were deployed on a Kevlar line from the side of the ship. Immediately upon recovery of the bottles, samples were filtered in-line through 0.2  $\mu\text{m}$  filter cartridges (Sartorius Sartobran filter capsule 5231307H5) by slight  $\text{N}_2$  overpressure into acid cleaned 1 L PTFE bottles for  $\text{O}_2^-$  and into LDPE bottles for trace metal analysis (both Nalgene).



**Experimental Details:**

Ultrapure (UP) water (resistivity  $> 18.2 \text{ M}\Omega \text{ cm}^{-1}$ ) for the total dissolved trace metal analysis was obtained in the laboratory in Kiel from a Millipore Synergy 185 system that was fed by an Elix-3 (Millipore) reverse osmosis system connected to the mains supply.

Ultrapure  $\text{HNO}_3$  and  $\text{HCl}$  were obtained by quartz (hereafter denoted as Q- $\text{HNO}_3$  and Q- $\text{HCl}$ ) sub-boiling distillation from analytical grade acids (Merck) in the laboratory in Kiel. For comparison purposes a commercial source of ultrapure  $\text{HCl}$  was also used in analysis (J.T. Baker, ULTREX II). Pipettes (Finnpipette) were calibrated frequently and trace metal clean pipette tips (Rainin RT-250 and RT-1000) were used as supplied. An inoLab pH 720 (WTW) was used to determine pH values on the NBS scale.

All plasticware and bottles (low density high polyethylene (LDPE) and Polytetrafluoroethylene (PTFE)) were extensively cleaned according to the GEOTRACES trace metal clean protocols<sup>1</sup>. In brief this consisted of sequential cleaning in a detergent solution and then soaking in acids for a period of weeks, followed by rinsing in UP water and allowing to dry on a Class 5 laminar flow bench before double bagging in polyethylene reclosable zipper bags (Minigrip™). All reagents and seawater samples were stored in these cleaned bottles. All the seawater used for  $\text{O}_2^-$  experiments was stored in PTFE bottles and the experiments also performed in these. Samples for dissolved trace metal analysis (filtered through  $0.2 \mu\text{m}$ ) were directly acidified with Q- $\text{HCl}$  to  $\text{pH} < 2$ , under a class 100-laminar flow bench. Sample processing and analysis steps were performed in laminar flow benches inside a class 100 clean room in Kiel.

**Determination of Mn, Fe, Cu and Ni in seawater.** Dissolved total trace metal (Copper (Cu), Iron (Fe) and Nickel (Ni)) concentrations were determined in the clean laboratory of the GEOMAR in Kiel using the graphite furnace atomic absorption (ETAAS, Perkin-Elmer Model 4100ZL) method after pre-concentration by simultaneous dithiocarbamate-freon extraction from seawater (250 - 300 g)<sup>2</sup>. The accuracy of the analytical procedure was evaluated by measurement of the SAFe intercomparison standard<sup>3</sup>. Our SAFe data (SAFe S:  $0.395 \pm 0.025 \text{ nM Cu}$ ,  $0.112 \pm 0.013 \text{ nM Fe}$ ,  $1.61 \pm 0.19 \text{ nM Ni}$ ; SAFe D2:  $1.480 \pm 0.481 \text{ nM Cu}$ ,  $0.829 \pm 0.127 \text{ nM Fe}$ ,  $6.59 \pm 0.76 \text{ nM Ni}$ ) are close to the average consensus values for Fe (SAFe S:  $0.090 \pm 0.007 \text{ nM}$ , D2:  $0.90 \pm 0.02 \text{ nM}$ ) and Cu (SAFe S:  $0.51 \pm 0.05 \text{ nM}$ , D2:  $2.25 \pm 0.11 \text{ nM}$ ). Our Ni values are slightly lower than the consensus values (SAFe S:  $2.31 \pm 0.01 \text{ nM}$ , D2:  $8.56 \pm 0.22 \text{ nM}$ )<sup>4</sup>. The precision for replicate analysis was between 3 - 5 % at the concentrations found in this study. The procedural (analytical) blank was  $0.041 \pm 0.024(\sigma_{\text{bl}}) \text{ nM (Fe)}$  and  $<1 \text{ pM (Cu)}$ . The accuracy of the method was evaluated by measuring SAFe and GEOTRACES intercalibration samples.

Dissolved Manganese (Mn) was also analysed in the clean laboratory in Kiel by graphite furnace atomic absorption (ETAAS, Perkin-Elmer Model 4100ZL) after solvent extraction modified after <sup>5</sup>. SAFe reference seawater D2 was determined as  $0.423 \pm 0.05$  nM (consensus value ( $0.35 \pm 0.06$  nM)).

The dissolved total trace metal concentrations are given in Table S 2.

**H<sub>2</sub>O<sub>2</sub> measurements.** Samples for H<sub>2</sub>O<sub>2</sub> were analysed within 1 – 2 h of collection using a flow injection chemiluminescence (FIA-CL) reagent injection method <sup>6</sup> as described previously <sup>7</sup>. Samples were analysed using 4 replicates: typical precision was 2 – 3 % through the concentration range 0.5 – 100 nM, the detection limit (3 s) was typically 0.2 nM.

**Calibration of the initial superoxide concentration.** In the present work we routinely measured the absorbance of the standard solution of KO<sub>2</sub> using UV spectrophotometry with either a 1 m LWCC-2100 (100 cm) pathlength liquid waveguide cell (World Precision Instruments, Sarasota, FL, USA) and an Ocean Optics USB4000 UV-VIS spectrophotometer in combination with an Ocean Optics DT-MINI-2-GS light source. Concentrations of H<sub>2</sub>O<sub>2</sub> and O<sub>2</sub><sup>-</sup> were determined by determining the least squares solution to the measured absorbance, at multiple wavelengths, by using published molar extinction coefficients for H<sub>2</sub>O<sub>2</sub> <sup>8</sup> and O<sub>2</sub><sup>-</sup> <sup>9</sup>. Mean initial concentrations in the primary KO<sub>2</sub> solution assessed in this way were  $900 \pm 50$  μM for H<sub>2</sub>O<sub>2</sub> and  $90 \pm 10$  μM O<sub>2</sub><sup>-</sup>. No DTPA or other complexing agents were added to our KO<sub>2</sub> primary solution. H<sub>2</sub>O<sub>2</sub> in the final seawater solutions was also assessed on occasion by the chemiluminescence flow injection method described above <sup>6</sup> and the results agreed well with the concentrations determined by direct spectrophotometry. For more information on specific calibration issues for O<sub>2</sub><sup>-</sup> the reader is referred to our earlier work <sup>10</sup>.

**Overview of the FeLume chemiluminescence system.** This system comprises a light tight box equipped with a Plexiglas spiral flow cell mounted below a photon counter (Hamamatsu HC-135-01) linked to a laptop computer via a Bluetooth connection controlled through a purpose built Labview<sup>TM</sup> (National Instruments) virtual instrument. For O<sub>2</sub><sup>-</sup> determination we ran the sample and the MCLA reagent directly into the flow cell using a peristaltic pump (Rainin<sup>TM</sup>, operating at 16.00 rpm,) with the sample line being pulled through the flow cell as this leads to the smallest amount of dead time in the system (typically 2 – 3 s). The overall flow rate through the cell was 8.25 mL min<sup>-1</sup>, comprising 5.0 mL min<sup>-1</sup> from the MCLA and 3.25 mL min<sup>-1</sup> from the sample. The transit time through the optical cell (300 μL) was therefore 2.18 s.

**Calculation of rate data for superoxide.** The raw chemiluminescence signal for the reaction between MCLA and  $O_2^-$  recorded by the computer was processed using a specially designed Labview™ VI constructed for this purpose using standard kinetic fitting procedures to determine both the 1<sup>st</sup> ( $k_{obs}$ ) and 2<sup>nd</sup> order ( $k_2$ ) rates simultaneously. The photon counter has a base counting period of 10 ms, for the present work we used average counts of an integration time of 200 ms. Dark background counts for this detector were typically 60 - 120 counts  $s^{-1}$ . Apparent reaction rates for Mn ( $k_{Mn}$ ), Cu ( $k_{Cu}$ ) and Fe ( $k_{Fe}$ ) with  $O_2^-$  were calculated via linear regression of  $k_{obs}$  versus the total metal added <sup>11</sup>. Using our experimental setup the minimum quantifiable values for  $k_{Mn}$ ,  $k_{Cu}$  and  $k_{Fe}$  is estimated at  $1 \times 10^6 \text{ M s}^{-1}$ .

**Model Calculations for  $O_2^-$  kinetics.** Numerical modelling of  $O_2^-$  reactions in seawater was performed using a fully explicit model written in C++ updated from an earlier version <sup>12</sup> to include Mn chemistry. Rate constants for the key reactions involved were compiled from those already published in the literature (see Table S 4).

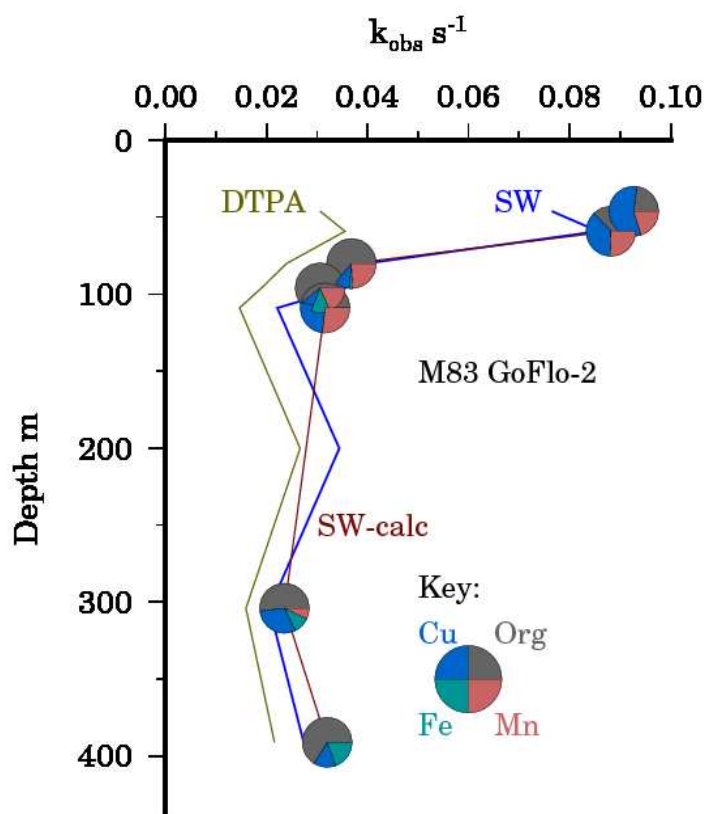


Figure S 3: In this depth profile of observed loss rate of  $O_2^-$ ,  $k_{obs}$ , at the GOFLO-Station 2 (on the shelf). The reaction with organic matter,  $k_{org}$ , is assumed to be equal to the measured reaction when DTPA is added,  $k_{DTPA}$  (beige line).  $k_{SW}$  is the reaction measured in unamended seawater (blue line).  $k_{SW-calc}$  is the calculated reaction with seawater (red line). With the help of the pie-charts the contribution from Organic matter, Cu, Fe and Mn on  $k_{SW-calc}$  is shown as explained for Figure 2.

### Sampling Methodology: Superoxide Kinetic Reactivity

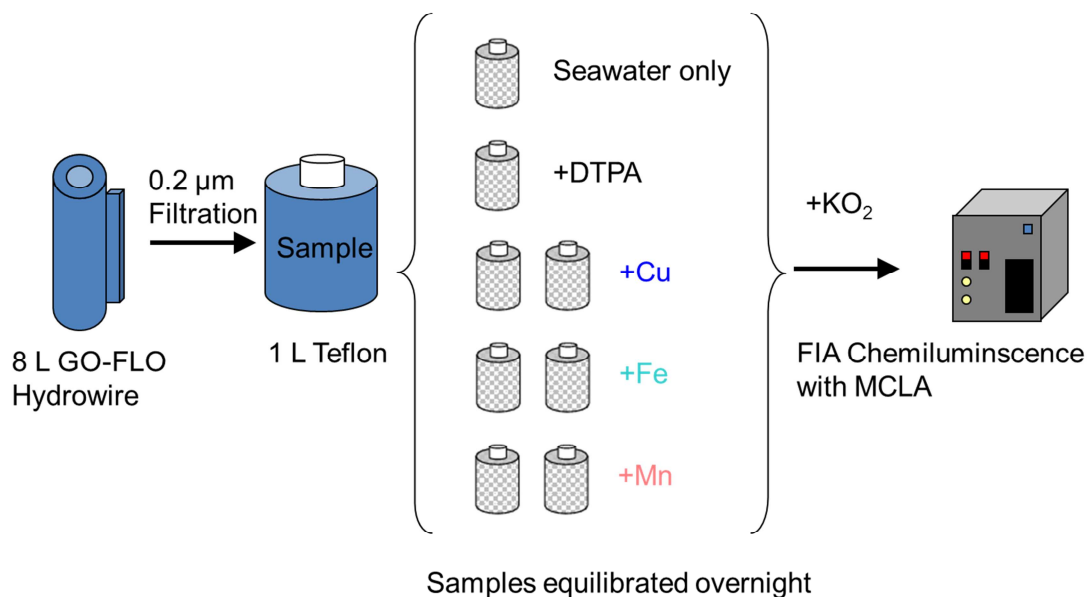


Figure S 4: Experimental design and description of the sampling protocol employed in this work which was further developed according to our previous work<sup>13</sup>.

Table S 2: M83/1 GoFlo-Station, depth (m) and total Cu, Fe, Mn and Ni (nmol L<sup>-1</sup>) concentrations measured by ETAAS. Numbers in brackets indicate samples suspected of contamination.

Station – Depth	Cu [nM]	Fe [nM]	Mn [nM]	Ni [nM]
1 – 19 m	0.741	1.024	2.45	5.486
1 – 40 m	-	-	2.056	-
1 – 140 m	0.830	0.716	0.59	2.317
1 – 200 m	0.627	0.895	1.65	2.283
1 – 600 m	0.998	1.325	0.62	6.065
2 – 46 m	0.851	1.232	2.72	3.016
2 – 59 m	0.905	2.167	3.36	3.050
2 – 80 m	0.692	1.445	1.26	2.556
2 – 96 m	0.827	2.543	0.883	5.367
2 – 109 m	(1.907)	1.361	3.52	(14.073)
2 – 200 m	0.783	4.477	1.08	3.868
2 – 304 m	0.815	2.256	0.55	3.987
2 – 391 m	0.859	5.211	0.906	(7.463)
3 – 20 m	0.938	0.552	3.08	3.510
3 – 40 m	0.875	0.883	1.73	2.624
3 – 80 m	1.021	0.714	0.615	2.828
3 – 100 m	0.772	1.771	0.826	3.050
3 – 200 m	0.917	1.515	0.573	3.493
3 – 300 m	0.780	1.739	0.570	4.123
3 – 400 m	0.916	2.029	0.675	5.231
4 – 20 m	0.550	0.851	2.25	2.470
4 – 40 m	0.594	0.754	2.30	1.550
4 – 60 m	0.600	0.312	1.29	1.431
4 – 80 m	0.605	0.324	1.17	4.208
4 – 100 m	0.531	0.691	1.02	2.385
4 – 200 m	0.649	1.359	0.415	2.794
4 – 300 m	0.585	1.065	0.42	3.459
4 – 400 m	0.823	1.295	0.457	(9.950)
5 – 20 m	0.679	1.248	2.54	2.266
5 – 40 m	0.667	0.457	1.92	2.010
5 – 60 m	0.506	0.220	1.50	1.261
5 – 80 m	0.649	0.297	1.17	5.418
5 – 100 m	0.709	0.886	0.724	3.612
5 – 200 m	0.690	1.397	0.315	3.425
5 – 300 m	0.709	1.076	0.382	3.135
5 – 400 m	0.764	1.402	0.462	5.265
6 – 20 m	0.512	0.415	2.37	1.397
6 – 40 m	0.586	0.573	2.09	1.585
6 – 60 m	0.608	0.199	1.87	1.653
6 – 80 m	0.518	0.149	1.28	2.641
6 – 100 m	0.693	0.333	0.83	3.347
6 – 200 m	0.700	0.842	0.399	3.391
6 – 300 m	0.656	0.860	0.319	3.152
6 – 400 m	0.808	0.963	0.326	5.486

**Table S 3: Compilation of specific metal decay rates of  $O_2^-$  in Tropical Atlantic seawater measured during M83/1 and calculated ones with least squares multiple regression analysis tool in Excel™ in brackets.**

Station – Depth	$\log k_{Cu}$	$\log k_{Fe}$	$\log k_{Mn}$	$k_{SW}$	$K_{DTPA}$
1 – 19 m	7.44 ± 0.12 (7.25 ± 0.25)	7.14 ± 0.08 (6.93 ± 0.44)	7.18 ± 0.08 (6.88 ± 0.35)	0.038	0.010 (0.006 ± 0.017)
1 – 40 m	7.30 ± 0.05 (6.97 ± 0.48)	6.35 ± 0.09 (-)	7.40 ± 0.04 (7.15 ± 0.21)	0.043	0.030 (0.024 ± 0.018)
1 – 140 m	7.33 ± 0.15 (7.17 ± 0.24)	7.00 ± 0.17 (7.73 ± 0.6)	6.13 ± 0.03 (7.03 ± 0.3)	0.025	0.014 (0.008 ± 0.013)
1 – 200 m	7.36 ± 0.01 (7.36 ± 0.15)	6.88 ± 0.52 (6.59 ± 0.73)	7.06 ± 0.11 (7.02 ± 0.27)	0.039	0.020 (0.017 ± 0.012)
1 – 600 m	7.42 ± 0.11 (7.25 ± 0.3)	7.37 ± 0.20 (7.14 ± 0.32)	- (-)	0.034	0.014 (0.008 ± 0.020)
2 – 46 m	7.73 ± 0.13	6.43 ± 0.14	7.29 ± 0.17	0.076	0.031
2 – 59 m	7.30 ± 0.17	< 6.0	< 6.0	0.086	0.036
2 – 80 m	6.55 ± 0.12	< 6.0	6.70 ± 0.05	0.040	0.024
2 – 96 m	6.38 ± 0.04	6.31 ± 0.04	6.58 ± 0.05	0.036	0.019
2 – 109 m	-	-	6.35 ± 0.28	0.022	0.015
2 – 200 m	6.38 ± 0.03	-	7.24 ± 0.02	0.034	0.027
2 – 304 m	6.94 ± 0.16	6.83 ± 0.09	6.81 ± 0.14	0.021	0.016
2 – 391 m	6.56 ± 0.15	-	6.67 ± 0.00	0.027	0.022
3 – 20 m	7.70 ± 0.14 (7.97 ± 0.21)	7.82 ± 0.19 (7.68 ± 0.39)	7.30 ± 0.01 (-)	0.065	0.045 (0.030 ± 0.077)
3 – 40 m	6.24 ± 1.27 (6.5 ± 0.52)	6.67 ± 0.16 (6.84 ± 0.22)	7.08 ± 0.08 (7.14 ± 0.21)	0.061	0.089 (0.024 ± 0.007)
3 – 80 m	7.13 ± 0.16 (6.98 ± 0.20)	- (-)	7.30 ± 0.01 (7.27 ± 0.09)	0.029	0.027 (0.013 ± 0.007)
3 – 100 m	6.42 ± 2.79 (6.78 ± 0.91)	- (-)	7.42 ± 0.02 (7.37 ± 0.19)	0.036	0.030 (0.017 ± 0.021)
3 – 200 m	- (-)	- (-)	7.54 ± 0.15 (7.51 ± 0.13)	0.044	0.016 (0.014 ± 0.019)
3 – 300 m	6.86 ± 0.29 (6.91 ± 0.18)	- (-)	7.40 ± 0.01 (7.45 ± 0.04)	0.037	0.035 (0.016 ± 0.006)
3 – 400 m	6.51 ± 4.22 (7.05 ± 0.9)	- (-)	7.35 ± 0.03 (7.31 ± 0.42)	0.030	0.016 (0.019 ± 0.039)
4 – 20 m	6.85 ± 1.35 (-)	7.22 ± 0.11 (6.50 ± 2.16)	7.57 ± 0.04 (7.38 ± 0.19)	0.046	0.017 (0.011 ± 0.030)
4 – 40 m	6.14 ± 0.95 (-)	6.98 ± 0.45 (6.97 ± 1.01)	6.71 ± 2.12 (7.07 ± 0.52)	0.044	0.014 (0.018 ± 0.040)
4 – 60 m	< 6.0 (-)	6.88 ± 0.04 (6.58 ± 0.71)	7.22 ± 0.08 (7.07 ± 0.17)	0.033	0.028 (0.023 ± 0.0103)

4 – 80 m	- (6.34 ± 1.44)	- (-)	6.72±0.08 (7.05 ± 0.2)	0.048	0.021 (0.024 ± 0.011)
4 – 100 m	7.31 ± 0.37 (7.13 ± 0.32)	6.83 ± 0.49 (6.51 ± 1.16)	7.20 ±0.04 (7.15 ± 0.21)	0.036	0.018 (0.012 ± 0.015)
4 – 200 m	6.91 ± 0.18 (6.44 ± 0.72)	- (-)	7.02 ± 0.01 (7.06 ± 0.15)	0.021	0.012 (0.014 ± 0.073)
4 – 300 m	6.37 ± 0.16 (6.19 ± 0.38)	< 6.0 (5.87 ± 0.63)	6.90 ± 0.07 (6.9 ± 0.06)	0.015	0.011 (0.011 ± 0.0 21)
4 – 400 m	6.56 ± 0.06 (6.37 ± 0.49)	6.34 ± 0.06 (5.99 ± 0.95)	7.04 ± 0.08 (6.99 ± 0.1)	0.017	0.011 (0.01 ± 0.004)
5 – 20 m	No data	No data	No data	No data	No data
5 – 40 m	No data	No data	No data	No data	No data
5 – 60 m	6.54±0.24 (6.69 ± 0.27)	- (-)	6.920.09 (6.9 ± 0.12)	0.031	0.017 (0.019 ± 0.005)
5 – 80 m	No data	No data	No data	No data	No data
5 – 100 m	6.45 ± 0.0 (6.6 ± 0.19)	- (5.82 ± 0.99)	6.96 ± 0.04 (7.01 ± 0.66)	0.020	0.010 (0.011 ± 0.003)
5 – 200 m	6.50 ± 0.2 (-)	- (7.47 ± 0.45)	7.09 ± 0.02 (-)	0.015	0.007 (0.019 ± 0.007)
5 – 300 m	6.09 ± 0.36 (6.06 ± 0.76)	Below detection (6.23 ± 0.42)	6.99 ± 0.07 (7.02 ± 0.07)	0.013	0.006 (0.007 ± 0.000)
5 – 400 m	No data	No data	No data		
6 – 20 m	7.16 ± 0.00 (7.11 ± 0.17)	6.86 ± 0.02 (6.77 ± 0.33)	7.35 ± 0.08 (7.29 ± 0.07)	0.048	0.050 (0.007 ± 0.008)
6 – 40 m	< 6.0 (6.96 ± 0.37)	6.25± 0.96 (6.89 ± 0.40)	7.17 ± 0.09 (7.31 ± 0.12)	0.054	0.044 (0.014 ± 0.012)
6 – 60 m	6.79 ± 0.94 (7.16 ± 0.69)	- (-)	- (7.16 ± 0.45)	0.063	0.051 (0.020 ± 0.035)
6 – 80 m	- (7.02 ± 0.59)	< 6.0 (6.85 ± 0.86)	6.91 ± 0.06 (7.12 ± 0.37)	0.044	0.040 (0.023 ± 0.021)
6 – 100 m	6.97 ± 0.22 (-)	6.33 ± 0.14 (-)	- (7.66 ± 0.51)	0.044	0.045 (0.026 ± 0.095)
6 – 200 m	6.38 ± 0.04 (6.41 ± 0.36)	- (-)	7.08 ± 0.07 (7.10 ± 0.07)	0.011	0.011 (0.007 ± 0.003)
6 – 300 m	No data	6.20 ± 0.04 (-)	7.24 ± 0.31 (-)	0.009	- (-)
6 – 400 m	6.85 ± 0.34 (6.51 ± 0.77)	< 6.0 (-)	7.17 ± 0.10 (7.10 ± 0.16)	0.009	0.011 (0.006 ± 0.009)

Notes: 95% CI listed for lower data.

Table S 4. 2<sup>nd</sup> Order Reaction Rate Constants ( $M^{-1} s^{-1}$ ) for Metal species with  $O_2^-$  modified after Heller and Croot (2010)<sup>13</sup>.

Species	$HO_2$	$O_2^-$
Cu(I)	$> 1*10^9$ (a) -	$\sim 1*10^{10}$ (a) $9.4\pm 0.8*10^9$ (b) $1.98\pm 0.05*10^9$ (c)
Cu(II)	$1.2*10^8$ (d) -	$1.1*10^{10}$ (d) $6.63 \pm 0.71*10^8$ (c)
Fe(II)	$1.2\pm 0.5*10^6$ (e) $1.2\pm 0.2*10^6$ (g)	$7.2*10^8$ (f) $1.0\pm 0.1*10^7$ (g)
Fe(III)	- $3.1*10^5$ (h)	$1.8*10^8$ (g) $1.5\pm 0.2*10^8$ (i)
Mn(II)		$5.4*10^7$ (j) $2.8*10^7$ (k)
Mn(III)		$1.7*10^7$ (l) $8.9*10^6$ (m)
$HO_2$	$8.3\pm 0.7*10^5$ (n)	$9.7\pm 0.6*10^7$ (n)
Cu(II)L	-	$2.9-8.1*10^8$ (o) $5\pm 3*10^7$ (p)
Fe(III)L	-	$9.3\pm 0.2*10^3$ (q) $2.3\pm 0.1*10^5$ (r)

Notes: The reader is also referred to the compilation of Bielski *et al.*<sup>9</sup>. In describing the experimental setup used in each work we use the following abbreviations: pulse radiolysis (p.r.), flash photolysis (f.p.),  $\gamma$  irradiation ( $\gamma$ -r), optical detection of superoxide (opt) and chemical detection of superoxide or equivalent (chem.). The pKa for  $HO_2$  is  $4.60 \pm 0.15$ <sup>14</sup>. All experiments are in the range 20 - 25°C.

(a)Cu(I), pH 5.3, p.r. opt.<sup>15</sup>. (b)Cu(I), p.r. opt.<sup>16</sup>. (c)Cu(I) and Cu(II) in seawater, p.r. opt.<sup>17</sup>. (d)Cu(II) and Cu(II)-arginine, p.r. opt.<sup>18</sup>. (e)Fe(II), pH 1, p.r. opt.<sup>19</sup>. (f)Fe(II) and Fe(III), p.r., opt<sup>20</sup>. (g)Fe(II) species, pH 1-7, p.r., opt<sup>21</sup>. (h)Fe(III) species, pH 2.74, p.r., opt<sup>22</sup>. (i)Fe(III)(OH) species, pH 1-7, p.r., opt<sup>21</sup>. (j) Mn(I) in sulphate, pH 7,  $\gamma$ -r, opt<sup>23</sup>. (k) Mn(I) in phosphate, pH 7,  $\gamma$ -r, opt<sup>23</sup>. (l) Mn(I) in pyrophosphate, pH 7,  $\gamma$ -r, opt<sup>23</sup>. (m)Mn(III) in phosphate, pH 7,  $\gamma$ -r, opt<sup>23</sup>. (n)As summarized in Bielski *et al.*<sup>9</sup>. (o)Natural seawater with Cu complexing ligands<sup>11</sup>. (p)Copper complexing ligands produced by *Synechococcus*<sup>11</sup>. (q)Fe(III) complexed with desferrioxamine B in bicarbonate buffered solution<sup>24</sup>. (r)Fe(III) complexed with natural organic matter in bicarbonate buffered solution<sup>24</sup>.



Table S 5: Compilation of ranges of specific metal reactions of superoxide in seawater during M83/1 and from other studies.

Study	Cruise	Station	Depth	Cu [nM]	Fe [nM]	Mn [nM]	log $k_{Cu}$	log $k_{Fe}$	log $k_{Mn}$	$k_{SW}$	$k_{DTPA}$
This study	RV Meteor M83/1 ETNA	GoFLo 1 (CVOO)	19-600	0.63- 1.00	0.72- 1.32	0.59- 2.06	7.30-7.44	6.35- 7.37	6.13- 7.40	0.025- 0.043	0.010- 0.030
		GoFLo 2	46-391	0.70- 0.90	1.23- 5.21		6.38-6.94	< 6-6.83	< 6.00- 7.24	0.021- 0.086	0.016- 0.36
		GoFLo 3	20-400	0.78- 1.02	0.55- 2.02	0.57- 3.08	6.24-7.70	6.67- 7.82	7.08- 7.54	0.029- 0.065	0.016- 0.089
		GoFLo 4	20-400	0.55- 0.82	0.31- 1.36	0.42- 2.30	< 6-7.31	< 6-7.22	6.71- 7.57	0.015- 0.048	0.011- 0.028
		GoFLo 5	20-400	0.51- 0.76	0.22- 1.40	0.31- 2.54	6.09-6.54	< 6-7.47	6.92- 7.09	0.013- 0.031	0.006- 0.017
		GoFLo 6	20-400	0.51- 0.80	0.15- 0.97		< 6.-7.16	< 6-6.86	6.91- 7.35	0.009- 0.063	0.011- 0.051
<sup>25</sup> Hansard <i>et al.</i> , 2011	GoA1-4 Gulf of Alaska					Added Mn: 3-24			6.78- 7.00		
<sup>13</sup> Heller and Croot, 2010a	RV Polar-stern (ANT24/3) Antarctica	230-6	25-1000	1.4-1.89	0.346- 1.78		7.27-7.85	< 6-7.64		0.014- 0.041	2.00x10 <sup>5</sup> - 9.36x10 <sup>4</sup>
		236-5	25-2800	1.07- 1.95	0.109- 1.91		< 6-7.79	< 6-7.43		0.008- 0.037	1.77x10 <sup>5</sup> - 7.21x10 <sup>4</sup>
		249-3	25-1000	0.85- 2.27	0.22- 0.666		6.4-7.9	< 6-7.79		0.009- 0.021	1.17x10 <sup>5</sup> - 4.46x10 <sup>4</sup>
<sup>26</sup> Heller and Croot, 2010b	RV Islandia ETNA	10 (CVOO)	10	0.78	0.6		7.5	7.19		0.023	0.013
<sup>27</sup> Heller and Croot, 2011	RV Islandia ETNA	8	5	0.68	0.81		7.4	6.28		0.036	0.013
Voelker <i>et al.</i> , 2000							*log $k_{CuL1}$ : < 8.00 log $k_{CuL2}$ : 8.46-8.91				

$K_{DTPA}$  should be  $10^4 \text{ M}^{-1} \text{ s}^{-1}$  is the 2<sup>nd</sup> order rate for superoxide decay.

**Table S 6: Normalized estimated % for each reaction pathway by multiple linear regression and used in the pie charts.**

Station - Depth	% DTPA	% Cu	% Fe	% Mn
1 – 19 m	12.05	29.41	19.37	39.17
1 – 40 m	39.49	13.32	0	47.19
1 – 140 m	29.47	43.08	13.50	13.95
1 – 200 m	43.84	36.32	8.88	10.97
1 – 600 m	19.81	44.16	45.46	0
2 – 46 m	20.46	50.39	0	29.15
2 – 59 m	35.57	36.23	0	28.02
2 – 80 m	59.65	9.16	1.69	29.50
2 – 96 m	54.86	7.61	11.12	26.41
2 – 109 m	43.70	25.26	0	31.04
2 – 200 m	No data	No data	No data	No data
2 – 304 m	49.67	29.27	10.28	10.77
2 – 391 m	60.12	13.08	0	26.80
3 – 20 m	78.12	0	0	21.88
3 – 40 m	42.45	4.85	10.67	42.04
3 – 80 m	43.92	19.27	0	36.81
3 – 100 m	40.75	11.39	0	47.86
3 – 200 m	44.02	0	0	58.19
3 – 300 m	40.75	16.55	0	42.70
3 – 400 m	43.80	24.03	0	32.17
4 – 20 m	13.67	0	6.45	79.88
4 – 40 m	No data	No data	No data	No data
4 – 60 m	60.74	0	3.16	40.07
4 – 80 m	62.67	3.38	0	33.95
4 – 100 m	33.56	20.05	6.19	40.19
4 – 200 m	68.61	8.63	0	22.77
4 – 300 m	69.35	5.26	4.83	20.57
4 – 400 m	59.49	10.96	7.60	21.96
5 – 20 m	No data	No data	No data	No data
5 – 40 m	No data	No data	No data	No data
5 – 60 m	62.36	8.22	0	29.75
5 – 80 m	No data	No data	No data	No data
5 – 100 m	57.06	14.72	3.05	25.17
5 – 200 m	41.74	0	89.31	0
5 – 300 m	54.92	6.40	14.28	24.39
5 – 400 m	No data	No data	No data	No data
6 – 20 m	14.93	13.37	4.94	66.73
6 – 40 m	31.31	12.19	10.04	46.46
6 – 60 m	39.37	17.31	0	43.32
6 – 80 m	58.87	13.82	2.65	24.66
6 – 100 m	58.88	0	0	41.15
6 – 200 m	58.88	15.77	0	25.35
6 – 300 m	No data	No data	No data	No data
6 – 400 m	48.39	21.71	0	29.90

## REFERENCES

1. Cutter, G. A.; Andersson, P.; Codispoti, L.; Croot, P. L.; Francois, R.; Lohan, M.; Obata, H.; Rutgers van der Loeff, M. Sampling and Sample-handling Protocols for GEOTRACES Cruises. <http://www.geotraces.org/libraries/documents/Intercalibration/Cookbook.pdf>.
2. (a) Bruland, K. W.; Franks, R. P.; Knauer, G. A.; Martin, J. H., Sampling and Analytical Methods for the Determination of Copper, Cadmium, Zinc, and Nickel at the Nanogram Per Liter Level in Sea-Water. *Analytica Chimica Acta* **1979**, *105* (1), 233-245; (b) Danielsson, L.-G.; Magnusson, B.; Westerlund, S., An improved metal extraction procedure for the determination of trace metals in sea water by atomic absorption spectrometry with electrothermal atomization. *Analytica Chimica Acta* **1978**, *98* (1), 47-57; (c) Grasshoff, K.; Kremling, K.; Ehrhardt, M., *Methods of seawater analysis*. Verlag Chemie: Weinheim, 1983.
3. Johnson, K. S.; Boyle, E.; Bruland, K.; Coale, K.; Measures, C.; Moffett, J.; Aguilar-islas, A.; Barbeau, K.; Berquist, B.; Bowie, A.; Buck, K.; Cai, Y.; Chase, Z.; Cullen, J.; Doi, T.; Elrod, V.; Fitzwater, S.; Gordon, M.; King, A.; Laan, P.; Laglera-Baquer, L.; Landing, W.; Lohan, M.; Mendez, J.; Milne, A.; Obata, H.; Ossiander, L.; Plant, J.; Sarthou, G.; Sedwick, P.; Smith, G. J.; Sohst, B.; Tanner, S.; Berg, S. v. d.; Wu, J., Developing Standards for Dissolved Iron in Seawater. *EOS, Transactions of the American Geophysical Union* **2007**, *88* (11), 131-132.
4. (a) Ellwood, M. J., Wintertime trace metal (Zn, Cu, Ni, Cd, Pb and Co) and nutrient distributions in the Subantarctic Zone between 40-52°S; 155-160°E. *Marine Chemistry* **2008**, *112* (1-2), 107; (b) Sohrin, Y.; Urushihara, S.; Nakatsuka, S.; Kono, T.; Higo, E.; Minami, T.; Norisuye, K.; Umetani, S., Multielemental Determination of GEOTRACES Key Trace Metals in Seawater by ICPMS after Preconcentration Using an Ethylenediaminetriacetic Acid Chelating Resin. *Analytical Chemistry* **2008**, *80* (16), 6267-6273.
5. Klinkhammer, G. P., Determination of manganese in sea water by flameless atomic absorption spectrometry after preconcentration with 8-hydroxyquinoline in chloroform. *Analytical Chemistry* **1980**, *52* (1), 117-120.
6. Yuan, J.; Shiller, A. M., Determination of Subnanomolar Levels of Hydrogen Peroxide in Seawater by Reagent-Injection Chemiluminescence Detection. *Analytical Chemistry* **1999**, *71* (10), 1975-1980.
7. Croot, P. L.; Streu, P.; Peeken, I.; Lochte, K.; Baker, A. R., Influence of the ITCZ on H<sub>2</sub>O<sub>2</sub> in near surface waters in the equatorial Atlantic Ocean. *Geophys. Res. Lett.* **2004**, *31* (23), L23S04.
8. (a) Taylor, R. C.; Cross, P. C., Light Absorption of Aqueous Hydrogen Peroxide Solutions in the Near Ultraviolet Region. *Journal of the American Chemical Society* **1949**, *71* (6), 2266-2268; (b) Baxendale, J. H.; Wilson, J. A., The photolysis of hydrogen peroxide at high light intensities. *Transactions of the Faraday Society* **1957**, *53*, 344-356.
9. Bielski, B. H. J.; Cabelli, D. E.; Arudi, R. L.; Ross, A. B., Reactivity Of HO<sub>2</sub>/O<sub>2</sub><sup>-</sup> Radicals In Aqueous-Solution. *Journal Of Physical And Chemical Reference Data* **1985**, *14* (4), 1041-1100.
10. Heller, M. I.; Croot, P. L., Application of a Superoxide (O<sub>2</sub><sup>-</sup>) thermal source (SOTS-1) for the determination and calibration of O<sub>2</sub><sup>-</sup> fluxes in seawater. *Analytica Chimica Acta* **2010**, *667*, 1-13.
11. Voelker, B. M.; Sedlak, D. L.; Zafiriou, O. C., Chemistry of Superoxide Radical in Seawater: Reactions with Organic Cu Complexes. *Environmental Science and Technology* **2000**, *34*, 1036-1042.
12. Croot, P. L.; Laan, P.; Nishioka, J.; Strass, V.; Cisewski, B.; Boye, M.; Timmermans, K.; Bellerby, R.; Goldson, L.; de Baar, H. J. W., Spatial and Temporal distribution of Fe(II)

- and H<sub>2</sub>O<sub>2</sub> during EISENEX, an open ocean mesoscale iron enrichment. *Marine Chemistry* **2005**, *95*, 65-88.
13. Heller, M. I.; Croot, P. L., Superoxide Decay Kinetics in the Southern Ocean. *Environ. Sci. Technol.* **2010**, *44* (1), 191-196.
  14. Zafiriou, O. C., Chemistry of superoxide ion (O<sub>2</sub><sup>-</sup>) in seawater. I. pK<sub>asw</sub><sup>\*</sup> (HOO) and uncatalysed dismutation kinetics studied by pulse radiolysis. *Marine Chemistry* **1990**, *30*, 31-43.
  15. Rabani, J.; Klug-Roth, D.; Lilie, J., Pulse radiolytic investigations of the catalyzed disproportionation of peroxy radicals. Aqueous cupric ions. *The Journal of Physical Chemistry* **1973**, *77* (9), 1169-1175.
  16. Piechowski von, M.; Nauser, T.; Hoigné, J.; Bühler, R., O<sub>2</sub><sup>-</sup> decay catalyzed by Cu<sup>2+</sup> and Cu<sup>+</sup> ions in aqueous solutions: a pulse radiolysis study for atmospheric chemistry. *Ber. Bunsenges. Phys. Chem.* **1993**, *6*, 762-771.
  17. Zafiriou, O. C.; Voelker, B. M.; Sedlak, D. L., Chemistry of the superoxide radical (O<sub>2</sub><sup>-</sup>) in seawater: Reactions with inorganic copper complexes. *Journal of Physical Chemistry A* **1998**, *102* (28), 5693-5700.
  18. Cabelli, D. E.; Bielski, B. H. J.; Holcman, J., Interaction between Copper(II)-Arginine Complexes and HO<sub>2</sub>/O<sub>2</sub><sup>-</sup> Radicals, a Pulse Radiolysis Study. *Journal of the American Chemical Society* **1987**, *109*, 3665-3669.
  19. Jayson, G. G.; Parsons, B. J.; Swallow, A. J., Oxidation Of Ferrous Ions By Perhydroxyl Radicals. *Journal Of The Chemical Society-Faraday Transactions I* **1973**, *69* (1), 236-242.
  20. Matthews, R. W., The radiation chemistry of aqueous ferrous sulfate solutions at natural pH. *Australian Journal of Chemistry* **1983**, *36*, 1305-1317.
  21. Rush, J. D.; Bielski, B. H. J., Pulse Radiolytic Studies of HO<sub>2</sub>/O<sub>2</sub><sup>-</sup> with Fe(II)/Fe(III) Ions. The reactivity of HO<sub>2</sub>/O<sub>2</sub><sup>-</sup> with Ferric Ions and Its Implication on the Occurrence of the Haber-Weiss Reaction. *Journal of Physical Chemistry* **1985**, *89*, 5062-5066.
  22. Sehested, K.; Bjergbakke, E.; Rasmussen, O. L.; Fricke, H., Reactions of H<sub>2</sub>O<sub>3</sub> in the Pulse □-Irradiated Fe(II)-O<sub>2</sub> System. *The Journal of Chemical Physics* **1969**, *51* (8), 3159-3166.
  23. Barnese, K.; Gralla, E. B.; Cabelli, D. E.; Selverstone Valentine, J., Manganous Phosphate Acts as a Superoxide Dismutase. *Journal of the American Chemical Society* **2008**, *130* (14), 4604-4606.
  24. Rose, A. L.; Waite, T. D., Reduction of organically complexed ferric iron by superoxide in a simulated natural water. *Environmental Science & Technology* **2005**, *39* (8), 2645-2650.
  25. Hansard, S. P.; Easter, H. D.; Voelker, B. M., Rapid Reaction of Nanomolar Mn(II) with Superoxide Radical in Seawater and Simulated Freshwater. *Environ. Sci. Technol.* **2011**, *45* (7), 2811-2817.
  26. Heller, M. I.; Croot, P. L., Kinetics of superoxide reactions with dissolved organic matter in tropical Atlantic surface waters near Cape Verde (TENATSO). *J. Geophys. Res.* **2010**, *115* (C12), C12038.
  27. Heller, M. I.; Croot, P. L., Superoxide decay as a probe for speciation changes during dust dissolution in Tropical Atlantic surface waters near Cape Verde. *Mar. Chem.* **2011**, *126* (1-4), 37-55.





# MANUSCRIPT 2

Reactivity of inorganic Mn and  
Mn Desferioxamine B with  $O_2$ ,  $O_2^-$   
and  $H_2O_2$  in seawater





# Reactivity of inorganic Mn and Mn Desferioxamine B with $O_2$ , $O_2^-$ and $H_2O_2$ in seawater

Kathrin Wuttig<sup>1</sup>, Maija I Heller<sup>1,2</sup> Peter L Croot<sup>3,4,\*</sup>

<sup>1</sup>GEOMAR Helmholtz Centre for Ocean Research Kiel, Marine Biogeochemistry,  
Düsternbrooker Weg 20, 24105 Kiel, Germany

<sup>2</sup>University of Southern California, Los Angeles, United States of America.

<sup>3</sup>Plymouth Marine Laboratory (PML), Plymouth, United Kingdom.

<sup>4</sup>Earth and Ocean Sciences, School of Natural Sciences, National University of  
Ireland, Galway (NUIG), Galway, Ireland.

\*Corresponding Author

Draft only – do not cite unless prior permission from the authors.

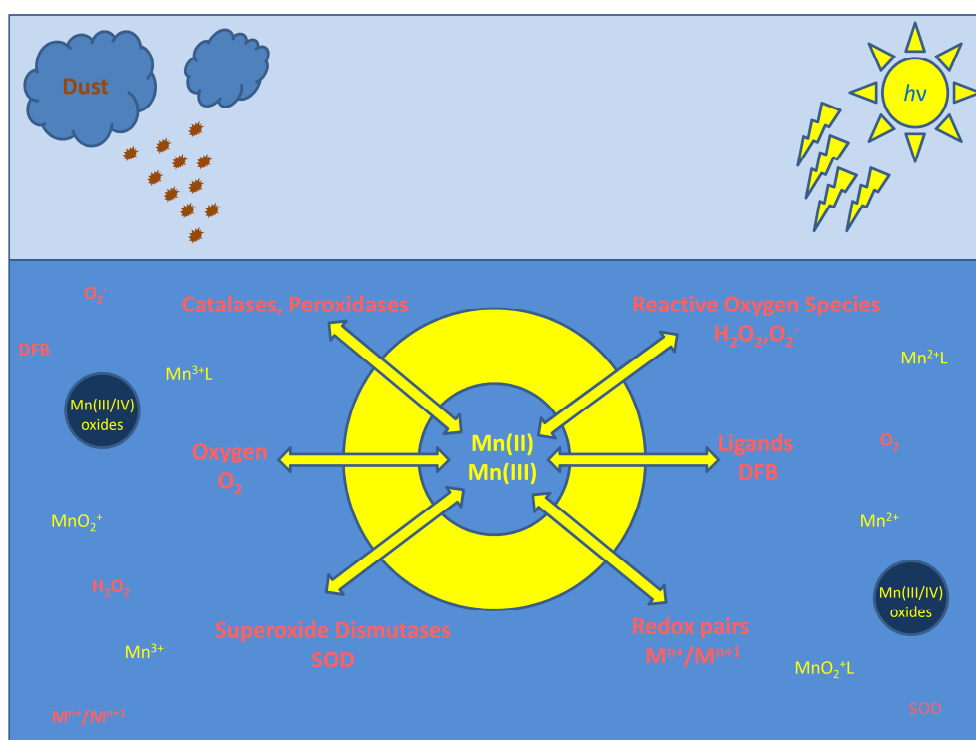
For submission to *Environmental Science and Technology*

This version April 16, 2013

(Word limit = 5487 words + 5 figures = 1500 words < 7000 words)

## ABSTRACT

Manganese (Mn) is a required element for oceanic phytoplankton as it plays a critical role in photosynthesis, through its unique redox chemistry, as the active site in photosystem II and in enzymes that act as defences against reactive oxygen species (ROS), most notably for protection against superoxide ( $O_2^-$ ), through the action of superoxide dismutase (SOD), and against hydrogen peroxide ( $H_2O_2$ ) via peroxidases and catalases. The distribution and redox speciation of Mn in the ocean is also apparently controlled by reactions with ROS. Here we examine the connections between ROS and dissolved Mn species in the upper ocean using field and laboratory experimental data. Our results suggest it is unlikely that significant concentrations of Mn(III) are produced in the euphotic zone, as in the absence of evidence for the existence of strong Mn(III) ligands, Mn(II) reacts with  $O_2^-$  to form the short lived transient manganous superoxide,  $MnO_2^+$ , which may react rapidly with other redox species in a similar manner to  $O_2^-$ . Experiments with the strong Mn(III) chelator, desferrioxamine B (DFB), in seawater indicated that the Mn(III) species is unlikely to form, as the pre-cursor Mn(II) complex under natural ambient conditions due to the high side reaction of DFB with Ca.



Abstract figure: showing the different Mn ROS reaction pathways, the main ROS and Mn sources and important species.

## 1 INTRODUCTION

Manganese (Mn) is an essential element for phytoplankton in the ocean due to its fundamental role in Photosystem II (PSII) in the 4 electron conversion of H<sub>2</sub>O to O<sub>2</sub><sup>1</sup>. Mn possesses a rich redox chemistry<sup>2</sup> and for this reason it is used by organisms to control levels of reactive oxygen species (ROS) inside cells as Mn complexes are capable of acting as superoxide dismutases (SODs), catalases and peroxidases<sup>3</sup>. Manganese induced growth limitation of phytoplankton has been found to occur below 100 pM Mn(II) in laboratory experiments<sup>4</sup> and there is yet no evidence for Mn limitation of phytoplankton growth in the field<sup>5,6</sup>, presumably as Mn concentrations in surface waters are typically > 100 pM even in the Southern Ocean<sup>7</sup>.

The main source of Mn to the open ocean is from the deposition of continental aerosols<sup>8,9</sup> with significant amounts of the Mn in the aerosol being easily solubilized<sup>10,11</sup>. Closer to the coast, oxygen poor shelf sediments can be important sources of Mn to the water column<sup>12,13</sup>. The residence time for Mn in the upper ocean has been estimated to be on the order of 4 – 5 years<sup>9,14</sup> and 60 years for the full water column<sup>15</sup>. While Mn(IV) is the thermodynamically favoured redox state in oxygenated seawater, kinetic limitations lead to the predominance of the soluble Mn(II) aquo ion, as the higher oxidation states, Mn(III) or Mn(IV), are poorly soluble and found almost exclusively in particles. The distribution and speciation of Mn in the surface ocean is strongly related to redox cycling through reactions with ROS. Particulate MnO<sub>2</sub> reacts with hydrogen peroxide (H<sub>2</sub>O<sub>2</sub>) rapidly to form Mn(II) and is believed to be the main reason for the retention and accumulation of Mn(II) in the euphotic zone<sup>16</sup>. The abiotic oxidation of Mn(II) in seawater by O<sub>2</sub> is very slow<sup>17,18</sup>, however the reaction is accelerated on particle surfaces<sup>19</sup>. Furthermore bacteria can facilitate Mn(II) oxidation by both direct (enzymatic) and indirect (e.g., non-enzymatic bacterial spore coat mediation) processes<sup>20,21</sup>. Oxidation of soluble Mn(II) ions to Mn(III/IV) oxides has been primarily attributed to direct enzymatic oxidation by microorganisms, via the production of superoxide (O<sub>2</sub><sup>-</sup>)<sup>22</sup>. Photo-oxidation in the presence of humic substances has also been suggested as a pathway for the formation of Mn oxides<sup>23</sup>. Soluble Mn(III) is rare in natural waters because it rapidly hydrolyses and precipitates as Mn(III) oxides or disproportionates into Mn(IV) and Mn(II)<sup>24,25</sup>, unless stabilized in complexes with ligands<sup>26,27</sup>.

Over the last two decades the role of Mn(III) in the marine environment has begun to be investigated in more detail<sup>27-29</sup>. However progress for resolving Mn(III) in the water column is limited by the detection limits of the current analytical methods being no lower than the 100 nM level<sup>30,31</sup>, almost a 100 times higher than oxic seawater concentrations. In the suboxic waters of the Black Sea concentrations of up to 5 μM Mn(III) have been reported<sup>30</sup> and it was suggested that this intermediate is stabilized by an unknown ligand, and formed

from the oxidation of Mn(II) and the reduction of particulate MnO<sub>2</sub>. Recently it was also suggested that Mn(III) may form in the oxic euphotic zone of the ocean via the Mn(II/III) redox couple catalysing the decay of O<sub>2</sub><sup>-</sup> <sup>32</sup>. However other laboratory studies indicate the Mn(III) only forms in reaction with O<sub>2</sub><sup>-</sup> when a strong Mn(III) ligand is present <sup>33-35</sup>. One group of ligands that could potentially fill this role are the hydroxamate siderophores as several of them are easily oxidized by air from the Mn(II) to Mn(III) complexes <sup>36-38</sup>.

In the present work we examined the interaction of the Mn and ROS redox cycles in the euphotic zone of the ocean through a combination of laboratory, field and modelling experiments. A companion paper <sup>39</sup> examines the overall role of metals and organics on the decay of O<sub>2</sub><sup>-</sup> in seawater. In this work we focus on the potential for Mn(III) formation in natural seawater and in the presence of the siderophore desferrioxamine B (DFB).

## 2 EXPERIMENTAL SECTION

**Material and Chemicals.** Seawater samples used in this work were collected on three separate research expeditions, full details can be found in the supplementary information accompanying this paper. Due to the low concentrations of Mn present in seawater, all laboratory work was performed in a trace metal clean chemistry laboratory under ISO Class 5 conditions. All reagents and seawater samples were stored in either FEP or LDPE bottles that had been extensively cleaned before use according to existing trace metal clean protocols (GEOTRACES). For shipboard work a specially designed containerized clean room (Clean Modules UK) belonging to the GEOMAR was employed. All chemicals that were used in this study were of ultrapure grade unless noted. Pipettes (Finnpipette) were calibrated monthly and trace metal clean pipette tips (Rainin RT-250 and RT-1000) were used as supplied. An inoLab pH 720 (WTW) was used to determine pH values on the NBS scale (pH<sub>NBS</sub>).

Ultrapure (UP) water (>18.2 MΩ ) was obtained in the laboratory and in the ship going clean container via a Millipore Synergy 185 system that was feed by an Elix-3 (Millipore) reverse osmosis system connected to the mains supply. Ultrapure HNO<sub>3</sub> and HCl were obtained by quartz (hereafter denoted as Q-HNO<sub>3</sub> and Q-HCl) sub-boiling distillation from analytical grade acids (Merck) in the laboratory in Kiel.

A primary 2-methy-6-(p-methoxyphenyl)-3,7-dihydroimidazol[1,2-α]pyrazin-3-one (MCLA) standard, 1 mM MCLA, was prepared by dissolving 10 mg of MCLA in 34.5 mL of MQ water; 1 mL aliquots of this solution were then pipetted into polyethylene vials and frozen at -80 °C until required for use. For the O<sub>2</sub><sup>-</sup> kinetic measurements a working MCLA standard, 1 μM, was prepared from a thawed vial of the primary stock by dilution into 1 L of UP water.

Fluorescence measurements (3D Excitation Emission Matrix) of oxyMCLA the decay product of MCLA were acquired using a Cary Eclipse fluorometer. This solution was buffered in 0.05 M sodium acetate and adjusted to  $\text{pH}_{\text{NBS}}$  of 6 with Q-HCl. Stock solutions (3.8 mM) of Diethylenetriaminepentaaceticacid (DTPA) were prepared by dissolving 0.6 g in 400 mL MQ water. All plasticware used in this work was extensively acid cleaned before use. Stock solutions (10 mM) of desferrioxamine B (DFB) were prepared by dissolving the mesylate salt (Sigma-Aldrich) directly in UP water.

**Synthesis and spectrophotometric determination of Mn(III) complexes:** Mn(III)acetate was purchased directly from Sigma Aldrich. A 10  $\mu\text{M}$  standard was prepared in ethanol to prevent dismutation. Mn(III)DFB was prepared by aerial oxidation of a solution containing 200  $\mu\text{M}$  Mn(II) and 400  $\mu\text{M}$  DFB in seawater. The pH of the solution was adjusted by the addition of 1 M sodium hydroxide (NaOH) (prepared from ultrapure NaOH pellets). The concentration of Mn(III)DFB was assessed by monitoring the absorbance at 310 nm ( $\epsilon = 2060 \pm 20 \text{ M}^{-1} \text{ cm}^{-1}$ )<sup>40</sup> using a Horiba Aqualog (1 cm cell) or with a 1 m LWCC-2100 (100 cm) pathlength liquid waveguide cell (World Precision Instruments, Sarasota, FL, USA) and an Ocean Optics USB4000 UV-VIS spectrophotometer in combination with an Ocean Optics DT-MINI-2-GS light source.

**Procedure to determine  $\text{O}_2^-$  reactivity in Seawater:** An aliquot of 20 mL of seawater was pipetted accurately into a Teflon bottle. The procedures were adapted as accordingly to our earlier work using  $\text{KO}_2$  as the  $\text{O}_2^-$  source<sup>41</sup>. Analysis of the loss rates was evaluated according to existing protocols<sup>42, 43</sup>.

**Dissolved  $\text{O}_2$  measurements:** Dissolved  $\text{O}_2$  was measured using an optode (Planar Oxygen-Sensitive Spot, SP-PSt3-NAU-D5-YOP, PreSens Precision Sensing GmbH) attached via silicon glue to the inside of a clear glass BOD bottle fitted with a glass stopper. The optode was illuminated by a fiber optic connected to a Fibox 3 (Fiber optic oxygen transmitter, PreSens Precision Sensing GmbH) equipped with a PT1000 temperature probe. The fiber optic was attached directly opposite the optode on the outside of the BOD bottle. Calibration was performed according to the manufacturer's instructions.

**$\text{H}_2\text{O}_2$  measurements:** Samples for  $\text{H}_2\text{O}_2$  were analysed directly using a flow injection chemiluminescence (FIA-CL) reagent injection method<sup>44</sup> as described previously<sup>45</sup>. Samples were analysed using 5 replicates: typical precision was 2 - 3 % through the concentration range 0.5 - 100 nM, the detection limit (3 s) is typically 0.2 nM.

### 3 RESULTS & DISCUSSION

The decay of an excess of a  $O_2^-$  in seawater amended with inorganic Mn(II) results in an increase in an apparent first order loss rate of  $O_2^-$  that increases linearly in proportion to Mn additions (Figure 1) as observed recently in other studies<sup>32, 39</sup>.

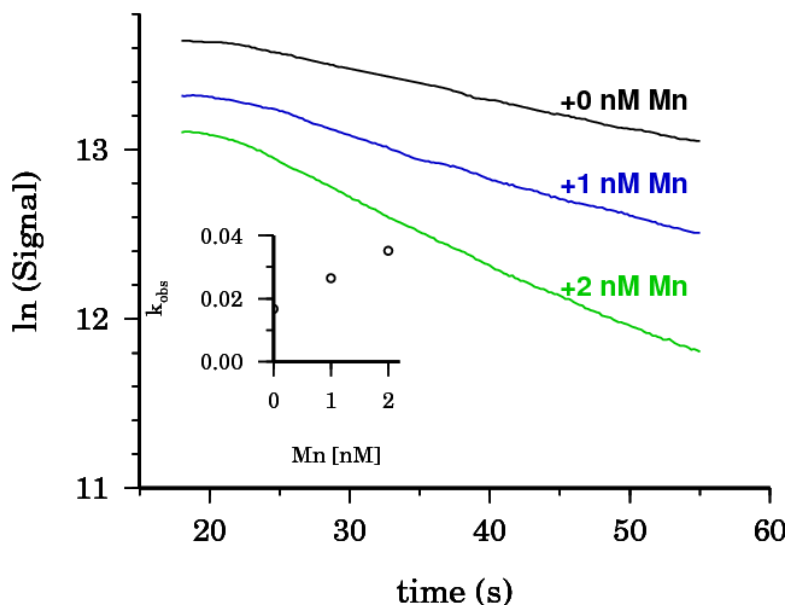
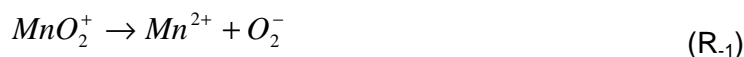


Figure 1: Mn reactivity 400m sample Station 4 M80 insert  $k_{\text{obs}}$  vs Mn concentration.

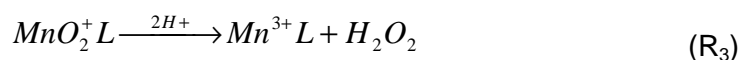
The apparent first order catalytic reaction rate,  $k_{\text{Mn}}$ , for Mn in the Eastern Tropical North Atlantic Ocean (ETNA) was found to be relatively constant  $\log k_{\text{Mn}} = 7.29 \pm 0.26$  ( $n = 35$ )<sup>39</sup>. Recently Hansard *et al.*<sup>32</sup> suggested that Mn can act as a catalytic SOD for  $O_2^-$  in seawater in the same manner as the Cu and Fe redox cycles<sup>42, 43</sup> with the formation of Mn(III) as part of the redox cycle<sup>32</sup>. However the presence of Mn(III) contrasts with the recent analysis by Barnese and colleagues<sup>33, 34</sup>, who found Mn(III) is only formed through reaction with  $O_2^-$  in the presence of strong Mn(III) stabilizing ligands (e.g. pyrophosphate and citrate) in a *non-catalytic stoichiometric* reaction that also produces  $H_2O_2$  but not  $O_2$ . In contrast the catalytic reaction is found with weak ligands (e.g. carbonate and phosphate) and involves a  $MnO_2^+$  intermediate, with no Mn(III) formation and the formation of  $H_2O_2$  and  $O_2$ . In this context the  $MnO_2^+$  species is interpreted as a manganous superoxide complex and not the alternative manganic peroxide species<sup>35, 46, 47</sup>. Thus it appears that the SOD behaviour of Mn in seawater must be achieved through the non redox Mn(II)/ $MnO_2^+$  pair.

## Reaction Modelling: Mn(II)/Mn(III) or Mn(II)/MnO<sub>2</sub><sup>+</sup> in the catalytic decomposition of O<sub>2</sub><sup>-</sup> in seawater.

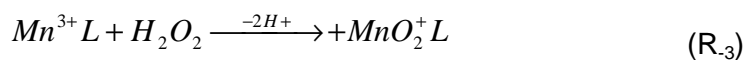
Previous studies<sup>33-35, 46-48</sup> have indicated that the initial reaction of O<sub>2</sub><sup>-</sup> with free Mn(II) is rapid (1.5 x 10<sup>8</sup> M<sup>-1</sup> s<sup>-1</sup>) and reversible, forming MnO<sub>2</sub><sup>+</sup>, the back reaction step is slower (6.5 x 10<sup>3</sup> s<sup>-1</sup> for aquo ion, 7 s<sup>-1</sup> for HCO<sub>3</sub><sup>-</sup> complex)



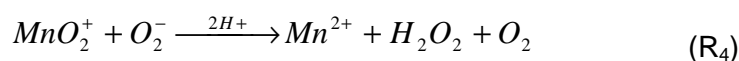
In the presence of a strong Mn(III) coordinating ligand the following reactions can also proceed, resulting in the stoichiometric production of H<sub>2</sub>O<sub>2</sub>:



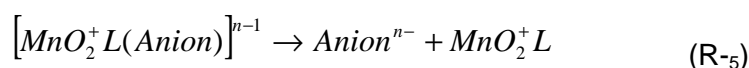
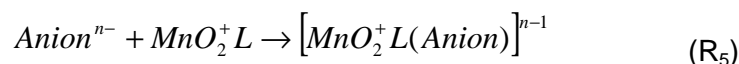
Strong Mn(III) complexes (e.g. pyrophosphate) apparently do not react with O<sub>2</sub><sup>-</sup><sup>34</sup>. However it is important to note the reaction 3 may also be reversible (see below).



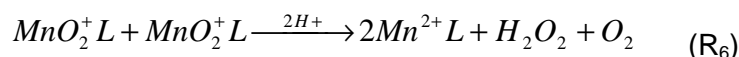
In the absence of a Mn(III) stabilizing ligand Jacobsen *et al.*<sup>48</sup> proposed that the reactions proceed according to R<sub>4</sub> (1.1 x 10<sup>6</sup> M<sup>-1</sup> s<sup>-1</sup>) forming a catalytic cycle with R<sub>1</sub> with a yield of 0.5 H<sub>2</sub>O<sub>2</sub> and O<sub>2</sub> per O<sub>2</sub><sup>-</sup>:



Barnese *et al.*<sup>34</sup> ruled out R<sub>4</sub> from their analysis due to consideration of the conditions employed in their work ([Mn(II)] > [O<sub>2</sub><sup>-</sup>]) and instead proposed the following scheme in which an additional anion reversibly binds to the MnO<sub>2</sub><sup>+</sup>L species:



The MnO<sub>2</sub><sup>+</sup>L species then can undergo dismutation to form H<sub>2</sub>O<sub>2</sub> and O<sub>2</sub>.



This overall reaction scheme suggests that for a Mn(II) complex to act as a successful SOD then  $k_1 \gg k_{-1}$  and this is satisfied with regard to the Mn(II) phosphate, citrate and carbonate complexes<sup>34</sup>. In the present work we note that at the concentrations of Mn(II) (0.2 – 5 nM) and  $O_2^-$  (~90 nM) employed in our  $KO_2$  addition experiments the reported rate constant for  $R_6$  is too slow and that  $R_4$  is a more likely pathway.

Hansard *et al.*<sup>32</sup> from their work in seawater postulated a further reaction,  $R_7$  (below) by which the Mn(III) formed via  $R_3$  reacted with  $O_2^-$  to complete a catalytic cycle that produced both  $O_2$  and  $H_2O_2$ :



The reader is referred to Table S1 for a compilation of the published rates for Mn reactions with ROS.

### **Speciation of inorganic Mn(II) in seawater and reactivity with $O_2^-$**

The speciation of inorganic Mn(II) in seawater is dominated by the free aquo ion, with smaller contributions from chloride, sulphate, and carbonate complexes<sup>17, 49</sup>. None of the complexing ligands identified as binding Mn(II) in seawater form strong Mn(III) complexing agents. See also the supplementary information for Mn speciation data in seawater. Comparing the inorganic Mn species in terms of their known reactivity with  $O_2^-$ , Barnese *et al.*<sup>34</sup> suggest that the back reaction for free Mn(II) and Mn sulphate species is sufficiently large to prevent them acting as efficient SODs (see Table S1), however if the pH is increased (>9) and  $MnCO_3$  becomes predominant the efficiency would increase due to the slower back reaction with this complex. There is no data for the  $MnCl^+$  complex with  $O_2^-$  but it may be assumed they react similarly to free Mn(II).

### **Stoichiometry of $H_2O_2$ formation from $O_2^-$ in seawater amended with Mn.**

In a further test we examined the stoichiometry of  $H_2O_2$  formation for Mn addition experiments in natural seawater in the presence of the thermal  $O_2^-$  source SOTS-1 which decays exponentially at constant temperature allowing determination of the  $O_2^-$  production rate<sup>41</sup>. Our data (Figure 2) indicates that the yields of  $H_2O_2$  were roughly half of the  $O_2^-$  reacted. In seawater samples, decay by Mn is not the only possible pathway for  $O_2^-$  decomposition<sup>39</sup>. If a Mn(III) complex is formed we would have expected a yield of 100% from the Mn pathway, which would lead to an increase in the  $H_2O_2$  yield with increasing Mn addition. In fact the opposite is observed indicating that we most likely have a catalytic SOD cycle via the intermediate  $MnO_2^+$  as proposed by Barnese *et al.*<sup>34</sup>. Thus based on the inorganic speciation of Mn(II) in seawater and the  $H_2O_2$  yield it does not appear feasible that



significant concentrations of Mn(III) are formed in seawater during reaction with  $O_2^-$ . However experiments in seawater with  $KO_2$  ( $[O_2^-] > [Mn(II)]$ ) and SOTS-1 ( $[O_2^-] < [Mn(II)]$ ) showed apparent catalytic dismutation of  $O_2^-$  and there were no obvious signs of a stoichiometric reaction between Mn(II) and  $O_2^-$ .

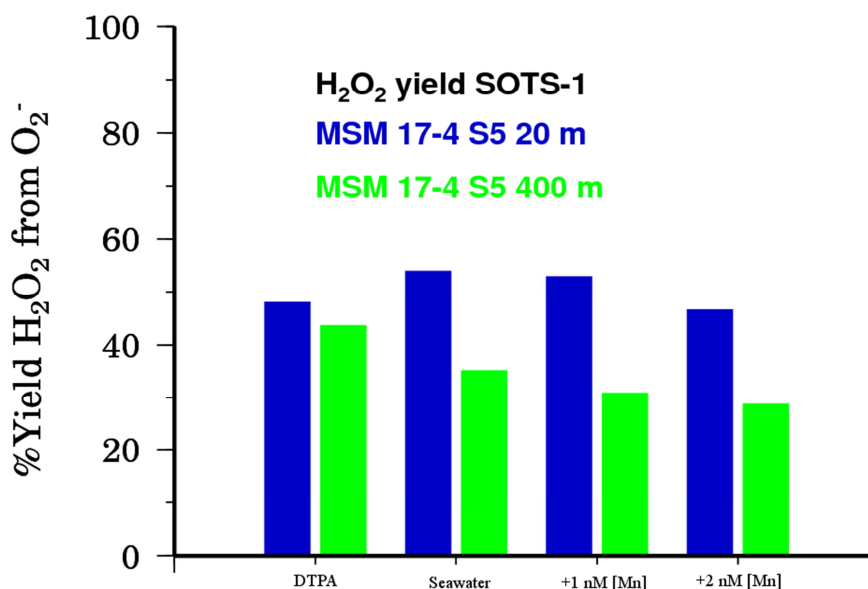
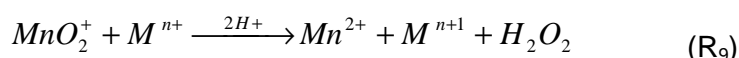
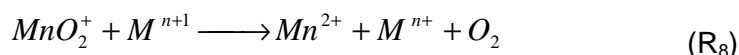


Figure 2: Yield of  $H_2O_2$  from Mn addition experiments to seawater amended with SOTS-1 as a superoxide source.

### $MnO_2^+$ reactivity with other redox species?

The predicted Mn(II) speciation in seawater appears at odds with a catalytic SOD cycle for  $O_2^-$  dismutation as earlier work had indicated that a catalytic SOD cycle was only possible with sulphate complexation, not phosphate, at Mn concentrations greater than  $100 \mu M$ <sup>35</sup>. Later however Barnese *et al.*<sup>34</sup> indicated that a catalytic SOD cycle was possible with phosphate and carbonate Mn(II) complexes. For Mn(II)/ $MnO_2^+$  to behave as a catalytic SOD in seawater and exhibit an overall first order decay, it requires that the back reaction  $k_1$  or  $k_2 \ll k_4 [O_2^-]$ . Based on the published kinetic data (Table S1) this condition is unlikely to be met under ambient seawater conditions for the inorganic Mn(II) species present in seawater as the back reaction  $k_1$  for the aquo or  $k_2$  for the sulphate complex are too fast ( $6500$  and  $8500 s^{-1}$  respectively) and steady state  $O_2^-$  concentrations too low (e.g.  $10 - 200 pM$ ) requiring a value of  $k_4$  that would be close to or above the diffusion limit. Previous workers have estimated the value of  $k_1$  or  $k_2$  by plotting  $k_{obs}$  against  $[Mn(II)]$ , for which they obtain  $k_1$  from the slope and  $k_1$  from the intercept. In the seawater case this is not a valid approach as the value of the intercept will also include contributions from other  $O_2^-$  dismutation pathways<sup>39</sup>.

One possible explanation for the apparent SOD behaviour then is that  $MnO_2^+$  is stabilized in seawater through complexation by  $Cl^-$  or other ligands present in seawater and this leads to a reduction in  $k_r$  resulting in a first order dependence on Mn(II) in the reaction. There are no previous studies reported in  $Cl^-$  media but several studies have noted an apparent rate dependence on ionic strength<sup>35, 46, 47</sup> but not to the degree that is required to stabilize  $MnO_2^+$ . In our seawater experiments we observed a mean value for  $k_{Mn} = 1.9 \times 10^7 M^{-1} s^{-1}$  which is very close to published values for the reaction of the aquo Mn(II) with  $O_2^-$  (Table S1). This suggests to us a possible mechanism by which the catalytic Mn and  $O_2^-$  cycles are completed by a reaction with another redox pair ( $M^{n+}/M^{n+1}$ ) as proposed below:



Thus the  $MnO_2^+$  is essentially reacting here similar to the free  $O_2^-$  complex. There is some precedent for this as it has been reported that  $MnO_2^+$  reacts faster with ascorbates than free  $O_2^-$ <sup>50</sup>. However we could find no other published data on the reactivity of  $MnO_2^+$  with other redox species. Our own data does show some evidence for cross reactivity between trace metal redox cycles as Figure 3 clearly shows the influence of the ambient Mn concentration on the apparent catalysis rates for  $O_2^-$  reactions with Cu and Fe. This is however not conclusive proof, as Mn while is not organically complexed in seawater, both Cu and Fe are extensively so, and this may simply reflect a common dependence on depth for the  $O_2^-$  reactive complexes of these metals.

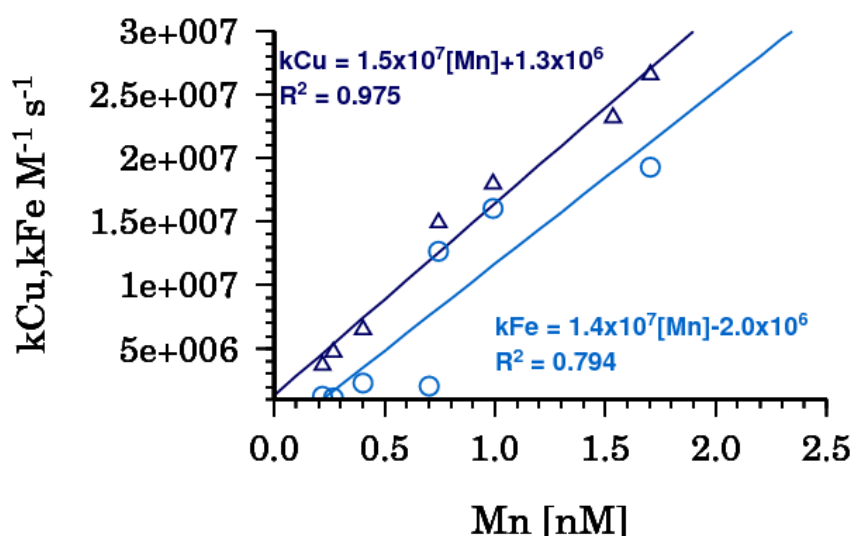


Figure 3:  $O_2^-$  reaction kinetics versus the ambient Mn concentration in seawater.

### Reactivity of simple Mn(III) complexes with $O_2^-$

The stoichiometric response seen upon the reaction of  $O_2^-$  with Mn(II) to form Mn(III) complexes of pyrophosphate or citrate strongly indicates that these Mn(III) complexes do not react significantly with  $O_2^-$ <sup>34</sup>. This suggests that stabilization of Mn(III) by complexation may lead to lower reactivity with  $O_2^-$  and thus it is unlikely that Mn(III) plays a role in the catalytic reaction observed here in seawater. Published rates for the reaction of  $O_2^-$  with Mn(III) complexes of EDTA ( $k = 5 \times 10^4 \text{ M}^{-1} \text{ s}^{-1}$ ) and CDTA ( $k = 1 \times 10^6 \text{ M}^{-1} \text{ s}^{-1}$ ) indicate that this reaction is significantly slower than that required here for a catalytic cycle and importantly it appears that the  $e^-$  exchange is not with Mn(III) but with the complexing ligand<sup>51</sup>.

### Formation of Mn(III) complexes in ambient seawater

Strong Mn(III) binding ligands however do exist in seawater, e.g. hydroxamate siderophores<sup>36</sup>, probably as Fe(III) ligands, but are only present at < 20 pM in the ETNA<sup>52</sup>. The paradigm of no Mn organic complexes in seawater has to date not been extensively tested owing to the analytical challenge of determining pM organic complexes in a total pool of nM inorganic Mn. However work by Mackey<sup>53</sup> did suggest that Mn organic complexes in seawater exist and can be retained on hydrophobic C18 columns. No data exists for Mn(III) complexes with humic matter, however in the present context, potential candidates are Mn porphyrins which can act as SOD mimics  $k_{\text{cat}} \sim 10^7 \text{ M}^{-1} \text{ s}^{-1}$ <sup>3, 54, 55</sup>.

### Formation and speciation of Mn(III)DFB in seawater

It is previously been shown in NaCl solutions (0.1 M) that the rate of formation of MnHDFB<sup>+</sup> from the aerial oxidation of Mn(II)-DFB species is related to the presence of [MnHDFB<sup>0</sup>] (rate =  $k[\text{Mn(II)DFB}][\text{O}_2]$ , pH 7.9,  $k = 0.15 \pm 0.02 \text{ M}^{-1} \text{ s}^{-1}$ ; pH 8.1  $k = 0.29 \pm 0.03 \text{ M}^{-1} \text{ s}^{-1}$ ; pH 8.6  $k = 0.34 \pm 0.07 \text{ M}^{-1} \text{ s}^{-1}$ )<sup>40</sup>. In seawater DFB is also complexed by  $\text{Ca}^{2+}$  and  $\text{Mg}^{2+}$  resulting in a substantial lowering of the effective conditional stability constant for the Mn(II)DFB species (see Table S3). Indeed the presence of 2 nM DFB in seawater leads to less than  $1 \times 10^{-4}$  of the total Mn being in the form of [MnHDFB<sup>0</sup>] (Figure S1). Thus the formation of MnHDFB<sup>+</sup> in seawater is potentially limited by the non-formation of the precursor MnHDFB<sup>0</sup> complex. Indeed for typical surface seawater at pH 8.2, only at levels above 200  $\mu\text{M}$  DFB does the MnHDFB<sup>0</sup> complex become significant (Figure S2).

Our experiments at pH 8.6 in seawater (Figure 4) amended with 400  $\mu\text{M}$  DFB had an initial formation rate of  $0.177 \pm 0.025 \text{ M}^{-1} \text{ s}^{-1}$  (95 % confidence interval), or approximately half the rate observed in 0.1 M NaCl<sup>40</sup>, consistent with the speciation in seawater under these conditions (see the SI) which indicate that ~38 % of the Mn was present as MnHDFB and ~12 % as MnH<sub>2</sub>DFB in our experiment, with the remainder as Mn inorganic species. We simultaneously observed  $\text{O}_2$  loss rates of  $25.5 \pm 0.3 \text{ nM s}^{-1}$  (95 % confidence interval) over

the first half hour. Mn(III)DFB formation rates during this time were  $12.8 \pm 1.8 \text{ nM s}^{-1}$  leading to a stoichiometry of 1:2 for MnDFB:O<sub>2</sub> when a ratio of 2:1 might be predicted from a balanced 2e<sup>-</sup> redox reaction:

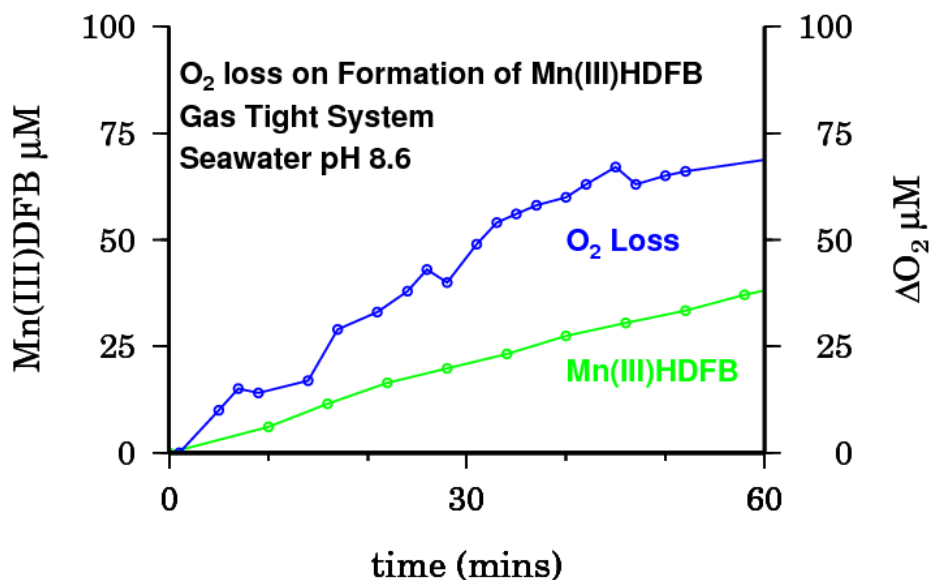
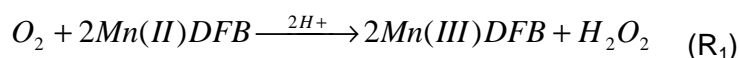


Figure 4: Formation of Mn(III)HDFB (green circles) in seawater and loss of O<sub>2</sub> (blue circles). Conditions: 200 mM Mn(II), 400 mM DFB, in seawater adjusted to pH 8.6.

This strongly suggests that the O<sub>2</sub><sup>-</sup> formed from the initial 1e<sup>-</sup> reduction of O<sub>2</sub> was also reacting with other redox species present in seawater resulting in a decreased MnDFB:O<sub>2</sub> stoichiometry, as presumably the O<sub>2</sub><sup>-</sup> oxidation of Mn(II)DFB was reduced due to the reduction of O<sub>2</sub><sup>-</sup> from these other reactions.

Electrochemical studies of Mn(III)DFB have found that the reduction wave is irreversible<sup>56</sup> though formal potentials have been estimated (pH 9.2, I = 0.1 M, 25 °C 176 mV (NHE)<sup>40</sup>; pH 9.5, I = 0.2 M, 0.47 V (NHE)<sup>38</sup>). Interestingly these studies conflict with studies in suboxic water where the reduction potential was reported to be -0.946 V (NHE)<sup>30</sup> close to the direct reduction of DFB itself -1.096 V (NHE). Thus in the latter case it is more likely to be a ligand centered reduction of the Mn(II)DFB that is observed.

We can use the formal potential for Mn(III)DFB + e<sup>-</sup> to examine if the reactions between the ROS species and Mn(II/III)DFB are thermodynamically feasible (Figures S3-S5). This type of analysis indicates that the oxidation of Mn(HDFB)<sup>0</sup> by O<sub>2</sub> should not occur spontaneously given the published formal potentials, however the conversion reaction between O<sub>2</sub><sup>-</sup> and Mn(HDFB)<sup>+</sup> should proceed. Based on the Nernst equation, the spontaneous oxidation of a

Mn(II) complex by  $O_2$  to the equivalent Mn(III) species requires a ligand that significantly stabilizes Mn(III) over Mn(II).

### **Mn(III)DFB – Catalytic or Stoichiometric reaction with $O_2^-$ ?**

Darr *et al.*<sup>57</sup> first reported the SOD properties of the complex formed from the reaction of  $MnO_2$  and DFB, a related study assessed its ability to protect a unicellular green alga from paraquat toxicity<sup>58</sup>. Beyer and Fridovich<sup>59</sup> reported the formation of a green Mn(III)DFB complex from the aerial oxidation of Mn(II) and DFB, they noted that the complex did not form in the absence of  $O_2$ . They were however able to produce the same green complex from a mixture of DFB with  $Mn(OH)_3$  produced by the Winkler method<sup>60</sup>. They also observed that Mn(III)DFB slowly decomposed to Mn(II) and  $MnO_2$ . A pink Mn(III)DFB has also been reported<sup>59</sup> after reacting DFB with  $MnO_2$  in the presence of ascorbate. Other studies have found the pink complex hard to prepare with reports of it converting to the green form upon isolation<sup>61</sup>.

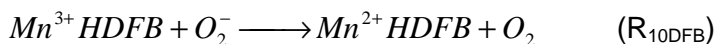
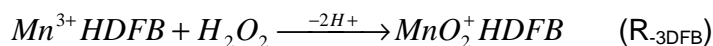
Initial studies with the green complex formed from aerial oxidation of Mn(II) with DFB suggested that the complex was a Mn(IV)DFB and it was oligomeric in solution<sup>62</sup>. Faulkner *et al.*<sup>56</sup> undertook a more extensive characterization of the green MnDFB complex and their results strongly indicated it was a 1:1 complex of Mn(III) with DFB. They also indicated that the Mn(III)DFB complex did exhibit SOD activity ( $k = 1 \times 10^6 \text{ s}^{-1}$ ), in contrast with the summary of earlier work by Gray and Carmichael<sup>63</sup> which suggested the SOD was due to Mn(II) released from the complex. Faulkner *et al.*<sup>56</sup> also found that the Mn(III) complex formed with a related siderophore, desferrioxamine E, was more resistant to exchange with EDTA than with DFB and was less reactive towards  $O_2^-$  ( $k = 9.5 \times 10^4 \text{ s}^{-1}$ ) based on the cytochrome c SOD assay.

Weiss *et al.*<sup>64</sup> studied the reactivity of Mn(II) and Mn complexes of DFB with  $O_2^-$  using stopped-flow analysis (HEPES buffer) and found that they had no detectable SOD activity ( $k_{\text{cat}} < 10^{5.5} \text{ M}^{-1} \text{ s}^{-1}$ ) using this approach. They did find however that MnDFB complexes did inhibit the reduction of cytochrome c by  $O_2^-$  generated by the xanthine/xanthine oxidase assay. These authors ascribed the inhibitory effects of MnDFB in the cytochrome c assay as being due to *stoichiometric*, not catalytic, reactions with  $O_2^-$  as had also been noted by Gray and Carmichael<sup>63</sup>. Our own work in seawater (Figures S7 and S8) found contradictory evidence for the kinetics of the reaction of  $O_2^-$  with  $Mn(HFDB)^+$  utilizing MCLA chemiluminescence. At nM levels of  $Mn(HFDB)^+$  (Figure S7) we found that the addition of  $KO_2$  lead to a quasi-stable signal, lacking the usual first order decay (e.g. as in Figure 1) that was proportional to the  $Mn(HFDB)^+$  concentrations but in excess of the added  $KO_2$  suggesting production of  $O_2^-$ . A potential source of this  $O_2^-$  could be from reaction between  $Mn(HFDB)^+$  and  $H_2O_2$  produced from the dismutation of the  $O_2^-$ . However with  $\mu\text{M}$

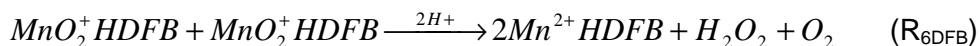
concentrations of  $\text{Mn}(\text{HFDB})^+$  a weak first order loss rate dependent on  $\text{Mn}(\text{HFDB})^+$  was observed (Figure S8) in line with earlier results suggesting a stoichiometric reaction<sup>63, 64</sup>. Earlier Faulkner *et al.*<sup>56</sup> observed that  $\text{Mn}(\text{II})$  was released from the related  $\text{Mn}(\text{III})$ -desferrioxmaine E complex after reaction with  $\text{O}_2^-$ , and based on the weak stability of the  $\text{Mn}(\text{II})\text{DFB}$  complex in seawater we would also predict that this occurs and prevents the reoxidation back to the  $\text{Mn}(\text{HFDB})^+$  complex. Additionally Hahn *et al.*<sup>65</sup> found that  $\text{Mn}(\text{HFDB})^+$  was able to rapidly oxidize  $\text{Fe}(\text{II})$  and  $\text{Cu}(\text{I})$  bound to DNA with the  $\text{Mn}(\text{II})$  formed lost from the DFB complex, which subsequently bound the oxidized  $\text{Fe}$  or  $\text{Cu}$ . This finding then would place limits on the existence of  $\text{Mn}(\text{HFDB})^+$  in suboxic waters with elevated  $\text{Fe}(\text{II})$  levels such as the Peruvian oxygen minimum zone<sup>66</sup>.

### Production of $\text{O}_2^-$ in reaction of $\text{Mn}(\text{III})\text{HDFB}$ with $\text{H}_2\text{O}_2$

Further experiments with MCLA indicated that  $\text{O}_2^-$  was formed in the presence of  $\text{Mn}(\text{HFDB})^+$  and an excess of  $\text{H}_2\text{O}_2$  (Figure S9) as MCLA was rapidly converted to the fluorescent product OxyMCLA<sup>67</sup>. MCLA reacts rapidly with both  $\text{O}_2^-$  ( $2.54 \times 10^8 \text{ M}^{-1} \text{ s}^{-1}$ <sup>68</sup>) and  $^1\text{O}_2$  ( $2.94 \times 10^9 \text{ M}^{-1} \text{ s}^{-1}$ <sup>69</sup>). In the present case the most likely reaction is thought to be the formation of a  $\text{Mn}(\text{III})$ -peroxy complex that undergoes an internal transition to form the  $\text{Mn}(\text{II})$ -superoxide complex analogous to  $\text{MnO}_2^+$ . This is based on previous work on the  $\text{Mn}(\text{III})$ -CyDTA complex which was found to react with  $\text{H}_2\text{O}_2$  with an overall 2:1 stoichiometry to give  $\text{Mn}(\text{II})$ -CyDTA and  $\text{O}_2$ <sup>70</sup>.  $\text{O}_2^-$  was an intermediate product of the reaction. Thus the following reaction scheme may apply (based on Jones and Hamm):



In addition to the reactions outlined by Jones and Hamm a further reaction is identified:



As noted above reaction  $\text{R}_{10\text{DFB}}$  is apparently very slow as the  $\text{Mn}(\text{HFDB})^+$  complex does not react rapidly with  $\text{O}_2^-$  analogous to the pyrophosphate and citrate complexes. Thus  $\text{O}_2$  is most likely formed through reaction  $\text{R}_{6\text{DFB}}$  or the self dismutation reaction. A similar reaction ( $\text{R}_{-3}$ ) was proposed for  $\text{Mn}(\text{III})$  with  $\text{H}_2\text{O}_2$ <sup>71</sup> and it was found that the rate increased as a function of pH (at pH 5.2,  $k_3 = 1.1 \times 10^5 \text{ M}^{-1} \text{ s}^{-1}$ ) in line with the increased reactivity of  $\text{Mn}(\text{OH})_n^{(3-n)+}$  analogous to increased reactivity of  $\text{Fe}(\text{III})$  hydroxy complexes due to faster water exchange rates with greater hydroxide complexation<sup>72</sup>. The production of  $\text{HO}_2$  has been suggested previously for the reaction of aquo  $\text{Mn}(\text{III})$  and  $\text{H}_2\text{O}_2$  in acid<sup>73</sup>, though a later

study indicated that  $O_2$  was formed without the apparent formation of  $O_2^-$  and suggested that  $MnO_2^+$  was formed instead<sup>74</sup>.

### **Catalase activity of Mn(III)DFB reactivity with $H_2O_2$**

Many Mn complexes are well known to act as both SODs and catalases, most notably the Salen based ligands<sup>75, 76</sup>. The production of  $O_2$  in the reaction of  $Mn(HDFB)^+$  with excess  $H_2O_2$  in seawater (Figure S10) was kinetically slow ( $k_{O_2} = 2 \pm 0.2 M^{-1} s^{-1}$ ). At high  $H_2O_2$  concentrations the solution eventually went clear indicating the decomposition of DFB (Figure 5). However it is difficult to quantify this loss spectrophotometrically as the decomposition products of DFB also complex Mn(III) and absorb in the same wavelength range. In these experiments we also saw no evidence of  $MnO_2$  formation. The lack of  $MnO_2$  formation is important, as it is well known that the reaction of  $MnO_2$  with  $H_2O_2$  produces  $O_2^-$  and  $O_2$  but not  $^1O_2$  or OH radicals<sup>77, 78</sup>.

Stadtman<sup>79</sup> had previously reported that DFB in the presence of Mn(II) and mM  $HCO_3^-$  stimulated the decomposition of  $H_2O_2$ , resulting in  $O_2$  evolution, though they made no reference to the potential role of  $Mn(HDFB)^+$ . In our own work we found no evidence for the oxidation of Mn(II)DFB to  $Mn(HDFB)^+$  in seawater by mM  $H_2O_2$  in the absence of  $O_2$  (data not shown). In seawater with lower concentrations of  $H_2O_2$  (Figure S11) it could be clearly observed that  $O_2$  consumption was also taking place indicating reactions with other organic molecules as the re-oxidation of Mn(II) to  $Mn(HDFB)^+$  in the presence of an excess of DFB would be too slow at this  $O_2$  concentration.

### **Existence of Mn(III) in the photic zone**

Our results indicate that given our current understanding of Mn redox chemistry in seawater it is unlikely that significant concentrations of Mn(III) complexes form in the photic zone of the ocean due to the combination of a lack of suitable ligands to stabilize Mn(III) combined with the reactivity of Mn(III) species with ROS. However our work has shown the complexity and interlinkages between Mn redox species and ROS in the ocean and how unravelling these reactions will lead to improved modelling of both pathways of ROS formation and destruction in the ocean and the residence time of Mn in the upper ocean.

## ACKNOWLEDGMENTS

We sincerely thank the officers and crew of the research vessels Meteor and Maria S. Merian for their help at sea. This study was financially supported by grants to PLC from the DFG (CR145/17-1 & SFB754) and BMBF. This work is a contribution of the Sonderforschungsbereich 754 "Climate – Biogeochemistry Interactions in the Tropical Ocean" ([www.sfb754.de](http://www.sfb754.de)). This work was supported by the BMBF Verbundprojekt SOPRAN (IG03) and forms part of the German contribution to SOLAS (Surface Ocean Lower Atmosphere Studies).

### Supporting Information Available

Full details of Station Locations and the experimental setup and related analysis methods are supplied as supplementary information. This information is available free of charge via the Internet at <http://pubs.acs.org>.



## REFERENCES

1. McEvoy, J. P.; Brudvig, G. W., Water-Splitting Chemistry of Photosystem II. *Chemical Reviews* **2006**, *106*, (11), 4455-4483.
2. Armstrong, F. A., Why did Nature choose manganese to make oxygen? *Philosophical Transactions of the Royal Society B: Biological Sciences* **2008**, *363*, (1494), 1263-1270.
3. Batinic-Haberle, I.; Reboucas, J. S.; Spasojevic, I., Superoxide Dismutase Mimics: Chemistry, Pharmacology, and Therapeutic Potential. *Antioxidants & Redox Signaling* **2010**, *13*, (6), 877-918.
4. Brand, L. E.; Sunda, W. G.; Guillard, R. R. L., Limitation of marine phytoplankton reproductive rates by zinc, manganese and iron. *Limnol. Oceanogr.* **1983**, *28*, 1182-1198.
5. Coale, K. H., Effects of Iron, Manganese, Copper, and Zinc Enrichments on Productivity and Biomass in the Sub-Arctic Pacific. *Limnol. Oceanogr.* **1991**, *36*, (8), 1851-1864.
6. Scharek, R.; van Leeuw, M. A.; de Baar, H. J. W., Responses of Southern Ocean phytoplankton to the addition of trace metals. *Deep-Sea Research Part II* **1997**, *44*, 209-228.
7. Middag, R.; de Baar, H. J. W.; Laan, P.; Cai, P. H.; van Ooijen, J. C., Dissolved manganese in the Atlantic sector of the Southern Ocean. *Deep Sea Research Part II: Topical Studies in Oceanography* **2011**, *58*, (25-26), 2661-2677.
8. Shiller, A. M., Manganese in surface waters of the Atlantic Ocean. *Geophysical Research Letters* **1997**, *24*, (12), 1495-1498.
9. Jickells, T. D., The inputs of dust derived elements to the Sargasso Sea; a synthesis. *Marine Chemistry* **1999**, *68*, 5-14.
10. Guieu, C.; Duce, R.; Arimoto, R., Dissolved input of manganese to the ocean: Aerosol source. *Journal of Geophysical Research* **1994**, *99*, 18789-18800.
11. Mendez, J.; Guieu, C.; Adkins, J., Atmospheric input of manganese and iron to the ocean: Seawater dissolution experiments with Saharan and North American dusts. *Marine Chemistry* **2010**, *120*, (1-4), 34-43.
12. Martin, J. H.; Knauer, G. A., Lateral Transport Of Mn In The Northeast Pacific Gyre Oxygen Minimum. *Nature* **1985**, *314*, (6011), 524-526.
13. Lewis, B. L.; Luther III, G. W., Processes controlling the distribution and cycling of manganese in the oxygen minimum zone of the Arabian Sea. *Deep-Sea Research II* **2000**, *47*, 1541-1561.
14. Martin, J. H.; Knauer, G. A., VERTEX: manganese transport through oxygen minima. *Earth and Planetary Science Letters* **1984**, *67*, (1), 35.
15. Martin, J. H.; Knauer, G. A., Manganese cycling in northeast Pacific waters. *Earth and Planetary Science Letters* **1980**, *51*, (2), 266-274.
16. Sunda, W. G.; Huntsman, S. A., Photoreduction of manganese oxides in seawater. *Mar. Chem.* **1994**, *46*, (1-2), 133-152.
17. Morgan, J. J., Kinetics of reaction between O<sub>2</sub> and Mn(II) species in aqueous solutions. *Geochim. Cosmochim. Acta* **2005**, *69*, (1), 35-48.
18. von Langen, P. J.; Johnson, K. S.; Coale, K. H.; Elrod, V. A., Oxidation kinetics of manganese (II) in seawater at nanomolar concentrations. *Geochim. Cosmochim. Acta* **1997**, *61*, (23), 4945-4954.
19. Davies, S. H. R.; Morgan, J. J., Manganese(II) oxidation kinetics on metal oxide surfaces. *Journal of Colloid and Interface Science* **1989**, *129*, (1), 63-77.
20. Tebo, B. M.; Bargar, J. R.; Clement, B. G.; Dick, G. J.; Murray, K. J.; Parker, D.; Verity, R.; Webb, S. M., Biogenic manganese oxides: Properties and mechanisms of formation. *Annu Rev Earth Pl Sc* **2004**, *32*, (1), 287-328.
21. Sunda, W. G.; Huntsman, S. A., Microbial oxidation of manganese in a North Carolina estuary. *Anglais* **1987**, *32*, (3), 552-564.

22. Learman, D. R.; Voelker, B. M.; Vazquez-Rodriguez, A. I.; Hansel, C. M., Formation of manganese oxides by bacterially generated superoxide. *Nature Geosci* **2011**, *4*, (2), 95-98.
23. Nico, P. S.; Anastasio, C.; Zasoski, R. J., Rapid photo-oxidation of Mn(II) mediated by humic substances. *Geochim. Cosmochim. Acta* **2002**, *66*, (23), 4047-4056.
24. Nealson, K. H.; Tebo, B. M.; Rosson, R. A.; Allen, I. L., Occurrence and Mechanisms of Microbial Oxidation of Manganese. In *Advances in Applied Microbiology*, Academic Press: 1988; Vol. Volume 33, pp 279-318.
25. Stumm, W.; Morgan, J. J., Aquatic Chemistry. *Wiley-Interscience, New York* (1996) **1996**, 1022 pp.
26. Klewicki, J. K.; Morgan, J. J., Kinetic Behavior of Mn(III) Complexes of Pyrophosphate, EDTA, and Citrate. *Environmental Science & Technology* **1998**, *32*, (19), 2916-2922.
27. Kostka, J. E.; Luther III, G. W.; Nealson, K. H., Chemical and biological reduction of Mn(III)-pyrophosphate complexes: Potential importance of dissolved Mn(III) as an environmental oxidant. *Geochim. Cosmochim. Acta* **1995**, *59*, (5), 885-894.
28. Schnetger, B.; Dellwig, O., Dissolved reactive manganese at pelagic redoxclines (part I): A method for determination based on field experiments. *Journal of Marine Systems* **2012**, *90*, (1), 23-30.
29. Luther III, G. W.; Ruppel, D. T.; Burkhard, C., Reactivity of Dissolved Mn(III) Complexes and Mn(IV) Species with Reductants: Mn Redox Chemistry Without a Dissolution Step? In *Mineral-Water Interfacial Reactions*, American Chemical Society: 1999; Vol. 715, pp 265-280.
30. Trouwborst, R. E.; Clement, B. G.; Tebo, B. M.; Glazer, B. T.; Luther, G. W., Soluble Mn(III) in suboxic zones. *Science* **2006**, *313*, (5795), 1955-1957.
31. Madison, A. S.; Tebo, B. M.; Luther III, G. W., Simultaneous determination of soluble manganese(III), manganese(II) and total manganese in natural (pore)waters. *Talanta* **2011**, *In Press, Corrected Proof*.
32. Hansard, S. P.; Easter, H. D.; Voelker, B. M., Rapid Reaction of Nanomolar Mn(II) with Superoxide Radical in Seawater and Simulated Freshwater. *Environ. Sci. Technol.* **2011**, *45*, (7), 2811-2817.
33. Barnese, K.; Gralla, E. B.; Cabelli, D. E.; Selverstone Valentine, J., Manganous Phosphate Acts as a Superoxide Dismutase. *Journal of the American Chemical Society* **2008**, *130*, (14), 4604-4606.
34. Barnese, K.; Gralla, E. B.; Valentine, J. S.; Cabelli, D. E., Biologically relevant mechanism for catalytic superoxide removal by simple manganese compounds. *Proceedings of the National Academy of Sciences* **2012**, *109*, (18), 6892-6897.
35. Cabelli, D. E.; Bielski, B. H. J., Pulse-Radiolysis Study Of The Kinetics And Mechanisms Of The Reactions Between Manganese(II) Complexes And HO<sub>2</sub>/O<sub>2</sub><sup>-</sup> Radicals .2. The Phosphate Complex And An Overview. *Journal Of Physical Chemistry* **1984**, *88*, (25), 6291-6294.
36. Duckworth, O. W.; Sposito, G., Siderophore-Manganese(III) Interactions. I. Air-Oxidation of Manganese(II) Promoted by Desferrioxamine B. *Environmental Science & Technology* **2005**, *39*, 6037-6044.
37. Harrington, J. M.; Parker, D. L.; Bargar, J. R.; Jarzecki, A. A.; Tebo, B. M.; Sposito, G.; Duckworth, O. W., Structural dependence of Mn complexation by siderophores: Donor group dependence on complex stability and reactivity. *Geochimica et Cosmochimica Acta* **2012**, *88*, (0), 106-119.
38. Szabó, O.; Farkas, E., Characterization of Mn(II) and Mn(III) binding capability of natural siderophores Desferrioxamine B and Desferricoprogen as well as model hydroxamic acids. *Inorganica Chimica Acta* **2011**, *In Press, Accepted Manuscript*.
39. Wuttig, K.; Heller, M. I.; Croot, P. L., Pathways of Superoxide (O<sub>2</sub><sup>-</sup>) decay in the Eastern Tropical North Atlantic. *submitted to Environmental Sciences and Technology* **2013**.
40. Duckworth, O. W.; Sposito, G., Siderophore-Manganese(III) Interactions. I. Air-Oxidation of Manganese(II) Promoted by Desferrioxamine B. *Environmental Science & Technology* **2005**, *39*, (16), 6037-6044.

41. Heller, M. I.; Croot, P. L., Application of a Superoxide ( $O_2^-$ ) thermal source (SOTS-1) for the determination and calibration of  $O_2^-$  fluxes in seawater. *Analytica Chimica Acta* **2010**, *667*, 1-13.
42. Heller, M. I.; Croot, P. L., Superoxide Decay Kinetics in the Southern Ocean. *Environmental Science & Technology* **2010**, *44*, (1), 191-196 DOI: 10.1021/es901766r.
43. Heller, M. I.; Croot, P. L., Superoxide decay as a probe for speciation changes during dust dissolution in Tropical Atlantic surface waters near Cape Verde. *Marine Chemistry* **2011**, *126*, (1-4), 37-55.
44. Yuan, J.; Shiller, A. M., Determination of Subnanomolar Levels of Hydrogen Peroxide in Seawater by Reagent-Injection Chemiluminescence Detection. *Analytical Chemistry* **1999**, *71*, (10), 1975-1980.
45. Croot, P. L.; Streu, P.; Peeken, I.; Lochte, K.; Baker, A. R., Influence of the ITCZ on  $H_2O_2$  in near surface waters in the equatorial Atlantic Ocean. *Geophysical Research Letters* **2004**, *31*, (23), L23S04.
46. Cabelli, D. E.; Bielski, B. H. J., Pulse-Radiolysis Study Of The Kinetics And Mechanisms Of The Reactions Between Manganese(II) Complexes And  $HO_2/O_2^-$  Radicals .1. Sulfate, Formate, And Pyrophosphate Complexes. *Journal Of Physical Chemistry* **1984**, *88*, (14), 3111-3115.
47. Pick-Kaplan, M.; Rabani, J., Pulse radiolytic studies of aqueous manganese(II) perchlorate solutions. *The Journal of Physical Chemistry* **1976**, *80*, (17), 1840-1843.
48. Jacobsen, F.; Holcman, J.; Sehested, K., Manganese(II)-Superoxide Complex in Aqueous Solution. *The Journal of Physical Chemistry A* **1997**, *101*, (7), 1324-1328.
49. Millero, F. J.; Hawke, D. J., Ionic interactions of divalent metals in natural waters. *Marine Chemistry* **1992**, *40*, (1-2), 19-48.
50. Cabelli, D. E., The interactions between  $MnO_2^+/Mn^{3+}$  complexes and ascorbates: A pulse radiolysis study. *Free Radical Biology and Medicine* **1989**, *6*, (2), 171-177.
51. Stein, J.; Fackler, J. P.; McClune, G. J.; Fee, J. A.; Chan, L. T., Superoxide and manganese(III). Reactions of manganese-EDTA and manganese-CyDTA complexes with molecular oxygen. X-ray structure of potassium manganese-EDTA.2 water. *Inorganic Chemistry* **1979**, *18*, (12), 3511-3519.
52. Mawji, E.; Gledhill, M.; Milton, J. A.; Tarran, G. A.; Ussher, S.; Thompson, A.; Wolff, G. A.; Worsfold, P. J.; Achterberg, E. P., Hydroxamate Siderophores: Occurrence and Importance in the Atlantic Ocean. *Environmental Science & Technology* **2008**, *42*, (23), 8675-8680.
53. Mackey, D. J., Metal-Organic Complexes in Seawater - an Investigation of Naturally Occurring Complexes of Cu, Zn, Fe, Mg, Ni, Cr, Mn and Cd using High-Performance Liquid Chromatography with Atomic Fluorescence Detection. *Marine Chemistry* **1983**, *13*, 169-180.
54. Faulkner, K. M.; Liochev, S. I.; Fridovich, I., Stable Mn(III) porphyrins mimic superoxide dismutase in vitro and substitute for it in vivo. *Journal of Biological Chemistry* **1994**, *269*, (38), 23471-23476.
55. Friedel, F. C.; Lieb, D.; Ivanović-Burmazović, I., Comparative studies on manganese-based SOD mimetics, including the phosphate effect, by using global spectral analysis. *Journal of Inorganic Biochemistry* **2012**, *109*, (0), 26-32.
56. Faulkner, K. M.; Stevens, R. D.; Fridovich, I., Characterization of Mn(III) Complexes of Linear and Cyclic Desferrioxamines as Mimics of Superoxide Dismutase Activity. *Archives of Biochemistry and Biophysics* **1994**, *310*, (2), 341-346.
57. Darr, D.; Zarilla, K. A.; Fridovich, I., A mimic of superoxide dismutase activity based upon desferrioxamine B and manganese(IV). *Archives of Biochemistry and Biophysics* **1987**, *258*, (2), 351.
58. Rabinowitch, H. D.; Privalle, C. T.; Fridovich, I., Effects of paraquat on the green alga *Dunaliella salina*: Protection by the mimic of superoxide dismutase, desferal-Mn(IV). *Free Radical Biology and Medicine* **1987**, *3*, (2), 125-131.

59. Beyer, W. F.; Fridovich, I., Characterization of a superoxide dismutase mimic prepared from desferrioxamine and MnO<sub>2</sub>. *Archives of Biochemistry and Biophysics* **1989**, *271*, (1), 149.
60. Winkler, L. W., Die Löslichkeit der Gase in Wasser. [Dritte Abhandlung]. *Berichte der deutschen chemischen Gesellschaft* **1901**, *34*, (2), 1408-1422.
61. Samuni, A.; Mitchel, J. B.; Degraff, W.; Krishna, C. M.; Samuni, U.; Russo, A., Nitroxide Sod-Mimics: Modes of Action. *Free Radical Research* **1991**, *12*, (1), 187-194.
62. Rush, J. D.; Maskos, Z.; Koppenol, W. H., The superoxide dismutase activities of two higher-valent manganese complexes, MnIV desferrioxamine and MnIII cyclam. *Archives of Biochemistry and Biophysics* **1991**, *289*, (1), 97-102.
63. Gray, B.; Carmichael, A. J., Kinetics of superoxide scavenging by dismutase enzymes and manganese mimics determined by electron spin resonance. *Biochem. J.* **1992**, *281*, (3), 795-802.
64. Weiss, R. H.; Flickinger, A. G.; Rivers, W. J.; Hardy, M. M.; Aston, K. W.; Ryan, U. S.; Riley, D. P., Evaluation of activity of putative superoxide dismutase mimics. Direct analysis by stopped-flow kinetics. *Journal Of Biological Chemistry* **1993**, *268*, (31), 23049-54.
65. Hahn, S. M.; Krishna, C. M.; Samuni, A.; Mitchell, J. B.; Russo, A., Mn(III)-desferrioxamine superoxide dismutase-mimic: Alternative modes of action. *Archives of Biochemistry and Biophysics* **1991**, *288*, (1), 215-219.
66. Hong, H.; Kester, D. R., Redox state of iron in offshore waters of Peru. *Limnol. Oceanogr.* **1986**, *31*, 512-524.
67. Kambayashi, Y.; Ogino, K., Reestimation of Cypridina Luciferin Analogs (MCLA) as a Chemiluminescence Probe to detect active oxygen species-Cautionary note for use of MCLA. *The Journal of Toxicological Sciences* **2003**, *28*, (3), 139.
68. Suzuki, N.; Suetsuna, K.; Mashiko, S.; Yoda, B.; Nomoto, T.; Toya, Y.; Inaba, H.; Goto, T., Reaction-Rates For The Chemiluminescence Of Cypridina Luciferin Analogs With Superoxide - A Quenching Experiment With Superoxide-Dismutase. *Agricultural And Biological Chemistry* **1991**, *55*, (1), 157-160.
69. Suzuki, N.; Mizumoto, I.; Toya, Y.; Nomoto, T.; Mashiko, S.; Inaba, H., Steady-State Near-Infrared Detection Of Singlet Molecular-Oxygen - A Stern-Volmer Quenching Experiment With Luminol, Superoxide-Dismutase, And Cypridina Luciferin Analogs. *Agricultural And Biological Chemistry* **1990**, *54*, (11), 2783-2787.
70. Jones, T. E.; Hamm, R. E., Kinetics of the reaction between 1,2-diaminocyclohexanetetraacetatomanganate(III) ion and hydrogen peroxide. *Inorganic Chemistry* **1974**, *13*, (8), 1940-1943.
71. Jacobsen, F.; Holcman, J.; Sehested, K., Oxidation of manganese(II) by ozone and reduction of manganese(III) by hydrogen peroxide in acidic solution. *International Journal Of Chemical Kinetics* **1998**, *30*, (3), 207-214.
72. Hudson, R. J. M.; Covault, D. T.; Morel, F. M. M., Investigations of iron coordination and redox reactions in seawater using <sup>59</sup>Fe radiometry and ion-pair solvent extraction of amphiphilic iron complexes. *Marine Chemistry* **1992**, *38*, 209-235.
73. Wells, C. F.; Mays, D., The kinetics of the reaction of aquomanganese(III) ions with hydrogen peroxide in perchlorate media. *Journal of the Chemical Society A: Inorganic, Physical, Theoretical* **1968**, 665-667.
74. Archibald, F. S.; Fridovich, I., The scavenging of superoxide radical by manganous complexes: In vitro. *Archives of Biochemistry and Biophysics* **1982**, *214*, (2), 452-463.
75. Abashkin, Y. G.; Burt, S. K., (salen)Mn(III) Compounds as Nonpeptidyl Mimics of Catalase. Mechanism-Based Tuning of Catalase Activity: A Theoretical Study. *Inorganic Chemistry* **2005**, *44*, (5), 1425-1432.
76. Baudry, M.; Etienne, S.; Bruce, A.; Palucki, M.; Jacobsen, E.; Malfroy, B., Salen-Manganese Complexes Are Superoxide Dismutase-Mimics. *Biochemical and Biophysical Research Communications* **1993**, *192*, (2), 964-968.

77. Furman, O.; Laine, D. F.; Blumenfeld, A.; Teel, A. L.; Shimizu, K.; Cheng, I. F.; Watts, R. J., Enhanced Reactivity of Superoxide in Water–Solid Matrices. *Environmental Science & Technology* **2009**, *43*, (5), 1528-1533.
78. Watts, R. J.; Sarasa, J.; Loge, F. J.; Teel, A. L., Oxidative and Reductive Pathways in Manganese-Catalyzed Fenton's Reactions. *Journal of Environmental Engineering* **2005**, *131*, (1), 158-164.
79. Stadtman, E. R.; Berlett, B. S.; Chock, P. B., Manganese-Dependent Disproportionation Of Hydrogen-Peroxide In Bicarbonate Buffer. *Proceedings Of The National Academy Of Sciences Of The United States Of America* **1990**, *87*, (1), 384-388.

## Supporting Information

To accompany the manuscript entitled

# Reactivity of inorganic Mn and Mn Desferrioxamine B with $O_2$ , $O_2^-$ and $H_2O_2$ in seawater

Kathrin Wuttig, Maija I. Heller and Peter L. Croot

Comprising :

30 Pages

3 Tables

11 Figures

**Supplementary Information:**

**Cautionary Tales for comparing  $O_2^-$  decay rates:** The published literature for the reactivity of Mn complexes with  $O_2^-$  is littered with apparently contradictory results, some of which is related to the choice of buffer and the detection system employed<sup>1, 2</sup>. Problems may also occur through other redox reactions involving probe compounds (e.g. oxidation of ferrocyanide, reduction of nitroblue tetrazolium (NBT)). In our evaluation of the literature we also came across two other critical problems:

- (1) The frequent use of the piperazine ring containing Good's buffer<sup>3</sup> HEPES (4-(2-hydroxyethyl)-1-piperazineethanesulfonic acid) without apparent recognition that this buffer is known to react with  $O_2^-$  producing HEPES radicals<sup>4</sup>. It has also been shown that  $H_2O_2$  oxidizes HEPES<sup>5</sup>. Indeed a number of studies have recommended that HEPES should not be used for  $O_2^-$  quantification<sup>6, 7</sup>.
- (2) The reporting of reaction rates for different Mn species but without consideration of the complexation effects of the buffer. In many cases where phosphate buffers have been used results are interpreted in terms of a synergistic effect of phosphate on the rates however a closer examination of the Mn speciation may reveal it is simply the reactivity of the Mn phosphate complexes in solution.

**Seawater sampling**

**Sampling Stations.** The seawater used in this study was collected during three research expeditions with the German research vessels RV Meteor and RV Maria S. Merian. The first cruise was performed in the Eastern Tropical North Atlantic (ETNA) during M83/1 (Las Palmas, Gran Canaria, Spain – Mindelo, Cape Verde), from 14 October to 13 November 2010. The second expedition took place in the ETNA during MSM17/4 (Dakar, Senegal to Las Palmas, Spain) from 10 March to 12 April 2011. The final cruise was in the Eastern Tropical Pacific (ETP) during M90 (Colon, Panama – Callao, Peru), from 26 October to 26 November 2012.

**Field Sample collection.** All analytical work at sea was performed in an over-pressurized ISO class 5 clean container, inside of which analysts wore the appropriate clean room apparel; overalls with hood (Tyvek), shoes (Abeba) and plastic gloves (Carl Roth). Seawater samples in this work were obtained from the whole water column using modified Teflon coated PVC General Oceanics (Miami, FL, USA) GoFlo bottles of 8 L in which the original drain cock was replaced by a Teflon stop cock. These bottles were deployed on a Kevlar line from the side of the ship. Immediately upon recovery of the bottles, samples were filtered in-line through 0.2  $\mu$ m filter cartridges (Sartorius Sartobran filter capsule 5231307H5) by  $N_2$  overpressure into acid cleaned 1 L Teflon bottles (Nalgene).

**Overview of the FeLume chemiluminescence system:** This system comprises a light tight box equipped with a Plexiglas spiral flow cell mounted below a photon counter (Hamamatsu HC-135-01) linked to a laptop computer via a Bluetooth connection controlled through a purpose built Labview™ (National Instruments) virtual instrument. For  $O_2^-$  determination we ran the sample and the MCLA reagent directly into the flow cell using a peristaltic pump (Gilson Minipuls 3, operating at 18 rpm,) with the sample line being pulled through the flow cell as this leads to the smallest amount of dead time in the system (typically 2 – 3 s). The overall flow rate through the cell was  $8.25 \text{ mL min}^{-1}$ , comprising  $5.0 \text{ mL min}^{-1}$  from the MCLA and  $3.25 \text{ mL min}^{-1}$  from the sample. The transit time through the optical cell ( $300 \mu\text{L}$ ) was therefore 2.18 s. For the precision and accuracy of the method, please, see assessment in Heller and Croot<sup>8</sup>. For more information on specific calibration issues and impurities for  $O_2^-$  the reader is referred to Heller and Croot<sup>9</sup>.

**Calculation of rate data for superoxide.** The raw chemiluminescence signal for the reaction between MCLA and  $O_2^-$  recorded by the computer was processed using a specially designed Labview™ VI constructed for this purpose using standard kinetic fitting procedures to determine both the 1<sup>st</sup> ( $k_{\text{obs}}$ ) and 2<sup>nd</sup> order ( $k_2$ ) rates simultaneously. The photon counter has a base counting period of 10 ms, for the present work we used average counts of an integration time of 200 ms. Dark background counts for this detector were typically 60 - 120 counts  $\text{s}^{-1}$ . Apparent reaction rates for Mn complexes with  $O_2^-$  were calculated via linear regression of  $k_{\text{obs}}$  versus the total metal added. Using our experimental setup the minimum values for  $k_{\text{obs}}$  that we can determine is estimated at  $1 \times 10^6 \text{ mol L}^{-1} \text{ s}^{-1}$ .

**Model Calculations for  $O_2^-$  kinetics.** Numerical modeling of  $O_2^-$  reactions in seawater was performed using a fully explicit model written in C++. Rate constants for the key reactions involved were compiled from those already published in the literature (see Table S2 in our companion paper<sup>10</sup>).



**Water exchange rates for Mn(II) and Mn(III) complexes:**

Water exchange rates for the  $d^5$  Mn(II) aquo ion have been determined,  $k_{ex} = 2.1 \times 10^7 \text{ s}^{-1}$ <sup>11</sup>. Measurements for the rate of water exchange for the  $d^4$  Mn(III) aquo ion do not exist as yet, but have been recently estimated by comparison with Fe at  $k_{ex} \sim 10^2 - 10^3 \text{ s}^{-1}$ <sup>12</sup>. Ligand exchange rates for the fluoride complexation of the aquo Mn(III) ion ( $k_{ex} = 1 \times 10^4 \text{ s}^{-1}$ , 10 °C) and Mn(OH)<sup>2+</sup> ion ( $k_{ex} \sim 10^4 - 10^5 \text{ s}^{-1}$ , 10 °C) have been reported and the fast rates ascribed to a strong Jahn-Teller effect<sup>13</sup>. The water loss kinetics of Mn(OH)<sub>2</sub><sup>+</sup> and Mn(OH)<sub>3</sub> are not determined but we would predict greater rates of water exchange in which water loss rates increase as the charge to radius ratio of the metal ion decreases analogous to that for Fe(III)<sup>14</sup>. Data for Mn(III) porphyrins indicates that exchange of axial ligands is rapid  $k_{ex} = 0.4 - 2.8 \times 10^7 \text{ s}^{-1}$  due to the charge density of the metal centre and the steric decompression of the complex<sup>12</sup>.

**Reactions of O<sub>2</sub><sup>-</sup> with Mn(II) organic complexes**

There are only a limited number of published data sets on the reactions of other Mn(II) organic complexes with O<sub>2</sub><sup>-</sup><sup>15</sup>. Fisher and colleagues<sup>16</sup> using O<sub>2</sub><sup>-</sup> detection with NBT reported a value of  $k = 6 \times 10^5 \text{ M}^{-1} \text{ s}^{-1}$  for the reaction of Mn(II) EDTA with O<sub>2</sub><sup>-</sup>, while a more recent study could only place an upper bound for this reaction of  $k < 3 \times 10^5 \text{ M}^{-1} \text{ s}^{-1}$  using spectrophotometry/stopped flow<sup>1</sup>. It is noted however that other studies have found no evidence for this reaction<sup>17-20</sup>.

### Thermodynamic calculations used in Figures S3-S5

Reduction reactions for relevant oxygen and Mn reactions normalized to one electron. All species are in aqueous form except for MnOOH. Activities of all reactants other than H<sup>+</sup> are at unity.

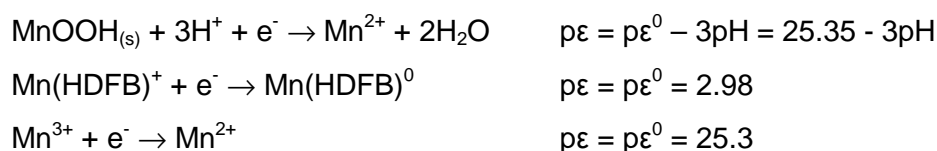
#### Oxygen Reactions

One electron transfer reactions only



#### Manganese Reactions

One electron transfer reactions only



References: Oxygen reactions <sup>21, 22</sup> MnDFB <sup>23</sup>

### Determination of required binding strength for Mn(III)L for spontaneous oxidation of Mn(II)L by O<sub>2</sub> using the Nernst equation.

$$pE^0_{\text{Mn(III)L/Mn(II)L}} = pE^0_{\text{Mn(III)/Mn(II)}} + \log \left( \frac{{}^cK_{[\text{Mn(II)L}]} }{{}^cK_{[\text{Mn(III)L}]} } \right)$$

where <sup>c</sup>K is the conditional stability constant for the complex of the form Mn<sup>n+</sup> + L<sup>m-</sup> → MnL<sup>(n-m)</sup> and pE<sup>0</sup> is the negative of the natural logarithm of the formal electron potential. pE = E / 0.059.

If ΔG < 0 for the 1 electron oxidation by O<sub>2</sub> to proceed then pE > 0 for the combination of the two 1 e<sup>-</sup> transfers, this condition is reached when pE<sup>0</sup><sub>Mn(III)L/Mn(II)L</sub> < -2.72. Then using pE = 25.3 for the Mn<sup>3+</sup> + e<sup>-</sup> → Mn<sup>2+</sup> results in log(<sup>c</sup>K<sub>[Mn(II)L] / <sup>c</sup>K<sub>[Mn(III)L]</sub>) < -28.02. Thus <sup>c</sup>K<sub>[Mn(III)L] / <sup>c</sup>K<sub>[Mn(II)L]</sub> > 10<sup>28.02</sup>.</sub></sub>

Notes: Complexation by Ca and Mg will result in the same lowering of the conditional stability constant for both Mn(II) and Mn(III) complexes if their stoichiometry is the same.

Table S1: Mn(II), Mn(III) and Mn(IV) reactivity with O<sub>2</sub>, HO<sub>2</sub>, O<sub>2</sub><sup>-</sup> and H<sub>2</sub>O<sub>2</sub>

Reactant	Products	Forward reaction $k_f$	Reverse reaction $k_r$	Ref
O <sup>2</sup> + MnOH <sup>+</sup>		$1.66 \times 10^{-2} \text{ M}^{-1} \text{ s}^{-1}$		24
O <sub>2</sub> + Mn(OH) <sub>2</sub>		$2.09 \times 10^1 \text{ M}^{-1} \text{ s}^{-1}$		24
O <sub>2</sub> + Mn(CO <sub>3</sub> ) <sub>2</sub> <sup>2-</sup>		$8.13 \times 10^{-2} \text{ M}^{-1} \text{ s}^{-1}$		24
O <sub>2</sub> + Mn <sup>(III)</sup> (Glu)	Mn(III)Glu + X	$2.8 \times 10^4 \text{ M}^{-1} \text{ s}^{-1}$		25
H <sub>2</sub> O <sub>2</sub> + Mn <sup>3+</sup>	MnO <sub>2</sub> <sup>+</sup> + 2H <sup>+</sup>	$2.8 \pm 0.3 \times 10^3 \text{ M}^{-1} \text{ s}^{-1}$		26
H <sub>2</sub> O <sub>2</sub> + Mn <sup>3+</sup>	Mn <sup>2+</sup> + HO <sub>2</sub> + H <sup>+</sup>	$2.8 \pm 0.3 \times 10^3 \text{ M}^{-1} \text{ s}^{-1}$	(see below)	27
H <sub>2</sub> O <sub>2</sub> + 2Mn <sup>3+</sup>	2Mn <sup>2+</sup> + O <sub>2</sub> + 2H <sup>+</sup>			28
H <sub>2</sub> O <sub>2</sub> + Mn <sup>(IV)</sup>	Mn <sup>2+</sup> + 2H <sup>+</sup> + O <sub>2</sub>	$k > 1 \times 10^6 \text{ M}^{-1} \text{ s}^{-1}$		27
H <sub>2</sub> O <sub>2</sub> + MnO <sub>2</sub>	Mn <sup>3+</sup> + O <sub>2</sub> <sup>-</sup> + 2H <sup>+</sup>	$7 \times 10^2 \text{ M}^{-1} \text{ s}^{-1}$		29
H <sub>2</sub> O <sub>2</sub> + Mn <sup>(III)</sup> gluconate		$2.5 \times 10^2 \text{ M}^{-1} \text{ s}^{-1}$		30
HO <sub>2</sub> + Mn <sup>2+</sup>	MnO <sub>2</sub> <sup>+</sup> + H <sup>+</sup>	$1.1 \pm 0.2 \times 10^6 \text{ M}^{-1} \text{ s}^{-1}$	$6.5 \pm 1.0 \times 10^3 \text{ M}^{-1} \text{ s}^{-1}$	26
HO <sub>2</sub> + Mn <sup>2+</sup> (Pyrophosphate)	Mn <sup>(III)</sup> Pyrophosphate + H <sub>2</sub> O <sup>-</sup>	$\sim 3 \times 10^5 \text{ M}^{-1} \text{ s}^{-1}$		31
O <sub>2</sub> <sup>-</sup> + Mn <sup>2+</sup>	MnO <sub>2</sub> <sup>+</sup>	$1.5 \pm 0.2 \times 10^8 \text{ M}^{-1} \text{ s}^{-1}$	$6.5 \pm 1.0 \times 10^3 \text{ s}^{-1}$	26
O <sub>2</sub> <sup>-</sup> + Mn <sup>2+</sup> (Sulfate)	MnO <sub>2</sub> <sup>+</sup> (Sulfate)	$4.0 \pm 0.5 \times 10^7 \text{ M}^{-1} \text{ s}^{-1}$	$8.5 \pm 2.0 \times 10^3 \text{ s}^{-1}$	26
O <sub>2</sub> <sup>-</sup> + Mn <sup>2+</sup> (Formate)	MnO <sub>2</sub> <sup>+</sup> (Formate)	$4.6 \times 10^7 \text{ M}^{-1} \text{ s}^{-1}$		32 33
O <sub>2</sub> <sup>-</sup> + Mn <sup>2+</sup> (Sulfate)	MnO <sub>2</sub> <sup>+</sup> (Sulfate)	$5.4 \times 10^7 \text{ M}^{-1} \text{ s}^{-1}$		32
O <sub>2</sub> <sup>-</sup> + Mn <sup>2+</sup> (Phosphate)	MnO <sub>2</sub> <sup>+</sup> (Phosphate)	$2.8 \times 10^7 \text{ M}^{-1} \text{ s}^{-1}$		32
O <sub>2</sub> <sup>-</sup> + Mn <sup>2+</sup> (Pyrophosphate)	Mn <sup>(III)</sup> Pyrophosphate + H <sub>2</sub> O <sup>-</sup>	$\sim 2 \times 10^7 \text{ M}^{-1} \text{ s}^{-1}$		31
O <sub>2</sub> <sup>-</sup> + Mn <sup>2+</sup> (Pyrophosphate)	MnO <sub>2</sub> <sup>+</sup> (Pyrophosphate)	$1.7 \times 10^7 \text{ M}^{-1} \text{ s}^{-1}$		32
O <sub>2</sub> <sup>-</sup> + Mn <sup>2+</sup> (Citrate)	MnO <sub>2</sub> <sup>+</sup> (Citrate)	$1.3 \times 10^7 \text{ M}^{-1} \text{ s}^{-1}$	$< 10 \text{ s}^{-1}$	34
O <sub>2</sub> <sup>-</sup> + MnHCO <sub>3</sub> <sup>+</sup>	MnO <sub>2</sub> HCO <sub>3</sub>	$1.4 \times 10^8 \text{ M}^{-1} \text{ s}^{-1}$	$7 \text{ s}^{-1}$	34
O <sub>2</sub> <sup>-</sup> + MnHPO <sub>4</sub>	MnO <sub>2</sub> (HPO <sub>4</sub> ) <sup>-</sup>	$2.3 \times 10^7 \text{ M}^{-1} \text{ s}^{-1}$	$10 \text{ s}^{-1}$	34
O <sub>2</sub> <sup>-</sup> + MnNTA		$4 \times 10^8 \text{ M}^{-1} \text{ s}^{-1}$		35
O <sub>2</sub> <sup>-</sup> + MnEDTA		$7.5 \times 10^6 \text{ M}^{-1} \text{ s}^{-1}$		35
O <sub>2</sub> <sup>-</sup> + Mn <sup>2+</sup>		$k_{\text{cat}} = 1.3 \times 10^6 \text{ M}^{-1} \text{ s}^{-1}$ (a)		20
O <sub>2</sub> <sup>-</sup> + Mn <sup>2+</sup>	MnO <sub>2</sub> <sup>+</sup>	$k_{\text{cat}} = 8.9 \times 10^6 \text{ M}^{-1} \text{ s}^{-1}$ (b)		32
O <sub>2</sub> <sup>-</sup> + Mn <sup>2+</sup>		$k_{\text{cat}} = 4 \times 10^6 \text{ M}^{-1} \text{ s}^{-1}$ (c)		18
O <sub>2</sub> <sup>-</sup> + Mn <sup>2+</sup>		$k_{\text{cat}} = 2.7 \pm 0.1 \times 10^6 \text{ M}^{-1} \text{ s}^{-1}$ (d) $k_{\text{cat}} = 4.5 \pm 0.3 \times 10^6 \text{ M}^{-1} \text{ s}^{-1}$ (e) $k_{\text{cat}} = 6.9 \pm 0.3 \times 10^6 \text{ M}^{-1} \text{ s}^{-1}$ (f)		1

$\text{HO}_2 + \text{Mn}^{3+}$		$k < 1 \times 10^5 \text{ M}^{-1} \text{ s}^{-1}$		26
$\text{O}_2^- + \text{Mn}^{3+}(\text{OAc}^-)_3$		No activity		1
$\text{O}_2^- + \text{Mn}^{(III)}\text{DFB}$		$k_{\text{cat}} = 1.5 \times 10^7 \text{ M}^{-1} \text{ s}^{-1}$ (g)		36
<hr/>				
$\text{MnO}_2^+\text{L}$ (L=Pyrophosphate)	$\text{Mn}^{3+}\text{L} + \text{H}_2\text{O}_2$	$> 2 \times 10^4 \text{ s}^{-1}$		33
$\text{MnO}_2^+\text{L}$ (L=Phosphate)	$\text{Mn}^{3+}\text{L} + \text{H}_2\text{O}_2$	$2 \times 10^3 \text{ s}^{-1}$		33
$\text{MnO}_2^+\text{L}$ (L=NTA)	$\text{Mn}^{3+}\text{L} + \text{H}_2\text{O}_2$	$3 \times 10^3 \text{ s}^{-1}$		35
$\text{MnO}_2^+\text{L}$ (L=EDTA)	$\text{Mn}^{3+}\text{L} + \text{H}_2\text{O}_2$	$9 \times 10^1 \text{ s}^{-1}$		35
$\text{MnO}_2^+\text{L}$ (L=Formate)	$\text{Mn}^{3+}\text{L} + \text{H}_2\text{O}_2$	$< 5 \text{ s}^{-1}$		33
$\text{MnO}_2^+\text{L}$ (L=Sulfate)	$\text{Mn}^{3+}\text{L} + \text{H}_2\text{O}_2$	$< 1.4 \text{ s}^{-1}$		33
<hr/>				
$\text{MnO}_2^+ + \text{MnO}_2^+ (+2\text{H}^+)$	$2\text{Mn}^{2+} + \text{H}_2\text{O}_2 + \text{O}_2$	$6.0 \pm 1.0 \times 10^6 \text{ M}^{-1} \text{ s}^{-1}$		26
$\text{MnO}_2^+\text{L} + \text{MnO}_2^+\text{L}$ (L= $\text{HCO}_3^-$ )	$2\text{Mn}^{2+}\text{L} + \text{H}_2\text{O}_2 + \text{O}_2$	$1.5 \times 10^6 \text{ M}^{-1} \text{ s}^{-1}$		34
$\text{MnO}_2^+\text{L} + \text{MnO}_2^+\text{L}$ (L= $\text{HPO}_4^{2-}$ )	$2\text{Mn}^{2+}\text{L} + \text{H}_2\text{O}_2 + \text{O}_2$	$8.9 \times 10^6 \text{ M}^{-1} \text{ s}^{-1}$		32,34
<hr/>				
$\text{HO}_2 + \text{MnO}_2^+ (+\text{H}^+)$	$\text{Mn}^{2+} + \text{H}_2\text{O}_2 + \text{O}_2$	$1.0 \pm 0.3 \times 10^7 \text{ M}^{-1} \text{ s}^{-1}$		26
$\text{O}_2^- + \text{MnO}_2^+(\text{sulfate}) (+2\text{H}^+)$	$\text{Mn}^{2+} + \text{H}_2\text{O}_2 + \text{O}_2$	$3.3 \times 10^7 \text{ M}^{-1} \text{ s}^{-1}$		33

Notes: (a) Pulse radiolysis, 0.05 M Potassium phosphate, pH 7.8, 25 °C. (b)  $^{60}\text{Co}$  gamma irradiation, 0.05 M phosphate medium, pH 7, 25 °C. (c) Xanthine oxidase/Xanthine, pH. (d) DMSO/ $\text{KO}_2$  Phosphate buffer pH 7.8, no apparent activity in HEPES at pH 7.8 or 8.1 (e) DMSO/ $\text{KO}_2$  Phosphate buffer pH 7.4, (f) DMSO/ $\text{KO}_2$  Phosphate buffer pH 7.0. (g) Xanthine oxidase/Xanthine, pH 7, Cytochrome c.

Table S2: Table: Mn(II) and Mn(III) Speciation in Seawater

Reactant			Ref.
$\text{Mn}^{2+} + \text{H}_2\text{O}$	$\text{MnOH}^+ + \text{H}^+$	$\text{Log } K_1 = -10.6$	37
$\text{Mn}^{2+} + 2\text{H}_2\text{O}$	$\text{Mn}(\text{OH})_2 + 2 \text{H}^+$	$\text{Log } \beta_2 = -22.2$	37
$\text{Mn}^{2+} + 3\text{H}_2\text{O}$	$\text{Mn}(\text{OH})_3^- + 3 \text{H}^+$	$\text{Log } \beta_3 = 34.8$	37
$\text{Mn}^{2+} + 4\text{H}_2\text{O}$	$\text{Mn}(\text{OH})_4^{2-} + 4 \text{H}^+$	$\text{Log } \beta_4 = -48.3$	37
$\text{Mn}^{2+} + \text{CO}_3^{2-}$	$\text{MnCO}_3$	$\text{Log } K = 4.4$	38
$\text{Mn}^{2+} + 2\text{CO}_3^{2-}$	$\text{Mn}(\text{CO}_3)_2^{2-}$	$\text{Log } K = 5.7$	38
$\text{Mn}^{2+} + \text{CO}_3^{2-} + \text{H}^+$	$\text{MnHCO}_3^+$	$\text{Log } K = 11.6$	38
$\text{Mn}^{2+} + \text{CO}_3^{2-} + \text{H}_2\text{O}$	$\text{MnOHCO}_3^-$	$\text{Log } K = -6.1$	38
$\text{Mn}^{2+} + \text{NH}_3$	$\text{MnNH}_3^{2+}$	$\text{Log } K = 1.0$	38
$\text{Mn}^{2+} + 2\text{NH}_3$	$\text{Mn}(\text{NH}_3)_2^{2+}$	$\text{Log } K = 1.5$	38
$\text{Mn}^{2+} + \text{Cl}^-$	$\text{MnCl}^-$	$\text{Log } K = 0.66$	38
$\text{Mn}^{2+} + \text{SO}_4^{2-}$	$\text{MnSO}_4$	$\text{Log } K = 2.3$	38
$\text{Mn}^{2+} + \text{F}^-$	$\text{MnF}^-$	$\text{Log } K = 1.3$	38
$\text{Mn}^{2+} + \text{O}_2$	$\text{Mn}^{3+} + \text{O}_2^-$	$\text{Log } K = -17.82$	38
$\text{MnOH}^+ + \text{O}_2$	$\text{MnOH}^{2+} + \text{O}_2^-$	$\text{Log } K = -9.2$	38
$\text{Mn}(\text{OH})_2 + \text{O}_2$	$\text{Mn}(\text{OH})_2^+ + \text{O}_2$	$\text{Log } K = -3.12$	38
<hr/>			
$\text{Mn}^{3+} + \text{H}_2\text{O}$	$\text{MnOH}^{2+} + \text{H}^+$	$K_1 = 1.0 \pm 0.2$	39
$\text{Mn}^{3+} + \text{H}_2\text{O}$	$\text{MnOH}^{2+} + \text{H}^+$	$^*K_1 = 0.4 \pm 0.1$	40
$\text{Mn}^{3+} + 2\text{H}_2\text{O}$	$\text{Mn}(\text{OH})_2^+ + 2 \text{H}^+$	$^*\beta_2 = 0.1 \pm 0.1$	40
$\text{MnOH}^{2+} + \text{H}_2\text{O}$	$\text{Mn}(\text{OH})_2^+ + \text{H}^+$	$K_2 = 5.0 \pm 0.1$	29
$\text{Mn}^{3+} + \text{H}_2\text{O}$	$\text{MnOH}^{2+} + \text{H}^+$	$\text{Log } K_1 = -0.12$	41
<hr/>			
$\text{Mn(III)} + \text{OH}^-$	$\text{Mn}(\text{OH})^{2+}$	$\text{Log } K_1 = 12.5$	42
$\text{Mn(III)} + 2\text{OH}^-$	$\text{Mn}(\text{OH})_2^+$	$\text{Log } \beta_2 = 24.0$	42
$\text{Mn(III)} + 3\text{OH}^-$	$\text{Mn}(\text{OH})_3$	$\text{Log } \beta_3 = 35.6$	42
<hr/>			
$2\text{Mn(III)} (+2\text{H}_2\text{O})$	$\text{MnO}_2 + 4\text{H}^+ + \text{Mn}^{2+}$	$\text{Log } K \sim 8.4$	40

Notes: 95% CI listed for lower data. Data in reference 43 was estimated from uptake of  $^{54}\text{Mn}$  onto particles.

**Table S3: Dissociation constants (pK) for Desferrixamine B and overall stability constants (log  $\beta_{pqr}$ ) Thermodynamic data for Mn(II) DFB Speciation in Seawater**

Metal		pK Lab <sup>a</sup>	pK Seawater <sup>b</sup>	Reference
H <sup>+</sup>	H <sup>+</sup> +L <sup>3-</sup>	10.84	10.85	43
	H <sup>+</sup> +HL <sup>2-</sup>	9.46	9.47	43
	H <sup>+</sup> +H <sub>2</sub> L <sup>-</sup>	9.00	9.00	43
	H <sup>+</sup> +H <sub>3</sub> L	8.30	8.30	43
Metal	M <sub>p</sub> L <sub>q</sub> H <sub>r</sub> p q r	Log $\beta_{pqr}$ (Lab) <sup>a</sup>	Log $\beta_{pqr}$ (seawater) <sup>b</sup>	Reference
Mn <sup>2+</sup>	1 1 0	6.81	6.83	44
	1 1 1	17.39	17.41	44
	1 1 2	25.51	25.53	44
	1 1 3	32.6	32.62	44
Mn <sup>3+</sup>	1 1 1	36.5	36.53	44
	1 1 1	39.56 <sup>c</sup>	39.24	23
Mg <sup>2+</sup>	1 1 0	2.8	2.82	43
	1 1 1	14.66	14.68	43
	1 1 2	23.85	23.87	43
Ca <sup>2+</sup>	1 1 0	3.03	3.05	43
	1 1 1	13.25	13.27	43
	1 1 2	22.41	22.43	43

Notes: <sup>a</sup>Conditions: I = 0.2 mol dm<sup>-3</sup> KCl, 25 °C. <sup>b</sup>Conditions: I = 0.7 mol dm<sup>-3</sup>, 25 °C (seawater), corrected using the Davies Equation. <sup>c</sup>Calculated from  $\beta_{111}=K_1K$  where log  $K = 28.6 \pm 0.5$ , for  $K = [\text{MnHDFB}]/[\text{Mn}][\text{HDFB}]$ , conditions: I = 0.1 mol dm<sup>-3</sup> NaCl, 25 °C. pK<sub>w</sub> = -13.63 (from Millero calculation at 25C and Ionic strength 0.7, equivalent to salinity 33.950)

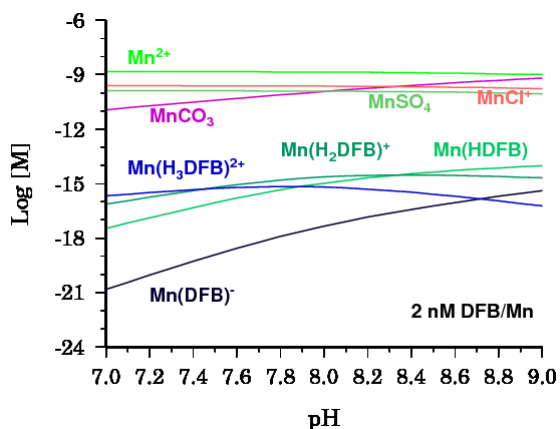


Figure S1: Calculated speciation of Mn(II) in seawater with 2 nM DFB.

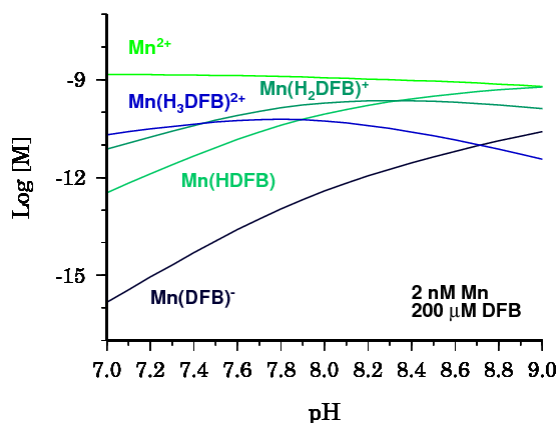


Figure S2: Calculated speciation of Mn(II) in seawater with 200 μM DFB. Other Mn inorganic species are not shown in order to highlight the Mn-DFB species.

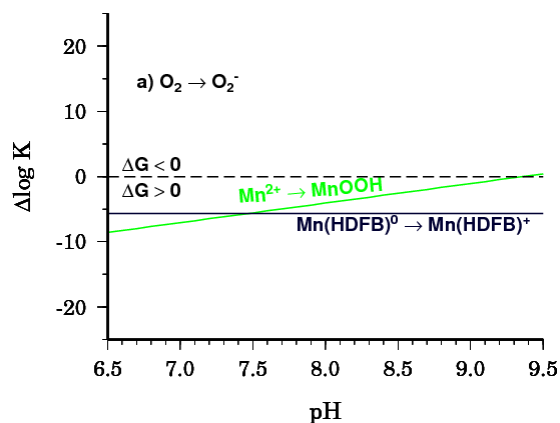


Figure S3: One-electron transfer reactions of Mn(II) and Mn(HDFB) in seawater with oxygen ( $O_2 \rightarrow O_2^-$ ).

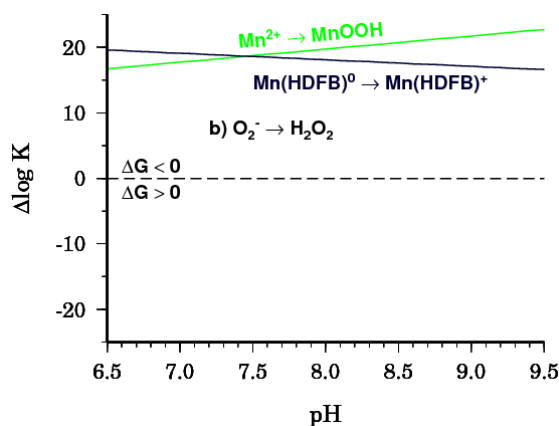


Figure S4: One-electron transfer reactions of Mn(II) and Mn(HDFB) in seawater with superoxide ( $O_2^- \rightarrow H_2O_2$ ).

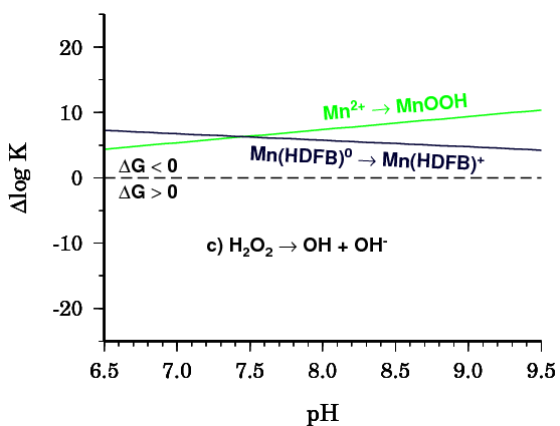


Figure S5: One-electron transfer reactions of Mn(II) and Mn(HDFB) in seawater with hydrogen peroxide ( $H_2O_2 \rightarrow OH + OH^-$ ).

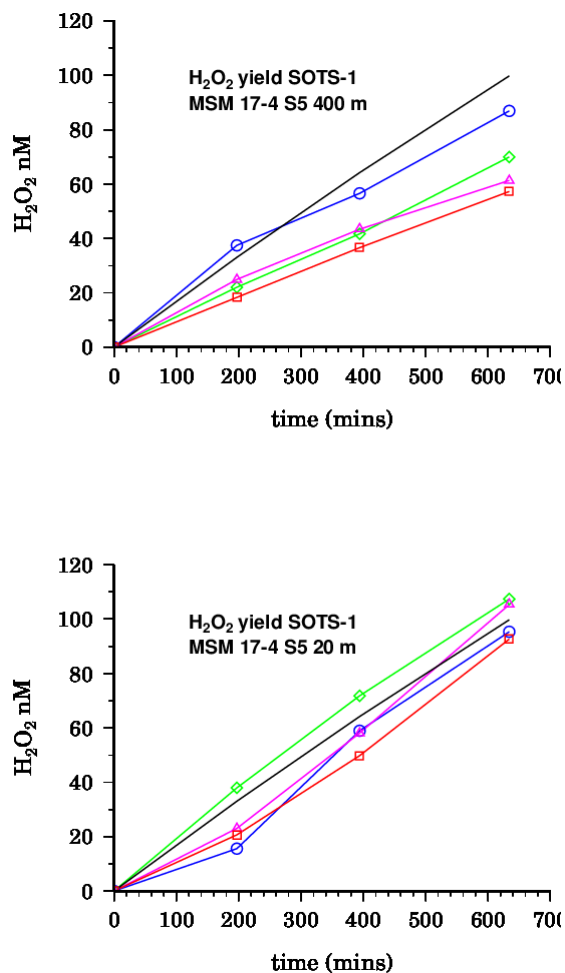


Figure S6: H<sub>2</sub>O<sub>2</sub> (nM) yield of SOTS of two different depths versus the time (min).

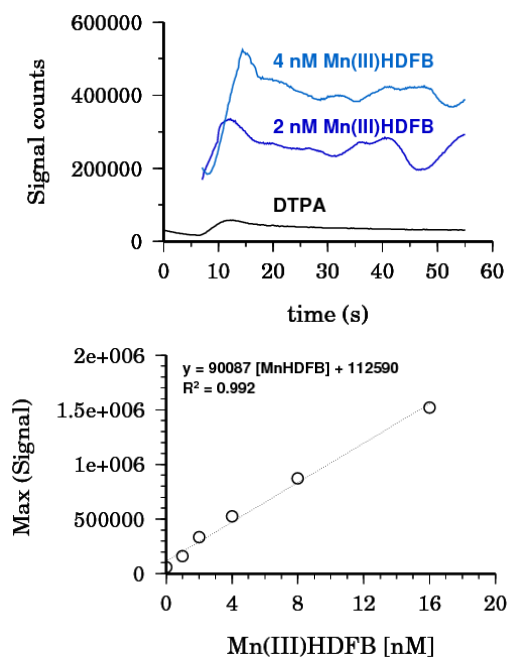


Figure S7: In the upper figure the signal counts of the O<sub>2</sub><sup>-</sup> FIA versus the time (s) is shown for an aliquot containing (1) DTPA (black), (2) 2 nM Mn(III)HDFB and (3) 4 nM Mn(III)HDFB. In the lower figure the linearity of the maximum signal of the O<sub>2</sub><sup>-</sup> FIA versus the Mn(III)HDFB (Mn) concentration is shown.

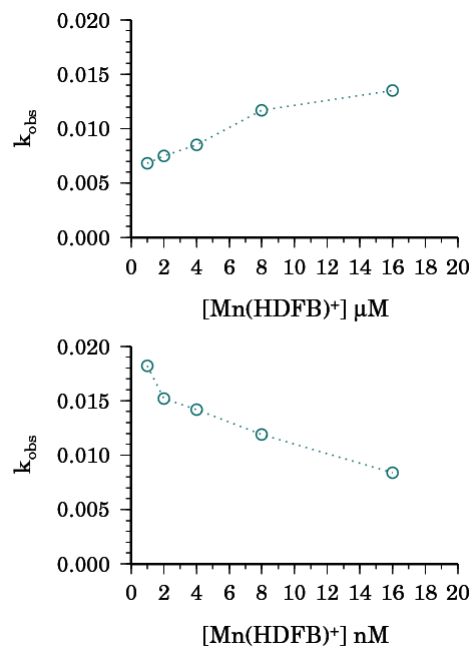


Figure S8: The observed loss rate of O<sub>2</sub><sup>-</sup> ( $k_{\text{obs}}$ ) versus Mn(HDFB)<sup>+</sup> (nM) is plotted in the upper panel for μM level ( $k_{\text{MnHDFB}^+} = 455 \pm 69 \text{ M}^{-1} \text{ s}^{-1}$ ) and in the lower panel for the nM level.



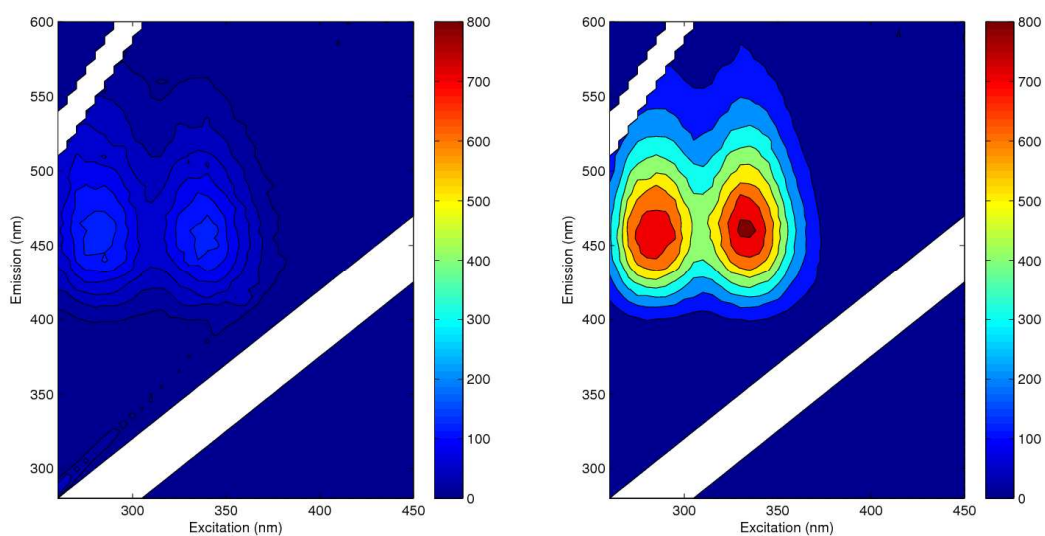


Figure S9: 3D Excitation Emission Matrix for (left) Mn(III)DFB and MCLA in seawater before and after (right) addition of  $\text{H}_2\text{O}_2$ . The EEM spectra is identical to that of OxyMCLA<sup>45, 46</sup> (Max emission at 455 nm with excitation at 285 and 335 nm) the end product of the reaction between  $\text{O}_2^-$  and MCLA.

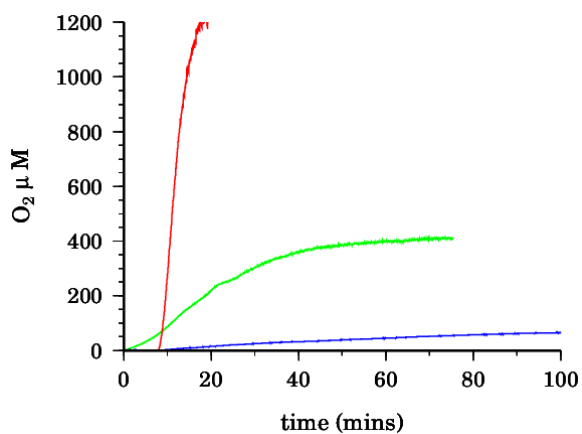


Figure S10: Production of  $\text{O}_2$  from addition of  $\text{H}_2\text{O}_2$  to Mn(HDFB)<sup>+</sup> in seawater.

Red line – 98  $\mu\text{M}$  Mn(HDFB)<sup>+</sup> and 138 mM  $\text{H}_2\text{O}_2$ ,  
Green line – 85.4  $\mu\text{M}$  Mn(HDFB)<sup>+</sup> and 27.9 mM  $\text{H}_2\text{O}_2$  and Blue line – 28.5  $\mu\text{M}$  Mn(HDFB)<sup>+</sup> and 27.9 mM  $\text{H}_2\text{O}_2$ .

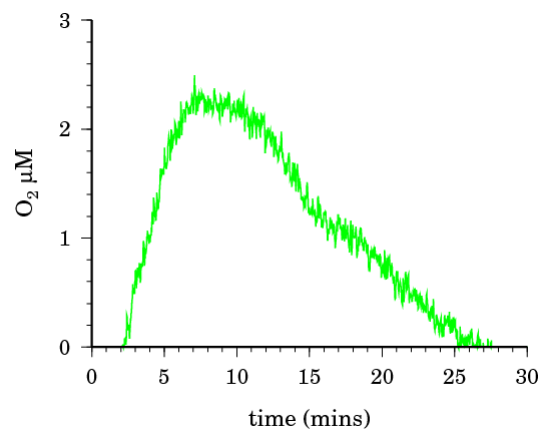


Figure S11: Production and consumption of  $\text{O}_2$  from addition of 98 mM  $\text{H}_2\text{O}_2$  to 10  $\mu\text{M}$  Mn(II) and 10  $\mu\text{M}$  DFB in deaerated seawater.

## REFERENCES

1. Friedel, F. C.; Lieb, D.; Ivanović-Burmazović, I., Comparative studies on manganese-based SOD mimetics, including the phosphate effect, by using global spectral analysis. *Journal of Inorganic Biochemistry* **2012**, *109*, (0), 26-32.
2. Batinic-Haberle, I.; Reboucas, J. S.; Spasojevic, I., Superoxide Dismutase Mimics: Chemistry, Pharmacology, and Therapeutic Potential. *Antioxidants & Redox Signaling* **2010**, *13*, (6), 877-918.
3. Good, N. E.; Winget, G. D.; Winter, W.; Connolly, T. N.; Izawa, S.; Singh, R. M., Hydrogen ion buffers for biological research. *Biochemistry* **1966**, *5*, (2), 467-77.
4. Grady, J. K.; Chasteen, N. D.; Harris, D. C., Radicals From Goods Buffers. *Analytical Biochemistry* **1988**, *173*, (1), 111-115.
5. Zhao, G. H.; Chasteen, N. D., Oxidation of Good's buffers by hydrogen peroxide. *Analytical Biochemistry* **2006**, *349*, (2), 262-267.
6. Kirsch, M.; Lomonosova, E. E.; Korth, H. G.; Sustmann, R.; de Groot, H., Hydrogen peroxide formation by reaction of peroxyxynitrite with HEPES and related tertiary amines - Implications for a general mechanism. *Journal Of Biological Chemistry* **1998**, *273*, (21), 12716-12724.
7. Hodges, G. R.; Ingold, K. U., Superoxide, amine buffers and tetranitromethane: A novel free radical chain reaction. *Free Radical Research* **2000**, *33*, (5), 547-550.
8. Heller, M. I.; Croot, P. L., Kinetics of superoxide reactions with dissolved organic matter in tropical Atlantic surface waters near Cape Verde (TENATSO). *J. Geophys. Res.* **2010**, *115*, (C12), C12038.
9. Heller, M. I.; Croot, P. L., Application of a Superoxide ( $O_2^-$ ) thermal source (SOTS-1) for the determination and calibration of  $O_2^-$  fluxes in seawater. *Analytica Chimica Acta* **2010**, *667*, 1-13.
10. Wuttig, K.; Heller, M. I.; Croot, P. L., Pathways of Superoxide ( $O_2^-$ ) decay in the Eastern Tropical North Atlantic. *submitted to Environmental Sciences and Technology* **2013**.
11. Helm, L.; Merbach, A. E., Water exchange on metal ions: experiments and simulations. *Coordination Chemistry Reviews* **1999**, *187*, (1), 151.
12. Budimir, A.; Kalmar, J.; Fabian, I.; Lente, G.; Banyai, I.; Batinic-Haberle, I.; Birus, M., Water exchange rates of water-soluble manganese(III) porphyrins of therapeutical potential. *Dalton Transactions* **2010**, *39*, (18), 4405-4410.
13. Diebler, H., Untersuchungen zur Komplexbildungskinetik des Ti(III) und Mn(III). *Zeitschrift für Physikalische Chemie* **1969**, *68*, (1\_2), 64-78.
14. Hudson, R. J. M.; Covault, D. T.; Morel, F. M. M., Investigations of iron coordination and redox reactions in seawater using  $^{59}Fe$  radiometry and ion-pair solvent extraction of amphiphilic iron complexes. *Marine Chemistry* **1992**, *38*, 209-235.
15. Bielski, B. H. J.; Cabelli, D. E.; Arudi, R. L.; Ross, A. B., Reactivity Of  $HO_2/O_2^-$  Radicals In Aqueous-Solution. *Journal Of Physical And Chemical Reference Data* **1985**, *14*, (4), 1041-1100.
16. Fisher, A. E. O.; Maxwell, S. C.; Naughton, D. P., Superoxide and hydrogen peroxide suppression by metal ions and their EDTA complexes. *Biochemical And Biophysical Research Communications* **2004**, *316*, (1), 48-51.
17. Stein, J.; Fackler, J. P.; McClune, G. J.; Fee, J. A.; Chan, L. T., Superoxide and manganese(III). Reactions of manganese-EDTA and manganese-CyDTA complexes with molecular oxygen. X-ray structure of potassium manganese-EDTA.2 water. *Inorganic Chemistry* **1979**, *18*, (12), 3511-3519.
18. Archibald, F. S.; Fridovich, I., The scavenging of superoxide radical by manganous complexes: In vitro. *Archives of Biochemistry and Biophysics* **1982**, *214*, (2), 452-463.
19. Baudry, M.; Etienne, S.; Bruce, A.; Palucki, M.; Jacobsen, E.; Malfroy, B., Salen-Manganese Complexes Are Superoxide Dismutase-Mimics. *Biochemical and Biophysical Research Communications* **1993**, *192*, (2), 964-968.

20. Spasojević, I.; Batinić-Haberle, I.; Stevens, R. D.; Hambright, P.; Thorpe, A. N.; Grodkowski, J.; Neta, P.; Fridovich, I., Manganese(III) Biliverdin IX Dimethyl Ester: A Powerful Catalytic Scavenger of Superoxide Employing the Mn(III)/Mn(IV) Redox Couple. *Inorganic Chemistry* **2001**, *40*, (4), 726-739.
21. Luther, G., The Role of One- and Two-Electron Transfer Reactions in Forming Thermodynamically Unstable Intermediates as Barriers in Multi-Electron Redox Reactions. *Aquatic Geochemistry* **2010**, *16*, (3), 395-420.
22. Luther, G. W., Thermodynamic Redox Calculations for One and Two Electron Transfer Steps: Implications for Halide Oxidation and Halogen Environmental Cycling. In *Aquatic Redox Chemistry*, American Chemical Society: 2011; Vol. 1071, pp 15-35.
23. Duckworth, O. W.; Sposito, G., Siderophore-Manganese(III) Interactions. I. Air-Oxidation of Manganese(II) Promoted by Desferrioxamine B. *Environmental Science & Technology* **2005**, *39*, (16), 6037-6044.
24. Morgan, J. J., Kinetics of reaction between O<sub>2</sub> and Mn(II) species in aqueous solutions. **2005**, *69*, (1), 35.
25. Bodini, M. E.; Sawyer, D. T., Electrochemical and Spectroscopic Studies of Manganese(II), -(III) and -(IV) Gluconate Complexes. 2. Reactivity and Equilibria with Molecular Oxygen and Hydrogen Peroxide. *Journal of the American Chemical Society* **1976**, *98*, (26), 8366-8371.
26. Jacobsen, F.; Holcman, J.; Sehested, K., Manganese(II)–Superoxide Complex in Aqueous Solution. *The Journal of Physical Chemistry A* **1997**, *101*, (7), 1324-1328.
27. Jacobsen, F.; Holcman, J.; Sehested, K., Oxidation of manganese(II) by ozone and reduction of manganese(III) by hydrogen peroxide in acidic solution. *International Journal Of Chemical Kinetics* **1998**, *30*, (3), 207-214.
28. Wells, C. F.; Mays, D., The kinetics of the reaction of aquomanganese(III) ions with hydrogen peroxide in perchlorate media. *Journal of the Chemical Society A: Inorganic, Physical, Theoretical* **1968**, 665-667.
29. Baral, S.; Lumepereira, C.; Janata, E.; Henglein, A., Chemistry Of Colloidal Manganese-Dioxide .2. Reaction With O<sub>2</sub><sup>-</sup> And H<sub>2</sub>O<sub>2</sub> (Pulse-Radiolysis And Stop Flow Studies). *Journal Of Physical Chemistry* **1985**, *89*, (26), 5779-5783.
30. Rerek, M. E.; Weil, I.; Hill, M., Kinetics and mechanism of the Mn(III)gluconate catalyzed decomposition of hydrogen peroxide. *Coordination Chemistry Reviews* **1990**, *105*, 251-268.
31. Cabelli, D. E.; Bielski, B. H. J., Pulse-Radiolysis Study Of The Kinetics And Mechanisms Of The Reactions Between Manganese(II) Complexes And HO<sub>2</sub>/O<sub>2</sub><sup>-</sup> Radicals .1. Sulfate, Formate, And Pyrophosphate Complexes. *Journal Of Physical Chemistry* **1984**, *88*, (14), 3111-3115.
32. Barnese, K.; Gralla, E. B.; Cabelli, D. E.; Selverstone Valentine, J., Manganous Phosphate Acts as a Superoxide Dismutase. *Journal of the American Chemical Society* **2008**, *130*, (14), 4604-4606.
33. Cabelli, D. E.; Bielski, B. H. J., Pulse-Radiolysis Study Of The Kinetics And Mechanisms Of The Reactions Between Manganese(II) Complexes And HO<sub>2</sub>/O<sub>2</sub><sup>-</sup> Radicals .2. The Phosphate Complex And An Overview. *Journal Of Physical Chemistry* **1984**, *88*, (25), 6291-6294.
34. Barnese, K.; Gralla, E. B.; Valentine, J. S.; Cabelli, D. E., Biologically relevant mechanism for catalytic superoxide removal by simple manganese compounds. *Proceedings of the National Academy of Sciences* **2012**, *109*, (18), 6892-6897.
35. Lati, J.; Meyerstein, D., Oxidation of first-row bivalent transition-metal complexes containing ethylenediaminetetra-acetate and nitrilotriacetate ligands by free radicals: a pulse-radiolysis study. *Journal of the Chemical Society, Dalton Transactions* **1978**, (9), 1105-1118.
36. Hahn, S. M.; Krishna, C. M.; Samuni, A.; Mitchell, J. B.; Russo, A., Mn(III)-desferrioxamine superoxide dismutase-mimic: Alternative modes of action. *Archives of Biochemistry and Biophysics* **1991**, *288*, (1), 215-219.

37. Baes, C. F.; Mesmer, R. E., *The Hydrolysis of Cations: A critical review of hydrolytic species and their stability constants in aqueous solution*. . Wiley: 1976.
38. Morgan, J. J., Kinetics of reaction between O<sub>2</sub> and Mn(II) species in aqueous solutions. *Geochimica Et Cosmochimica Acta* **2005**, *69*, (1), 35-48.
39. Rosseinsky, D. R.; Nicol, M. J.; Kite, K.; Hill, R. J., Manganese(III) and its hydroxo- and chloro-complexes in aqueous perchloric acid: comparison with similar transition-metal(III) complexes. *Journal of the Chemical Society, Faraday Transactions 1: Physical Chemistry in Condensed Phases* **1974**, *70*, (0), 2232-2238.
40. Biedermann, G.; Palombari, R., On the Hydrolysis of the Manganese(III) Ion *Acta Chemica Scandinavica* **1978**, *32*, 381-390.
41. Sisley, M. J.; Jordan, R. B., First Hydrolysis Constants of Hexaaquacobalt(III) and -manganese(III): □ Longstanding Issues Resolved. *Inorganic Chemistry* **2006**, *45*, (26), 10758-10763.
42. Novikov, A. I.; Shaffert, A. A.; Pavlova, T. D., Sorption of the <sup>54</sup>Mn radionuclide by oxides and hydroxides under redox and complexation conditions. II. Sorption of <sup>54</sup>Mn(III, IV, VI, VII). *Radiokhimiya* **1987**, *29*, (3), 361-367.
43. Farkas, E.; Enyedy, É. A.; Csóka, H., A comparison between the chelating properties of some dihydroxamic acids, desferrioxamine B and acetohydroxamic acid. *Polyhedron* **1999**, *18*, (18), 2391-2398.
44. Szabó, O.; Farkas, E., Characterization of Mn(II) and Mn(III) binding capability of natural siderophores Desferrioxamine B and Desferricoprofen as well as model hydroxamic acids. *Inorganica Chimica Acta* **2011**, *In Press, Accepted Manuscript*.
45. Kambayashi, Y.; Ogino, K., Reestimation of Cypridina Luciferin Analogs (MCLA) as a Chemiluminescence Probe to detect active oxygen species-Cautious note for use of MCLA. *The Journal of Toxicological Sciences* **2003**, *28*, (3), 139.
46. Fujimori, K.; Komiyama, T.; Tabata, H.; Nojima, T.; Ishiguro, K.; Sa-waki, Y.; Tatsuzawa, H.; Nakano, M., Chemiluminescence of Cypridina Luciferin Analogs. Part 3. MCLA Chemiluminescence with Singlet Oxygen Generated by the Retro-Diels-Alder Reaction of a Naphthalene Endoperoxide. *Photochemistry and Photobiology* **1998**, *68*, (2), 143-149.





# **M**ANUSCRIPT 3

Contrasting behavior of cadmium,  
iron and manganese in the Eastern  
Tropical Atlantic





# Contrasting behavior of cadmium, iron and manganese in the Eastern Tropical Atlantic

**K. Wuttig<sup>1</sup>, T. Wagener<sup>1,2</sup>, D. Booge<sup>1</sup>, P. Streu<sup>1</sup> and P. L. Croot<sup>1,3</sup>**

<sup>1</sup>FB2 Marine Biogeochemistry, Chemical Oceanography, GEOMAR Helmholtz-Zentrum für Ozeanforschung Kiel, Kiel, Germany

<sup>2</sup>now at: Université d'Aix-Marseille, CNRS/ INSU, IRD, Institut Méditerranéen d'Océanologie (MIO), UM 110, 13288 Marseille, France

<sup>3</sup>now at: Earth and Ocean Sciences, School of Natural Sciences, National University of Ireland, Galway (NUIG), Galway, Ireland

Correspondence to: K. Wuttig ([kwuttig@geomar.de](mailto:kwuttig@geomar.de))

Manuscript in prep. for submission to Global Biogeochem. Cycles.

## ABSTRACT

Seawater samples (20 – 400 m) were measured for dissolved cadmium (Cd), iron (Fe), and manganese (Mn) in the Eastern Tropical Atlantic (ETA) ocean on a transect along 23°W from 5°S to 17°N and at the Cape Verde Ocean Observatory (CVOO) time-series station (Cape Verde Islands). The distribution of these trace metals was compared to oxygen and nutrient (nitrate, nitrite and phosphate) distributions and the main hydrological features. In this region Fe and Mn are clearly influenced by Aeolian sources due to surface deposition of Saharan dust. Mn was depleted with depth and from north to south. Fe was depleted in a subsurface minimum between 40 - 80 m coinciding together with the observed nitrite ( $\text{NO}_2^-$ ) and chlorophyll-*a* maximum. On the equator Fe exhibits a clear signal for the core of the Equatorial Undercurrent (EUC) at 60 m with elevated Fe of  $0.84 \text{ nmol L}^{-1}$  in comparison to concentrations of the surrounding water masses. Cd was not influenced by dust deposition and showed very low surface concentrations ( $<10 \text{ pmol L}^{-1}$  in the upper 60 m) which increased steadily with depth (nutrient like behavior) by roughly  $100 \text{ pmol L}^{-1}$  per 100 m (from 100 - 400 m). Cd was highly correlated to phosphate (P) and the Cd/P ratio revealed two different slopes and ratios. The surface ratio was  $16.6 \text{ pmol}/\mu\text{mol}$  and the deep ratio was  $237.4 \text{ pmol}/\mu\text{mol}$  and exhibited higher P, but comparably even higher Cd values than in the surface.

## 1 INTRODUCTION

Alongside the macronutrients (e.g. phosphate (in the following just P), nitrate ( $\text{NO}_3^-$ ) and nitrite ( $\text{NO}_2^-$ )), a number of bio-essential micronutrients like the trace metals iron (Fe), manganese (Mn) and cadmium (Cd) have been moved into the spotlight of attention in the last few years. These and other trace metals are vital for the growth of phytoplankton in the oceans as for example for macronutrient uptake, as cofactors or in respiration processes. In some regions trace metals can be the limiting factor (Morel *et al.*, 1991). As the name implies, the concentrations of trace metals in the oceans are very low (in the nano- and even picomolar range) (Morel and Price, 2003). Both the macro- and the micronutrients can be supplied to the surface ocean from the atmosphere. For some metals like Fe and Mn which are abundant in crustal dust, atmospheric dust deposition has been argued to be the main supply to the ocean (Duce *et al.*, 1991). Other important pathways can be riverine input, sediments and fluvial and hydrothermal vents. The oligotrophic Eastern Tropical Atlantic (ETA) ocean, where this study was conducted, is highly impacted by the influence of Saharan dust as a natural source for the input of macro- (like phosphorous) and micronutrients (Fe and Mn) (Jickells, 1995). Though recent work has also suggested that supply from the continental shelf may also be important closer to the coast of West Africa

(Lam *et al.*, 2012). Riverine supply to the ETA is limited only to the Senegalese shelf region (Cotrim da Cunha *et al.*, 2009).

In this region Mills *et al.* (2004) performed bioassay experiments by adding dust to filtered seawater and observed an increase of chlorophyll-*a*. The authors showed that some processes like nitrogen fixation are not only limited by either macro- or micronutrients, but by the combination of Fe and P. Saito *et al.* (2008) have suggested that three types of limitation exist: Type I, the independent co-limitation like N and P (Benitez-Nelson, 2000), type II, the biochemical substitution like Fe and Mn in superoxide dismutases (SODs) (Wolfe-Simon *et al.*, 2005) and type III, a dependent nutrient co-limitation. An example for type III can be the co-limitation of Fe and P (Mills *et al.*, 2004). For phytoplankton, Fe is the key bio-essential trace metal due to its necessity in its photosystems I and II (PSI and PSII) and in the microbial loop for nitrogen fixation (Moore *et al.*, 2009). Mn plays a prominent role for photosynthesis thanks to its unique role in PSII (Parkhill *et al.*, 2001) and as a central-active metal cofactor in defense mechanisms such as SODs (Wolfe-Simon *et al.*, 2006). Mn as the metal centre in Mn SODs can be outcompeted by cellular Fe and the antioxidant effect of Mn SOD minimized (Aguirre and Culotta, 2012). Cd can be utilized in the enzyme carbonic anhydrase by marine diatoms when Zinc (Zn) limited (Lane and Morel, 2000), but at the same time Cd can be toxic for phytoplankton and therefore it exudates strong Cd binding ligands (phytochelatin) for detoxification (Lee *et al.*, 1996).

Not only do the trace metals limit the biological reproduction, species composition and growth rates, but the other way round as well. Biota can influence the initial concentration of trace metals in seawater, their chemical speciation (e.g. Fe(II) and Fe(III) (Gledhill and Buck, 2012; Zhuang *et al.*, 1992)) and the redox cycling of trace metals (Sunda, 2012) as the phytoplankton produces chelating ligands to stabilize one chemical species to make it more bioavailable as in the case of Fe. Recently a *Prochlorococcus* sp. strain has been shown to upregulate its siderophore transport proteins when less Fe was available (Malmstrom *et al.*, 2013).

The finding of the biological usage of Cd by Lane and Morel (2000) provided an explanation for the nutrient-like behavior of Cd in seawater. Like many other trace metals Cd is depleted in the surface due to uptake by phytoplankton. Many other trace metals exhibit this kind of depth profile, because they are strongly mediated by biota with a similar distribution to macronutrients. An exception is Mn which is mostly not limited in surface waters and which is often dominated by scavenging, but due to its uptake in phytoplankton, it belongs into the category of hybrid-type behavior. Fe also is a member of this category as it behaves mostly like a nutrient, except in areas of high dust input with high surface concentrations, it shows a mixed behavior of nutrient-like and scavenged (Bruland and Lohan, 2003).

The expansive Atlantic oxygen minimum zone (OMZ) is located between 100 and 700 m depth with its core around 400 m and dissolved oxygen of  $\sim 40 \mu\text{mol kg}^{-1}$  (Karstensen *et al.*, 2008). Oxygen has been shown to influence the trace metal speciation as in the case of Fe. In suboxic waters ( $< 5 \mu\text{mol L}^{-1}$ ) of the OMZ significant amounts of the short-lived Fe(II) have been determined (Hong and Kester, 1986; Hopkinson and Barbeau, 2007; Moffett *et al.*, 2007). The changes in the oxygen concentration can also affect the Mn biogeochemical cycle. According to the redox chain, particulate  $\text{MnO}_2$  is reduced under suboxic conditions to soluble Mn(II) (Rue *et al.*, 1997). As a result a secondary Mn(II) maximum was observed in the OMZ in the Arabian Sea and the North Pacific (Johnson *et al.*, 1992; Lewis and Luther III, 2000). Soluble Mn(III) was detected with concentrations up to  $5 \mu\text{mol L}^{-1}$  in suboxic waters of the Black Sea and contributed up to 100 % of the total Mn pool (Trouwborst *et al.*, 2006).

As all three trace metals play critical roles in marine metabolisms, it is of interest to measure the concentrations of these trace metals together and we report in this paper vertical profiles (20 – 400 m) along 23°W in the strongly dust influenced ETA starting with the Cape Verdean Ocean Observatory (former TENATSO, now CVOO) time series station close to the Cape Verdean Archipelago down to 5°S. In the Pacific Equatorial Undercurrent (EUC) large fluxes of trace metals, especially of Fe, are observed (Gordon *et al.*, 1997; Slemons *et al.*, 2012). The objectives for this paper in regard to this transect were: (1) the trace metal concentration in the Atlantic Equatorial Undercurrent (EUC), (2) the role of the low oxygen concentration on Fe and Mn and (3) the Cd/P ratio.

## 2 MATERIALS AND METHODS

### 2.1 Field Sample collection

Figure 1 shows the M80/1 cruise track (in red) in the ETA open ocean in autumn 2010.

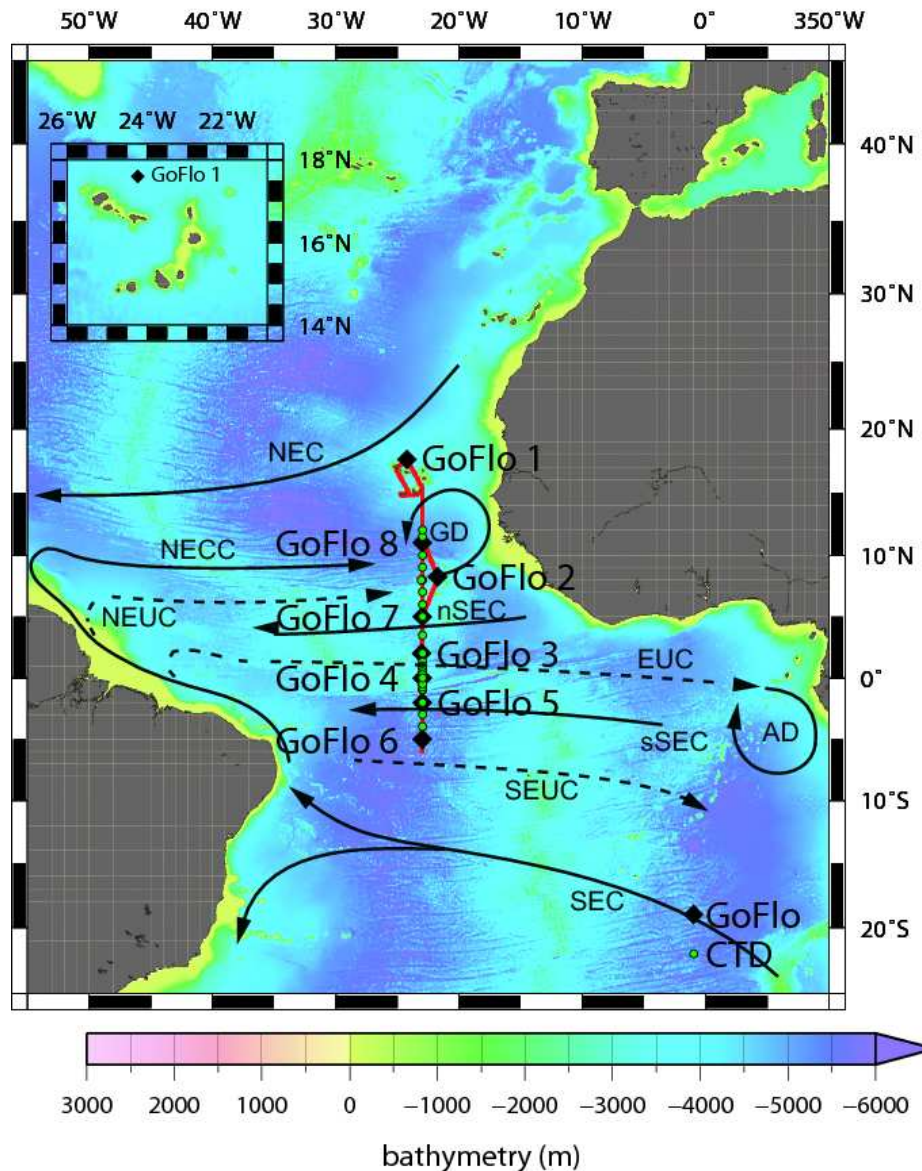


Figure 1. The hydrographic setting of the ETA with its main currents is plotted. Shown are the North Equatorial Current (NEC), the Guinea Dome (GD), the North Equatorial Countercurrent (NECC), the North Equatorial Undercurrent (NEUC), the South Equatorial Current (SEC) with its northern (nSEC) and southern (sSEC) branches, the Equatorial Undercurrent (EUC), the South Equatorial Undercurrent (SEUC) and the Angola Dome (AD). The GoFlo-section on M80/1 is shown in red and the 8 GoFlo-stations, starting with CVOO (GoFlo-station 1) and then along 23°W, are plotted as black dots (plotted with GMT, <http://gmt.soest.hawaii.edu/>). Trace Metal section with 8 GoFlo-stations as black diamonds (2 casts with 4 GoFlos per GoFlo-station) starting with CVOO (GoFlo-station 1) and then along 23°W (plotted with GMT, <http://gmt.soest.hawaii.edu/>). The M80/1 cruise track in the ETA is shown in red. The CTD-stations are shown as green dots. The Cape Verdean Archipelago with GoFlo-station 1 is highlighted in the left high corner.

Samples were taken on board of the German research vessel Meteor (Table 2) for trace metals and at 28 CTD-stations (green dots) for all ancillary parameters. The first station was located at the CVOO time-series station close to the Cap Verde Island, Sao Vicente (17.35°N 24.15°W) (cvo0.geomar.de). The second station was located at 8.15°N 21.45°W and the other stations (3 - 8) were occupied on a 23°W transect between 11°N and 5°S in the ETA ocean (Figure 1). Each GoFlo-station consisted of two casts with 4 GoFlos each. Samples were taken in the upper 400 m of the water column.

All trace metal clean analytical work at sea was performed in an over-pressurized ISO class 5 clean container, inside of which analysts wore the appropriate clean room apparel; overalls with hood (Tyvek), shoes (Abeba) and plastic gloves (Carl Roth). Seawater samples in this work were obtained from the water column using modified Teflon coated PVC General Oceanics (Miami, FL, USA) GoFlo bottles of 8 L in which the original drain cock was replaced by a Teflon stop cock. These bottles were deployed on a Kevlar line from the side of the ship. Immediately upon recovery of the GoFlo bottles, samples were filtered in-line through 0.2 µm filter cartridges (Sartorius Sartobran filter capsule 5231307H5) by N<sub>2</sub> overpressure into acid cleaned bottles. Directly following the filtration, the samples for dissolved trace metal analysis (in 1 L LDPE bottles) were acidified with 2 mL Q-HCl to pH < 2 under a class 100-laminar flow bench and then protected by double bags (Minigrip™). They were bagged and stored in blue plastic boxes until further sample processing and analysis steps which were performed under HEPA filtered air on laminar flow benches inside a class 5 clean room in Kiel.

Samples for oxygen, macronutrients and chlorophyll-*a* measurements were obtained from a Seabird™ CTD rosette systems with one Digiquartz pressure and one chlorophyll-*a* sensor and double sensor packages for temperature, conductivity and oxygen (Brandt *et al.*, 2011).

## 2.2 Reagents and bottles

All reagents used were of highest purity available (Fischer Scientific and Sigma-Aldrich) and were prepared using deionized (18 MΩ cm<sup>-1</sup> resistivity) water (MQ water) from a Milli-Q purification system (Millipore). Sub-boiled quartz-distilled hydrochloric acid (hereafter Q-HCl) was made by single distillation from 25 % HCl. All plasticware and bottles (low density high polyethylene (LDPE) and Polytetrafluoroethylene (PTFE) (Nalgene)) used for acidified seawater samples for the total trace metal analysis were cleaned according to the trace metal clean procedures (Bruland *et al.*, 1979; Cutter *et al.*, 2010).

## 2.3 Chemical Analysis

### 2.3.1 Dissolved total trace metal analysis

Dissolved trace metal (Cd and Fe) concentrations were determined in the ISO class 5 clean laboratory of the GEOMAR in Kiel using the graphite furnace atomic absorption (ETAAS, Perkin-Elmer Model 4100ZL) method after pre-concentration by simultaneous dithiocarbamate-freon extraction from seawater (100 - 250 g) (Danielsson *et al.*, 1978; Grasshoff *et al.*, 1983). Hereafter we will only discuss dissolved trace metal concentrations, but will simply refer to them as Cd and Fe. The accuracy of the method was evaluated by measuring SAFe and GEOTRACES intercalibration samples. We also reextracted the samples in order to determine extraction efficiency and/or blank contributions and did not find any significant re-extraction blank for Fe. As Baars *et al.* (for submission) found recovery problems for this extraction method for their Antarctic Cd concentrations in seawater samples acidified with Q-HCl, therefore we calculated the recovery for our Cd values. Based on the re-extraction blanks the recovery of Cd was >85%. This means that our higher Cd concentrations may be underestimated. Baars *et al.* (for submission) have shown that these recovery problems are severe in the Antarctic as they seem to be a function of Cd complexation and primary productivity. Thus we assume that this problem should not be as severe in the ETA.

### 2.3.2 Dissolved Manganese (Mn) analysis

Samples for Mn were measured with a flow injection system (FIA) combined with spectrophotometric detection modified slightly after Aguilar-Islas *et al.* (2006). Subsamples (50 mL) were taken from the 1 L bottles and acidified with Q-HCl to pH 1.7 and measured two years of storage in the clean laboratory Kiel. The method used for the M80/1 samples is described elsewhere (Wuttig *et al.*, 2012), but was refined and the variable wavelength spectrophotometer (USB-4000, Ocean Optics, Inc.) was coupled with the help of optical fibers (QP400-025-SR) to an external UV/VIS-light source (Micropak DT-Mini-2GS, Ocean Optics, Inc.) and to a 10 cm Liquid Waveguide Capillary Cell (LWCC-2010, World Precision Instruments, Inc.) which replaced the 1 cm quartz flow-through cell (100-QS, 10.00 mm, Hellma GmbH & Co. KG), whereas the sensitivity was enhanced and the detection limit lowered significantly. The signal was spectrophotometrically detected at 620 nm. The loading time onto the column was enhanced from 120 to 180 s in comparison to a former study for the Mediterranean (Mn concentrations of  $3.60 \pm 0.30 \text{ nmol L}^{-1}$  (Wuttig *et al.*, 2012)) to achieve an increase of sensitivity in the open ocean samples. The electrically actuated 10-port sample valve was replaced by an electrically actuated 26-port sample valve (both VICI, Valco Instruments) whereby the Mn-FIA could be run nonstop for about a week.

Calibration curves were determined daily by the addition of standards (0 - 10 nmol L<sup>-1</sup>) produced by serial dilution of a 1000 ppm Mn(II) Standard (Fluka) into 0.2 µm filtered Tropical Atlantic seawater (M80/2).

Samples, standard additions and blanks were measured in quadruplicates. Analytical precision (expressed as percent relative standard deviation) was typically < 8 %. The accuracy of the analytical procedure was evaluated by daily measurements of SAFe intercalibration samples S and D2. SAFe values determined as follows: 0.85 ± 0.14 nmol L<sup>-1</sup> (S) and 0.35 ± 0.09 nmol L<sup>-1</sup> (D2) of Mn (n = 8) (consensus values are 0.79 ± 0.06 nmol L<sup>-1</sup> and 0.35 ± 0.06 nmol L<sup>-1</sup>, respectively). The detection limit (3σ of the blank) for the Mn flow injection system used here was estimated in the lab in Kiel by repeated measurements of low Mn Antarctic seawater (< 0.2 nmol L<sup>-1</sup>; collected during ANTXXIV-3) at 150 pmol L<sup>-1</sup>.

### 2.3.3 Ancillary parameters

Seawater samples for macronutrient analyses were taken from the Niskin bottles mounted on a Seabird<sup>TM</sup> CTD rosette systems (Brandt *et al.*, 2011) into 60 mL polypropylene (PP) bottles (Nalgene) and directly frozen at -20°C. After thawing they were directly analyzed at the GEOMAR with a continuous-flow-autoanalyzer system build after Grasshoff *et al.* (2007). For precision, duplicates were sampled and analyzed at each station. Dissolved oxygen was measured by classic Winkler titration and fluorescence chlorophyll-*a* was measured by standard procedures (Grasshoff *et al.*, 2007).



### 3 RESULTS

#### 3.1 Hydrography and currents

In Figure 1 we only present the most prominent currents and features in the ETA which are important for our findings in the upper 400 m of the water column in in the area of our sampled 23°W transect in the ETA.

For detailed information on the hydrography and currents, see, for example, (Brandt *et al.*, 2008; Brandt *et al.*, 2010; Brandt *et al.*, 2006; Stramma *et al.*, 2003; Stramma *et al.*, 2005; Stramma and Schott, 1999).

The Tropical Surface Water (TSW) is the mixed, near surface layer in this region with about 27°C (Figure 1). Underneath the TSW a sharp thermocline with a 10°C temperature decrease over 50 m can be found (Stramma *et al.*, 2003; Stramma and Schott, 1999).

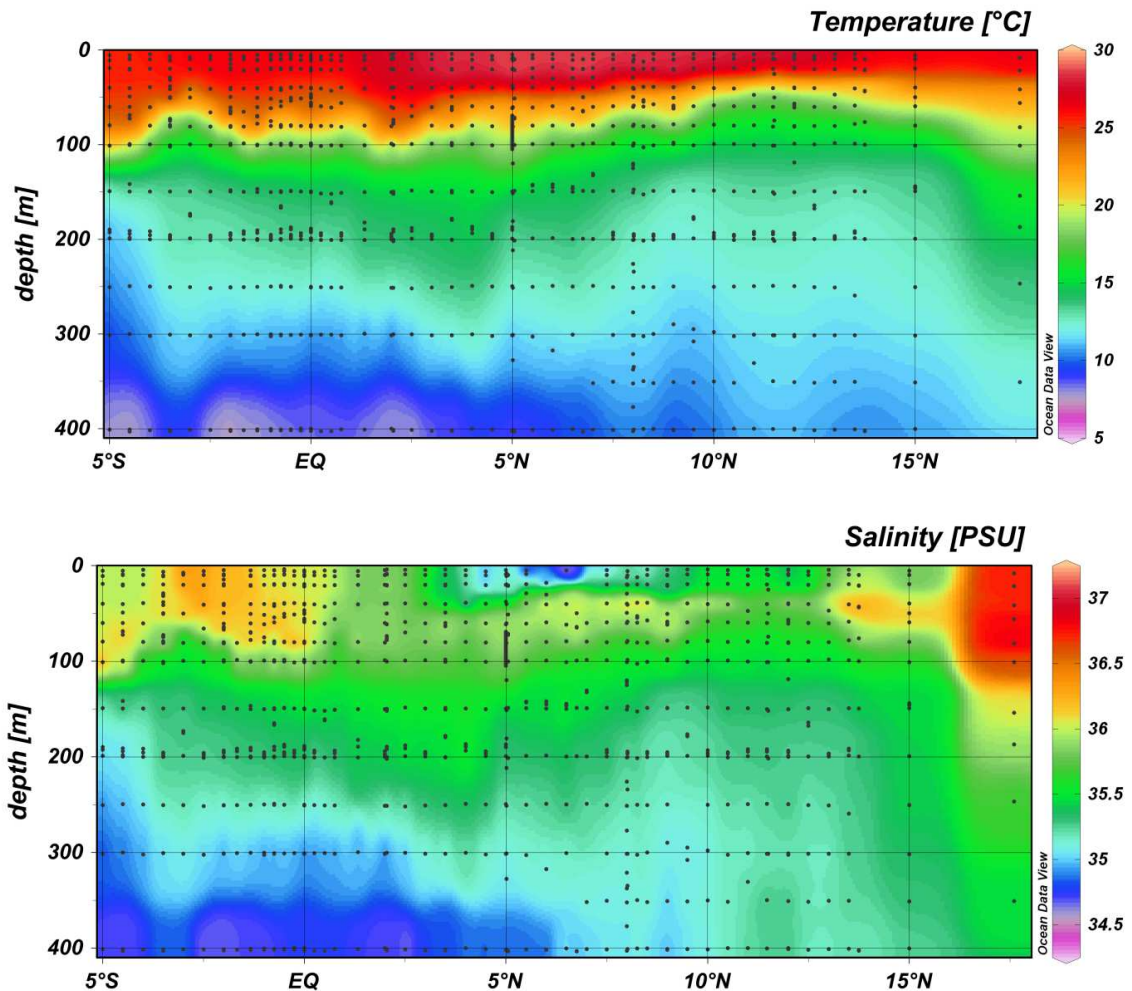


Figure 2: Two dimensional plots of salinity and temperature (in °C) in the upper 400 m of the ETA water column on M80/1 from south to north (along 23°W and at CVOO) (plotted with ODV (Schlitzer, 2012)).

The authors show that in this region there are a number of zonal current and counter current bands of smaller meridional and vertical extent. The main water pathway to the tropical Atlantic is the South Equatorial Current (SEC). Two of its westward flowing branches (the northern (nSEC) and the eastern (eSEC)) were observed in the surface waters surrounding the Equatorial Undercurrent (EUC). The EUC was one of the most dominant features observed (Brandt *et al.*, 2011) with its core at 60 – 80 m depths on the equator and it flows from the western boundary towards the eastern equatorial Atlantic (Schott *et al.*, 2003 and Brandt *et al.*, 2006). Another branch was the also eastward flowing Southern Equatorial Undercurrent (SEUC) with its center around 4.25°S and its northern pendant (NEUC) between 4 - 6°N. North 6°N bands of the eastward flowing North Equatorial Countercurrent (NECC) were observed (Brandt *et al.*, 2011).

Another important feature in the ETA is the Inter-Tropical Convergence Zone (ITCZ) which varies seasonally and during the northern autumn the band of rainfall is north of the equator (~10°N) while during northern winter is located nearly on the equator (Sultan and Janicot, 2000). In Figure 2 the salinity in the upper 400 m on 23°W from south to north is shown and it decreased from north to south. At CVOO ( $36.73 \pm 0.14$  PSU) and from 0.5°N to 3.5°S (>36 PSU) salinity was enhanced in the surface 100 m whereas from 4.5°N to 7°N it was depleted (<35 PSU) in the upper 30 m with its core in the north (5.5 – 7°N).

### 3.2 Ancillary parameters

In Figure 3 oxygen, apparent oxygen utilization (AOU) and chlorophyll-*a* are plotted as two dimensional plots of latitude (south to north as shown in Figure 1) and depth (0 - 400 m, in the case of chlorophyll-*a* 0 - 200 m). Oxygen was typically depleted with depth (especially below 60 m) reaching its minimum from 7° to 13°N in the Eastern Tropical North Atlantic Oxygen Minimum Zone (ETNA-OMZ) with values down to  $40 \mu\text{mol kg}^{-1}$ . Between 2.5°N and 2.5°S oxygen was enhanced at 400 m whereas this increased oxygen zone was narrower (0 – 1.3°N) above (150 – 300 m).

Between 5°N and 15°N (300 – 400 m) AOU reached its maximum with  $>200 \mu\text{mol kg}^{-1}$ . In comparison to the surrounding waters at depth the AOU was lower around the equator. As expected AOU increased with depth due to remineralization.

The maximum in chlorophyll-*a* was observed between 30 and 60 m ( $0.3 - 0.7 \mu\text{g L}^{-1}$ ).

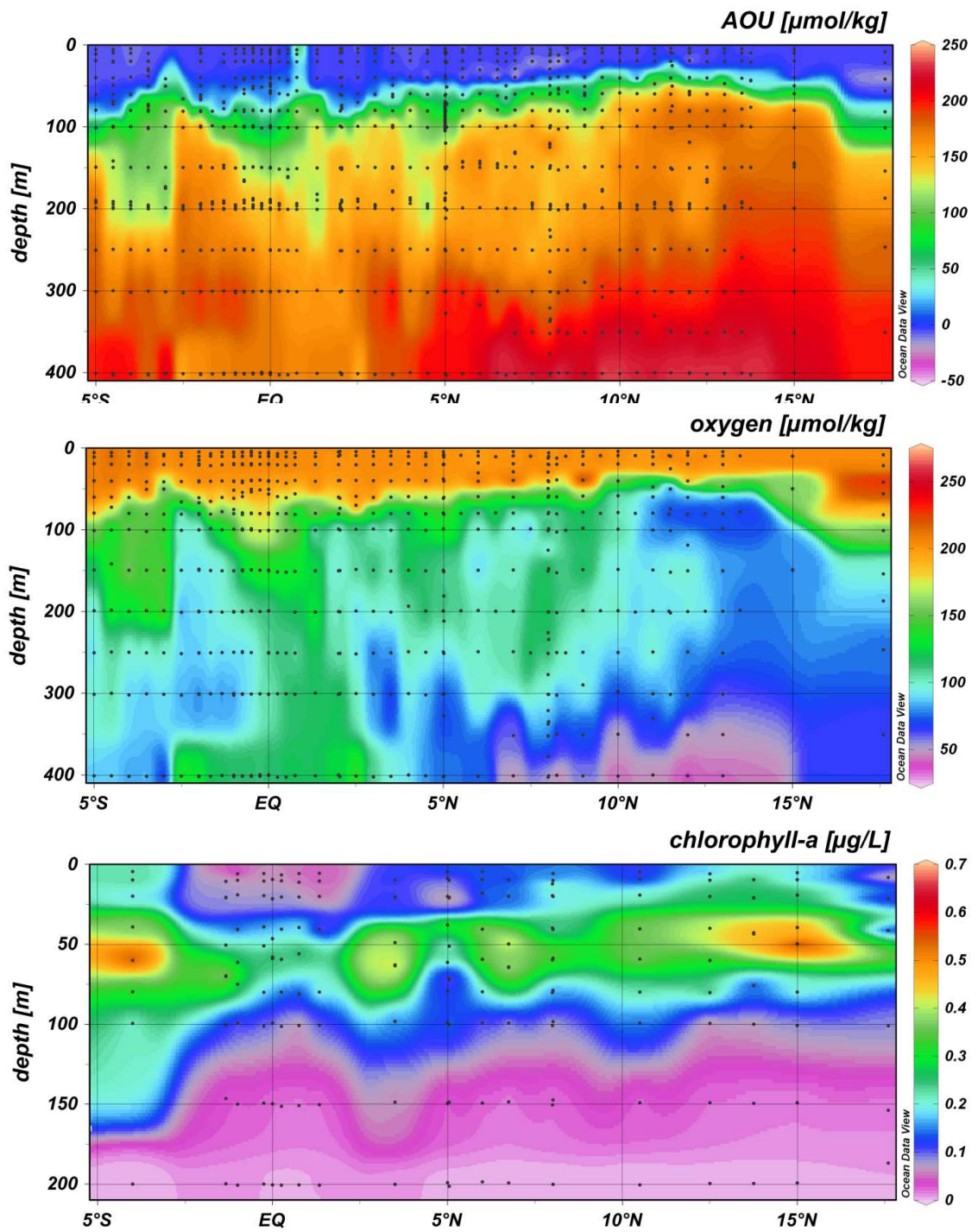


Figure 3. Two dimensional plots of dissolved oxygen (in  $\mu\text{mol kg}^{-1}$ ), apparent oxygen utilization (AOU in  $\mu\text{mol kg}^{-1}$ ) and chlorophyll-a (in  $\mu\text{g L}^{-1}$ ) in the upper 400 m of the ETA water column on M80/1 from south to north (along 23°W and at CVOO). The discrete samples taken with the CTD are shown as black dots (plotted with ODV (Schlitzer, 2012)).

The  $\text{NO}_2^-$  maximum ( $0.10 - 0.45 \mu\text{mol L}^{-1}$ ) was observed from 30 to 100 m (with its maximum at 60 – 100 m) with the rest of the water column being depleted below  $0.10 \mu\text{mol L}^{-1}$  as shown in Figure 4. This is imbedded into waters of low  $\text{NO}_2^-$  in the surface waters and below 150 – 200 m depth where it is really depleted. A slight variation was observed on the equator and  $2^\circ\text{S}$  were  $\text{NO}_2^-$  penetrated down to 200 and even 300 m.

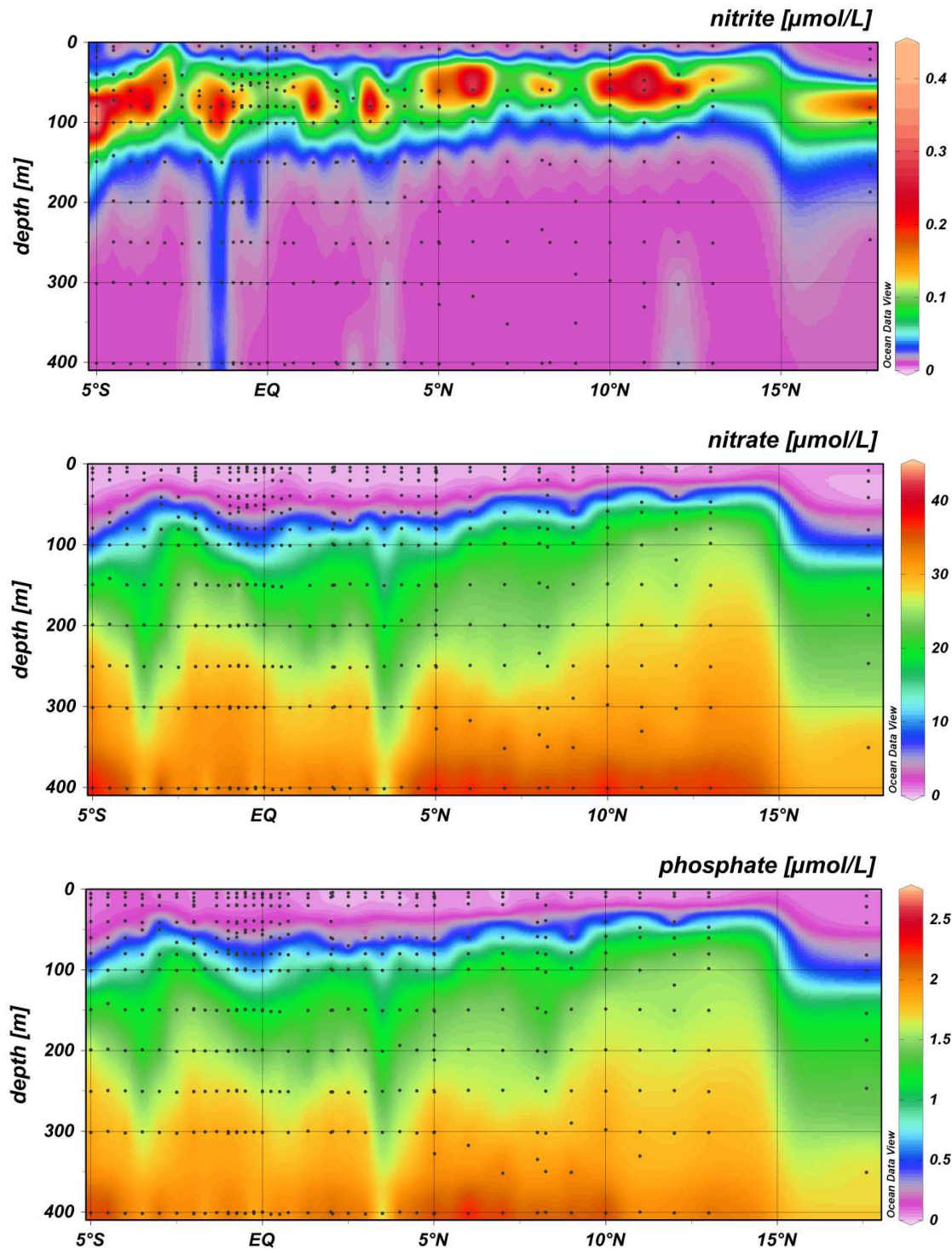


Figure 4. Two dimensional plot of the nutrients nitrite ( $\text{NO}_2^-$ ), nitrate ( $\text{NO}_3^-$ ) and phosphate ( $\text{PO}_4^{3-}$ ) (in  $\mu\text{mol L}^{-1}$ ) plotted in the same way as figure 3.

The other two macronutrients ( $\text{NO}_3^-$  and P) are shown in Figure 4 and exhibit typical nutrient like depth profiles. The surface shows the lowest concentrations of  $\text{NO}_3^-$  ( $<0.5 \mu\text{mol L}^{-1}$ ) and an increase with depth with a maximum at 400 m between  $4.5^\circ\text{N}$  and  $13^\circ\text{N}$  ( $>36 \mu\text{mol L}^{-1}$ ). The same feature was observed for P with surface concentrations of  $< 0.1 \mu\text{mol L}^{-1}$  and an increase with depth to  $\sim 2 \mu\text{mol L}^{-1}$ . The maximum core of  $2.2 - 2.3 \mu\text{mol L}^{-1}$  was observed at 400 m between  $6^\circ\text{N}$  and  $7^\circ\text{N}$ . At CVOO the P concentration was lower throughout the whole water column compared to the rest of the transect.

### 3.3 Section of dissolved Cadmium (Cd)

Figure 5 shows the Cd concentration as a function of latitude (south to north as shown in Figure 5) in the ETA upper 400 m of the water column. The depth profiles at all of the sampled GoFlo-stations revealed the typical nutrient type behavior with very low concentrations in the euphotic and increasing concentrations with depth. Cd showed depleted concentrations in the surface (20 m) samples ( $3 - 11 \text{ pmol L}^{-1}$ ). Cd remained depleted ( $< 30 \text{ pmol L}^{-1}$ ) at all stations in the upper 80 m of the water column with the only exception of  $86 \text{ pmol L}^{-1}$  Cd at 80 m of GoFlo-station 2 ( $8^\circ 15' \text{N}$ ,  $21^\circ 45' \text{W}$ ). At some stations the depletion remained down to 100 m, or even to 200 m at GoFlo-station 3 at  $2^\circ\text{N}$  with less than  $5 \text{ pmol L}^{-1}$  down to 80 m,  $12 \text{ pmol L}^{-1}$  at 100 m and  $21 \text{ pmol L}^{-1}$  at 200 m. Below the euphotic zone, Cd concentrations increased rapidly with depth (max.  $472 \text{ pmol L}^{-1}$  at 400 m at GoFlo-station 7 at  $5^\circ\text{N}$ ). Most stations show this feature, just some less pronounced than others. An exception was GoFlo-station 4 on the equator with similarly low concentrations as at  $2^\circ\text{N}$  throughout the euphotic zone, but then the lowest concentrations at depth ( $125 \text{ pmol L}^{-1}$  at 200 m,  $140 \text{ pmol L}^{-1}$  at 300 m and  $244 \text{ pmol L}^{-1}$  at 200 m).

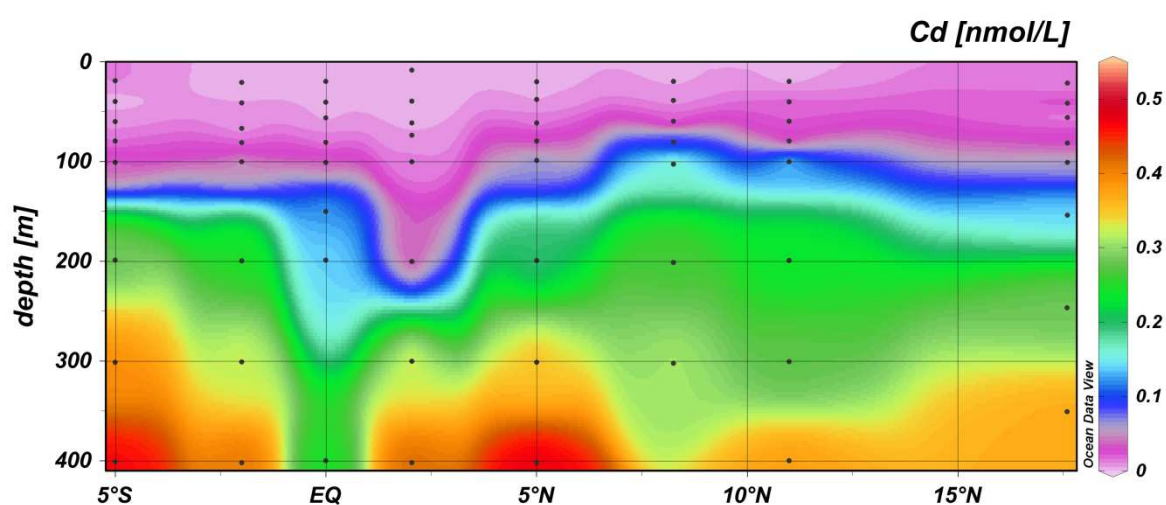


Figure 5. Two dimensional plot of dissolved Cadmium (Cd) (in  $\text{nmol L}^{-1}$ ) as a function of the upper 400 m of the water column versus latitude (south to north). The discrete samples taken with the GoFlo bottles are shown as black dots.

### 3.4 Section of dissolved Iron (Fe)

In Figure 6 the Fe concentrations are displayed as a function of latitude. South of the equator up to 2°N Fe was distributed with its typical nutrient like depth profile.

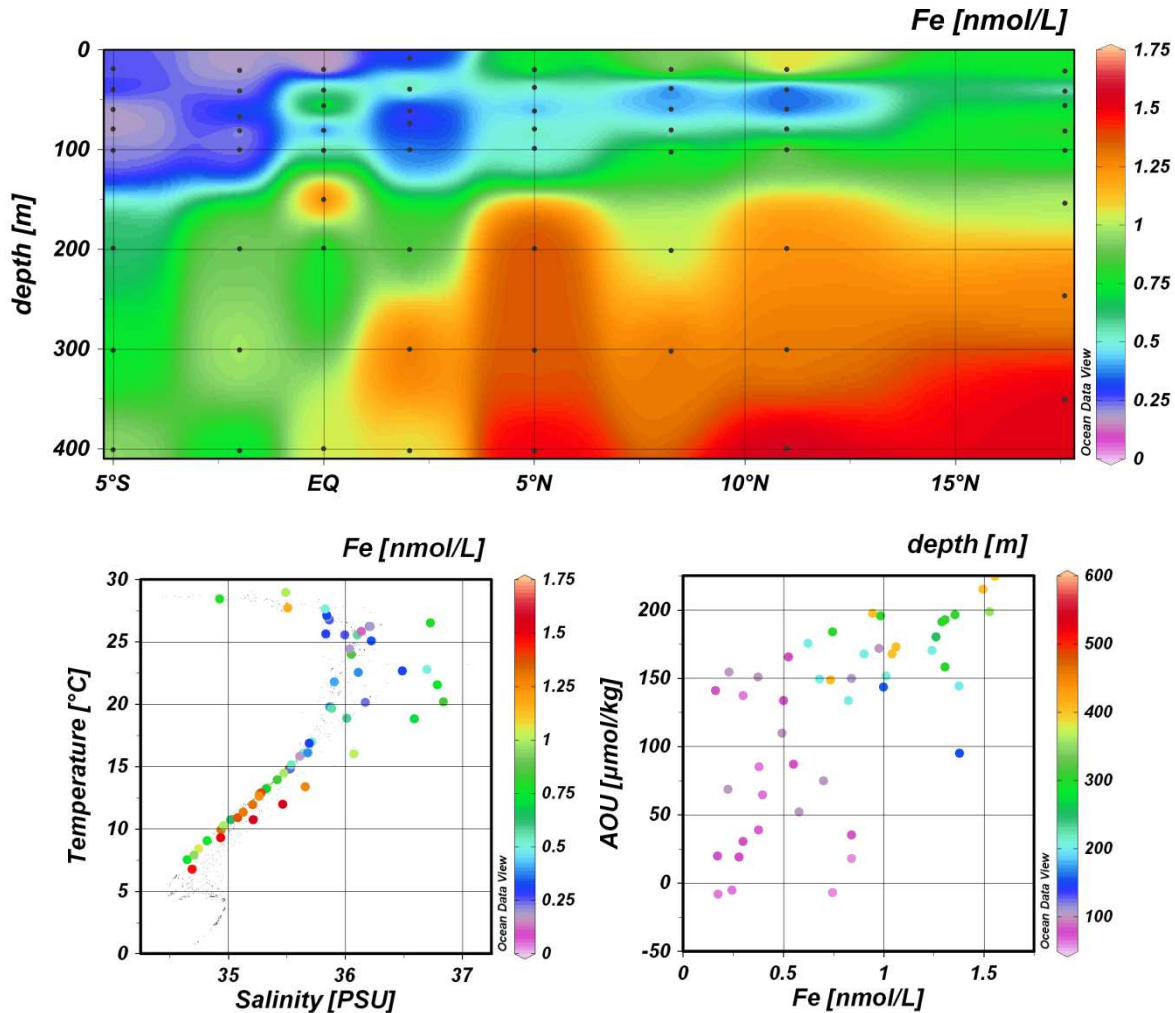


Figure 6. On top two dimensional plot of dissolved iron (Fe) (in  $\text{nmol L}^{-1}$ ) plotted in the same way as Figure 5. Below on the left: temperature (in  $^{\circ}\text{C}$ ) versus salinity (PSU) diagram with color of the dots scaled to the Fe concentration (in  $\text{nmol L}^{-1}$ ). The outliers with higher salinity from the line of other samples were from CVOO and the dark blue is from the EUC. Below on the right: the Fe concentration (in  $\text{nmol L}^{-1}$ ) is plotted versus the apparent oxygen utilization (AOU) (in  $\mu\text{mol kg}^{-1}$ ) the and in color the sampling depth (in m).

The lowest concentrations were observed in the surface and penetrating deeper down in the south ( $20 - 100 \text{ m} < 0.40 \text{ nmol L}^{-1}$  at  $2^{\circ}\text{S}$  and  $5^{\circ}\text{S}$ ) than in the north with its higher deep concentrations ( $\sim 0.57 \text{ nmol L}^{-1}$  at  $40 \text{ m}$  at  $0^{\circ}\text{N}$  and  $2^{\circ}\text{N}$ ). The lowest surface concentration was observed on the equator with  $0.11 \text{ nmol L}^{-1}$ . The deep ( $400 \text{ m}$ ) concentrations increased from south ( $< 0.96 \text{ nmol L}^{-1}$ ) to the Equator ( $\sim 1.00 \text{ nmol L}^{-1}$ ) and further to the north ( $\sim 1.50 \text{ nmol L}^{-1}$ ). This feature was also observed at  $200$  and  $300 \text{ m}$  depth. Between  $40$  and  $100 \text{ m}$  the concentrations were nearly as low as the observed surface concentrations in the Southern Hemisphere of our transect, but then increased towards the north. Though between

the equator and 11°N the concentrations in this 60 m range were lower than in the surrounding water masses in the surface and below this “tongue”. In this region it becomes clear that Fe does not reveal a purely nutrient-like, but a hybrid-type behavior as it is biologically used at these depths. Two more high points stick out on the equator. On one hand the comparably high Fe values between 40 and 60 m ( $0.559$  and  $0.840$   $\text{nmol L}^{-1}$ ) and on the other  $1.377$   $\text{nmol L}^{-1}$  at 150 m.

### 3.5 Section of dissolved Manganese (Mn)

In Figure 7 the Mn concentration is plotted as a function of the trace metal section at 23°W and the depth (0 – 400 m).

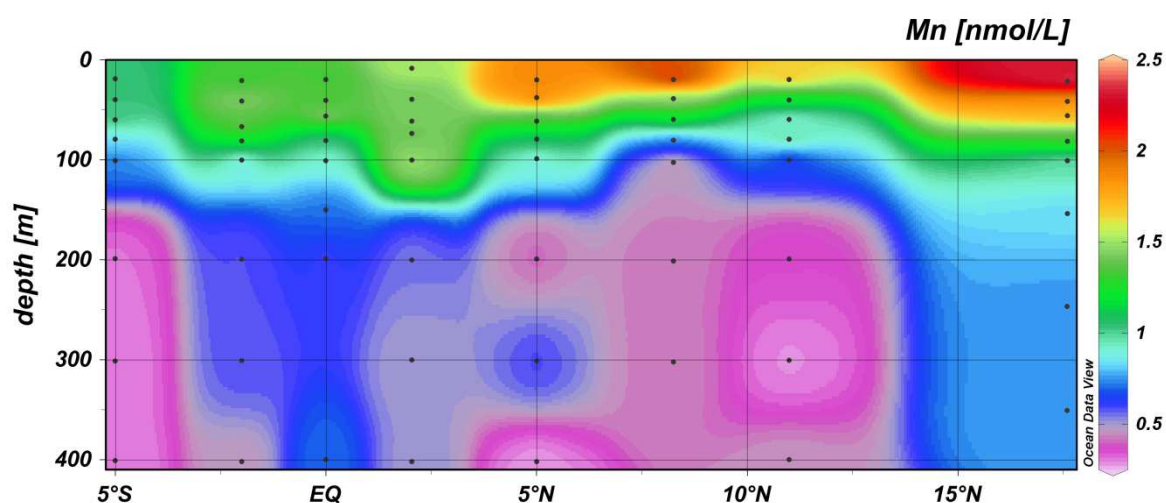


Figure 7. Two dimensional plot of dissolved Manganese (Mn) (in  $\text{nmol L}^{-1}$ ) which is plotted in the same way as Figure 5.

At all the sampled GoFlo-stations the Mn concentrations show typical scavenged depth profiles with high surface concentrations and depletion with depths. The most elevated Mn concentrations were found in the surface waters of CVOO with  $2.38$   $\text{nmol L}^{-1}$  and at 8°N with  $2.10$   $\text{nmol L}^{-1}$ . Heading from CVOO to the south on the 23°W transect, the Mn surface concentrations kept decreasing towards the South with  $1.31$   $\text{nmol L}^{-1}$  found on the equator and only  $1.04$   $\text{nmol L}^{-1}$  at 5°S. At 2°N the Mn concentration in the upper 100 m nearly did not vary at all  $1.45 \pm 0.05$   $\text{nmol L}^{-1}$  and was then depleted to  $0.51 \pm 0.02$   $\text{nmol L}^{-1}$ . As expected for a scavenged distributed trace metal the Mn concentrations were high in the surface and then quickly depleted with depths at all the sampled stations. Though this feature was far less pronounced at CVOO with the highest surface concentration detected on this cruise, still high values in the top 80 m were observed and remained pretty constant from 100 – 350 m ( $0.80 \pm 0.66$   $\text{nmol L}^{-1}$ ) compared to the depleted Mn concentrations of  $0.42 \pm 0.11$   $\text{nmol L}^{-1}$  at depth (without CVOO and the equator station). Another exceptional station at depth was the one on the equator with  $0.72 \pm 0.11$   $\text{nmol L}^{-1}$  compared to the other sampled stations.

## 4 DISCUSSION

### 4.1 Dissolved Cadmium (Cd) and Phosphate (P)

Due to the high dust inputs to the Eastern Tropical North Atlantic (ETNA), some of the P in this region is introduced to the surface ocean via mineral aerosols (Mahowald *et al.*, 2008). As typically a low surface residence time for aerosols is found, this means that solubility is an important factor and the soluble part of the aerosol total phosphorous is thought to be phosphate with a content of approximately 10% in Saharan dust (Baker *et al.*, 2006). The P surface minimum ( $<0.1 \mu\text{mol L}^{-1}$ ) in our data was shallower ( $<40 \text{ m}$ ) between  $6^{\circ}\text{N}$  and  $13^{\circ}\text{N}$  compared to the rest of the transect. At  $6^{\circ}\text{N}$  and  $7^{\circ}\text{N}$  the core of the P maximum was observed at  $400 \text{ m}$ . Baker *et al.* (2007) and Mills *et al.* (2004) found the P inputs to be insufficient for N-fixation in this region. Upwelling brings micro- and macronutrient rich waters up from below. Cd and  $\text{PO}_4^{3-}$  have been shown to be upwelled uniformly from subsurface waters and continental runoff (Boyle *et al.*, 1981; Bruland, 1980; Van Der Loeff *et al.*, 1997), but Cd is depleted before  $\text{PO}_4^{3-}$  in the surface waters and out of upwelling regions Cd is depleted first (Van Der Loeff *et al.*, 1997). Close to the West African higher  $\text{PO}_4^{3-}$  were observed in the surface waters (at  $25 \text{ m}$  depth), but further away from the coast in the open ocean, close to the Cape Verdean Islands and close to the equator the concentrations are low (Mather *et al.*, 2008). Though the Northern Atlantic subtropical gyre has this higher dust impact, the region is nonetheless depleted in  $\text{PO}_4^{3-}$  as a result to the higher nitrogen fixation due to the high Fe and P input (Mills *et al.*, 2004). At  $50 \text{ m}$  elevated  $\text{PO}_4^{3-}$  concentrations can be observed close to the West African coast due to upwelling. The equatorial upwelling is also a source of  $\text{PO}_4^{3-}$  which can be observed below  $150 \text{ m}$  and is more pronounced in the eastern than in the western basin (Levitus *et al.*, 1993). These observations are comparable to our results on the  $23^{\circ}\text{W}$  transect where  $\text{PO}_4^{3-}$  behaved with its typical nutrient like behavior with depleted surface concentrations ( $< 0.02 \mu\text{mol L}^{-1}$ ) and  $2.06 \pm 0.11 \mu\text{mol L}^{-1}$  at  $400 \text{ m}$ . In contrast to the dust-derived  $\text{PO}_4^{3-}$ , the main source of Cd is vertical mixing from below whilst atmospheric deposition and influence by the Inter-Tropical Convergence Zone (ITCZ) are insignificant (Pohl *et al.*, 2011; Van Der Loeff *et al.*, 1997). In the upper  $60 \text{ m}$  Cd concentrations remained below  $10 \text{ pmol L}^{-1}$  which is in good agreement with the values report by Pohl *et al.* (2011) for this region. We found that Cd was low in the surface/euphotic zone throughout the region but the lowest in equatorial region due to primary productivity. These are typical Cd values in the open Atlantic Ocean. Cd concentrations are found in the low  $\text{pmol L}^{-1}$  range in the surface and in the high  $\text{pmol L}^{-1}$ /nearly  $\text{nmol L}^{-1}$  range in the deep ocean (Löscher *et al.*, 1997). We observed at all stations below the TSW with its steady low Cd concentrations a sharp increase with depth by roughly  $100 \text{ pmol L}^{-1}$  per  $100 \text{ m}$  (from



100 – 400 m). Therefore we also divided our results into two Cd/P ratios (in pmol/ $\mu$ mol): the surface Cd/P ratio and the deep Cd/P <sup>3-</sup> ratio. Dissolved Cd/P ratios (pmol/ $\mu$ mol) are shown in Figure 8 and were low in the euphotic zone (80 - 100 m depending on the station) below 100 m with a few exceptions where the PO<sub>4</sub><sup>3-</sup> was really depleted.

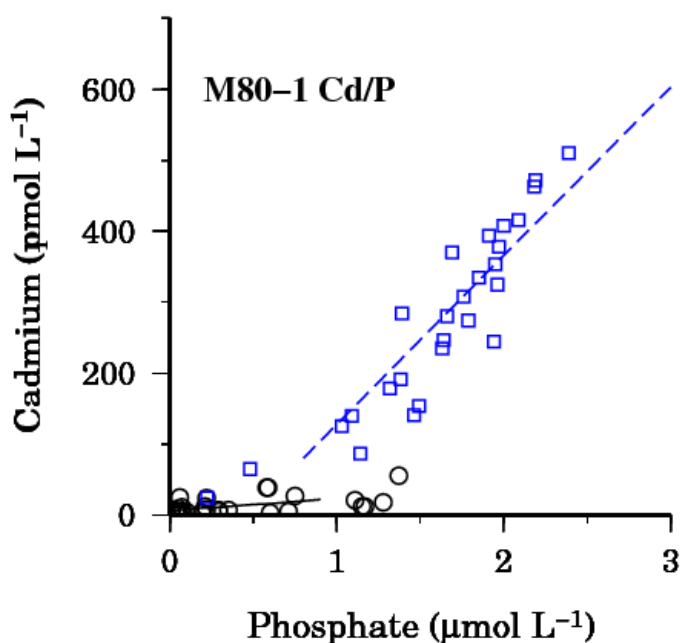


Figure 8. Dissolved Cadmium (Cd) (in pmol L<sup>-1</sup>) versus phosphate (P) (in  $\mu$ mol L<sup>-1</sup>) concentrations in the upper 400 m of the water column on the trace metal section. The two Cd/P ratios are expressed as (i) for the Cd depleted surface water (0 – 100 m) (black circles and the Cd/P ratio as a black line) and (ii) for 100 – 400 m of the water column (blue squares and the Cd/P ratio as a dashed blue line).

This ratio increased with depth to approximately 200 at 400 m. This increase was linear with different slopes and intercepts for the different positions. These values are reported in Table 3. The steepest slopes were observed at 2°S, 2°N and 11°N with 422 – 461 pmol/ $\mu$ mol together with the most negative intercept ranging from -459 to -542 pmol/ $\mu$ mol. The two stations 5°S and 5°N of the equator revealed slopes of 265 pmol/ $\mu$ mol and 309 pmol/ $\mu$ mol. The lowest slopes and smallest intercept were observed on the equator (slope = 141 pmol/ $\mu$ mol, intercept = -39 pmol/ $\mu$ mol) and at CVOO (slope = 231 pmol/ $\mu$ mol, intercept = -48 pmol/ $\mu$ mol). The deep ratio with 237.4 pmol/ $\mu$ mol exhibited higher P, but also comparably higher Cd values than in the surface. Our reported Cd/P deep ratio is similar to the deep Atlantic ratio compiled and found by Löscher *et al.* (1997). North of our sampling area Kremling and Streu (1993) found an average Cd/P ratio in the ETA of  $140 \pm 60$  pmol/ $\mu$ mol. The compiled data set for the global ocean by de Baar *et al.* (1994) show Cd/P ratios which are comparable to our deep ratio. Cd/P ratios can be grouped along isopycnal surfaces. The Cd/P ratio of 240 pmol/ $\mu$ mol for the surface waters (0 - 700 m) of the

Atlantic Ocean and of 252 pmol/ $\mu$ mol for the North Atlantic Central Water (NACW) (Yeats, 1998) are similar with our deep ratio of 237.4 pmol/ $\mu$ mol (100 – 400 m).

As a result of higher biological fractionation (Saager, 1994) in the surface, this ratio was significantly lower with 16.6 pmol/ $\mu$ mol than the deep ratio. It has been shown that in the oligotrophic surface waters of the Atlantic Ocean the Cd/P ratios are significantly lower than in the deep due to favored mineralization of P (de Baar *et al.*, 1994; Kremling and Streu, 1993; Yeats *et al.*, 1995). This decoupling of Cd and P in the surface ocean is a result to biologically produced organic chelators which can bind up to 70 % of the dissolved Cd. In comparison Cd at depth is believed to be bound by mostly inorganic chloride components with little to no organic complexation (Bruland, 1992) though there is no data from the Tropical Atlantic and recent data from the Atlantic sector of the Southern Ocean (Baars *et al.* submitted) suggests there is organic complexation of Cd in deep waters there. The surface variations in Cd/P has been shown to be due to Fe limitation in high nutrient low chlorophyll (HNLC) areas (Cullen, 2006; Lane *et al.*, 2009). Similarly in laboratory studies Finkel *et al.* (2007) observed that phytoplankton growth can lead to variations of Cd/P e.g. diatoms were found to increase the Cd/P ratio due to a metabolic demand of Cd.

## 4.2 Dissolved Iron (Fe) and Nitrite (NO<sub>2</sub><sup>-</sup>)

The main pathway for Fe to the oligotrophic ETA is via Saharan dust deposition (Jickells, 1995). It has been shown that for Fe the wet deposition outcompetes dry deposition in areas of the ITCZ and can be an order of magnitude greater than Fe introduced to the surface ocean by dry deposition, but dry deposition dominates in regions without rainfall (Sarhou *et al.*, 2003). Though in the ITCZ this does not account for N as both deposition types were comparable and the wet deposition decreased westwards with distance from the African coast (Baker *et al.*, 2007). Saharan dust deposition was found to be depleted southwards of the ITCZ as shown for the Aeolian tracer of dust aluminum (Al) (Measures, 1995). These observations correlate nicely with our findings of Fe in the ETA. From 5°S to 2°N we observed Fe with a nutrient like depth profile. Fe concentrations in the surface waters of 5°–23°N under the Saharan Dust Plume were the peak Fe concentrations depleting southwards down to 5°S. Barrett *et al.* (2012) found the highest Fe surface concentrations between ~10° and 20°N as a result of high dust input and scavenging from lithogenic particles. South of the Cape Verdean Islands Rijkenberg *et al.* (2012) found that vertical diffusive mixing can outcompete the dust input as a source for Fe between 100 and 300 m which fits our elevated Fe concentrations between 200 and 400 m between 5 and 23°N. They consider that the concurrence of the nutricline and ferricline confirm this finding and that in the Atlantic oxygen minimum zone (OMZ) Fe is re-solubilized from sinking particles. Fe can be solubilized and bound by organic ligands in the OMZ (Witter *et al.*, 2000). In the euphotic zone the ligands

outcompete the Fe and hence nearly 100 % of Fe is organically complexed (Gledhill and van den Berg, 1994). Our results confirm these findings as we observed a correlation between 60 and 100 m for high  $\text{NO}_2^-$  and low Fe concentrations. At 2°N we observed a minimum in Fe of  $0.24 \text{ nmol L}^{-1}$  at 60 m and  $0.28 \text{ nmol L}^{-1}$  at 80 m together with depleted  $\text{NO}_2^-$  concentrations ( $0.01$  and  $0.06 \text{ } \mu\text{mol L}^{-1}$ ) compared to other  $\text{NO}_2^-$  concentrations at similar depth (up to  $0.40 \text{ } \mu\text{mol L}^{-1}$ ). These minima were observed in the near-surface layer TSW which is a western flowing current from the West African coast (Stramma *et al.*, 2003) with high biological uptake.

A recent study by Noble *et al.* (2012) showed on a west-east transect in the Southern Tropical Atlantic that the two strongly dust/terrestrially influenced trace metals Fe and Mn can be exponentially removed relative to the distance from the coast and relative to the concentration of dissolved oxygen. Similar patterns have been observed in other regions related to distance from the shore (Croot and Hunter, 1998; Johnson *et al.*, 1999; Luther III *et al.*, 1997). In Figure 6, Fe is plotted versus AOU below the mixed layer depth (100 – 600 m). A cluster for the samples around 100 m was observed and a second smaller area for the samples taken at greater depth.

On the equator we found some anomalies in our Fe data which has not been observed yet as far as we know. We measured comparably high Fe values at 40 and 60 m ( $0.56$  and  $0.84 \text{ nmol L}^{-1}$ ) and at 150 m ( $1.38 \text{ nmol L}^{-1}$ ). This enrichment in Fe can be due to high Fe values transported eastwards with the EUC. The Fe peak data was found on the edges of the EUC. In the upper part it coincides with the salinity maximum of the subtropical underwater which was pronounced when the samples were taken. The peak Fe data at 150 m was on the lower edge of the EUC (Brandt, personal communication).

### 4.3 Dissolved Manganese (Mn)

Already, Kremling (1985) observed clear patterns for the Mn concentrations in the Atlantic with the highest surface concentrations in the area of the Saharan dust.  $2.74 \pm 1.01 \text{ nmol L}^{-1}$  were determined in areas of Aeolian influence, whereas in surface areas without this influence they ranged around  $1.0 \text{ nmol L}^{-1}$  (Kremling, 1985). High Mn due to dry deposition around the Cape Verdean Islands and highest surface values in the ITCZ as a matter of wet deposition (up to  $4.8 \text{ nmol L}^{-1}$ ) were observed by Pohl *et al.* (2011). The ITCZ can have a significant influence on the photodissolution of Mn from particles (Sunda and Huntsman, 1994) due to the high inputs of hydrogen peroxide ( $\text{H}_2\text{O}_2$ ) with the precipitation (Croot *et al.*, 2004). Models predict high Aeolian dust deposition to the ETNA (Vink and Measures, 2001) in comparison to the Eastern Subtropical Northern Atlantic (ESNA) (Mahowald *et al.*, 2005). As expected for an element introduced mainly by dust to the surface ocean in the region of our transect (Shiller, 1997), Mn exhibits typical scavenged depth profiles at all stations on the

23°W transect. This distribution has been observed for Mn in the eastern Atlantic Ocean with similar concentrations to our findings. The surface concentrations ranged from 0.90 to 2.12 nmol L<sup>-1</sup> and at depth Mn was depleted to ~0.2 nmol L<sup>-1</sup> as a result to scavenging (Statham *et al.*, 1998). The surface concentrations were comparable to previous studies with a Mn peak at CVOO with 2.38 nmol L<sup>-1</sup>. Mn concentrations show a similar feature like Fe in the surface with high surface concentrations at CVOO. Clearly Mn is elevated in the whole water column at CVOO compared to the more southern stations due to continental runoff as it has been observed for the coast of West Africa (Lam *et al.*, 2012).

## ACKNOWLEDGMENTS

This work is a contribution of the Collaborative Research Centre 754 “Climate – Biogeochemistry Interactions in the Tropical Ocean” ([www.sfb754.de](http://www.sfb754.de)), which is supported by the German Research Association (DFG) and a contribution of the BMBF Verbundprojekt SOPRAN (FKZ 03F0462A and 03F0611A) (<http://sopran.pangaea.de>) that forms part of the German contribution to SOLAS (Surface Ocean Lower Atmosphere Studies). Funding for the participation of K. Wuttig was provided by a grant from the DFG awarded to P. L. Croot (CR145/17-1). T. Wagener was supported by a Marie Curie IEF (Grant agreement No.: PIEF-GA-2009-236694, DAPOP). The officers and crew of the research vessel FS Meteor are gratefully acknowledged for their help in performing sampling at sea along with the chief scientist P. Brandt and the M80/1 scientists. Special thanks to V. Hormann for the salinity measurements and to P.Brandt, A. Funk and G. Krahnemann (all GEOMAR) for providing the physical oceanographic data. The authors gratefully acknowledge the members of the trace metal speciation group at GEOMAR who helped directly with this project: O. Baars, A. Dammshäuser, M. Dunker and M. I. Heller. Special thanks go to T. Steinhoff, T. Stöven, S. Fessler, M. Lohmann and F. Malien (GEOMAR) for sampling, their nutrient laboratory work and T. Stöven for measuring the Winkler oxygen samples. T. Großkopf (GEOMAR) and V. Meldo (INDP) are gratefully acknowledged for providing the chlorophyll-a data. Special thanks to Geoffrey (Geo) Smith at UCSC for taking care of the logistics for the SAFe and GEOTRACES samples.

## REFERENCES

- Aguilar-Islas, A.M., Resing, J.A. and Bruland, K.W., 2006. Catalytically enhanced spectrophotometric determination of manganese in seawater by flow-injection analysis with a commercially available resin for on-line preconcentration. *Limnology and Oceanography-Methods*, 4: 105-113.
- Aguirre, J.D. and Culotta, V.C., 2012. Battles with Iron: Manganese in Oxidative Stress Protection. *Journal of Biological Chemistry*, 287(17): 13541-13548.
- Baars, O., Croot, P.L., Abouchami, W., Galer, S.J.G. and Boye, M., for submission. Distribution and speciation of dissolved cadmium in the Southern Ocean and its relation to phosphate.
- Baker, A.R., Jickells, T.D., Witt, M. and Linge, K.L., 2006. Trends in the solubility of iron, aluminium, manganese and phosphorus in aerosol collected over the Atlantic Ocean. *Marine Chemistry*, 98(1): 43-58.
- Baker, A.R. *et al.*, 2007. Dry and wet deposition of nutrients from the tropical Atlantic atmosphere: Links to primary productivity and nitrogen fixation. *Deep Sea Research Part I: Oceanographic Research Papers*, 54(10): 1704-1720.
- Barrett, P.M. *et al.*, 2012. The trace element composition of suspended particulate matter in the upper 1000m of the eastern North Atlantic Ocean: A16N. *Marine Chemistry*, 142-144(0): 41-53.
- Benitez-Nelson, C.R., 2000. The biogeochemical cycling of phosphorus in marine systems. *Earth-Science Reviews*, 51(1-4): 109-135.
- Boyle, E.A., Husteded, S.S. and Jones, S.P., 1981. On the distribution of copper, nickel, and cadmium in the surface waters of the North Atlantic and North Pacific Ocean. *Journal of Geophysical Research: Oceans*, 86(C9): 8048-8066.
- Brandt, P. *et al.*, 2011. Circulation and Oxygen Distribution in the Tropical Atlantic Cruise No. 80, Leg 1; October 26 to November 23, 2009 Mindelo (Cape Verde) to Mindelo (Cape Verde), Hamburg, Germany, Leitstelle Deutsche Forschungsschiffe, Inst. f. Meereskunde.
- Brandt, P. *et al.*, 2008. Oxygen tongues and zonal currents in the equatorial Atlantic. *Journal of Geophysical Research-Oceans*, 113(C4): C04012.
- Brandt, P. *et al.*, 2010. Changes in the Ventilation of the Oxygen Minimum Zone of the Tropical North Atlantic. *Journal of Physical Oceanography*, 40(8): 1784-1801.
- Brandt, P. *et al.*, 2006. Circulation in the central equatorial Atlantic: Mean and intraseasonal to seasonal variability. *Geophysical Research Letters*, 33(7): L07609.
- Bruland, K.W., 1980. Oceanographic distributions of cadmium, zinc, nickel, and copper in the North Pacific. *Earth and Planetary Science Letters*, 47(2): 176-198.
- Bruland, K.W., 1992. Complexation of cadmium by natural organic ligands in the central North Pacific. *Limnol. Oceanogr.*, 37(5): 1008-1017.
- Bruland, K.W., Franks, R.P., Knauer, G.A. and Martin, J.H., 1979. Sampling and Analytical Methods for the Determination of Copper, Cadmium, Zinc, and Nickel at the Nanogram Per Liter Level in Sea-Water. *Analytica Chimica Acta*, 105(1): 233-245.
- Bruland, K.W. and Lohan, M.C., 2003. 6.02 - Controls of Trace Metals in Seawater. In: D.H. Editors-in-Chief: Heinrich and K.T. Karl (Editors), *Treatise on Geochemistry*. Pergamon, Oxford, pp. 23-47.
- Cotrim da Cunha, L., Croot, P.L. and LaRoche, J., 2009. Influence of river discharge in the tropical and subtropical North Atlantic Ocean. *Limnology and Oceanography*, 54(2): 644-U1.
- Croot, P.L. and Hunter, K.A., 1998. Trace metal distributions across the continental shelf near Otago Peninsula, New Zealand. *Marine Chemistry*, 62(3-4): 185-201.
- Croot, P.L., Streu, P., Peeken, I., Lochte, K. and Baker, A.R., 2004. Influence of the ITCZ on H<sub>2</sub>O<sub>2</sub> in near surface waters in the equatorial Atlantic Ocean. *Geophys. Res. Lett.*, 31(23): L23S04.

- Cullen, J.T., 2006. On the nonlinear relationship between dissolved cadmium and phosphate in the modern global ocean : Could chronic iron limitation of phytoplankton growth cause the kink? *Limnol. Oceanogr.*, 51(3): 12.
- Cutter, G.A. *et al.*, 2010. Sampling and Sample-handling Protocols for GEOTRACES Cruises. In: G.S.a.I. Committee (Editor).
- Danielsson, L.-G., Magnusson, B. and Westerlund, S., 1978. An improved metal extraction procedure for the determination of trace metals in sea water by atomic absorption spectrometry with electrothermal atomization. *Analytica Chimica Acta*, 98(1): 47-57.
- de Baar, H.J.W., Saager, P.M., Nolting, R.F. and van der Meer, J., 1994. Cadmium versus phosphate in the world ocean. *Marine Chemistry*, 46(3): 261-281.
- Duce, R.A. *et al.*, 1991. The atmospheric input of trace species to the world ocean. *Global Biogeochemical Cycles*, 5(3): 193-259.
- Finkel, Z.V., Quigg, A.S., Chiampì, R.K., Schofield, O.E. and Falkowski, P.G., 2007. Phylogenetic diversity in cadmium: phosphorus ratio regulation by marine phytoplankton. *Limnol. Oceanogr.*, 52(3): 8.
- Gledhill, M. and Buck, K.N., 2012. The organic complexation of iron in the marine environment: a review. *Frontiers in Microbiology*, 3.
- Gledhill, M. and van den Berg, C.M.G., 1994. Determination of complexation of iron(III) with natural organic complexing ligands in seawater using cathodic stripping voltammetry. *Marine Chemistry*, 47(1): 41-54.
- Gordon, R.M., Coale, K.H. and Johnson, K.S., 1997. Iron distributions in the equatorial Pacific: Implications for new production. *Limnology and Oceanography*, 42(3): 419-431.
- Grasshoff, K., Ehrhardt, M. and Kremling, K., 2007. *Methods of Seawater Analysis*. Wiley-VCH Verlag GmbH, Weinheim (FRG), pp. i-xxxii.
- Grasshoff, K., Kremling, K. and Ehrhardt, M., 1983. *Methods of seawater analysis*. Verlag Chemie, Weinheim.
- Hong, H. and Kester, D.R., 1986. Redox state of iron in offshore waters of Peru. *Limnology and Oceanography*, 31: 512-524.
- Hopkinson, B.M. and Barbeau, K.A., 2007. Organic and redox speciation of iron in the eastern tropical North Pacific suboxic zone. *Marine Chemistry*, 106(1–2): 2-17.
- Jickells, T., 1995. Atmospheric inputs of metals and nutrients to the oceans: their magnitude and effects. *Marine Chemistry*, 48(3–4): 199-214.
- Johnson, K.S. *et al.*, 1992. Manganese Flux from Continental Margin Sediments in a Transect Through the Oxygen Minimum, pp. 1242-1245.
- Johnson, K.S., Chavez, F.P. and Friederich, G.E., 1999. Continental-shelf sediment as a primary source of iron for coastal phytoplankton. *Nature*, 398(6729): 697-700.
- Karstensen, J., Stramma, L. and Visbeck, M., 2008. Oxygen minimum zones in the eastern tropical Atlantic and Pacific oceans. *Progress in Oceanography*, 77(4): 331-350.
- Kremling, K., 1985. The distribution of cadmium, copper, nickel, manganese, and aluminium in surface waters of the open Atlantic and European shelf area. *Deep Sea Research Part A. Oceanographic Research Papers*, 32(5): 531-555.
- Kremling, K. and Streu, P., 1993. Saharan dust influenced trace element fluxes in deep North Atlantic subtropical waters. *Deep Sea Research Part I: Oceanographic Research Papers*, 40(6): 1155-1168.
- Lam, P.J., Ohnemus, D.C. and Marcus, M.A., 2012. The speciation of marine particulate iron adjacent to active and passive continental margins. *Geochimica Et Cosmochimica Acta*, 80(0): 108-124.
- Lane, E.S., Semeniuk, D.M., Strzepek, R.F., Cullen, J.T. and Maldonado, M.T., 2009. Effects of iron limitation on intracellular cadmium of cultured phytoplankton: Implications for surface dissolved cadmium to phosphate ratios. *Marine Chemistry*, 115(3–4): 155-162.
- Lane, T.W. and Morel, F.M.M., 2000. A biological function for cadmium in marine diatoms. *Proceedings of the National Academy of Sciences*, 97(9): 4627-4631.
- Lee, J.G., Ahner, B.A. and Morel, F.M.M., 1996. Export of Cadmium and Phytochelatin by the Marine Diatom *Thalassiosira weissflogii*. *Environmental Science & Technology*, 30(6): 1814-1821.

- Levitus, S., Conkright, M.E., Reid, J.L., Najjar, R.G. and Mantyla, A., 1993. Distribution of nitrate, phosphate and silicate in the world oceans. *Progress in Oceanography*, 31(3): 245-273.
- Lewis, B.L. and Luther III, G.W., 2000. Processes controlling the distribution and cycling of manganese in the oxygen minimum zone of the Arabian Sea. *Deep Sea Research Part II: Topical Studies in Oceanography*, 47(7-8): 1541-1561.
- Löscher, B.M., van der Meer, J., de Baar, H.J.W., Saager, P.M. and de Jong, J.T.M., 1997. The global Cd/phosphate relationship in deep ocean waters and the need for accuracy. *Marine Chemistry*, 59(1-2): 87-93.
- Luther III, G.W., Sundby, B., Lewis, B.L., Brendel, P.J. and Silverberg, N., 1997. Interactions of manganese with the nitrogen cycle: Alternative pathways to dinitrogen. *Geochimica et Cosmochimica Acta*, 61(19): 4043-4052.
- Mahowald, N. *et al.*, 2008. Global distribution of atmospheric phosphorus sources, concentrations and deposition rates, and anthropogenic impacts. *Global Biogeochem. Cycles*, 22(4): GB4026.
- Mahowald, N.M. *et al.*, 2005. Atmospheric global dust cycle and iron inputs to the ocean. *Global Biogeochem. Cycles*, 19(4): GB4025.
- Malmstrom, R.R. *et al.*, 2013. Ecology of uncultured *Prochlorococcus* clades revealed through single-cell genomics and biogeographic analysis. *ISME J*, 7(1): 184-198.
- Mather, R.L. *et al.*, 2008. Phosphorus cycling in the North and South Atlantic Ocean subtropical gyres. *Nature Geosci*, 1(7): 439-443.
- Measures, C.I., 1995. The distribution of Al in the IOC stations of the eastern Atlantic between 30 °S and 34 °N. *Marine Chemistry*, 49(4): 267-281.
- Mills, M.M., Ridame, C., Davey, M., La Roche, J. and Geider, R.J., 2004. Iron and phosphorus co-limit nitrogen fixation in the eastern tropical North Atlantic. *Nature*, 429(6989): 292-4.
- Moffett, J.W., Goepfert, T.J. and Naqvi, S.W.A., 2007. Reduced iron associated with secondary nitrite maxima in the Arabian Sea. *Deep Sea Research Part I: Oceanographic Research Papers*, 54(8): 1341-1349.
- Moore, M.C. *et al.*, 2009. Large-scale distribution of Atlantic nitrogen fixation controlled by iron availability. *Nature Geosci*, 2(12): 867-871.
- Morel, F.M.M., Hudson, R.J.M. and Price, N.M., 1991. Limitation of productivity by trace metals in the sea. *Limnol. Oceanogr.*, 36(8).
- Morel, F.M.M. and Price, N.M., 2003. The Biogeochemical Cycles of Trace Metals in the Oceans. *Science*, 300(5621): 944-947.
- Noble, A.E. *et al.*, 2012. Basin-scale inputs of cobalt, iron, and manganese from the Benguela-Angola front to the South Atlantic Ocean. *Limnology and Oceanography*, 57(4): 989-1010.
- Parkhill, J.-P., Maillet, G. and Cullen, J.J., 2001. FLUORESCENCE-BASED MAXIMAL QUANTUM YIELD FOR PSII AS A DIAGNOSTIC OF NUTRIENT STRESS. *Journal of Phycology*, 37(4): 517-529.
- Pohl, C. *et al.*, 2011. Synoptic transects on the distribution of trace elements (Hg, Pb, Cd, Cu, Ni, Zn, Co, Mn, Fe, and Al) in surface waters of the Northern- and Southern East Atlantic. *Journal of Marine Systems*, 84(1-2): 28-41.
- Rijkenberg, M.J.A. *et al.*, 2012. Fluxes and distribution of dissolved iron in the eastern (sub-) tropical North Atlantic Ocean. *Global Biogeochem. Cycles*, 26(3): GB3004.
- Rue, E.L., Smith, G.J., Cutter, G.A. and Bruland, K.W., 1997. The response of trace element redox couples to suboxic conditions in the water column. *Deep Sea Research Part I: Oceanographic Research Papers*, 44(1): 113-134.
- Saager, P.M., 1994. On the relationships between dissolved trace metals and nutrients in seawater.
- Saito, M.A., Goepfert, T.J. and Ritt, J.T., 2008. Some thoughts on the concept of colimitation: Three definitions and the importance of bioavailability. *Limnol. Oceanogr.*, 53(1): 276-290.

- Sarthou, G. *et al.*, 2003. Atmospheric iron deposition and sea-surface dissolved iron concentrations in the eastern Atlantic Ocean. *Deep-Sea Research Part I- Oceanographic Research Papers*, 50(10-11): 1339-1352.
- Schlitzer, R., 2012. Ocean Data View.
- Shiller, A.M., 1997. Manganese in surface waters of the Atlantic Ocean. *Geophys. Res. Lett.*, 24(12): 1495-1498.
- Slemons, L., Paul, B., Resing, J. and Murray, J.W., 2012. Particulate iron, aluminum, and manganese in the Pacific equatorial undercurrent and low latitude western boundary current sources. *Marine Chemistry*, 142-144(0): 54-67.
- Statham, P.J., Yeats, P.A. and Landing, W.M., 1998. Manganese in the eastern Atlantic Ocean: processes influencing deep and surface water distributions. *Marine Chemistry*, 61(1-2): 55-68.
- Stramma, L., Fischer, J., Brandt, P. and Schott, F., 2003. Circulation, variability and near-equatorial meridional flow in the central tropical Atlantic. In: G.J. Goni and P. Malanotte-Rizzoli (Editors), Elsevier Oceanography Series. Elsevier, pp. 1-22.
- Stramma, L., Hüttl, S. and Schafstall, J., 2005. Water masses and currents in the upper tropical northeast Atlantic off northwest Africa. *J. Geophys. Res.*, 110(C12): C12006.
- Stramma, L. and Schott, F., 1999. The mean flow field of the tropical Atlantic Ocean. *Deep Sea Research Part II: Topical Studies in Oceanography*, 46(1-2): 279-303.
- Sultan, B. and Janicot, S., 2000. Abrupt shift of the ITCZ over West Africa and intra-seasonal variability. *Geophysical Research Letters*, 27(20): 3353-3356.
- Sunda, W., 2012. Feedback interactions between trace metal nutrients and phytoplankton in the ocean. *Frontiers in Microbiology*, 3.
- Sunda, W.G. and Huntsman, S.A., 1994. Photoreduction of manganese oxides in seawater. *Marine Chemistry*, 46(1-2): 133-152.
- Trouwborst, R.E., Clement, B.G., Tebo, B.M., Glazer, B.T. and Luther, G.W., 2006. Soluble Mn(III) in suboxic zones. *Science*, 313(5795): 1955-1957.
- Van Der Loeff, M.R., Helmers, E. and Kattner, G., 1997. Continuous transects of cadmium, copper, and aluminium in surface waters of the Atlantic Ocean, 50°N to 50°S: correspondence and contrast with nutrient-like behaviour. *Geochimica Et Cosmochimica Acta*, 61(1): 47-61.
- Vink, S. and Measures, C.I., 2001. The role of dust deposition in determining surface water distributions of Al and Fe in the South West Atlantic. *Deep Sea Research Part II: Topical Studies in Oceanography*, 48(13): 2787-2809.
- Witter, A.E., Hutchins, D.A., Butler, A. and Luther lii, G.W., 2000. Determination of conditional stability constants and kinetic constants for strong model Fe-binding ligands in seawater. *Marine Chemistry*, 69(1-2): 1-17.
- Wolfe-Simon, F., Grzebyk, D., Schofield, O. and Falkowski, P.G., 2005. THE ROLE AND EVOLUTION OF SUPEROXIDE DISMUTASES IN ALGAE1. *Journal of Phycology*, 41(3): 453-465.
- Wolfe-Simon, F., Starovoytov, V., Reinfelder, J.R., Schofield, O. and Falkowski, P.G., 2006. Localization and Role of Manganese Superoxide Dismutase in a Marine Diatom. *Plant Physiology*, 142(4): 1701-1709.
- Wuttig, K. *et al.*, 2012. Impacts of dust deposition on dissolved trace metal concentrations (Mn, Al and Fe) during a mesocosm experiment. *Biogeosciences Discuss.*, 9(10): 13857-13897.
- Yeats, P.A., 1998. An isopycnal analysis of cadmium distributions in the Atlantic Ocean. *Marine Chemistry*, 61(1-2): 15-23.
- Yeats, P.A., Westerlund, S. and Flegal, A.R., 1995. Cadmium, copper and nickel distributions at four stations in the eastern central and south Atlantic. *Marine Chemistry*, 49(4): 283-293.
- Zhuang, G., Yi, Z., Duce, R.A. and Brown, P.R., 1992. Chemistry of iron in marine aerosols. *Global Biogeochemical Cycles*, 6(2): 161-173.



Table 2. 8 GoFlo-stations on the Meteor cruise M80/1.

GoFlo-station	Meteor-Station	Date	Time (UTC)	Latitude	Longitude	Water Depth (m)	Wind
1	ME801/1071-1	10/26/09	20:42	17°36.04' N	24°14.6 1' W	3590	ENE 6
2	ME801/1081-1	10/30/09	04:56	08°14.99' N	21°44.9 9' W	4392.2	NE 6
3	ME801/1090-1	11/01/09	15:47	02°02.50' N	23°02.0 1' W	4363.1	SE 7
4	ME801/1115-1	11/04/09	21:20	00°00.06' N	23°00.0 2' W	3956.4	SE 7
5	ME801/1139-1	11/07/09	16:35	01°59.99' S	23°00.0 0' W	5234.2	ESE 6
6	ME801/1148-1	11/09/09	09:28	04°59.99' S	23°00.0 4' W	5195.4	SE 7
7	ME801/1178-1	11/16/09	03:43	05°00.01' N	22°58.0 0' W	4191	ESE 6
8	ME801/1206-1	11/20/09	00:47	11°00.00' N	23°00.0 2' W	5145.8	NNE 6

Table 3. Cd/PO<sub>4</sub><sup>3-</sup> ratio (pmol/μmol), its slope, intercept and number (N) and depths (m) used for the calculation.

GoFlo-station	Latitude	Longitude	Depth used (m)	Slope	Intercept	n	R <sup>2</sup>
1	17°36.04' N	24°14.61' W	80-350	230.9	-48.3	5	0.9372
2	08°14.99' N	21°44.99' W	80, 100, 300	346.3	-296.5	3	0.9808
3	02°02.50' N	23°02.01' W	100-400	422	-458.6	4	0.9958
4	00°00.06' N	23°00.02' W	100-400	140.5	-38.7	4	0.947
5	01°59.99' S	23°00.00' W	80-400	461.3	-542.3	5	0.9607
6	04°59.99' S	23°00.04' W	100-400	264.8	-126	4	0.9854
7	05°00.01' N	22°58.00' W	80-600	308.6	-227.9	6	0.9904
8	11°00.00' N	23°00.02' W	100-400	447.3	-509.6	4	0.9787



# MANUSCRIPT 4

Impacts of dust deposition on  
dissolved trace metal  
concentrations (Mn, Al and Fe)  
during a mesocosm experiment





## Impacts of dust deposition on dissolved trace metal concentrations (Mn, Al and Fe) during a mesocosm experiment

K. Wuttig<sup>1</sup>, T. Wagener<sup>1,2</sup>, M. Bressac<sup>3,4</sup>, A. Dammshäuser<sup>1</sup>, P. Streu<sup>1</sup>, C. Guieu<sup>3,4</sup>, and P. L. Croot<sup>1,\*</sup>

<sup>1</sup>GEOMAR Helmholtz Centre for Ocean Research Kiel, Marine Biogeochemistry, Düsternbrooker Weg 20, 24105 Kiel, Germany

<sup>2</sup>Université d'Aix-Marseille, CNRS/INSU, IRD, Institut Méditerranéen d'Océanologie (MIO), UM 110, 13288 Marseille, France

<sup>3</sup>Laboratoire d'Océanographie de Villefranche-sur-Mer, CNRS-INSU, UMR 7093, Observatoire Océanologique, 06230, Villefranche-sur-Mer, France

<sup>4</sup>Université Pierre et Marie Curie - Paris 6, UMR7093, LOV, Observatoire Océanologique, Villefranche-sur-Mer, France

\* now at: Earth and Ocean Sciences, School of Natural Sciences, National University of Ireland, Galway (NUIG), Galway, Ireland

Correspondence to: K. Wuttig (kwuttig@geomar.de)

Received: 26 September 2012 – Published in Biogeosciences Discuss.: 11 October 2012

Revised: 1 March 2013 – Accepted: 21 March 2013 – Published: 18 April 2013

**Abstract.** The deposition of atmospheric dust is the primary process supplying trace elements abundant in crustal rocks (e.g. Al, Mn and Fe) to the surface ocean. Upon deposition, the residence time in surface waters for each of these elements differs according to their chemical speciation and biological utilization. Presently, however, the chemical and physical processes occurring after atmospheric deposition are poorly constrained, principally because of the difficulty in following natural dust events in situ. In the present work we examined the temporal changes in the biogeochemistry of crustal metals (in particular Al, Mn and Fe) after an artificial dust deposition event. The experiment was contained inside trace metal clean mesocosms (0–12.5 m depths) deployed in the surface waters of the northwestern Mediterranean, close to the coast of Corsica within the frame of the DUNE project (a DUst experiment in a low Nutrient, low chlorophyll Ecosystem). Two consecutive artificial dust deposition events, each mimicking a wet deposition of  $10 \text{ g m}^{-2}$  of dust, were performed during the course of this DUNE-2 experiment. The changes in dissolved manganese (Mn), iron (Fe) and aluminum (Al) concentrations were followed immediately after the seeding with dust and over the following week. The Mn, Fe and Al inventories and loss or dissolution rates were determined. The evolution of the inventories after the two consecutive additions of dust showed distinct behaviors

for dissolved Mn, Al and Fe. Even though the mixing conditions differed from one seeding to the other, Mn and Al showed clear increases directly after both seedings due to dissolution processes. Three days after the dust additions, Al concentrations decreased as a consequence of scavenging on sinking particles. Al appeared to be highly affected by the concentrations of biogenic particles, with an order of magnitude difference in its loss rates related to the increase of biomass after the addition of dust. In the case of dissolved Fe, it appears that the first dust addition resulted in a decrease as it was scavenged by sinking dust particles, whereas the second seeding induced dissolution of Fe from the dust particles due to the excess Fe binding ligand concentrations present at that time. This difference, which might be related to a change in Fe binding ligand concentration in the mesocosms, highlights the complex processes that control the solubility of Fe. Based on the inventories at the mesocosm scale, the estimations of the fractional solubility of metals from dust particles in seawater were  $1.44 \pm 0.19 \%$  and  $0.91 \pm 0.83 \%$  for Al and  $41 \pm 9$  and  $27 \pm 19 \%$  for Mn for the first and the second dust addition. These values are in good agreement with laboratory-based estimates. For Fe no fractional solubility was obtained after the first seeding, but  $0.12 \pm 0.03 \%$  was estimated after the second seeding. Overall, the trace metal dataset presented here makes a significant

contribution to enhancing our knowledge on the processes influencing trace metal release from Saharan dust and the subsequent processes of bio-uptake and scavenging in a low nutrient, low chlorophyll area.

## 1 Introduction

Marine oligotrophic areas, also described as low nutrient, low chlorophyll (LNLC) areas, represent 60 % of the global ocean (Longhurst et al., 1995) and are suggested to contribute up to 50 % oceanic carbon export from the surface to the deep ocean (Emerson et al., 1997). These areas are characterized by low nutrient concentrations in oceanic surface waters resulting in reduced biological activity (Carr et al., 2006; Longhurst et al., 1995). Vast surfaces of these LNLC areas are subject to fluxes of lithogenic material through the atmospheric deposition of desert dust particles. Microcosm experiments performed previously in the oligotrophic eastern Mediterranean by Herut et al. (2005) found that the addition of fresh mineral dust to seawater resulted in the release of nutrients and to a positive growth response by biota; however, they did not find a response of biota to pre-leached dust, suggesting it was the presence of water soluble components in the dust that provided the nutrient stimulus. Due to the elemental composition of the earth crust, the flux of dust particles constitutes a major source of trace metals to the surface ocean (Duce et al., 1991; K. Desboeufs, personal communication, 2013). For this reason, in addition to macronutrients (phosphorus and nitrogen) transported by dust particles, it has been suggested that the response of the biota to dust might be (partially) controlled by trace metals. During the last twenty years, due to its importance in high nutrient, low chlorophyll (HNLC) areas, iron (Fe) has received much attention (Jickells et al., 2005), but in recent years, a number of studies have pointed to the importance of studying other trace elements in order to more completely describe the overall biogeochemical functioning of these LNLC areas (e.g. Heller and Croot, 2010; Noble et al., 2008; Obata et al., 2008; Saito and Moffett, 2002).

In order to assess the impact of atmospherically deposited micronutrients on the biogeochemical functioning of the LNLC areas, a variety of complex factors controlling the solubility of trace metals – from the solid form in a dust particle to the dissolved form once it enters the water – have to be taken into account (Baker and Croot, 2010). Indeed, in addition to atmospheric factors controlling the inherent solubility of the metal in the particle (size of the particles (Baker and Jickells, 2006), mineralogy (Journet et al., 2008), chemical composition (Sedwick et al., 2007)), there are a number of factors that can be important once the particle is deposited in seawater. These factors can be the initial concentration of dissolved metals in seawater (Liu and Millero, 2002; Mendez et al., 2010), photochemical processing (Fe(III) to Fe(II))

(Zhuang et al., 1992) and lability in the atmosphere and in seawater (Spokes and Jickells, 1996). Additional factors can be the mixing layer structure (Croot et al., 2007; Moore et al., 2006) as well as specific chelating substances in seawater at the time of the deposition, as in the case of Fe (Gledhill and Buck, 2012; Wagener et al., 2008).

The Mediterranean Sea is a LNLC area, especially in summer when the surface is strongly stratified. The atmospheric load over the Mediterranean has been estimated to reach up to one billion tonnes per year, which is one of the highest dust loads reaching a LNLC area (Guerzoni et al., 1999). In Corsica, dust deposition events of  $\sim 22 \text{ g m}^{-2}$  have been observed (e.g. Bonnet and Guieu, 2006). The Mediterranean is a suitable place to assess the impact of dust deposition on LNLC areas. This is the objective of the project DUNE (a DUst experiment in a low Nutrient low chlorophyll Ecosystem) based on an original experimental approach: dust addition experiments into large, clean mesocosms. This experimental design constitutes an opportunity to study processes once particles have deposited at the surface ocean in a realistic way (Guieu et al., 2009, 2010).

During the first campaign in 2008 (DUNE-1), it was demonstrated that the mesocosms were sufficiently trace metal clean to study the Fe cycle (Wagener et al., 2010). Two major results concerning Fe chemistry were gained from this first experiment:

1. A clear decrease of the dissolved iron (Fe) inventory in the mesocosms, in which a wet deposition was simulated, compared to the mesocosms without addition of dust, has been observed. A simple 1-D model of the mesocosms demonstrated that during the experiment the addition of dust was a sink rather than a source of Fe due to scavenging on dust particles (Ye et al., 2011).
2. Additionally, a second addition of simulated aeolian dust in batch experiments performed with filtered seawater, obtained from the corresponding mesocosms 168 h after the first seeding, showed a clear increase in the Fe solubility. Wagener et al. (2010) postulated that the dust addition could have induced the production of Fe binding ligands and therefore increased significantly the solubility of Fe. This would imply that a second addition of dust to the mesocosms might have a stimulatory effect on Fe dissolution and a contrasting impact from the first addition.

A second experimental campaign was performed in June and July 2010 (DUNE-2) (Guieu et al., 2013). Based on the experience gained during the DUNE-1 experiment, the strategy for studying trace metals was slightly changed. Understanding the processes that govern the fluxes of Fe to seawater is a critical challenge in chemical oceanography today. While the importance of Fe to primary productivity in the ocean is well demonstrated (Blain et al., 2007; Boyd et al., 2000), we are only now beginning to examine the exchange

of Fe between different chemical forms in seawater (Croot and Heller, 2012; Gledhill and Buck, 2012; Baker and Croot, 2010). The ability of Fe to form organic complexes (Croot and Heller, 2012; Gledhill and Buck, 2012) helps to elevate Fe levels above the low solubility of inorganic Fe(III) in seawater (Liu and Millero, 2002); however, colloidal Fe still dominates the dissolved fraction (Bergquist et al., 2007). The chemical reactivity and biological requirement for Fe result in it being easily scavenged onto other particles and subsequently lost from the euphotic zone. For this reason, Fe binding ligand measurements have been performed in addition to the dissolved Fe concentration measurements. Moreover, two additional dissolved trace metals have been examined during DUNE-2: the biogeochemically important micronutrient manganese (Mn) and the crustal metal aluminum (Al). In contrast to Fe, there is no organic speciation known for Al and it is also considered to be negligible for Mn (Roitz and Bruland, 1997; Sañudo-Wilhelmy et al., 1996). Al is a major and relatively invariant component of the earth crust and is not known to be actively assimilated by organisms. However, Al is strongly influenced by scavenging mechanisms and is therefore considered to be a potentially useful tracer for lithogenic input on relatively short time scales (Dammshäuser et al., 2011). On the other hand, Mn is a bioactive metal with a complex chemistry in seawater. While most of the Mn exists as soluble Mn(II) which is not thought to be organically complexed, dissolved Mn(III) and Mn(IV) organic species are possible, but have not yet been observed in oxygenated seawater. Soluble Mn(III) is rare in natural waters because it hydrolyzes and precipitates as Mn(III) oxides or disproportionate into Mn(IV) oxides plus Mn(II) (Nealson et al., 1988; Stumm and Morgan, 1996). Another important difference compared to DUNE-1 is that DUNE-2 was carried out with two consecutive seedings with the same amount of evapocondensed dust. After measuring the initial concentrations, the seeding with dust was performed and all experimental variables were determined with a higher resolution in the first day and then daily for one week. After the second addition of dust the variables were measured again for one week with a similar resolution in order to assess if the biogeochemical response to a second seeding could be influenced by the response to the former seeding.

This paper presents the dissolved trace metal inventories of Fe, Mn and Al during the DUNE-2 experiment. Based on the revised experimental strategy after the DUNE-1 experiment, the specific objectives of this study are (1) to assess dissolution and loss rates of these trace metals after two consecutive additions of dust and (2) to quantify the processes involved at different time scales.

## 2 Materials and methods

### 2.1 Experimental design and sampling

In June 2010, seven trace metal clean mesocosms were deployed in the Bay of Elbo in the conservation area of Scandola, Corsica (42.374° N, 8.554° E) during typical oligotrophic summer conditions (Millot, 1999). Marine oligotrophic areas, also described as low nutrient, low chlorophyll (LNLC) areas, are typically defined by a chlorophyll *a* content of less than 0.1 mg m<sup>-3</sup> (Carr et al., 2006; Longhurst et al., 1995). Giovagnetti et al. (2012) showed that during the DUNE-2 experiment the chlorophyll *a* content always remained below this threshold even after the seedings. Their initial chlorophyll *a* concentration was 0.02–0.03 mg m<sup>-3</sup>. The DUNE-2 mesocosm experiment design was based on the exact same protocol as described in detail earlier (Guieu et al., 2010) for the DUNE-1 experiment in 2008. The mesocosms were entirely made out of plastic and were composed of a cylindrical section of 12 m length and 2.3 m in diameter. The conical bottom started at 12 m depth and ended with a sediment trap at 14.5 m depth. In each mesocosm, the total seawater volume was 52 m<sup>3</sup> and, in general, the biological, chemical and physical properties of the water column were retained within the mesocosms. To protect the mesocosms against naturally occurring dust events, they were covered with a transparent cover which was designed to let natural light pass and to allow gas exchanges between the water body and the atmosphere. The three mesocosms to which the dust was added are referred to here as D1, D2 and D3 and “dust seeded mesocosms”. Further, three trace-metal clean mesocosms were kept without seeding as the control mesocosms (labeled here C1, C2 and C3). For comparison between the control mesocosms and the environment, samples were also taken outside the mesocosms.

The seeding with dust was performed using the following protocol. After deploying the mesocosms, they were left open for 24 h in order to let the water masses inside equilibrate with the water masses outside of the mesocosms. After closing the mesocosms, *t*<sub>0</sub> was sampled and then the mesocosms were seeded. Two consecutive seedings with cloud processed dust (Guieu et al., 2010) were performed at an interval of one week. Each seeding was followed for a week with high resolution sampling in the first 24 h and subsequent daily sampling. Therefore, DUNE-2 had a higher time resolution than DUNE-1 where sampling was performed daily for most parameters (Guieu et al., 2010). For each of the two consecutive seedings, 41.5 g of evapocondensed dust was diluted in ultrapure water (hereafter referred to as MQ water – see below) and sprayed with an all-plastic spray bottle onto the surface of each of the mesocosms. This corresponds to a simulated wet deposition of 10 g m<sup>-2</sup> for each seeding. The first seeding took place on 26 June 2010 at 09:00 UTC (*t*<sub>0</sub>), the second on 3 July 2010 at 07:00 UTC (*t*<sub>166</sub>).

In each of the six sampled mesocosms, flexible reinforced PVC tubings were installed at 0.1, 5 and 10 m depth. Sampling was performed with a Teflon<sup>TM</sup> (polytetrafluoroethylene) diaphragm pumping system. For dissolved trace metals, samples were filtered inline through 0.2 µm filter cartridges (Sartorius Sartobran filter capsule 5231307H5, Germany). Additionally to DUNE-1, two dust seeded mesocosms (D1 and D2) were deployed with three supplementary tubings installed at 2.5, 7.5 and 12.5 m depth in order to improve the resolution in the water body and to be able to follow the processes after a simulated dust storm on a smaller scale.

## 2.2 Chemical Analysis

### 2.2.1 Reagents and bottles

Strict attention was paid to avoiding contamination in this study. All manipulations were performed in class 100-laminar flow benches. All reagents that were used were of highest purity available (Fisher Scientific and Sigma-Aldrich) and were prepared using deionized (18 MΩ cm<sup>-1</sup> resistivity) water (MQ water) from a Milli-Q purification system (Millipore). Sub-boiled quartz-distilled hydrochloric acid (hereafter Q-HCl) was made by single distillation from 25 % HCl. All plasticware and bottles (low density high polyethylene (LDPE) and polytetrafluoroethylene (PTFE)) used for acidified seawater samples for the total trace metal analysis were cleaned according to the trace metal clean procedures (Bruland et al., 1979; Cutter et al., 2010) and then protected by double bags (Minigrip<sup>TM</sup>). The filtered samples for dissolved trace metal analysis were directly acidified with Q-HCl to pH 1.7 under a class 100-laminar flow bench in the lab at the port facilities used for servicing the mesocosms. Samples for Fe binding ligands were directly frozen (-20 °C) upon collection in Corsica, transported frozen to Marseille, and thawed immediately prior to analysis. Sample processing and analysis steps were performed in laminar flow benches inside class 100 clean rooms in Kiel (Germany) and in Villefranche-sur-Mer (France).

In this paper we only discuss the dissolved trace metals (referred to as Mn, Fe and Al).

### 2.2.2 Dissolved manganese analysis

Samples for dissolved manganese (Mn) were analyzed on site. The acidified samples were spectrophotometrically analyzed using a slightly modified flow-injection analysis system (FIA) built following Aguilar-Islas et al. (2006). We used one 8-channel peristaltic pump (Rainin), two electronically actuated 6-port valves, one electronically actuated 10-port sample valve (all VICI, Valco Instruments), one dry bath (Fisher) kept at 35 °C and a variable wavelength spectrophotometer (USB-4000, Ocean Optics, Inc.) with an internal Ocean Optics light source and a 1 cm quartz flow-through cell (100-QS, 10.00 mm, Hellma GmbH and Co.

KG). The flow rates were identical with those in Aguilar-Islas et al. (2006). The filtered and acidified seawater sample was preconditioned for 30 s by flushing with 0.05 mol L<sup>-1</sup> ammonium borate rinse solution on a pre-concentration column (GLOBAL-FIA) filled with Toyopearl AF-Chelate-650M resin. The timing parameters were for preconditioning, loading, rinse and elution of the column: 30, 120, 30, 180 s, respectively.

Calibration curves were determined daily by the addition of standards (0–10 nmol L<sup>-1</sup>) produced by serial dilution of a 1000 ppm Mn(II) standard (Fluka) into 0.2 µm filtered Mediterranean seawater which had been taken before the first seeding at 5 m depth outside of the mesocosms at our external reference point (t<sub>0</sub>, outside, 5 m). For external validation, selected samples were also analyzed in the clean laboratory in Kiel by graphite furnace atomic absorption (ETAAS, Perkin-Elmer Model 4100ZL; this method is described in detail below).

Samples, standard additions and blanks were measured in triplicates. Analytical precision (expressed as percent relative standard deviation) was typically < 8 % at 3.6 nmol L<sup>-1</sup> under the conditions employed here. The accuracy of the analytical procedure was evaluated by daily measurements of SAFe intercalibration samples S and D2. It should be noted, however, that the SAFe concentrations are over a lower range (< 1 nmol L<sup>-1</sup>) than the seawater samples from the mesocosms (< 3.5 nmol L<sup>-1</sup>), which leads to lower precision for the SAFe samples using our system optimized for Mediterranean surface waters. SAFe values determined while in Corsica were as follows: 0.85 ± 0.14 nmol L<sup>-1</sup> (S) and 0.35 ± 0.09 nmol L<sup>-1</sup> (D2) of Mn (*n* = 8) (consensus values are 0.79 ± 0.06 nmol L<sup>-1</sup> and 0.35 ± 0.06 nmol L<sup>-1</sup>, respectively). We used a large volume of secondary standard (0.2 µm filtered Mediterranean seawater (t<sub>0</sub>, outside, 5 m)) throughout this work as the seawater in which standard additions were prepared. The complete Mn-FIA measurements over the course of the work in Corsica resulted in a value of 3.60 ± 0.30 nmol L<sup>-1</sup>, which was in good agreement with values measured by ETAAS in Kiel: 3.55 ± 0.08 nmol L<sup>-1</sup>. The detection limit (3σ of the blank) for the Mn flow injection system used here was estimated in the lab in Kiel by repeated measurements of low Mn Antarctic seawater (< 0.2 nmol L<sup>-1</sup>; collected during ANTXXIV-3) at 150 pmol L<sup>-1</sup>. The use of a low Mn or Mn free seawater is preferred to running MQ blanks, as both in Corsica and in Kiel we found that there was detectable Mn in the MQ systems due to problems with the ion-exchange units of the systems.

A few samples of Mn, as a comparison to the direct analysis in Corsica (FIA), were analyzed by graphite furnace atomic absorption (ETAAS, Perkin-Elmer Model 4100ZL) in the clean laboratory in Kiel using solvent extraction modified after Klinkhammer (1980). Briefly, 200 g of filtered and acidified seawater were extracted with 8-hydroxyquinoline in distilled chloroform as Mn-oxinates,



back-extracted with  $3 \text{ mol L}^{-1}$  distilled  $\text{HNO}_3$  and then analyzed with ETAAS. SAFe reference seawater D1 was determined as  $0.423 \pm 0.05 \text{ nmol L}^{-1}$  (consensus value  $(0.35 \pm 0.06 \text{ nmol L}^{-1})$ ); these Mn values for the validation are given in the supplementary information.

### 2.2.3 Dissolved iron and Fe binding ligand analysis

Fe concentrations were analyzed at Laboratoire d'Océanographie de Villefranche-sur-Mer between 4 and 10 months after the experiment. A flow injection system with online preconcentration and chemiluminescence detection was used as described in Bonnet and Guieu (2006). The detection limit (DL) was  $25 \text{ pmol L}^{-1}$  on average and blanks were between 50 and  $150 \text{ pmol L}^{-1}$ . An internal acidified seawater standard was measured in order to control the stability of the analysis during each series of measurements. The reliability of the method was controlled by analyzing the D2 SAFe seawater standard (Johnson et al., 2007), which was determined as  $0.84 \pm 0.04 \text{ nmol L}^{-1}$  of Fe ( $n = 5$ ) (consensus value is  $0.90 \pm 0.02 \text{ nmol L}^{-1}$ ).

The concentration of Fe complexing ligands, [L] was determined by cathodic stripping voltammetry using the competitive ligand 2-(2-thiazolyazo)-p-cresol (TAC) (Croot and Johansson, 2000) at Institut Méditerranéen d'Océanologie, Marseille (France) 18 months after the experiment. After thawing of the samples, [L] complexing ligands were determined following the exact same protocol as described in Wagener et al. (2008). A  $\mu$ -Autolab voltammeter coupled to a Metrohm VA663 electrode stand with a static mercury drop working electrode, a double junction Ag/AgCl reference electrode and carbon rod counter electrode was used. The titration data were calculated using a single ligand fit with the van den Berg/Ruzic linearization method (see, for example, Croot and Johansson, 2000).

### 2.2.4 Dissolved aluminum analysis

The aluminum analysis was conducted at GEOMAR, Kiel, a few months after the experiment using the fluorometric method described by Hydes and Liss (1976). In short, the reagent lumogallion was added to the sample, which was then buffered to pH 5 with ammonium-acetate, and heated to  $40\text{--}50^\circ\text{C}$  for 3 h to accelerate complex formation. The fluorescence of the sample was measured with a Hitachi FL 2700 Fluorescence Spectrophotometer (excitation wavelength 497 nm, emission wavelength 572 nm). The detection limit varied between 0.1 and  $0.3 \text{ nmol L}^{-1}$ , the blank values between 0.4 and  $0.6 \text{ nmol L}^{-1}$  for the different days of analysis. In the SAFe reference seawater S1 (S1 543, S1 474),  $1.81 \pm 0.24 \text{ nmol L}^{-1}$  of Al ( $n = 4$ ) were determined (consensus value is  $1.74 \pm 0.09 \text{ nmol L}^{-1}$ ).

## 3 Results

The complete set of data is available as supplementary information to this paper.

The nomenclature for samples of the DUNE-2 experiment is as follows: dust seeded mesocosms D1, D2 and D3; unseeded control mesocosms C1, C2 and C3; and the sampling outside the mesocosms. Samples were taken at 0.1, 2.5, 5.0, 7.5, 10.0 and 12.5 m depth. The time  $t_x$  is expressed in hours ( $x$ ) since the first dust addition and in parentheses  $t_x(y)$  the time (in h) since the second dust addition. The samples outside the mesocosms were taken as an external reference point to the control mesocosms and the concentrations are not reported in the figures, but are available in the supplementary information.

### 3.1 Evolution of dissolved manganese (Mn)

Figure 1 shows the evolution of the concentration of Mn as a function of time after the first seeding and depth in each of the mesocosms. The initial Mn concentrations outside, in the control and dust seeded mesocosms were  $3.4 \pm 0.6 \text{ nmol L}^{-1}$ . Directly on the first day ( $t_{23}$ ) after the first dust addition, the Mn concentrations increased to  $4.9 \pm 0.4 \text{ nmol L}^{-1}$  in the surface and at mid-depth (D1 and D2). D3 was not sampled at  $t_{23}$  after the first addition. At  $t_{48}$  the same trend as in D1 and D2 was seen with a continuation of the increase in Mn which was most pronounced in the surface. After the continuous increase since the first seeding with dust, at  $t_{71}$  Mn reached its maximum in all three dust seeded mesocosms and in D1 at 5 m depth the concentration was as elevated as  $7.2 \text{ nmol L}^{-1}$ . After this initial elevation of Mn, overall the concentration then decreased slowly in all three dust seeded mesocosms with time down to  $3.0\text{--}4.6 \text{ nmol L}^{-1}$  after a week. These values were in the range of the values before the first seeding.

After the second dust addition to the surface of the dust seeded mesocosms, the increase in Mn was more pronounced than after the first addition. Concentrations of Mn in the surface (0.1 m) in the first few hours after the second seeding increased strongly, especially in D2 to  $13.2 \text{ nmol L}^{-1}$  at  $t_{171}(5)$  and  $11 \text{ nmol L}^{-1}$  at  $t_{175}(9)$ . In these first 24 h after the second dust addition the concentrations of Mn at 5 m and 10 m remained constant at 3.2 to  $4.4 \text{ nmol L}^{-1}$ . While the values in the surface decreased slowly after the first strong pulse following the second addition, the Mn values increased at 5 m at  $t_{191}(24)$  and even more at  $t_{215}(49)$ . At all depths the Mn concentrations in the dust seeded mesocosms decreased again with time down to  $3\text{--}5 \text{ nmol L}^{-1}$  after  $t_{287}(121)$  (with the exception of D3 10 m with a Mn concentration of  $5.7 \text{ nmol L}^{-1}$ ).

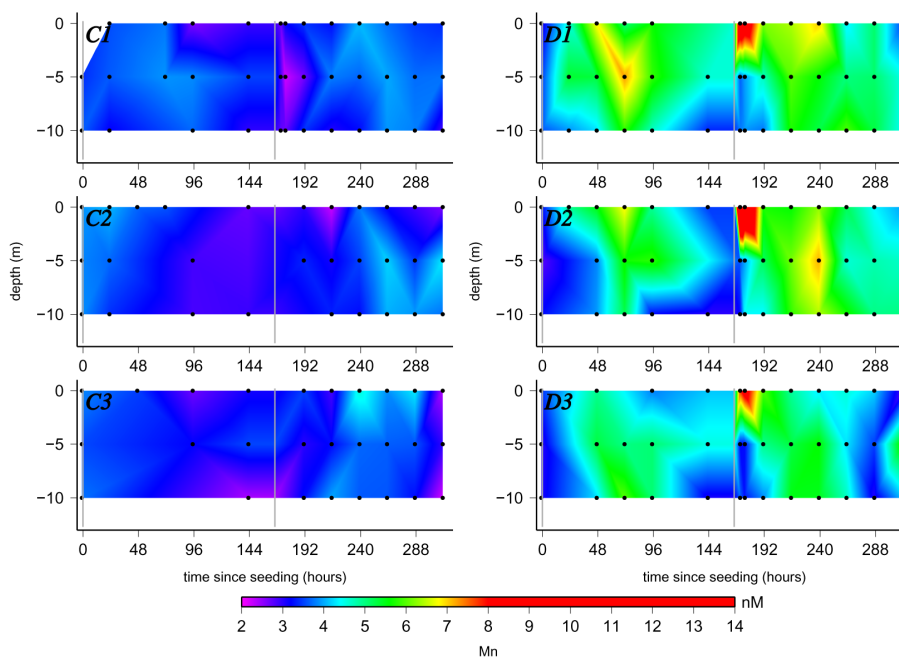


**Fig. 1.** Evolution of dissolved manganese (Mn) in the 6 mesocosms (left hand side – control mesocosms: C1, C2 and C3; right hand side – dust seeded mesocosms: D1, D2 and D3). The graphs are plotted as the time since the first seeding (h) versus the depth (m) in the mesocosms. Black dots show the points where samples were taken. The two grey vertical bars highlight the time points when the seeding took place ( $t_0$  and  $t_{166(0)}$ ).

### 3.2 Evolution of dissolved iron concentration (Fe) and Fe binding ligands (L)

In Fig. 2, the evolution of Fe values in the control and dust seeded mesocosms are shown. The initial Fe values before the dust addition varied between 2.2 and 4.4 nmol L<sup>-1</sup> inside the mesocosms and outside (values available in the supplementary information). After the first addition of dust at  $t_{10}$ , there was a direct decrease in the Fe concentrations to 2.5–2.9 nmol L<sup>-1</sup> in the surface of the dust seeded mesocosms and values as low as 1.5 nmol L<sup>-1</sup> were measured in D2 and D3. At  $t_{23}$  the values inside the control mesocosms still ranged from 3.0 to 3.5 nmol L<sup>-1</sup>. With more time elapsing, this decrease in the Fe concentrations continued in the dust seeded mesocosms but also occurred in the control mesocosms and outside. After  $t_{143}$  the Fe values in the control mesocosms varied from 1.4–2.1 nmol L<sup>-1</sup> and in the dust seeded mesocosms from 1.6–2.0 nmol L<sup>-1</sup>.

After the second dust addition, a significant increase in Fe was observed in the dust seeded mesocosms, whereas Fe values remained constant in control mesocosms. Directly after this addition there was a strong increase in the surface with a maximum at  $t_{191(25)}$ . In D1 and D2, the Fe concentration increased up to 6.1 nmol L<sup>-1</sup> at 2.5 m and up to 3.8 nmol L<sup>-1</sup> in the surface of D3. In the first 24 h after the second addition the Fe values had increased in all the dust seeded mesocosms. However, after  $t_{215(49)}$ , the Fe concentrations de-

creased quickly again down to 1.0–1.8 nmol L<sup>-1</sup>. This range remained the same until the end of the experiment.

Fe complexing ligands in the dissolved phase [L'] were measured on a limited subset of samples collected at 5 m depth. The evolution of the arithmetical means [L'] for the dust seeded and the control mesocosms is presented in Fig. 3. Before and after the first seeding, ligands were close to saturation or over-saturated, i.e.  $([L] + [\text{FeL}]) < \text{total dissolved Fe}$ , with values ranging from 1.3 to 3.3 nmol L<sup>-1</sup> at  $t_0$ – $t_{143}$ . In the control mesocosms the values remained in this range for the whole experiment. The saturation and over-saturation made a full analysis of the ligand complexation parameters complicated as the ambient system was already over titrated. This situation indicated a limited capacity to take up more Fe in the dissolved phase and a potential for greater scavenging rates as increases in dissolved Fe can only be achieved by processes that do not impact the ligand concentration. This is because as the soluble and colloidal ligand pools are saturated, and the inorganic solubility is also maximized, any more Fe that dissolves will lead to Fe being incorporated into existing colloidal aggregates or onto particles. However, after the second dust addition, the ligand concentration rose significantly in the dust seeded samples with values reaching 6.8 nmol L<sup>-1</sup> at  $t_{191(25)}$ , indicating a higher complexing capacity for Fe. At  $t_{239(73)}$  and  $t_{311(145)}$  the values decreased to 5.2–5.3 nmol L<sup>-1</sup>.

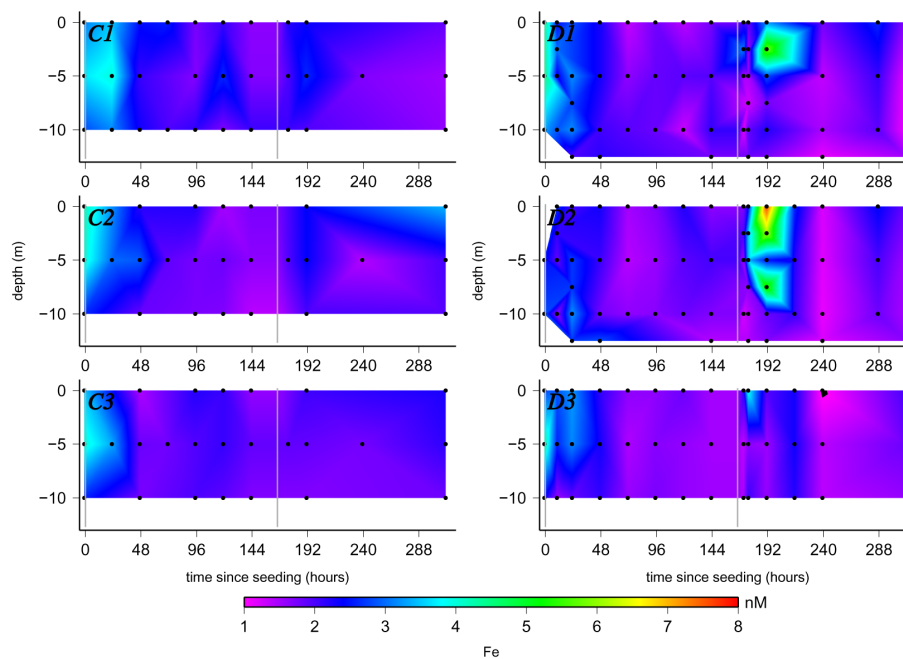


Fig. 2. Evolution of dissolved iron (Fe) in the 6 mesocosms. This graph is plotted in the same way as Fig. 1.

### 3.3 Evolution of dissolved aluminum (Al)

The evolution of the concentrations of Al is displayed in Fig. 4. In all three control mesocosms, similar features were observed: the values decreased nearly linearly with time over the two weeks of the experiments, from  $44 \text{ nmol L}^{-1}$  to  $38 \text{ nmol L}^{-1}$ . Values from outside the mesocosms were in the same range as those in the control mesocosms.

In the dust seeded mesocosms, directly after the first addition of dust at  $t_{10}$ , the surface Al values increased to  $54 \text{ nmol L}^{-1}$  and the rest of the water column was also elevated ( $48\text{--}50 \text{ nmol L}^{-1}$ ). The increase continued throughout the dust seeded mesocosms ( $50\text{--}56 \text{ nmol L}^{-1}$ ), but most distinctive in the surface with concentrations up to  $60\text{--}63 \text{ nmol L}^{-1}$  at  $t_{47}$ . At the end of the first dust addition the Al concentrations were constant in all dust seeded mesocosms at approximately  $55 \text{ nmol L}^{-1}$ .

After the second dust addition the Al concentrations increased by approximately  $10 \text{ nmol L}^{-1}$  ( $t_{215}(49)$ ), for example up to  $78 \text{ nmol L}^{-1}$  in the surface in D1. At  $t_{239}(73)$ , the minimum value was  $58 \text{ nmol L}^{-1}$  and the maximum was reached with  $66 \text{ nmol L}^{-1}$  at several depths. At the end of the experiment, the values decreased to  $53 \text{ nmol L}^{-1}$  in D1 and  $55\text{--}60 \text{ nmol L}^{-1}$  in D2. In D3, a similar decrease with time could be observed, but the initial increase after the second addition was smaller compared to D1 and D2. At the end of the experiment ( $t_{311}(145)$ ), the values dropped to  $42\text{--}46 \text{ nmol L}^{-1}$ .

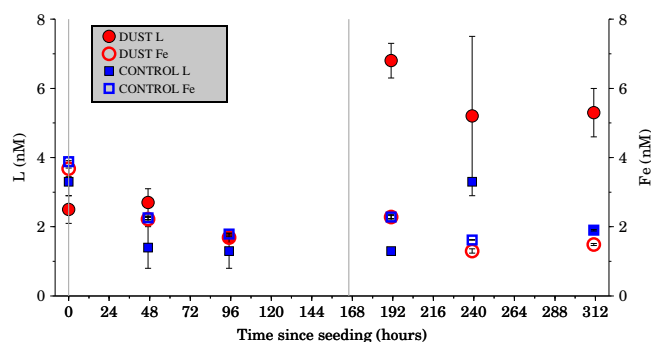
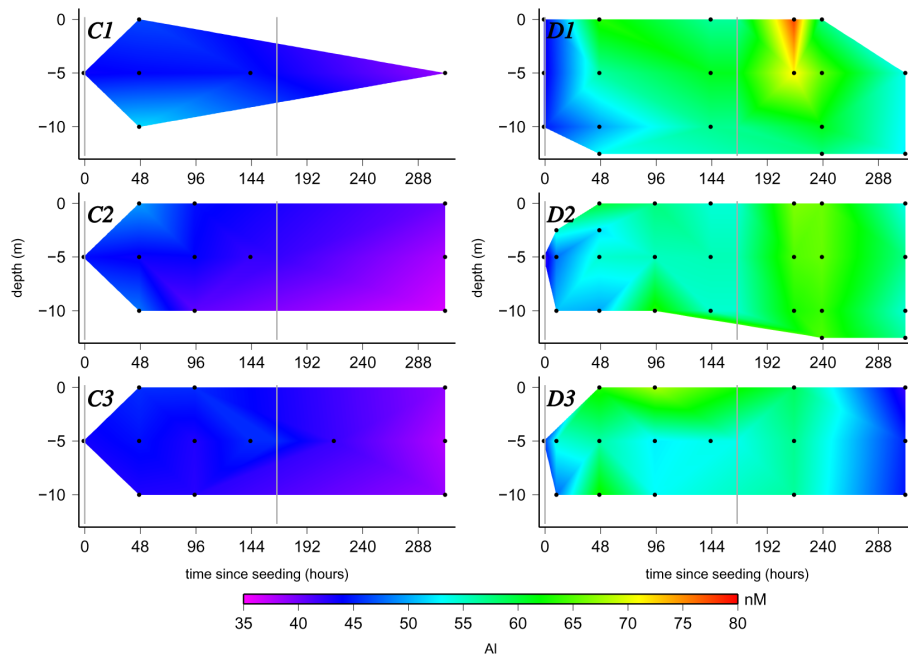


Fig. 3. Evolution of the arithmetical means of the iron binding ligand (L) concentrations ( $\text{nmol L}^{-1}$ ) of the dust seeded mesocosms (red circles) and the control mesocosms (blue squares) at 5 m depth with time since the seeding. The evolution of the arithmetical means of the dissolved iron (Fe) concentrations ( $\text{nmol L}^{-1}$ ) of the dust seeded mesocosms (red empty circles) and the control mesocosms (blue empty squares) at 5 m depth with time since the seeding.

## 4 Discussion

### 4.1 Trace metal concentrations at the DUNE site

All the total dissolved trace metal concentrations measured at the DUNE sampling site before the seeding are representative for the western Mediterranean basin (Boyle et al., 1985; Copin-Montegut et al., 1986; Kremling and Petersen, 1981; Morley et al., 1997; Sherrell and Boyle, 1988; Yoon et al., 1999). The average values of the total dissolved trace metal concentrations ( $\pm$  standard deviation) before the addition of



**Fig. 4.** The evolution of dissolved aluminum (Al) in the 6 mesocosms. This graph is plotted in the same way as Fig. 1.

dust at 5 m depths at the DUNE site are given in Table 1. For all the trace metals measured during DUNE-2, no significant differences could be observed between the initial values inside and outside the mesocosms. This indicates that the deployment protocol of the mesocosms, developed for the DUNE experiment (Guieu et al., 2010), does not contaminate the water column trapped inside for the trace element measured in this study. The concentrations are given as supplementary information and will not be discussed here any further. This is in agreement with the results obtained for Fe during DUNE-1 (Wagener et al., 2010).

Sherrell and Boyle (1988) report a limited set of data for total and dissolved Fe in the western Mediterranean. They found maximal values in the core of the Atlantic inflow jet to the Mediterranean in the Strait of Gibraltar of  $53.0 \text{ nmol kg}^{-1}$  total Fe, with dissolved Fe making up only 30 % of this value, indicating a high particulate load. Outside this plume of Fe, total surface concentrations were around  $5 \text{ nmol kg}^{-1}$ . The range of reported Fe concentrations is similar to those previously published for the western Mediterranean basin (Bonnet and Guieu, 2004; Sarthou and Jeandel, 2001; van den Berg, 1995). However, the initial Fe values in the mesocosms were in the higher range of reported data for the open waters of the western Mediterranean Sea, but similar coastal Fe concentrations were determined in the Bay of Villefranche at different times of the year (Bressac and Guieu, 2013). A study by Statham et al. (1985) of Mn concentrations in the Mediterranean also showed a surface enrichment up to  $4.19 \text{ nmol L}^{-1}$ . Our observed Al concentrations are in the same range as previously reported surface values of about

$56 \text{ nmol L}^{-1}$  close to our study site off the coast of Corsica in 1977 (Caschetto and Wollast, 1979). Similar Al concentrations have also been observed in the western Mediterranean basin (Chou and Wollast, 1997; Hydes et al., 1988; van den Berg et al., 1994).

#### 4.2 Changes in trace metal inventories: dissolution and scavenging after the seeding

The temperatures measured at four depths (0, 3, 6 and 10 m) inside and outside the mesocosms are the only available physical continuously monitored parameters measured during the entire experiment. In Fig. 5a, the calculated temperature difference between the surface and the bottom of the mesocosm is plotted (0–10 m). The temperature difference between 0 and 10 m measured inside the mesocosm is therefore used as an indicator for mixing or thermal stratification in the mesocosm in order to discuss the changes in the inventories within the mesocosms. If there was little or no temperature difference between 0 and 10 m, we interpreted this as an indication that the water column in the mesocosm was well-mixed. The more significant the temperature difference, the more likely the mesocosm was stratified. The main feature this proxy provides is that the course of the experiment can be separated into four periods. A relatively well-mixed mesocosm during the first four days (t96) of the experiment, followed by a stratification of the water column (t96–t180). The second addition of dust therefore occurred in a more stratified water column than the first one. After t180 the water column was mixed again until t240 when a new stratification followed until the end of the experiment (Bressac et al., 2013).

**Table 1.** Trace metal concentrations before the start of the experiment.

	Concentration (nmol L <sup>-1</sup> ) inside the mesocosms <sup>c</sup>	Concentration (nmol L <sup>-1</sup> ) outside the mesocosms <sup>d</sup>
Al (FIA)	43.8 ± 1.4	36.97 <sup>a</sup>
Cd (ETAAS) <sup>e</sup>	0.052 ± 0.007	0.05 <sup>b</sup>
Co (ETAAS) <sup>e</sup>	0.099 ± 0.007	0.12 <sup>b</sup>
Cu (ETAAS) <sup>e</sup>	1.83 ± 0.30	1.42 <sup>b</sup>
Fe (FIA)	3.78 ± 0.67	4.44
Mn (FIA)	3.36 ± 0.37	3.50
Ni (ETAAS) <sup>e</sup>	3.47 ± 0.40	3.34 <sup>b</sup>
Pb (ETAAS) <sup>e</sup>	0.104 ± 0.017	0.09 <sup>b</sup>
Zn (ETAAS) <sup>e</sup>	2.14 ± 0.67	1.01 <sup>b</sup>

<sup>a</sup> This value was measured at t47 after the start of the experiment.

<sup>b</sup> These values were measured at t143(–23) after the start of the experiment. <sup>c</sup> The errors presented with the mean values in this table correspond to the standard deviation ( $1\sigma$ ) calculated on the values at 5 m in the 6 mesocosms directly after their deployment.

<sup>d</sup> We only had one reference point outside the mesocosms and therefore cannot give an error for the outside concentrations. <sup>e</sup> The graphite furnace atomic absorption method (ETAAS) for the dissolved trace metal concentrations (cadmium (Cd), cobalt (Co), copper (Cu), nickel (Ni), lead (Pb) and zinc (Zn)) is described in the supplementary information (Grasshoff et al., 1983; Danielsson et al., 1978).

Mesocosms are closed systems without lateral advection. Therefore, after the addition of dust, its effect on the cycling of trace metals can be completely assessed by using inventories over the water column of the mesocosms. For this reason the inventories were calculated for all three trace metals for each 5 m depth layer (0–5 m and 5–10 m). The final conical section of the mesocosms was neglected. The few missing values were interpolated if necessary by using the average values between two depths, or the values at the extremes (surface and bottom). The inventories for the 5 m increments were then added up as an inventory for the corresponding mesocosm at the corresponding time point  $t_x$ . Figure 5 shows the evolution of the Mn (B), Fe (C) and Al (D) inventories as a function of the time since the addition of dust. The plotted inventories were calculated as arithmetical means for the control and the dust seeded mesocosms. For all three elements (Fe, Al and Mn), the inventories in the dust seeded and control mesocosms were equivalent before the start of the experiment. The Mn and Al dust seeded inventories were always higher than the Mn and Al control inventories, which remained constant or decreased slightly throughout the whole experiment, whereas the inventories in the dust seeded mesocosms showed a remarkable increase during t47–t73 after both the seedings, followed by a decrease in the inventories in the following days. Fe inventories showed a different trend with a distinct quicker and stronger decrease in the dust seeded compared to the control mesocosms after the first dust seeding. This decrease until t73 was

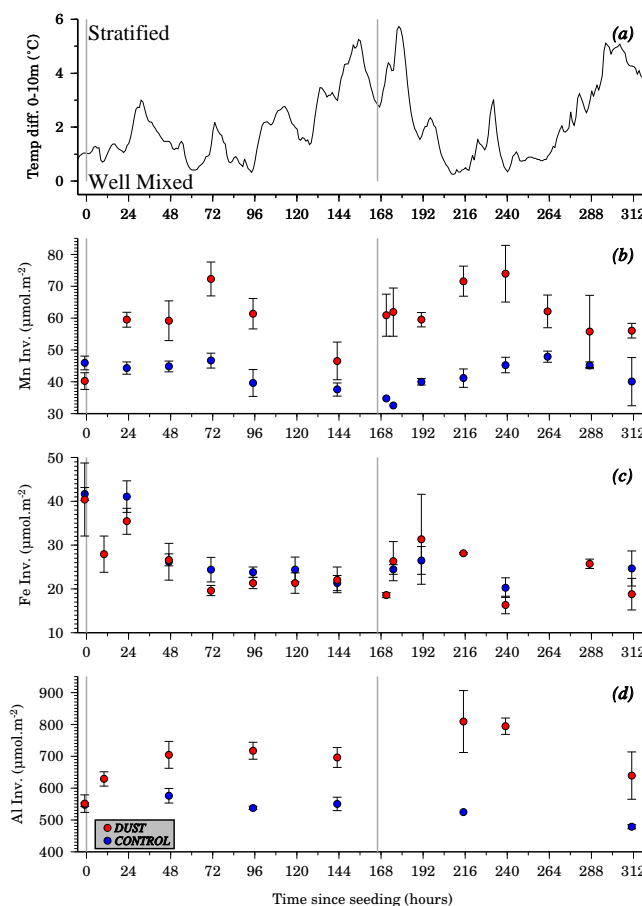


**Fig. 5.** Evolution of the temperature difference (0–10 m) (a) and the arithmetical means of the dissolved trace metal inventories ( $\mu\text{mol m}^{-2}$ ) (Mn (b), Fe (c) and Al (d) from top to bottom) of the dust seeded mesocosms (red circles) and the control mesocosms (blue circles).

followed by constant inventories during the rest of the experiment. Only a very transient, but strong increase could be observed in the dust seeded mesocosms one day after the second addition of dust (t191(25)).

Based on these inventory calculations, changes are discussed (1) in terms of absolute inventories based on estimations of trace metal solubilities from dust particles and (2) in terms of relative changes of the inventories based on estimations of dissolution and loss rates of the three elements.

#### 4.2.1 Estimation of dissolution during the mesocosm experiment

The fractional solubility (FracSol %) of an element from the dissolution of dust particles in seawater (Baker and Croot, 2010) is typically expressed as the percentage of the soluble element compared to the total element in the dust particle. This percentage allows an estimation of the impact of the atmospheric particle flux on the dissolved (and bioavailable)

stock in the ocean (Landing and Paytan, 2010). In recent years, two major experimental protocols have been used to assess the solubility of collected dust particles in seawater: flow through protocols (e.g. Buck et al., 2006) and batch experiments (e.g. Bonnet and Guieu, 2004). As discussed in Wagener et al. (2010), mesocosms allow us to estimate solubility from dust particles in a somewhat *in situ* way: the settling of the particles through the water column and interactions with naturally occurring particles are both integrated in this approach. However, two main limitations are inherent to this approach: (1) the dust addition is based on artificially produced dust particles which might not completely reproduce natural particles and (2) the results obtained are only relevant for the area where the mesocosms have been deployed. For a given element at a given time, the fractional solubility is the ratio between the increase in the dissolved metal concentrations ( $[M]$ ) due to dust dissolution in seawater (in this case integrated over the entire mesocosm) and the total amount of this element introduced with the dust particles ( $\Sigma M_{\text{Dust}}$ ) – as indicated below.

Here, the solubility of each element from the added dust is estimated at the time point ( $t$ ) when the inventory of this dissolved element in the mesocosms is at its maximum after the dust addition. In the present work we utilized Eq. (1) (below) for the phase of the first dust addition, in which the amount of the dissolved element introduced by the dust is estimated as the difference between the inventories in the dust seeded mesocosms (DM) and the control mesocosms (CM). The total amount of the element introduced by dust is estimated from the amount of dust introduced to the mesocosm and its elemental composition (K. Desboeufs, personal communication, 2013). It is assumed here that no dust was lost when it was sprayed at the surface of the mesocosm (see Sect. 2.1.):

$$\text{FracSol} (\%) = \frac{\max \left\{ A \left( \left| \int_z^0 [M]_{\text{DM}} \partial z \right|_t - \left| \int_z^0 [M]_{\text{CM}} \partial z \right|_t \right) \right\}}{\Sigma M_{\text{Dust}}} \quad (1)$$

#### Case 1: first addition

Where  $A$  is the surface area of the mesocosm and assuming it is a perfect cylinder,  $t$  represents the time since the first dust addition.

It is important to notice that in the case of this experiment, using the difference of the inventories between dust seeded and control mesocosms to estimate the dissolved amount allows us to take into consideration the ongoing changes in the dissolved concentrations observed in the control mesocosms during the experiment. The inventory changes for the dissolved metals in the control mesocosms are independent of the added dust and must therefore not be taken into account in the solubility calculation. This is an important difference with classical abiotic batch protocols where the amount of dissolved element is estimated from the difference in concen-

tration before and after the dust addition. However, in order to estimate FracSol % induced by the second dust addition only, the amount of the dissolved element introduced needs to be calculated by comparison with the inventories in the dust mesocosms (DM) immediately prior to the second seeding (t143(-23)) and we therefore utilized Eq. (2) for the second seeding. An estimation of FracSol % based on Eq. (1) for the second dust addition would cumulate the effect of the two additions. Values of fractional solubility are reported in Table 2.

$$\text{FracSol} (\%) = \frac{\max \left\{ A \left( \left| \int_z^0 [M]_{\text{DM}} \partial z \right|_t - \left| \int_z^0 [M]_{\text{DM}} \partial z \right|_{\text{t143}} \right) \right\}}{\Sigma M_{\text{Dust}}} \quad (2)$$

#### Case 2: second addition

The fractional solubility for Al after the first and second dust addition was, respectively,  $1.44 \pm 0.19 \%$  and  $0.91 \pm 0.83 \%$ . There is no significant difference between these additions and the high variability for the second addition, which is due to the much lower values for Al observed in D3. In this mesocosm, significantly higher concentrations of bacteria were also observed, indicating that some other processes were occurring in this mesocosm compared to D1 and D2. Our data are consistent with results from Measures et al. (2010) who measured fractional Al solubilities of 0.087 to 14.3 % (average 4.6 %) in seawater with Hawaiian aerosol samples. For Saharan dust, fractional Al solubilities of 1.9–5.5 % in pH 4.7 solutions have been published by Baker et al. (2006), so our data are consistent with these results given the higher pH in seawater. For Mn, the fractional solubilities are higher, but after both dust additions in the same order of magnitude with values of  $41 \pm 9$  and  $27 \pm 19 \%$ . Recently, Mendez et al. (2010) reported values of 12 to 14 % for Saharan dust in laboratory experiments with seawater, while Baker et al. (2006) reported values of 50–64 % in pH 4.7 solutions. Earlier, Guieu et al. (1994) have shown fractional Mn solubilities of 30–35 % in pH 7 solutions. Values obtained with the “mesocosm” method are thus comparable to other experimental setups.

During the DUNE-1 experiment no dissolution from the dust particles was observed for Fe and therefore no value for the fractional solubility of Fe was obtainable (Wagener et al., 2010). Here, during DUNE-2, the same result was obtained after the first seeding, but a fractional solubility of  $0.12 \pm 0.03 \%$  was estimated after the second addition of dust. The reasons for this change in the amount of the dissolved element introduced by the dust and the induced fractional solubility are discussed in Sect. 4.4. Literature values for fractional Fe solubility range over more than three orders of magnitude (Baker and Croot, 2010; Sholkovitz et al., 2012) with large differences depending on atmospheric and

**Table 2.** Estimation of the elemental relative dissolution of dust in seawater.

		Mn	Fe	Al
Elemental dust addition ( $\mu\text{mol m}^{-2}$ ) <sup>a</sup>		63.7	4136	15271
First seeding	Difference of inventories Average maximum in the dust seeded mesocosms minus average control mesocosms ( $\mu\text{mol m}^{-2}$ ) <sup>b</sup>	25.6 $\pm$ 5.8	NA	177 $\pm$ 24
	Dissolution (%) <sup>c</sup>	40 $\pm$ 9	NA	1.2 $\pm$ 0.2
	Time when dust seeded mesocosms inventories reached their maxima (h)	t71	NA	t47
Second seeding	Difference of inventories Average maximum in the dust seeded mesocosms minus dust seeded mesocosms prior to second addition ( $\mu\text{mol m}^{-2}$ ) <sup>b</sup>	17.1 $\pm$ 11.8 <sup>d</sup>	4.9 $\pm$ 1.2	112 $\pm$ 103 <sup>d</sup>
	Dissolution (%) <sup>c</sup>	27 $\pm$ 19 <sup>d</sup>	0.12 $\pm$ 0.03	0.73 $\pm$ 0.67 <sup>d</sup>
	Time when dust seeded mesocosms inventories reached their maxima (h)	t239	t191	t215

<sup>a</sup> Estimation based on the addition of  $10 \text{ g m}^{-2}$  of dust with an elemental composition of Mn = 0.0342 %, Fe = 2.26 % and Al = 3.32 % (Desboeufs, personal communication, 2013). <sup>b</sup> Estimated with mean values for control and dust seeded mesocosms. <sup>c</sup> Estimated as the ratio between the difference of inventories and the amount of element added with dust. <sup>d</sup> High variability here related to differences in D3, also seen in bacterial numbers and phytoplankton abundance.

marine processes as well as on the experimental design used. In summary, based on a much more realistic protocol than the commonly used laboratory protocols, the fractional solubility of Mn and the fractional solubility of Al in dust are in the range of previously published values. This overall gives more confidence in consensus ranges for fractional Al and Mn solubility from dust. For Fe, the complex processes that control the fractional solubility are clearly shown here, and indicate that the use of a single absolute value for the fractional solubility of Fe is not realistic.

#### 4.2.2 Dissolution and loss rates

The rates of the decreases or increases in the inventories were quantified by estimating loss and dissolution rates. These estimated rates for Mn, Al and Fe are reported in Table 3.

An overall trend, observed for the three dissolved trace metals, was a general decrease in the inventories in the control mesocosms with low loss rates. This could correspond to scavenging onto particles, which is a common physical-chemical process occurring in the ocean for trace metals (Turekian, 1977). The loss rate was well defined for Al, which is not known to have a bioactive role, whereas some variations over the general decreasing trend were observed for Fe and Mn. This might be due to changes in biological utilization in response to the changes in stratification in the mesocosms.

In the dust seeded mesocosms, the inventories of Mn and Al increased with apparent dissolution rates which were quite similar for both dust additions. It is interesting to note that,

even if the dust additions occurred under different stratification conditions (Fig. 5a), the increase in the inventories and the dissolution rates were the same when integrated over the entire mesocosm. However, Fig. 1 clearly shows that the increase in Mn concentrations was occurring throughout the whole water column for the first compared to the second seeding, in which the increase was concentrated in the first few meters of the mesocosms. This implies that the overall rate of dissolution and fractional solubility was apparently not affected by the vertical mixing of the water column, but that mixing diluted the maximal concentration observed for the dissolved elements. This has important implications, illustrating that the sampling resolution can impact the assessment of the influence of dust addition. For example, the determination of vertical gradients, using finer spatial sampling resolution within the mesocosms, helps better define the processes occurring.

The loss rates of Al and Mn behaved differently. Mn showed quite equivalent loss rates for the first and the second seeding, whereas the Al loss rate was approximately one order of magnitude higher after the second seeding ( $-1.9 \mu\text{mol m}^{-2} \text{ d}^{-1}$ ) in comparison to after the first one ( $-0.07 \mu\text{mol m}^{-2} \text{ d}^{-1}$ ). Scavenging of Al is sensitive to the amount of biogenic particles in seawater (Moran and Moore, 1988). During DUNE-2, an increase of chlorophyll *a* in the dust seeded mesocosms is reported by Giovagnetti et al. (2012), suggesting an increase of biomass, which could explain the observed significant change in the loss rates for Al. Correlations of leachable Al and chlorophyll *a* were also previously observed by Moran and Moore (1988), suggesting

**Table 3.** Mn, Fe and Al dissolution and loss rates in  $\mu\text{mol m}^{-2} \text{d}^{-1}$  ( $\pm 1\sigma$ ). They were calculated as the increase/decline of each metal in each of the dust seeded mesocosms by applying a linear regression to the inventory as a function of time. For the dissolution rates the calculation was started at the point before each of the seedings until the point in time when the concentration reached its maximum. For the loss rates the calculation was started at the point after each of the seedings when the concentration was the highest.

dissolved trace metal	seeding	Dissolution rates ( $\mu\text{mol m}^{-2} \text{d}^{-1}$ )	Time intervals (h) used	loss rate [ $\mu\text{mol m}^{-2} \text{d}^{-1}$ ]	Time intervals (h) used
Mn	1	$0.43 \pm 0.09$	t0–t71	$-0.35 \pm 0.04$	t71–t143
Mn	2	$0.27 \pm 0.05$	t143(–23)–t239(73)	$-0.25 \pm 0.08$	t239(73)–t311(145)
	Control			$-0.006 \pm 0.013$	t0–t311(145)
Fe	1	NA	NA	NA	NA
Fe	2	$0.67 \pm 0.15$	t171(5)–t191(25)	NA	NA
	Control	NA	NA	$-0.01 \pm 0.01$	t47–t311(145)
Al	1	$2.8 \pm 1.3$	t0–t47	$-0.07 \pm 0.17$	t47–t143
Al	2	1, 1	t143(–23)–t215(49)	$-1.9 \pm 0.3$	t215(49)–t311(145)
	Control			$-0.24 \pm 0.07$	t0–t311(145)

a link between scavenging of Al and chlorophyll *a*. During DUNE-2 we also observed a similar correlation (Fig. 6) using the chlorophyll *a* inventory (Giovagnetti et al., 2012). Figure 6 shows an increase of the chlorophyll *a* inventory related to an increase of the Al loss rate. Previous studies in the vicinity of Corsica have shown that Al is strongly covariant with silicate (Mackenzie et al., 1978), suggesting removal of dissolved Al by incorporation in diatoms with subsequent remineralization at depth. In the present case, however, non-siliceous pico-plankton (*Synechococcus* and *Prochlorococcus*) and nano-plankton (Haptophytes and Chlorophytes) showed the major response to the dust additions, particularly after the second addition (Giovagnetti et al., 2012). Therefore, it appears that the loss of dissolved Al was related to adsorption into organic matter on these cells and not incorporation into biogenic silica. Stratification after the second dust addition may have accentuated this Al removal at this time, as higher concentrations of cyanobacteria and haptophytes were also observed at this time in the surface waters (Giovagnetti et al., 2012).

In the case of Mn, there was no appreciable difference in the loss rate after the first and second additions of dust, suggesting that the loss of Mn was not affected by uptake or adsorption into phytoplankton. Scavenging of Mn by particles requires the oxidation of Mn(II) prior to particle loss, as Mn(II) is only weakly complexed or adsorbed to particles (Yeats and Strain, 1990; Sunda and Huntsman, 1987). Abiotic oxidation of Mn(II) is normally considered to be too slow to account for the adsorbed loss rates and instead it is believed that bacterial oxidation is the major pathway in the ocean (Morgan, 2005; von Langen et al., 1997). During this experiment bacterial numbers were relatively constant throughout the experiment in all mesocosms, suggesting that the Mn oxidation rate was relatively constant (Pulido-Villena et al., 2013). The dissolved Mn loss rates observed here are equivalent to 6.5–10.8 %  $\text{d}^{-1}$  of the dissolved

Mn pool, which is significantly above the range of rates (0.2–1.5 %  $\text{d}^{-1}$ ) observed in oligotrophic regions (Moffett, 1997) but similar to that seen in coastal regions (Sunda and Huntsman, 1987). Thus, the turnover time of the Mn pool was about 10 to 16 days in the dust amended mesocosms. The slower turnover of Mn in the control mesocosms presumably indicates that Mn oxidation by bacteria may have been limited by another substrate, in this case presumably suitable organic carbon sources. Our rates are also integrated over the whole day and it is also likely that a diel cycle in Mn oxidation was occurring due to photo-reduction of  $\text{MnO}_2$  via reaction with humics or photo-produced  $\text{H}_2\text{O}_2$ , and potential photo-inhibition of Mn oxidizing bacteria, as it has been observed in coastal waters and the Sargasso Sea (Sunda and Huntsman, 1988, 1990). Thus, it is likely that Mn oxidation rates were maximal at night.

Changes in the Fe inventories were complex with regard to the dust addition. In the first day (t0–t23), the loss rate in the dust seeded mesocosms was  $-45.5 \mu\text{mol m}^{-2} \text{d}^{-1}$ , whereas it was slightly positive in that time frame in the control mesocosms. The control inventories only started to decrease after t23. The loss rate in the dust seeded mesocosms on the first day was comparable to the one reported for DUNE-1. This might demonstrate an assimilable scavenging onto dust particles, which had been demonstrated for DUNE-1 (Wagner et al., 2010). Until t72, an overall sharp decrease in the loss rates was observed in both the control and the dust seeded mesocosms. This decrease had not been observed in the control mesocosms during DUNE-1. A plausible reason for this decrease could be adsorption onto the mesocosms' plastic walls, by which the walls were not in equilibrium with the seawater initially during DUNE-2. It has been demonstrated in bottle experiments (e.g. Fischer et al., 2007), that this could represent up to 50 % of Fe in bottles. But, as the surface to volume ratio is much lower for large mesocosms,



wall adsorption cannot explain entirely the Fe loss in the control mesocosms.

After the second addition, a transient dissolution of Fe was observed within the first day (t166(0)–t191(25)) with a dissolution rate of  $0.67 \pm 0.15 \mu\text{mol m}^{-2} \text{d}^{-1}$ , which was higher than the loss rate observed after the first seeding. In the earlier DUNE-1 experiment, Wagener et al. (2010) estimated a maximal biological uptake of Fe in the mesocosms of 0.5 to  $1.0 \mu\text{mol m}^{-2} \text{d}^{-1}$  for the productive conditions encountered during this experiment. During DUNE-2, the productive conditions were in the same order of magnitude compared to DUNE-1 in terms of autotrophic and heterotrophic organisms. We therefore postulate that dissolution from dust particles could therefore sustain biological activity in terms of relieving any potential Fe limitation. This transient dissolution observed after the second addition corresponds with a significant increase in Fe binding ligands in the dust seeded mesocosms in comparison to the control mesocosms (Fig. 3). The ligand concentration increased about  $5 \text{ nmol L}^{-1}$  between the mean concentrations measured at t95 before the second dust addition and the mean concentrations measured at t191(25) after the second dust addition. This increase of the Fe binding capacity is compatible with the transient increase in Fe concentration, with values up to  $7.64 \text{ nmol L}^{-1}$  observed at t191(25) in the surface of D2. In any case, the observed excess of ligands would have helped to maintain Fe in solution and drive the observed transient dissolution on addition of the dust. A similar occurrence was also seen during SOIREE, Southern Ocean Fe enrichment, where Fe binding ligand concentrations increased after successive Fe additions, leading to an increase in the retention of Fe in the water column (Croot et al., 2001).

#### 4.3 Insights into the time scales and possible mechanisms of dissolution and scavenging processes during a dust event

Our unique dataset allows a first order look at the scavenging mechanisms following atmospheric deposition events. Previous work on this has been done over much larger temporal (week to month) and vertical (hundreds of meters) scales through the use of sediment traps (Brust et al., 2011; Brust and Waniek, 2010). The DUNE-2 experiment is unique in the sense that optical measurements in the water column were made simultaneously, allowing an assessment of the particle residence time. This particulate export was controlled partly by the formation of organic–mineral aggregates (Bressac et al., 2012). The mass of material exported into the sediment traps (collected every 24 h) was the highest at t48. At the end of the first seeding experiment, the optical parameters were homogenous from 0 to 10 m depth, but still slightly higher than before the first addition of dust (Bressac et al., 2012). During the second part of the DUNE-2 experiment, optical measurements were also performed in order to follow the particle dynamics (Bressac et al., 2013). These optical

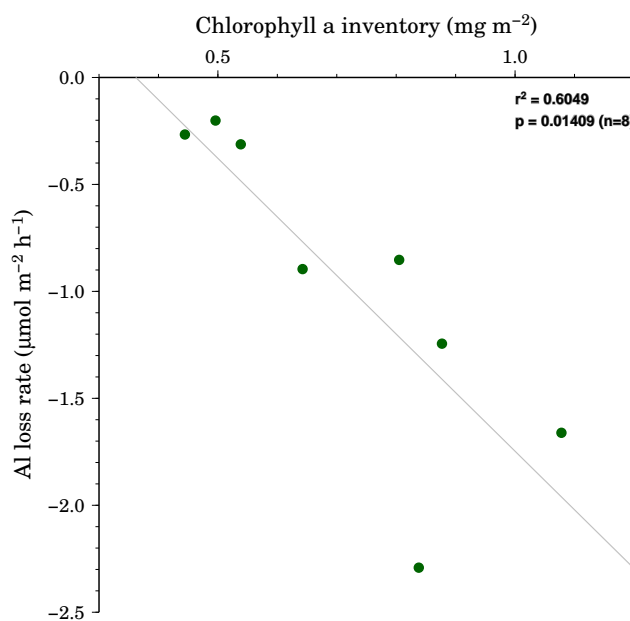


Fig. 6. Correlation of Al loss rate vs. the chlorophyll *a* inventory.

measurements revealed an accumulation of particles in the upper 2.5 m layer directly following the second dust addition, likely due to the stratification of the water column (Fig. 5a). This particle maximum was apparently partly due to increases in phytoplankton abundance triggered by the second dust addition (Giovagnetti et al., 2012). This longer residence time of particles in the subsurface could explain the high Fe dissolution observed after the second addition of dust. However, the mass of material exported into the sediment traps was the highest at t191(25). Indeed, the mixing of the water column occurred between t179(13) (maximum of the temperature difference (0–10 m)) and t215(49) (Fig. 5a). Simultaneously, a sudden decrease of the beam attenuation in the subsurface was observed between t176(8) and t191(25), revealing the activation of the particulate export (Bressac et al., 2013). The optical measurements indicate that part of the Saharan dust was rapidly lost from the mixed layer (estimated sinking rates  $\sim 24\text{--}86 \text{ m d}^{-1}$ ). As reported above, after the first seeding with dust, part of the Saharan dust pool was rapidly exported. The physical characteristics of the water column differed widely between both dust addition experiments. This difference in physical conditions, especially marked during the first hours after the seedings, likely impacted the particulate export dynamics and could partly explain the differences observed in the kinetic dissolution between the two additions of dust. These findings are important in the present context as they represent the removal of particulates and the adsorbed or scavenged metals they contain. Our observations are consistent with field studies from the Atlantic Ocean which have shown that the residence time of Fe in surface waters is strongly influenced by Saharan

dust deposition (Croot et al., 2004), while that of Mn and Al are much less so (Jickells et al., 1994; Jickells, 1999). In the case of Fe in the surface waters, Croot et al. (2004) showed that the fractional mean residence time was shortened with increasing Saharan dust fluxes. Earlier laboratory studies have shown that scavenging and export are controlled by the formation of organic–mineral aggregates (Balistrieri et al., 1981; Hunter, 1983), with scavenging related to particle concentration (Honeyman et al., 1988). For particle reactive elements, e.g. Fe, the transfer of colloidal to particulate phases (colloidal pumping) is also important (Honeyman and Santschi, 1991). Combining the optical data with the dissolved trace metal data suggests that the larger dust particles sunk out quickly (Bressac et al., 2013) but played a small role in scavenging both Mn and Al from the water column, as release processes dominated at that time. Thus, scavenging by smaller particles (dust and phytoplankton/bacteria) appears to be the more important removal term over the duration of the experiment. In particular, the production of organic material by bacteria and phytoplankton would lead to increased formation of organic–mineral aggregates and lead to increased scavenging.

#### 4.4 Effect of two successive dust additions on the biogeochemistry of trace metals

During the DUNE-1-P experiment, batch reactor dissolution experiments of dust performed with filtered seawater collected in the dust seeded and the control mesocosms have shown that the solubility of Fe increased significantly in the dust seeded mesocosms 7 d after the addition of dust (Wagener et al., 2010). A probable mechanism could be the production of specific Fe binding ligands by heterotrophic bacteria in the dust seeded mesocosms in response to a change in the bioavailability of Fe after the settling of particles. This hypothesis was supported by observations of changes in the diversity of the bacterial community attached to the dust particles (Laghdass et al., 2011).

Here during DUNE-2, this hypothesis was completely verified for Fe where a comparable response to the first addition of dust was observed with an increased scavenging of Fe, whereas after the second addition of dust, dissolution of Fe from the dust particles was observed. No additional dust dissolution batch reactor experiments were performed during DUNE-2, but Fe binding ligand measurements by ligand competition and cathodic stripping voltammetry showed a significant increase of Fe binding ligands at t191(25), in complete accordance with the increase in Fe solubility observed for DUNE-1. As mentioned earlier, this increase in Fe binding ligands can explain the transient increase in Fe inventory. However, it is interesting to note that the increase of Fe concentration by the second addition of dust was only very limited in time (24 h), whereas the ligand concentration in the dust seeded mesocosms remained high until the end of the experiment. The Fe inventory after the second dust ad-

dition rapidly decreased to the pre-addition values when a massive export of lithogenic particles was observed with the release of the stratification of the water column (Fig. 5a). We observed different behavior for Mn and Al in comparison to Fe and this can be explained by differences in their speciation in seawater. Whereas the solubility of Mn and Al is controlled solely by inorganic species, the solubility of soluble and colloidal Fe is controlled by organic complexes (Gledhill and Buck, 2012). Indeed, opposing effects were observed for Al and Fe. The consecutive additions of dust did not impact the dissolution of Al but did impact the loss rate through the increase of scavenging onto biogenic particles induced by biomass increase subsequent to the first dust addition. However, this mechanism was not observed for Mn, which is certainly subject to more complex redox and photochemical processes (Sunda and Huntsman, 1987, 1988). Overall, this demonstrates that the biogeochemistry of the surface ocean responds in a nonlinear way to the atmospheric flux of dust to the seawater. The frequency of the depositions needs to be taken into account because it will condition the impact of the deposited particles. This has important consequences on the time scales that have to be studied in order to obtain a realistic picture of the impact of dust deposition.

**Supplementary material related to this article is available online at: <http://www.biogeosciences.net/10/2583/2013/bg-10-2583-2013-supplement.zip>.**

*Acknowledgements.* This study was financially supported by ANR-DUNE under the contract ANR-07-BLAN-0126-01. Funding for the participation of K. Wuttig and support of the work performed during DUNE-2 were provided by grants from the DFG to P. L. Croot (CR145/15-1 and CR145/17-1). The financial support by the BMBF Verbundprojekt SOPRAN (FKZ 03F0462A and 03F0611A), which is a German contribution to SOLAS (Surface Ocean – Lower Atmosphere Studies), is also gratefully acknowledged. T. Wagener was supported by a Marie Curie IEF (Grant agreement No. PIEF-GA-2009-236694, DAPOP). M. Bressac acknowledges a PhD grant provided by the ACRI-ST company and the French National Association for Research and Technology (ANRT). J. M. Dominici and collaborators of the Réserve naturelle de Scandola, Parc naturel régional de Corse are gratefully acknowledged for their cooperation and help in performing the experiment in the Bay of Elbo. We thank all of the participants of the DUNE-2 experiment for their involvement. Special thanks are also due to F. Malien and M. Lohmann (GEOMAR) for their nutrient laboratory work on very short notice and to Sandrine Chifflet (MIO) for all her Fe binding ligand measurements. We would like to acknowledge the editor and four anonymous reviewers for improving this paper.

The service charges for this open access publication have been covered by a Research Centre of the Helmholtz Association.

Edited by: E. Marañón

## References

- Aguilar-Islas, A. M., Resing, J. A., and Bruland, K. W.: Catalytically enhanced spectrophotometric determination of manganese in seawater by flow-injection analysis with a commercially available resin for on-line preconcentration, *Limnol. Oceanogr. Meth.*, 4, 105–113, doi:10.4319/lom.2006.4.105, 2006.
- Baker, A. R. and Croot, P. L.: Atmospheric and marine controls on aerosol iron solubility in seawater, *Mar. Chem.*, 120, 4–13, doi:10.1016/j.marchem.2008.09.003, 2010.
- Baker, A. R. and Jickells, T. D.: Mineral particle size as a control on aerosol iron solubility, *Geophys. Res. Lett.*, 33, L17608, doi:10.1029/2006gl026557, 2006.
- Baker, A. R., Jickells, T. D., Witt, M., and Linge, K. L.: Trends in the solubility of iron, aluminium, manganese and phosphorus in aerosol collected over the atlantic ocean, *Mar. Chem.*, 98, 43–58, doi:10.1016/j.marchem.2005.06.004, 2006.
- Balistrieri, L., Brewer, P. G., and Murray, J. W.: Scavenging residence times of trace-metals and surface-chemistry of sinking particles in the deep ocean, *Deep-Sea Res.*, 28, 101–121, doi:10.1016/0198-0149(81)90085-6, 1981.
- Bergquist, B. A., Wu, J., and Boyle, E. A.: Variability in oceanic dissolved iron is dominated by the colloidal fraction, *Geochim. Cosmochim. Acta*, 71, 2960–2974, 2007.
- Blain, S., Queguiner, B., Armand, L., Belviso, S., Bombled, B., Bopp, L., Bowie, A., Brunet, C., Brussaard, C., Carlotti, F., Christaki, U., Corbiere, A., Durand, I., Ebersbach, F., Fuda, J. L., Garcia, N., Gerringa, L., Griffiths, B., Guigue, C., Guillermin, C., Jacquet, S., Jeandel, C., Laan, P., Lefevre, D., Lo Monaco, C., Malits, A., Mosseri, J., Obernosterer, I., Park, Y. H., Picherl, M., Pondaven, P., Remenyi, T., Sandroni, V., Sarthou, G., Savoye, N., Scouarnec, L., Souhaut, M., Thuiller, D., Timmermans, K., Trull, T., Uitz, J., van Beek, P., Veldhuis, M., Vincent, D., Viollier, E., Vong, L., and Wagener, T.: Effect of natural iron fertilization on carbon sequestration in the southern ocean, *Nature*, 446, 1070–1071, 2007.
- Bonnet, S. and Guieu, C.: Dissolution of atmospheric iron in seawater, *Geophys. Res. Lett.*, 31, L03303, doi:10.1029/2003gl018423, 2004.
- Bonnet, S. and Guieu, C.: Atmospheric forcing on the annual iron cycle in the western mediterranean sea: A 1-year survey, *J. Geophys. Res.-Oceans*, 111, C09010, doi:10.1029/2005jc003213, 2006.
- Boyd, P. W., Watson, A., Law, C. S., Abraham, E., Trull, T., Murdoch, R., Bakker, D. C. E., Bowie, A. R., Buesseler, K. O., Chang, H., Charette, M., Croot, P. L., Downing, K., Frew, R., Gall, M., Hadfield, M., Hall, J., Harvey, M., Jameson, G., LaRoche, J., Liddicoat, M., Ling, R., Maldonado, M., McKay, R. M., Nodder, S., Pickmere, S., Pridmore, R., Rintoul, S., Safi, K., Sutton, P., Strzepek, R., Tannenberger, K., Turner, S., Waite, A., and Zeldis, J.: Mesoscale iron fertilisation elevates phytoplankton stocks in the polar southern ocean, *Nature*, 407, 695–702, 2000.
- Boyle, E. A., Chapnick, S. D., Bai, X. X., and Spivack, A.: Trace-metal enrichments in the mediterranean-sea, *Earth Planet. Sci. Lett.*, 74, 405–419, doi:10.1016/s0012-821x(85)80011-x, 1985.
- Bressac, M. and Guieu, C.: Organic complexation versus scavenging: What really happens to new atmospheric iron in the ocean surface?, *Global Biogeochem. Cy.*, in revision, 2013.
- Bressac, M., Guieu, C., Doxaran, D., Bourrin, F., Obolensky, G., and Grisoni, J.-M.: A mesocosm experiment coupled with optical measurements to assess the fate and sinking of atmospheric particles in clear oligotrophic waters, *Geo-Mar. Lett.*, 32, 153–164, doi:10.1007/s00367-011-0269-4, 2012.
- Bressac, M., Guieu, C., Doxaran, D., Bourrin, F., Leblond, N., and Ridame, C.: Quantification of the lithogenic carbon pump following a dust event, *Biogeosciences (BG)*, in preparation, 2013.
- Bruland, K. W., Franks, R. P., Knauer, G. A., and Martin, J. H.: Sampling and analytical methods for the determination of copper, cadmium, zinc, and nickel at the nanogram per liter level in seawater, *Anal. Chimica Acta*, 105, 233–245, doi:10.1016/s0003-2670(01)83754-5, 1979.
- Brust, J. and Waniek, J. J.: Atmospheric dust contribution to deep-sea particle fluxes in the subtropical northeast atlantic, *Deep-Sea Res. Pt. I*, 57, 988–998, doi:10.1016/j.dsr.2010.04.011, 2010.
- Brust, J., Schulz-Bull, D. E., Leipe, T., Chavagnac, V., and Waniek, J. J.: Descending particles: From the atmosphere to the deep ocean—a time series study in the subtropical ne atlantic, *Geophys. Res. Lett.*, 38, L06603, doi:10.1029/2010gl045399, 2011.
- Buck, C. S., Landing, W. M., Resing, J. A., and Lebon, G. T.: Aerosol iron and aluminum solubility in the northwest pacific ocean: Results from the 2002 ioc cruise, *Geochim. Geophys. Geosy.*, 7, Q04m07, doi:10.1029/2005gc000977, 2006.
- Carr, M.-E., Friedrichs, M. A. M., Schmeltz, M., Noguchi Aita, M., Antoine, D., Arrigo, K. R., Asanuma, I., Aumont, O., Barber, R., Behrenfeld, M., Bidigare, R., Buitenhuis, E. T., Campbell, J., Ciotti, A., Dierssen, H., Dowell, M., Dunne, J., Esaias, W., Gentili, B., Gregg, W., Groom, S., Hoepffner, N., Ishizaka, J., Kameda, T., Le Quéré, C., Lohrenz, S., Marra, J., Mélin, F., Moore, K., Morel, A., Reddy, T. E., Ryan, J., Scardi, M., Smyth, T., Turpie, K., Tilstone, G., Waters, K., and Yamanaka, Y.: A comparison of global estimates of marine primary production from ocean color, *Deep-Sea Res. Pt. II*, 53, 741–770, doi:10.1016/j.dsr2.2006.01.028, 2006.
- Caschetto, S. and Wollast, R.: Vertical distribution of dissolved aluminium in the mediterranean sea, *Mar. Chem.*, 7, 141–155, doi:10.1016/0304-4203(79)90006-9, 1979.
- Chou, L. and Wollast, R.: Biogeochemical behavior and mass balance of dissolved aluminum in the western mediterranean sea, *Deep Sea Research Part II: Topical Studies in Oceanography*, 44, 741–768, doi:10.1016/s0967-0645(96)00092-6, 1997.
- Copin-Montegut, G., Courau, P., and Nicolas, E.: Distribution and transfer of trace elements in the western mediterranean, *Mar. Chem.*, 18, 189–195, doi:10.1016/0304-4203(86)90007-1, 1986.
- Croot, P. L. and Heller, M. I.: The importance of kinetics and redox in the biogeochemical cycling of iron in the surface ocean, *Frontiers in Microbiology*, 3, 219, doi:10.3389/fmicb.2012.00219, 2012.
- Croot, P. L. and Johansson, M.: Determination of iron speciation by cathodic stripping voltammetry in seawater using the competing ligand 2-(2-thiazolylazo)-p-cresol (tac), *Electroanalysis*, 12, 565–576, 2000.
- Croot, P. L., Bowie, A. R., Frew, R. D., Maldonado, M., Hall, J. A., Safi, K. A., La Roche, J., Boyd, P. W., and Law, C. S.: Retention of dissolved iron and  $Fe^{II}$  in an iron induced southern ocean phytoplankton bloom, *Geophys. Res. Lett.*, 28, 3425–3428, doi:10.1029/2001gl013023, 2001.

- Croot, P. L., Streu, P., and Baker, A. R.: Short residence time for iron in surface seawater impacted by atmospheric dry deposition from saharan dust events, *Geophys. Res. Lett.*, 31, L23S08, doi:10.1029/2004gl020153, 2004.
- Croot, P. L., Passow, U., Assmy, P., Jansen, S., and Strass, V. H.: Surface active substances in the upper water column during a southern ocean iron fertilization experiment (eifex), *Geophys. Res. Lett.*, 34, L03612, doi:10.1029/2006gl028080, 2007.
- Cutter, G. A., Andersson, P., Codispoti, L., Croot, P. L., Francois, R., Lohan, M., Obata, H., and Rutgers van der Loeff, M.: Sampling and Sample-handling Protocols for GEOTRACES Cruises: <http://www.geotraces.org/libraries/documents/Intercalibration/Cookbook.pdf>, 2010.
- Dammshäuser, A., Wagener, T., and Croot, P. L.: Surface water dissolved aluminum and titanium: Tracers for specific time scales of dust deposition to the atlantic?, *Geophys. Res. Lett.*, 38, L24601, doi:10.1029/2011gl049847, 2011.
- Danielsson, L.-G., Magnusson, B., and Westerlund, S.: An improved metal extraction procedure for the determination of trace metals in sea water by atomic absorption spectrometry with electrothermal atomization, *Analyt. Chimica Acta*, 98, 47–57, doi:10.1016/s0003-2670(01)83237-2, 1978.
- Duce, R. A., Liss, P. S., Merrill, J. T., Atlas, E. L., Buat-Menard, P., Hicks, B. B., Miller, J. M., Prospero, J. M., Arimoto, R., Church, T. M., Ellis, W., Galloway, J. N., Hansen, L., Jickells, T. D., Knap, A. H., Reinhardt, K. H., Schneider, B., Soudine, A., Tokos, J. J., Tsunogai, S., Wollast, R., and Zhou, M.: The atmospheric input of trace species to the world ocean, *Glob. Biogeochem. Cy.*, 5, 193–259, doi:10.1029/91gb01778, 1991.
- Emerson, S., Quay, P., Karl, D., Winn, C., Tupas, L., and Landry, M.: Experimental determination of the organic carbon flux from open-ocean surface waters, *Nature*, 389, 951–954, 1997.
- Fischer, A. C., Kroon, J. J., Verburg, T. G., Teunissen, T., and Wolterbeek, H. T.: On the relevance of iron adsorption to container materials in small-volume experiments on iron marine chemistry: 55Fe-aided assessment of capacity, affinity and kinetics, *Mar. Chem.*, 107, 533–546, 2007.
- Giovagnetti, V., Brunet, C., Conversano, F., Tramontano, F., Obernosterer, I., Ridame, C., and Guieu, C.: Assessing the role of dust deposition on phytoplankton ecophysiology and succession in a low-nutrient low-chlorophyll ecosystem: A mesocosm experiment in the mediterranean sea, *Biogeosciences Discuss.*, 9, 19199–19243, doi:10.5194/bgd-9-19199-2012, 2012.
- Gledhill, M. and Buck, K. N.: The organic complexation of iron in the marine environment: A review, *Front. Microbiol.*, 3, doi:10.3389/fmicb.2012.00069, 2012.
- Grasshoff, K., Kremling, K., and Ehrhardt, M.: *Methods of seawater analysis*, Verlag Chemie, Weinheim, 1983.
- Guerzoni, S., Molinaroli, E., Rossini, P., Rampazzo, G., Quarantotto, G., de Falco, G., and Cristini, S.: Role of desert aerosol in metal fluxes in the mediterranean area, *Chemosphere*, 39, 229–246, doi:10.1016/s0045-6535(99)00105-8, 1999.
- Guieu, C., Duce, R., and Arimoto, R.: Dissolved input of manganese to the ocean: Aerosol source, *J. Geophys. Res.*, 99, 18789–18800, 1994.
- Guieu, C., Loye-Pilot, M. D., and Ridame, C.: DUNE –a Dust experiment in a low Nutrient, low Chlorophyll Ecosystem – Quantifying the role of atmospheric input on marine ecosystem using large clean mesocosms, *SOLAS Newsletter*, 9, 36–37, 2009.
- Guieu, C., Dulac, F., Desboeufs, K., Wagener, T., Pulido-Villena, E., Grisoni, J.-M., Louis, F., Ridame, C., Blain, S., Brunet, C., Nguyen, E. B., Tran, S., Labiadh, M., and Dominici, J.-M.: Large clean mesocosms and simulated dust deposition: A new methodology to investigate responses of marine oligotrophic ecosystems to atmospheric inputs, *Biogeosciences*, 7, 2765–2784, doi:10.5194/bg-7-2765-2010, 2010.
- Guieu, C., Dulac, F., Ridame, C., and Pondaven, P.: Introduction to the DUNE project: a DUST experiment in a low Nutrient, low chlorophyll Ecosystem, *Biogeosciences (BG)*, in preparation, 2013.
- Heller, M. I. and Croot, P. L.: Kinetics of superoxide reactions with dissolved organic matter in tropical Atlantic surface waters near Cape Verde (TENATSO), *J. Geophys. Res.*, 115, C12038, doi:10.1029/2009jc006021, 2010.
- Herut, B., Zohary, T., Krom, M. D., Mantoura, R. F. C., Pitta, P., Psarra, S., Rassoulzadegan, F., Tanaka, T., and Frede Thingstad, T.: Response of east mediterranean surface water to saharan dust: On-board microcosm experiment and field observations, *Deep-Sea Res. Pt. II*, 52, 3024–3040, doi:10.1016/j.dsr2.2005.09.003, 2005.
- Honeyman, B. D. and Santschi, P. H.: Coupling adsorption and particle aggregation: Laboratory studies of “colloidal pumping” using iron-59fe-labeled hematite, *Environ. Sci. Technol.*, 25, 1739–1747, doi:10.1021/es00022a010, 1991.
- Honeyman, B. D., Balistieri, L. S., and Murray, J. W.: Oceanic trace metal scavenging: The importance of particle concentration, *Deep-Sea Res.*, 35, 227–246, 1988.
- Hunter, K. A.: The adsorptive properties of sinking particles in the deep ocean, *Deep-Sea Res.*, 30, 669–675, 1983.
- Hydes, D. J. and Liss, P. S.: Fluorimetric method for the determination of low concentrations of dissolved aluminium in natural waters, *Analyst*, 101, 922–931, 1976.
- Hydes, D. J., de Lange, G. J., and de Baar, H. J. W.: Dissolved aluminium in the mediterranean, *Geochim. Cosmochim. Acta*, 52, 2107–2114, doi:10.1016/0016-7037(88)90190-1, 1988.
- Jickells, T. D.: The inputs of dust derived elements to the sargasso sea; a synthesis, *Mar. Chem.*, 68, 5–14, 1999.
- Jickells, T., Church, T., Veron, A., and Arimoto, R.: Atmospheric inputs of manganese and aluminum to the sargasso sea and their relation to surface-water concentrations, *Mar. Chem.*, 46, 283–292, doi:10.1016/0304-4203(94)90083-3, 1994.
- Jickells, T. D., An, Z. S., Andersen, K. K., Baker, A. R., Bergametti, G., Brooks, N., Cao, J. J., Boyd, P. W., Duce, R. A., Hunter, K. A., Kawahata, H., Kubilay, N., laRoche, J., Liss, P. S., Mahowald, N., Prospero, J. M., Ridgwell, A. J., Tegen, I., and Torres, R.: Global iron connections between desert dust, ocean biogeochemistry, and climate, *Science*, 308, 67–71, doi:10.1126/science.1105959, 2005.
- Johnson, K. S., Elrod, V., Fitzwater, S., Plant, J., Boyle, E., Bergquist, B., Bruland, K., Aguilar-Islas, A., Buck, K., Lohan, M., Smith, G. J., Sohst, B., Coale, K., Gordon, M., Tanner, S., Measures, C., Moffett, J., Barbeau, K., King, A., Bowie, A., Chase, Z., Cullen, J., Laan, P., Landing, W., Mendez, J., Milne, A., Obata, H., Doi, T., Ossiander, L., Sarthou, G., Sedwick, P., Van den Berg, S., Laglera-Baquer, L., Wu, J.-f., and Cai, Y.: Developing standards for dissolved iron in seawater, *Eos Trans. AGU*, 88, 2007.

- Journet, E., Desboeufs, K. V., Caqueneau, S., and Colin, J.-L.: Mineralogy as a critical factor of dust iron solubility, *Geophys. Res. Lett.*, 35, L07805, doi:10.1029/2007gl031589, 2008.
- Klinkhammer, G. P.: Determination of manganese in sea water by flameless atomic absorption spectrometry after preconcentration with 8-hydroxyquinoline in chloroform, *Analytical Chemistry*, 52, 117–120, doi:10.1021/ac50051a028, 1980.
- Kremling, K. and Petersen, H.: The distribution of zinc, cadmium, copper, manganese and iron in waters of the open mediterranean sea, *Meteor Forschungsergeb Reihe A/B*, 23, 5–14, 1981.
- Laghdass, M., Blain, S., Besseling, M., Catala, P., Guieu, C., and Obernosterer, I.: Effects of saharan dust on the microbial community during a large in situ mesocosm experiment in the nw mediterranean sea, *Aquat. Microb. Ecol.*, 62, 201–213, doi:10.3354/Ame01466, 2011.
- Landing, W. M. and Paytan, A.: Marine chemistry special issue: Aerosol chemistry and impacts on the ocean, *Mar. Chem.*, 120, 1–3, doi:10.1016/j.marchem.2010.04.001, 2010.
- Liu, X. and Millero, F. J.: The solubility of iron in seawater, *Mar. Chem.*, 77, 43–54, 2002.
- Longhurst, A., Sathyendranath, S., Platt, T., and Caverhill, C.: An estimate of global primary production in the ocean from satellite radiometer data, *J. Plankt. Res.*, 17, 1245–1271, doi:10.1093/plankt/17.6.1245, 1995.
- Mackenzie, F. T., Stoffyn, M., and Wollast, R.: Aluminum in seawater: Control by biological activity, *Science*, 199, 680–682, doi:10.1126/science.199.4329.680, 1978.
- Measures, C. I., Sato, T., Vink, S., Howell, S., and Li, Y. H.: The fractional solubility of aluminium from mineral aerosols collected in hawaii and implications for atmospheric deposition of biogeochemically important trace elements, *Mar. Chem.*, 120, 144–153, doi:10.1016/j.marchem.2009.01.014, 2010.
- Mendez, J., Guieu, C., and Adkins, J.: Atmospheric input of manganese and iron to the ocean: Seawater dissolution experiments with saharan and north american dusts, *Mar. Chem.*, 120, 34–43, doi:10.1016/j.marchem.2008.08.006, 2010.
- Millot, C.: Circulation in the western mediterranean sea, *Journal of Marine Systems*, 20, 423–442, doi:10.1016/s0924-7963(98)00078-5, 1999.
- Moffett, J. W.: The importance of microbial Mn oxidation in the upper ocean: a comparison of the Sargasso Sea and equatorial Pacific, *Deep-Sea Res. Pt. I*, 44, 1277–1291, doi:10.1016/s0967-0637(97)00032-0, 1997.
- Moore, J. K., Doney, S. C., Lindsay, K., Mahowald, N., and Michaels, A. F.: Nitrogen fixation amplifies the ocean biogeochemical response to decadal timescale variations in mineral dust deposition, *Tellus B*, 58, 560–572, 2006.
- Moran, S. B. and Moore, R. M.: Temporal variations in dissolved and particulate aluminum during a spring bloom, *Estuarine, Coastal and Shelf Science*, 27, 205–215, doi:10.1016/0272-7714(88)90090-x, 1988.
- Morgan, J. J.: Kinetics of reaction between o<sub>2</sub> and mn(ii) species in aqueous solutions, 69, 35–48, doi:10.1016/j.gca.2004.06.013, 2005.
- Morley, N. H., Burton, J. D., Tankere, S. P. C., and Martin, J. M.: Distribution and behaviour of some dissolved trace metals in the western mediterranean sea, *Deep-Sea Res. Pt. II*, 44, 675–691, doi:10.1016/s0967-0645(96)00098-7, 1997.
- Nealson, K. H., Tebo, B. M., Rosson, R. A., and Allen, I. L.: Occurrence and mechanisms of microbial oxidation of manganese, in: *Advances in applied microbiology*, Academic Press, 279–318, 1988.
- Noble, A. E., Saito, M. A., Maiti, K., and Benitez-Nelson, C. R.: Cobalt, manganese, and iron near the hawaiian islands: A potential concentrating mechanism for cobalt within a cyclonic eddy and implications for the hybrid-type trace metals, *Deep-Sea Res. Pt. II*, 55, 1473–1490, doi:10.1016/j.dsr2.2008.02.010, 2008.
- Obata, H., Shitashima, K., Isshik, K., and Nakayama, E.: Iron, manganese and aluminum in upper waters of the western south pacific ocean and its adjacent seas, *J. Oceanogr.*, 64, 233–245, 2008.
- Pulido-Villena, E., Baudoux, A.-C., Obernosterer, I., Catala, P., and Guieu, C.: Enhanced carbon remineralization by the microbial food web after dust deposition: Results from a mesocosm study, *Biogeosciences Discuss.*, in preparation, 2013.
- Roitz, J. S. and Bruland, K. W.: Determination of dissolved manganese(II) in coastal and estuarine waters by differential pulse cathodic stripping voltammetry, *Analyt. Chimica Acta*, 344, 175–180, doi:10.1016/s0003-2670(97)00041-x, 1997.
- Saito, M. A. and Moffett, J. W.: Temporal and spatial variability of cobalt in the atlantic ocean, *Geochim. Cosmochim. Acta*, 66, 1943–1953, doi:10.1016/s0016-7037(02)00829-3, 2002.
- Sañudo-Wilhelmy, S. A., Rivera-Duarte, I., and Russell Flegal, A.: Distribution of colloidal trace metals in the san francisco bay estuary, *Geochim. Cosmochim. Acta*, 60, 4933–4944, doi:10.1016/s0016-7037(96)00284-0, 1996.
- Sarthou, G. and Jeandel, C.: Seasonal variations of iron concentrations in the ligurian sea and iron budget in the western mediterranean sea, *Mar. Chem.*, 74, 115–129, 2001.
- Sedwick, P. N., Sholkovitz, E. R., and Church, T. M.: Impact of anthropogenic combustion emissions on the fractional solubility of aerosol iron: Evidence from the sargasso sea, *Geochem. Geophys. Geosy.*, 8, Q10Q06, doi:10.1029/2007gc001586, 2007.
- Sherrell, R. M. and Boyle, E. A.: Zinc, chromium, vanadium and iron in the mediterranean sea, *Deep-Sea Res. Pt. A*, 35, 1319–1334, doi:10.1016/0198-0149(88)90085-4, 1988.
- Sholkovitz, E. R., Sedwick, P. N., Church, T. M., Baker, A. R., and Powell, C. F.: Fractional solubility of aerosol iron: Synthesis of a global-scale data set, *Geochim. Cosmochim. Acta*, 89, 173–189, doi:10.1016/j.gca.2012.04.022, 2012.
- Spokes, L. J., and Jickells, T. D.: Factors controlling the solubility of aerosol trace metals in the atmosphere and on mixing into seawater, *Aquat. Geochem.*, 1, 355–374, doi:10.1007/bf00702739, 1996.
- Statham, P. J., Burton, J. D., and Hydes, D. J.: Cd and Mn in the Alboran Sea and adjacent North Atlantic: geochemical implications for the Mediterranean, *Nature*, 313, 565–567, 1985.
- Stumm, W. and Morgan, J. J.: *Aquatic chemistry*, Wiley-Interscience, New York, 1022 pp., 1996.
- Sunda, W. G. and Huntsman, S. A.: Microbial oxidation of manganese in a north carolina estuary, *Anglais*, 32, 552–564, 1987.
- Sunda, W. G. and Huntsman, S. A.: Effect of sunlight on redox cycles of manganese in the southwestern sargasso sea, *Deep-Sea Res. Pt. A*, 35, 1297–1317, 1988.
- Sunda, W. G. and Huntsman, S. A.: Diel cycles in microbial manganese oxidation and manganese redox speciation in coastal waters of the bahama-islands, *Limnol. Oceanogr.*, 35, 325–338,

- 1990.
- Turekian, K. K.: The fate of metals in the oceans, *Geochim. Cosmochim. Acta*, 41, 1139–1144, doi:10.1016/0016-7037(77)90109-0, 1977.
- van den Berg, C. M. G., Boussemart, M., Yokoi, K., Prartono, T., and Campos, M. L. A. M.: Speciation of aluminium, chromium and titanium in the nw mediterranean, *Mar. Chem.*, 45, 267–282, doi:10.1016/0304-4203(94)90074-4, 1994.
- van den Berg, C. M. G.: Evidence for organic complexation of iron in seawater, *Mar. Chem.*, 50, 139–157, 1995.
- von Langen, P. J., Johnson, K. S., Coale, K. H., and Elrod, V. A.: Oxidation kinetics of manganese (II) in seawater at nanomolar concentrations, *Geochim. Cosmochim. Acta*, 61, 4945–4954, doi:10.1016/s0016-7037(97)00355-4, 1997.
- Wagener, T., Pulido-Villena, E., and Guieu, C.: Dust iron dissolution in seawater: Results from a one-year time-series in the mediterranean sea, *Geophys. Res. Lett.*, 35, L16601, doi:10.1029/2008GL034581, 2008.
- Wagener, T., Guieu, C., and Leblond, N.: Effects of dust deposition on iron cycle in the surface mediterranean sea: Results from a mesocosm seeding experiment, *Biogeosciences*, 7, 3769–3781, doi:10.5194/bg-7-3769-2010, 2010.
- Ye, Y., Wagener, T., Völker, C., Guieu, C., and Wolf-Gladrow, D. A.: Dust deposition: Iron source or sink? A case study, *Biogeosciences*, 8, 2107–2124, doi:10.5194/bg-8-2107-2011, 2011.
- Yeats, P. A. and Strain, P. M.: The oxidation of manganese in seawater: Rate constants based on field data, *Estuarine, Coast. Shelf Sci.*, 31, 11–24, 1990.
- Yoon, Y. Y., Martin, J. M., and Cotte, M. H.: Dissolved trace metals in the western mediterranean sea: Total concentration and fraction isolated by c18 sep-pak technique, *Mar. Chem.*, 66, 129–148, doi:10.1016/s0304-4203(99)00033-x, 1999.
- Zhuang, G., Yi, Z., Duce, R. A., and Brown, P. R.: Chemistry of iron in marine aerosols, *Global Biogeochem. Cy.*, 6, 161–173, doi:10.1029/92gb00756, 1992.







**F**INAL **C**ONCLUSIONS  
AND  
**F**UTURE **P**ERSPECTIVES



## 5 FINAL CONCLUSIONS AND FUTURE PERSPECTIVES

The major goals of this thesis were to investigate the biogeochemistry of the biologically important micronutrient Mn in the upper ocean with emphasis on the processes affecting its distribution, sources and sinks. A new aspect of this work was to examine the biogeochemical interactions between Mn and ROS within the euphotic zone as earlier studies had demonstrated the importance of reactions between Mn and ROS but had not clearly elucidated exact pathways or chemical mechanisms. The ROS species  $O_2^-$  and  $H_2O_2$  can act as both an oxidant or reductant in seawater and thus directly influence the cycling between the three main redox states of Mn: Mn(II), Mn(III) and Mn(IV). The redox states of Mn are characterized by different solubilities (e.g. Mn(II) is soluble, whereas Mn(IV) is insoluble) and chemical reactivity. My thesis work was designed to address identified knowledge gaps, through a combination of laboratory work and field studies performed in contrasting environments; OMZ off Peru, the Mediterranean, the Mauritanian shelf and the oligotrophic Atlantic Ocean. My thesis work has demonstrated the importance and quantified the roles that  $O_2$  and  $H_2O_2$  play in determining the bioavailability and residence time of Mn in the ocean. More specifically, the results reported in this thesis have greatly improved our understanding of the different reaction pathways and mechanisms of Mn, as well as associated dissolution processes. The major results of this thesis are summarized below. Subsequently the main pathways for ROS and Mn redox cycling in the sunlit ocean are addressed. Finally, future perspectives of further work on this topic will be given towards the end of this chapter.

- **Mn method**

In the course of this work a Mn FIA was constructed as outlined by Aguilar-Islas *et al.* (2006) with some modifications to substantially improve the sensitivity and sample throughput of measurements for Mn (II) concentrations in the nanomolar and picomolar range. The accuracy and precision of this method was compared to the established Mn(II) oxine extraction method and showed good agreement. The main advantage of the Mn FIA measurements used in this study was the substantially improved rate of sample analysis and the ability to conduct measurements at sea.

- **Sampling for Mn**

Mn samples were processed from trace metal clean GoFlo-bottles and from the Niskin-bottles of a CTD rosette system and it was shown that samples from the CTD rosette could be collected without Mn contamination. As sampling with the GoFlo-bottles is very time-consuming and laborious, the ability to take non-contaminated samples for Mn using the CTD system allows a considerable higher resolution for

depth profiles and transects could be achieved than sampling solely with GoFlo-bottles.

- **Mn sources and sinks**

Mn was measured in different oceans and environments: the Mediterranean, the Pacific and the Atlantic. Sampling took place in the surface of the coastal and open ocean as well as in the OMZ of the Atlantic and the Pacific Ocean. Mn distributions and cycling were compared to other important trace metals. Mn sources could be clearly identified based on the increase of the Mn concentrations e.g. in coastal areas close to sediments and especially in the ITCZ due to wet deposition of Saharan dust. On the Mauritanian shelf the Mn concentrations in the water column were enhanced in the water column consistent with either a Mn flux from the sediments and/or from aeolian deposition of Saharan dust.

- **Mn in the OMZ and the Eastern Tropical Atlantic Ocean**

For the Atlantic and in the Pacific different Mn distributions were shown. In the Eastern Tropical Atlantic, the Mn concentration along with the concentration of the key micronutrient Fe was strongly enhanced by the deposition of Saharan dust to the surface. The strongest influence was observed in the ITCZ due to wet deposition. Mn was depleted with depth and from north to south. No secondary Mn maximum was observed in the Atlantic OMZ in contrast to the Arabian Sea this secondary Mn(II) maximum was observed under anoxic conditions due to the reduction of Mn(IV)O<sub>2</sub> with HS<sup>-</sup> to Mn(II) and SO<sub>4</sub> (Johnson *et al.*, 1992; Lewis and Luther III, 2000). The reason that no secondary Mn(II) maximum in the Atlantic could be observed was that the O<sub>2</sub> concentrations are not as low as in the Arabian Sea or the Pacific Ocean.

- **Fe and Cd in the Atlantic Ocean**

In contrast to the Mn distribution in the Atlantic, additional transport pathways and biological utilization were seen for Cd and Fe. In the equatorial upwelling Mn was slightly increased whilst Cd concentrations were significantly enhanced and no difference was observed for Fe. In the euphotic zone Fe exhibited its biological influence in the form of a distinct subsurface minimum which was correlated to a chlorophyll-a and a nitrite maxima. However an additional transport pathway of Fe was shown in the eastward flowing EUC which didn't show any difference in the Mn or Cd, but which had been shown before for the Pacific EUC (Slemons *et al.*, 2012).

- **Mn in the Eastern Tropical Pacific Ocean and the OMZ off Peru**

In contrast to the Atlantic, in the Pacific a secondary Mn maximum was detected in the OMZ where the nitrite was below its detection limit. Elevated surface concentrations were detected at 14°S and 5°S due to a combination of eddy transport of Mn rich waters from the Peruvian coastal margins and possible dust deposition.

- ***In-situ* dust dissolution study**

Contrasts and similarities between Mn and other trace metals were also shown in a dust dissolution process study in trace metal clean mesocosms in the LNLC Mediterranean. Trace metal biogeochemical processes after two consecutive dust depositions with evapocondensed dust were followed in-situ. Al is a tracer for dust on short time scales and was used to follow the dissolution processes from dust. After both dust seedings the Al concentration increased and started to decrease three days after the dust additions due to scavenging onto biogenic particles. The Al loss rate was coupled to the increase of the biomass after the seeding with dust. Mn was also clearly increased directly after both dust additions although the mixing conditions varied. In contrast to the predominant inorganic form of Mn, Fe is mainly controlled by organic complexation. This was evident after the second seeding. After the first dust addition the dissolved Fe concentrations decreased due to scavenging, but after the second addition Fe was dissolved from dust due to the presence of, and increase in, Fe binding ligands in seawater.

- **Mn dissolution from Saharan dust and loss rates and fractional solubility**

The Mn dissolution were estimated as  $0.43 \pm 0.09 \mu\text{mol m}^2 \text{d}^{-1}$  and  $0.27 \pm 0.05 \mu\text{mol m}^2 \text{d}^{-1}$ , the Mn loss rates as  $-0.35 \pm 0.04 \mu\text{mol m}^2 \text{d}^{-1}$  and  $0.25 \pm 0.08 \mu\text{mol m}^2 \text{d}^{-1}$  for the first and the second dust addition. In the case of Al the dissolution rates for both seedings were also comparable whereas the loss rate after the first addition was nearly one order of magnitude lower compared to the loss rate after the second seeding. The increase in the loss rate was linked to the correlated enhancement of biomass. It was only possible to calculate a single Fe loss rate after the second dust addition. This different behavior of Mn compared to Al and Fe is caused by its complex photochemical and redox processes.

The fractional solubility was estimated to be similar after both dust seedings as  $41 \pm 9\%$  and  $27 \pm 19\%$  for Mn for the first and the second dust addition. To conclude, this demonstrates clearly that the biogeochemistry does not respond linearly to the input of dust and that the frequency and time scales of repeated atmospheric dust fluxes might have very different impacts.

- **$\text{O}_2^-$  decay due to Mn and organics in the Eastern Tropical Atlantic Ocean**

Furthermore the pathways of  $\text{O}_2^-$  and  $\text{H}_2\text{O}_2$  and the processes involved with these ROS and inorganic Mn(II) and Mn(III)DFB in the ETA were investigated. The ETA is an area highly influenced by Atmospheric dust fluxes to the surface waters and also by sediment resuspension. In this area Mn(II) and organic matter are the major contributors to the  $\text{O}_2^-$  decay.  $\text{O}_2^-$  decays with inorganic Mn(II) following a first order

loss rate with the constant  $\log k_{\text{Min}} = 7.29 \pm 0.26$  ( $n = 35$ ). In contrast to our results Cu was found to be the major sink in the Southern Ocean (Heller and Croot, 2010d). This difference is probably caused by strong Cu binding ligands that are produced by both *Synechococcus* and *Prochlorococcus*. Organic complexes as also in the case of Fe seem to be relatively inert when it comes to reactions with  $\text{O}_2^-$ .







# REFERENCES

## 6 REFERENCES

- Aguilar-Islas, A.M. and Bruland, K.W., 2006. Dissolved manganese and silicic acid in the Columbia River plume: A major source to the California current and coastal waters off Washington and Oregon. *Marine Chemistry*, 101(3–4): 233-247.
- Aguilar-Islas, A.M., Resing, J.A. and Bruland, K.W., 2006. Catalytically enhanced spectrophotometric determination of manganese in seawater by flow-injection analysis with a commercially available resin for on-line preconcentration. *Limnology and Oceanography-Methods*, 4: 105-113.
- Baker, A.R., Jickells, T.D., Witt, M. and Linge, K.L., 2006. Trends in the solubility of iron, aluminium, manganese and phosphorus in aerosol collected over the Atlantic Ocean. *Marine Chemistry*, 98(1): 43-58.
- Barnese, K., Gralla, E.B., Cabelli, D.E. and Selverstone Valentine, J., 2008. Manganous Phosphate Acts as a Superoxide Dismutase. *Journal of the American Chemical Society*, 130(14): 4604-4606.
- Barnese, K., Gralla, E.B., Valentine, J.S. and Cabelli, D.E., 2012. Biologically relevant mechanism for catalytic superoxide removal by simple manganese compounds. *Proceedings of the National Academy of Sciences*, 109(18): 6892-6897.
- Barth, A., Alvera-Azcárate, A., Rixen, M. and Beckers, J.M., 2005. Two-way nested model of mesoscale circulation features in the Ligurian Sea. *Progress in Oceanography*, 66(2–4): 171-189.
- Batinic-Haberle, I., Reboucas, J.S. and Spasojevic, I., 2010. Superoxide Dismutase Mimics: Chemistry, Pharmacology, and Therapeutic Potential. *Antioxidants & Redox Signaling*, 13(6): 877-918.
- Bento, I., Martins, L.O., Gato Lopes, G., Armenia Carrondo, M. and Lindley, P.F., 2005. Dioxygen reduction by multi-copper oxidases; a structural perspective. *Dalton Transactions*, 0(21): 3507-3513.
- Bertino, D.J. and Zepp, R.G., 1991. Effects of solar radiation on manganese oxide reactions with selected organic compounds. *Environmental Science & Technology*, 25(7): 1267-1273.
- Bonnet, S. and Guieu, C., 2006. Atmospheric forcing on the annual iron cycle in the western Mediterranean Sea: A 1-year survey. *Journal of Geophysical Research-Oceans*, 111(C9).
- Bonnet, S., Guieu, C., Chiaverini, J., Ras, J. and Stock, A., 2005. Effect of atmospheric nutrients on the autotrophic communities in a low nutrient, low chlorophyll system. *Limnol. Oceanogr.*, 50(6): 10.
- Brand, L.E., Sunda, W.G. and Guillard, R.R.L., 1983. Limitation of Marine-Phytoplankton Reproductive Rates by Zinc, Manganese, and Iron. *Limnology and Oceanography*, 28(6): 1182-1198.
- Brandt, P. et al., 2011. Circulation and Oxygen Distribution in the Tropical Atlantic Cruise No. 80, Leg 1; October 26 to November 23, 2009 Mindelo (Cape Verde) to Mindelo (Cape Verde), Hamburg, Germany, Leitstelle Deutsche Forschungsschiffe, Inst. f. Meereskunde.
- Bressac, M. et al., this issue. Quantification of the lithogenic carbon pump following a dust event. *Biogeosciences (BG)*.
- Brudvig, G.W., 2008. Water oxidation chemistry of photosystem II. *Philosophical Transactions of the Royal Society B: Biological Sciences*, 363(1494): 1211-1219.
- Bruland, K.W., 2011. Consensus Values for the GEOTRACES 2008 and SAFe Reference Samples, University of California Santa Cruz  
Ocean Sciences Department  
CHEMICAL OCEANOGRAPHY.
- Bruland, K.W., Franks, R.P., Knauer, G.A. and Martin, J.H., 1979. Sampling and Analytical Methods for the Determination of Copper, Cadmium, Zinc, and Nickel at the Nanogram Per Liter Level in Sea-Water. *Analytica Chimica Acta*, 105(1): 233-245.

- Bruland, K.W. and Lohan, M.C., 2003. 6.02 - Controls of Trace Metals in Seawater. In: D.H. Editors-in-Chief: Heinrich and K.T. Karl (Editors), *Treatise on Geochemistry*. Pergamon, Oxford, pp. 23-47.
- Byrne, R.H., 1988. Seawater trace metal speciation. *Applied Geochemistry*, 3(1): 85.
- Cabelli, D.E. and Bielski, B.H.J., 1984a. Pulse radiolysis study of the kinetics and mechanisms of the reactions between manganese(II) complexes and perhydroxyl (HO<sub>2</sub>)/hydroperoxide (O<sub>2</sub><sup>-</sup>) radicals. 2. The phosphate complex and an overview. *The Journal of Physical Chemistry*, 88(25): 6291-6294.
- Cabelli, D.E. and Bielski, B.H.J., 1984b. Pulse radiolysis study of the kinetics and mechanisms of the reactions between manganese(II) complexes and perhydroxyl (HO<sub>2</sub>)/superoxide (O<sub>2</sub><sup>-</sup>) radicals. 1. Sulfate, formate and pyrophosphate complexes. *The Journal of Physical Chemistry*, 88(14): 3111-3115.
- Canfield, D.E. et al., 1993. Pathways of organic carbon oxidation in three continental margin sediments. *Marine Geology*, 113(1-2): 27-40.
- Carr, M.-E. et al., 2006. A comparison of global estimates of marine primary production from ocean color. *Deep Sea Research Part II: Topical Studies in Oceanography*, 53(5-7): 741-770.
- Chester, R. and Stoner, J.H., 1974. The distribution of zinc, nickel, manganese, cadmium, copper, and iron in some surface waters from the world ocean. *Marine Chemistry*, 2(1): 17-32.
- Creamean, J.M. et al., 2013. Dust and Biological Aerosols from the Sahara and Asia Influence Precipitation in the Western U.S. *Science*.
- Croot, P.L., Bluhm, K., Heller, M.I. and Wuttig, K., subm. Transient redox species as tracers of oceanographic mixing and transport. *Journal of Marine Systems*.
- Croot, P.L. and Laan, P., 2002. Continuous shipboard determination of Fe(II) in polar waters using flow injection analysis with chemiluminescence detection. *Analytica Chimica Acta*, 466(2): 261-273.
- Croot, P.L., Streu, P., Malien, F. and Wuttig, K., in prep. Trace Metal Distributions in the Peruvian Oxygen Minimum Zone. *Global Biogeochem. Cycles*.
- Croot, P.L., Streu, P., Peeken, I., Lochte, K. and Baker, A.R., 2004. Influence of the ITCZ on H<sub>2</sub>O<sub>2</sub> in near surface waters in the equatorial Atlantic Ocean. *Geophys. Res. Lett.*, 31(23): L23S04.
- Cutter, G.A. et al., 2010. Sampling and Sample-handling Protocols for GEOTRACES Cruises. In: G.S.a.I. Committee (Editor).
- Czeschel, R., Stramma, L. and Johnson, G.C., 2012. Oxygen decreases and variability in the eastern equatorial Pacific. *Journal of Geophysical Research: Oceans*, 117(C11): C11019.
- Czeschel, R. et al., 2011. Middepth circulation of the eastern tropical South Pacific and its link to the oxygen minimum zone. *Journal of Geophysical Research-Oceans*, 116: 13.
- Dammshäuser, A., Wagener, T. and Croot, P.L., 2011. Surface water dissolved aluminum and titanium: Tracers for specific time scales of dust deposition to the Atlantic? *Geophysical Research Letters*, 38(24): L24601.
- Danielsson, L.-G., Magnusson, B. and Westerlund, S., 1978. An improved metal extraction procedure for the determination of trace metals in sea water by atomic absorption spectrometry with electrothermal atomization. *Analytica Chimica Acta*, 98(1): 47-57.
- Dellwig, O., Schnetger, B., Brumsack, H.-J., Grossart, H.-P. and Umlauf, L., 2011. Dissolved reactive manganese at pelagic redoxclines (part II): Hydrodynamic conditions for accumulation. *Journal of Marine Systems*(0).
- Duce, R.A. et al., 1991. The atmospheric input of trace species to the world ocean. *Global Biogeochemical Cycles*, 5(3): 193-259.
- Elderfield, H., 1976. Manganese fluxes to the oceans. *Marine Chemistry*, 4(2): 103-132.
- Emerson, S. et al., 1982. Environmental oxidation rate of manganese(II): bacterial catalysis. *Geochimica Et Cosmochimica Acta*, 46(6): 1073-1079.

- Faulkner, K.M., Stevens, R.D. and Fridovich, I., 1994. Characterization of Mn(III) Complexes of Linear and Cyclic Desferrioxamines as Mimics of Superoxide Dismutase Activity. *Archives of Biochemistry and Biophysics*, 310(2): 341-346.
- Fridovich, I., 1995. Superoxide Radical and Superoxide Dismutases. *Annual Review of Biochemistry*, 64(1): 97-112.
- Fuenzalida, R., Schneider, W., Garcés-Vargas, J., Bravo, L. and Lange, C., 2009. Vertical and horizontal extension of the oxygen minimum zone in the eastern South Pacific Ocean. *Deep Sea Research Part II: Topical Studies in Oceanography*, 56(16): 992-1003.
- Ginoux, P. et al., 2001. Sources and distributions of dust aerosols simulated with the GOCART model. *Journal of Geophysical Research: Atmospheres*, 106(D17): 20255-20273.
- Giovagnetti, V. et al., 2012. Assessing the role of dust deposition on phytoplankton ecophysiology and succession in a low-nutrient low-chlorophyll ecosystem: a mesocosm experiment in the Mediterranean Sea. *Biogeosciences Discuss.*, 9(12): 19199-19243.
- Grasshoff, K., Kremling, K. and Ehrhardt, M., 1983. *Methods of seawater analysis*. Verlag Chemie, Weinheim.
- Guieu, C. et al., 2010. Large clean mesocosms and simulated dust deposition: a new methodology to investigate responses of marine oligotrophic ecosystems to atmospheric inputs. *Biogeosciences*, 7(9): 2765-2784.
- Guieu, C., Dulac, F., Ridame, C. and Pondaven, P., this issue. Introduction to the DUNE project: a DUst experiment in a low Nutrient, low chlorophyll Ecosystem. *Biogeosciences (BG)*.
- Hansard, S.P., Easter, H.D. and Voelker, B.M., 2011. Rapid Reaction of Nanomolar Mn(II) with Superoxide Radical in Seawater and Simulated Freshwater. *Environmental Science & Technology*, 45(7): 2811-2817.
- Hansel, C.M. and Francis, C.A., 2006. Coupled Photochemical and Enzymatic Mn(II) Oxidation Pathways of a Planktonic Roseobacter-Like Bacterium. *Applied and Environmental Microbiology*, 72(5): 3543-3549.
- Hatakka, A., 1994. Lignin-modifying enzymes from selected white-rot fungi: production and role from in lignin degradation. *FEMS Microbiology Reviews*, 13(2-3): 125-135.
- Heller, M.I. and Croot, P.L., 2010a. Application of a Superoxide ( $O_2^-$ ) thermal source (SOTS-1) for the determination and calibration of  $O_2^-$  fluxes in seawater. *Analytica Chimica Acta*, 667: 1-13.
- Heller, M.I. and Croot, P.L., 2010b. Kinetics of superoxide reactions with dissolved organic matter in tropical Atlantic surface waters near Cape Verde (TENATSO). *J. Geophys. Res.*, 115(C12): C12038.
- Heller, M.I. and Croot, P.L., 2010c. Superoxide Decay Kinetics in the Southern Ocean. *Environmental Science & Technology*, 44(1): 191-196 DOI: 10.1021/es901766r.
- Heller, M.I. and Croot, P.L., 2011. Superoxide decay as a probe for speciation changes during dust dissolution in Tropical Atlantic surface waters near Cape Verde. *Marine Chemistry*, 126(1-4): 37-55.
- Herut, B. et al., 2005. Response of East Mediterranean surface water to Saharan dust: On-board microcosm experiment and field observations. *Deep Sea Research Part II: Topical Studies in Oceanography*, 52(22-23): 3024-3040.
- Huntsman, S.A. and Sunda, W.G., 1980. The role of trace metals in regulating phytoplankton growth with emphasis on Fe, Mn and Cu [iron, manganese, copper]. In: I. Morris (Editor), *The Physiological Ecology of Phytoplankton*. Blackwell, London, pp. 258-328.
- Jacobsen, F., Holcman, J. and Sehested, K., 1997. Manganese(II)-Superoxide Complex in Aqueous Solution. *The Journal of Physical Chemistry A*, 101(7): 1324-1328.
- Jickells, T., 1995. Atmospheric inputs of metals and nutrients to the oceans: their magnitude and effects. *Marine Chemistry*, 48(3-4): 199-214.

- Jickells, T., Church, T., Veron, A. and Arimoto, R., 1994. Atmospheric Inputs of Manganese and Aluminum to the Sargasso Sea and Their Relation to Surface-Water Concentrations. *Marine Chemistry*, 46(3): 283-292.
- Jickells, T.D., 1999. The inputs of dust derived elements to the Sargasso Sea; a synthesis. *Marine Chemistry*, 68(1-2): 5-14.
- Jickells, T.D. et al., 2005. Global Iron Connections Between Desert Dust, Ocean Biogeochemistry, and Climate. *Science*, 308(5718): 67-71.
- Johnson, K.S. et al., 1992. Manganese Flux from Continental Margin Sediments in a Transect Through the Oxygen Minimum. *Science*, 257(5074): 1242-1245.
- Kanungo, S.B., Parida, K.M. and Sant, B.R., 1981. Studies on MnO<sub>2</sub>—III. The kinetics and the mechanism for the catalytic decomposition of H<sub>2</sub>O<sub>2</sub> over different crystalline modifications of MnO<sub>2</sub>. *Electrochimica Acta*, 26(8): 1157-1167.
- Karstensen, J., Stramma, L. and Visbeck, M., 2008. Oxygen minimum zones in the eastern tropical Atlantic and Pacific oceans. *Progress in Oceanography*, 77(4): 331-350.
- Klewicki, J.K. and Morgan, J.J., 1998. Kinetic Behavior of Mn(III) Complexes of Pyrophosphate, EDTA, and Citrate. *Environmental Science & Technology*, 32(19): 2916-2922.
- Klinkhammer, G., Rona, P., Greaves, M. and Elderfield, H., 1985. Hydrothermal manganese plumes in the Mid-Atlantic Ridge rift valley. *Nature*, 314(6013): 727-731.
- Klinkhammer, G.P., 1980. Determination of manganese in sea water by flameless atomic absorption spectrometry after preconcentration with 8-hydroxyquinoline in chloroform. *Analytical Chemistry*, 52(1): 117-120.
- Klinkhammer, G.P. and Bender, M.L., 1980. The distribution of manganese in the Pacific Ocean. *Earth and Planetary Science Letters*, 46(3): 361-384.
- Kostka, J.E., Luther III, G.W. and Neelson, K.H., 1995. Chemical and biological reduction of Mn(III)-pyrophosphate complexes: Potential importance of dissolved Mn(III) as an environmental oxidant. *Geochimica et Cosmochimica Acta*, 59(5): 885-894.
- Kremling, K., 1983. Trace metal fronts in European shelf waters. *Nature*, 303(5914): 225-227.
- Landing, W.M. and Bruland, K.W., 1980. Manganese in the North Pacific. *Earth and Planetary Science Letters*, 49(1): 45-56.
- Landing, W.M. and Bruland, K.W., 1987. The contrasting biogeochemistry of iron and manganese in the Pacific Ocean. *Geochimica Et Cosmochimica Acta*, 51(1): 29-43.
- Lewis, B.L. and Luther III, G.W., 2000. Processes controlling the distribution and cycling of manganese in the oxygen minimum zone of the Arabian Sea. *Deep Sea Research Part II: Topical Studies in Oceanography*, 47(7-8): 1541-1561.
- Li, T. et al., 2002. Differential Expression and Localization of Mn and Fe Superoxide Dismutases in the Heterocystous Cyanobacterium *Anabaena* sp. Strain PCC 7120. *Journal of Bacteriology*, 184(18): 5096-5103.
- Loye-Pilot, M.D. and Martin, J.M., 1996. Saharan dust input to the western Mediterranean: An eleven year record in Corsica. In: S. Guerzoni and R. Chester (Editors), *The Impact of Desert Dust Across the Mediterranean*. Springer, New York, pp. 191-199.
- Luther III, G.W., 2005. Manganese(II) Oxidation and Mn(IV) Reduction in the Environment—Two One-Electron Transfer Steps Versus a Single Two-Electron Step. *Geomicrobiology Journal*, 22(3-4): 195-203.
- Luther III, G.W., 2010. The Role of One- and Two-Electron Transfer Reactions in Forming Thermodynamically Unstable Intermediates as Barriers in Multi-Electron Redox Reactions. *Aquatic Geochemistry*, 16(3): 395-420.
- Mahowald, N.M. and Luo, C., 2003. A less dusty future? *Geophysical Research Letters*, 30(17): 1903.
- Martin, J.H. and Knauer, G.A., 1983. VERTEX: Manganese transport with CaCO<sub>3</sub>. *Deep Sea Research Part A. Oceanographic Research Papers*, 30(4): 411-425.
- Martin, J.H. and Knauer, G.A., 1984. VERTEX: manganese transport through oxygen minima. *Earth and Planetary Science Letters*, 67(1): 35-47.

- Matsunaga, K., Ohyama, T., Kuma, K., Kudo, I. and Suzuki, Y., 1995. Photoreduction of manganese dioxide in seawater by organic substances under ultraviolet or sunlight. *Water Research*, 29(2): 757-759.
- McEvoy, J.P. and Brudvig, G.W., 2006. Water-Splitting Chemistry of Photosystem II. *Chemical Reviews*, 106(11): 4455-4483.
- Middag, R., de Baar, H.J.W., Laan, P., Cai, P.H. and van Ooijen, J.C., 2011a. Dissolved manganese in the Atlantic sector of the Southern Ocean. *Deep Sea Research Part II: Topical Studies in Oceanography*, 58(25-26): 2661-2677.
- Middag, R., de Baar, H.J.W., Laan, P. and Klunder, M.B., 2011b. Fluvial and hydrothermal input of manganese into the Arctic Ocean. *Geochimica et Cosmochimica Acta*, 75(9): 2393-2408.
- Miller, A.-F., 2004. Superoxide dismutases: active sites that save, but a protein that kills. *Current Opinion in Chemical Biology*, 8(2): 162-168.
- Milne, A., Landing, W., Bizimis, M. and Morton, P., 2010. Determination of Mn, Fe, Co, Ni, Cu, Zn, Cd and Pb in seawater using high resolution magnetic sector inductively coupled mass spectrometry (HR-ICP-MS). *Analytica Chimica Acta*, 665(2): 200-207.
- Morgan, J.J., 2005. Kinetics of reaction between O<sub>2</sub> and Mn(II) species in aqueous solutions. *Geochimica Et Cosmochimica Acta*, 69(1): 35-48.
- Nakabayashi, S. et al., 2002. Variation in iron(III) solubility and iron concentration in the northwestern North Pacific Ocean. *Limnology and Oceanography*, 47(3): 885-892.
- NASA-EO, 2011. <http://earthobservatory.nasa.gov/>.
- Nealson, K.H., Tebo, B.M., Rosson, R.A. and Allen, I.L., 1988. Occurrence and Mechanisms of Microbial Oxidation of Manganese, *Advances in Applied Microbiology*. Academic Press, pp. 279-318.
- Nico, P.S., Anastasio, C. and Zasoski, R.J., 2002. Rapid photo-oxidation of Mn(II) mediated by humic substances. *Geochimica et Cosmochimica Acta*, 66(23): 4047-4056.
- Nozaki, Y., 1997. A fresh look at element distribution in the North Pacific Ocean. *Eos, Transactions American Geophysical Union*, 78(21): 221-221.
- Pakhomova, S. and Yakushev, E., 2011. Manganese and Iron at the Redox Interfaces in the Black Sea, the Baltic Sea, and the Oslo Fjord [Without Title]. *The Handbook of Environmental Chemistry*. Springer Berlin / Heidelberg, pp. 1-27.
- Parkhill, J.-P., Maillet, G. and Cullen, J.J., 2001. FLUORESCENCE-BASED MAXIMAL QUANTUM YIELD FOR PSII AS A DIAGNOSTIC OF NUTRIENT STRESS. *Journal of Phycology*, 37(4): 517-529.
- Paulmier, A., Ruiz-Pino, D. and Garçon, V., 2008. The oxygen minimum zone (OMZ) off Chile as intense source of CO<sub>2</sub> and N<sub>2</sub>O. *Continental Shelf Research*, 28(20): 2746-2756.
- Peers, G. and Price, N.M., 2004. A role for manganese in superoxide dismutases and growth of iron-deficient diatoms. *Limnology and Oceanography*, 49(5): 1774-1783.
- Pohl, C. et al., 2011. Synoptic transects on the distribution of trace elements (Hg, Pb, Cd, Cu, Ni, Zn, Co, Mn, Fe, and Al) in surface waters of the Northern- and Southern East Atlantic. *Journal of Marine Systems*, 84(1-2): 28-41.
- Post, J.E., 1999. Manganese oxide minerals: Crystal structures and economic and environmental significance. *Proceedings of the National Academy of Sciences*, 96(7): 3447-3454.
- Roitz, J.S. and Bruland, K.W., 1997. Determination of dissolved manganese(II) in coastal and estuarine waters by differential pulse cathodic stripping voltammetry. *Analytica Chimica Acta*, 344(3): 175-180.
- Rue, E.L., Smith, G.J., Cutter, G.A. and Bruland, K.W., 1997. The response of trace element redox couples to suboxic conditions in the water column. *Deep Sea Research Part I: Oceanographic Research Papers*, 44(1): 113-134.
- Shelley, R.U., Zachhuber, B., Sedwick, P.N., Worsfold, P.J. and Lohan, M.C., 2010. Determination of total dissolved cobalt in UV-irradiated seawater using flow injection

- with chemiluminescence detection. *Limnology and Oceanography-Methods*, 8: 352-362.
- Shiller, A.M., 1997. Manganese in surface waters of the Atlantic Ocean. *Geophys. Res. Lett.*, 24(12): 1495-1498.
- Siedler, G., Zangenberg, N., Onken, R. and Morlière, A., 1992. Seasonal changes in the tropical Atlantic circulation: Observation and simulation of the Guinea Dome. *Journal of Geophysical Research: Oceans*, 97(C1): 703-715.
- Slemons, L., Paul, B., Resing, J. and Murray, J.W., 2012. Particulate iron, aluminum, and manganese in the Pacific equatorial undercurrent and low latitude western boundary current sources. *Marine Chemistry*, 142-144(0): 54-67.
- Statham, P.J., Yeats, P.A. and Landing, W.M., 1998. Manganese in the eastern Atlantic Ocean: processes influencing deep and surface water distributions. *Marine Chemistry*, 61(1-2): 55-68.
- Stein, J., Fackler, J.P., McClune, G.J., Fee, J.A. and Chan, L.T., 1979. Superoxide and manganese(III). Reactions of manganese-EDTA and manganese-CyDTA complexes with molecular oxygen. X-ray structure of potassium manganese-EDTA.2 water. *Inorganic Chemistry*, 18(12): 3511-3519.
- Stone, A.T., 1987. Microbial metabolites and the reductive dissolution of manganese oxides: Oxalate and pyruvate. *Geochimica Et Cosmochimica Acta*, 51(4): 919-925.
- Stramma, L., Fischer, J., Brandt, P. and Schott, F., 2003. Circulation, variability and near-equatorial meridional flow in the central tropical Atlantic. In: G.J. Goni and P. Malanotte-Rizzoli (Editors), Elsevier Oceanography Series. Elsevier, pp. 1-22.
- Stramma, L., Johnson, G.C., Firing, E. and Schmidtko, S., 2010a. Eastern Pacific oxygen minimum zones: Supply paths and multidecadal changes. *Journal of Geophysical Research: Oceans*, 115(C9): C09011.
- Stramma, L., Johnson, G.C., Sprintall, J. and Mohrholz, V., 2008. Expanding Oxygen-Minimum Zones in the Tropical Oceans. *Science*, 320(5876): 655-658.
- Stramma, L., Schmidtko, S., Levin, L.A. and Johnson, G.C., 2010b. Ocean oxygen minima expansions and their biological impacts. *Deep Sea Research Part I: Oceanographic Research Papers*, 57(4): 587-595.
- Stramma, L. and Schott, F., 1999. The mean flow field of the tropical Atlantic Ocean. *Deep Sea Research Part II: Topical Studies in Oceanography*, 46(1-2): 279-303.
- Stramma, L., Visbeck, M., Brandt, P., Tanhua, T. and Wallace, D., 2009. Deoxygenation in the oxygen minimum zone of the eastern tropical North Atlantic. *Geophysical Research Letters*, 36(20): L20607.
- Stumm, W. and Morgan, J.J., 1996. *Aquatic Chemistry*. Wiley-Interscience, New York (1996): 1022 pp.
- Sultan, B. and Janicot, S., 2000. Abrupt shift of the ITCZ over West Africa and intra-seasonal variability. *Geophysical Research Letters*, 27(20): 3353-3356.
- Sunda, W. and Huntsman, S., 1983. Effect of competitive interactions between manganese and copper on cellular manganese and growth in estuarine and oceanic species of the diatom *Thalassiosira*. *Limnol. Oceanogr.*, 28(5): 924-934.
- Sunda, W.G., 1984. Measurement of manganese, zinc and cadmium complexation in seawater using Chelex ion exchange equilibria. *Marine Chemistry*, 14(4): 365-378.
- Sunda, W.G. and Huntsman, S.A., 1986. Relationships among Growth-Rate, Cellular Manganese Concentrations and Manganese Transport Kinetics in Estuarine and Oceanic Species of the Diatom *Thalassiosira*. *Journal of Phycology*, 22(3): 259-270.
- Sunda, W.G. and Huntsman, S.A., 1987. Microbial oxidation of manganese in a North Carolina estuary. *Limnology and Oceanography*, 32(3): 552-564.
- Sunda, W.G. and Huntsman, S.A., 1988. Effect of sunlight on redox cycles of manganese in the southwestern Sargasso Sea. *Deep Sea Research Part A. Oceanographic Research Papers*, 35(8): 1297-1317.

- Sunda, W.G. and Huntsman, S.A., 1990. Diel cycles in microbial manganese oxidation and manganese redox speciation in coastal waters of the Bahama Islands, 35. American Society of Limnology and Oceanography, Waco, TX, ETATS-UNIS, 14 pp.
- Sunda, W.G. and Huntsman, S.A., 1994. Photoreduction of manganese oxides in seawater. *Marine Chemistry*, 46(1-2): 133-152.
- Sunda, W.G. and Kieber, D.J., 1994. Oxidation of humic substances by manganese oxides yields low-molecular-weight organic substrates. *Nature*, 367(6458): 62-64.
- Tchernia, P., 1980. Descriptive regional oceanography, Volume 3, 1st edition Pergamon Press Oxford and New York.
- Tebo, B. and Emerson, S., 1986. Microbial manganese(II) oxidation in the marine environment: a quantitative study. *Biogeochemistry*, 2(2): 149-161.
- Tebo, B.M., Clement, B.G. and Dick, G.J., 2007. Biotransformations of manganese. In: C.J. Hurst et al. (Editors), *Manual of environmental microbiology* pp. 1223-1238
- Tebo, B.M., Johnson, H.A., McCarthy, J.K. and Templeton, A.S., 2005. Geomicrobiology of manganese(II) oxidation. *Trends in Microbiology*, 13(9): 421-428.
- Tegen, I., Werner, M., Harrison, S.P. and Kohfeld, K.E., 2004. Relative importance of climate and land use in determining present and future global soil dust emission. *Geophysical Research Letters*, 31(5): L05105.
- Ternon, E. et al., 2010. The impact of Saharan dust on the particulate export in the water column of the North Western Mediterranean Sea. *Biogeosciences Discuss. (BGD)*, 6(6): 10737-10773.
- Trouwborst, R.E., Clement, B.G., Tebo, B.M., Glazer, B.T. and Luther, G.W., 2006. Soluble Mn(III) in Suboxic Zones. *Science*, 313(5795): 1955-1957.
- Van Der Loeff, M.R., Helmers, E. and Kattner, G., 1997. Continuous transects of cadmium, copper, and aluminium in surface waters of the Atlantic Ocean, 50°N to 50°S: correspondence and contrast with nutrient-like behaviour. *Geochimica Et Cosmochimica Acta*, 61(1): 47-61.
- von Langen, P.J., Johnson, K.S., Coale, K.H. and Elrod, V.A., 1997. Oxidation kinetics of manganese (II) in seawater at nanomolar concentrations. *Geochimica Et Cosmochimica Acta*, 61(23): 4945-4954.
- Webb, S.M., Dick, G.J., Bargar, J.R. and Tebo, B.M., 2005. Evidence for the presence of Mn(III) intermediates in the bacterial oxidation of Mn(II). *Proceedings of the National Academy of Sciences of the United States of America*, 102(15): 5558-5563.
- Wedepohl, H.K., 1995. The composition of the continental crust. *Geochimica Et Cosmochimica Acta*, 59(7): 1217-1232.
- Wintjens, R. et al., 2004. Specificity and Phenetic Relationships of Iron- and Manganese-containing Superoxide Dismutases on the Basis of Structure and Sequence Comparisons. *Journal of Biological Chemistry*, 279(10): 9248-9254.
- Wolfe-Simon, F., Grzebyk, D., Schofield, O. and Falkowski, P.G., 2005. The role and evolution of superoxide dismutases in algae. *Journal Of Phycology*, 41(3): 453-465.
- Wolfe-Simon, F., Starovoytov, V., Reinfelder, J.R., Schofield, O. and Falkowski, P.G., 2006. Localization and Role of Manganese Superoxide Dismutase in a Marine Diatom. *Plant Physiology*, 142(4): 1701-1709.
- Wuttig, K., Heller, M.I. and Croot, P.L., subm., 2013a. Pathways of O<sub>2</sub><sup>-</sup> decay in the Tropical Atlantic. *Environmental Science & Technology*.
- Wuttig, K., Heller, M.I. and Croot, P.L., subm., 2013b. Reactivity of Mn(II/III)-Desferrioxamine B with O<sub>2</sub>, O<sub>2</sub><sup>-</sup> and H<sub>2</sub>O<sub>2</sub> in seawater. *Environmental Science & Technology*.
- Wuttig, K., Wagener, T., Booge, D., Streu, P. and Croot, P.L., in prep., 2013. Contrasting behavior of cadmium, iron and manganese in the Eastern Tropical Atlantic. *Global Biogeochem. Cycles*.
- Wuttig, K. et al., 2013. Impacts of dust deposition on dissolved trace metal concentrations (Mn, Al and Fe) during a mesocosm experiment. *Biogeosciences*, 10: 2583-2600.
- Xyla, A.G. et al., 1992. Reductive dissolution of manganese(III, IV) (hydr)oxides by oxalate: the effect of pH and light. *Langmuir*, 8(1): 95-103.



- 
- Yeats, P.A. and Strain, P.M., 1990. The oxidation of manganese in seawater: Rate constants based on field data. *Estuarine, Coastal and Shelf Science*, 31(1): 11-24.
- Yuan, J. and Shiller, A.M., 1999. Determination of Subnanomolar Levels of Hydrogen Peroxide in Seawater by Reagent-Injection Chemiluminescence Detection. *Analytical Chemistry*, 71(10): 1975-1980.

## 7 ABBREVIATIONS

Al	Aluminium
Cd	Cadmium
CDOM	Chromophoric dissolved organic matter
Co	Cobalt
Cu	Copper
CuL	Cu complex with the organic ligand L
CSV	Cathodic stripping voltammetry
DEF-B	Desferioxamine B
DL	Detection Limit
DMSO	Dimethyl sulfoxide
DTPA	Diethylenetriaminepentaacetic acid
DUNE	a <b>D</b> Ust experiment in a low <b>N</b> utrient, low chlorophyll <b>E</b> cosystem
EDTA	Ethylenediaminetetraacetic acid
ETP	Eastern Tropical Pacific
ETA	Eastern Tropical Atlantic
ETAAS	Electrothermal Atomic Absorption Spectroscopy
ETNA	Eastern Tropical North Atlantic
Fe	Iron
FeL	Fe complex with the organic ligand L
H <sub>2</sub> O <sub>2</sub>	Hydrogen peroxide
Q-HCl	Hydrochloric acid distilled with a sub-boiling quartz still
HNLC	High Nutrient, Low Chlorophyll
Q-HNO <sub>3</sub>	Nitric acid distilled with a sub-boiling quartz still
HOAc	Acetic acid
ITCZ	Inter Tropical Convergence Zone

$k_{\text{DTPA}} (\text{s}^{-1})$	reaction in seawater with DTPA
$k_{\text{M}} (\text{M}^{-1} \text{s}^{-1})$	metal (Cu, Fe and Mn) reaction rate constant in seawater calculated from regression analysis of the observed first order decay rates
$k_{\text{obs}} (\text{s}^{-1})$	from the metal addition experiments
$k_{\text{SW}} (\text{s}^{-1})$	reaction in unamended seawater
L	Organic binding ligand
LDPE	Low density high polyethylene
LNLC	Low Nutrient, Low Chlorophyll
M80/1	Expedition 80, leg 1 on the German RV Meteor
M83/1	Expedition 83, leg 1 on the German RV Meteor
MCLA	2-methyl-6-(p-methoxyphenyl)-3,7-dihydroimidazol[1,2- $\alpha$ ]pyrazin-3-one
MCO	Multicopper Oxidase
MSM17/4	Expedition 17, leg 4 on the German RV Maria S. Merian
Mn	Manganese
Mn(III)DEF-B	Mn(III)-Desferioxamine B
NH <sub>3</sub>	Ammonia
Ni	Nickel
O <sub>2</sub>	Oxygen
O <sub>2</sub> <sup>-</sup>	Superoxide radical
OMZ	Oxygen Minimum Zone
Pb	Lead
PTFE	Polytetrafluoroethylene
ROS	Reactive Oxygen species
SOD	Superoxide dismutase
SOTS	Bis(4-carboxybenzyl)hyponitrite
Zn	Zink

## DANKSAGUNG

Allen voran möchte ich meinem Betreuer Peter L. Croot danken - für das interessante Doktorarbeitsthema, die interessanten Projekte und Fahrten und vor allem die prompten Antworten auf „tausend und eine“ Frage. Wenn ich gedanklich oder schriftlich stecken blieb, konnte er mir immer weiterhelfen. Auch wenn es manchmal wegen der großen Entfernung schwierig war, habe ich immer Hilfe erhalten, wenn ich sie benötigt habe und man kann auch via Skype oder Email diskutieren. Thanks a lot.

Ich möchte mich bei meinem Doktorvater Prof. Dr. Arne Körtzinger für die Unterstützung und die Möglichkeit der Durchführung dieser Doktorarbeit am GEOMAR bedanken.

Bei Thibaut Wagener und Maija I. Heller möchte ich mich für die gute Zusammenarbeit auf See, die Diskussion unserer Daten und das Schreiben der Manuskripte bedanken. Dies gilt auch für meine anderen Koautoren, sowie die Fahrtleiter (v.a. Lothar Stramma), -teilnehmer und die super Zusammenarbeit bei den Mesokosmen. Merci beaucoup.

Mein Dank gilt auch der ganzen momentanen und ehemaligen Spurenmetallgruppe des GEOMAR mit Oliver Baars, Katrin Bluhm, Anna Dammshäuser, Mirja Dunker, Friederike Lübben, Dörte Nischkowski, Christian Schlosser und Peter Streu. Ein großer Dank geht auch Eike Breitbarth für die Fortsetzung meiner Finanzierung und für die ganze Hilfe in letzter Minute.

Ein riesiger Dank geht an die Mädels und Pinky aus der HPA. Auch wenn es manchmal laut ist bei uns im Büro, haben wir doch den besten Blick und v.a. die netteste Gemeinschaft und man hört unser Gelächter gerne bis in die PO. Ich danke euch allen für das Korrekturlesen, insbesondere Cathleen, die Hilfestellungen, wenn es um Programme, Intranet oder auch das normale Alltagsleben ging. Danke auch an die tolle Gemeinschaft und die schöne Zeit in und mit der ganzen Meereschemie. Danke auch für das Korrekturlesen Anke Schneider, Damian Grundle, Linn Hoffmann und insbesondere Christa Marandino. Thanks!

Meinen Freunden und meiner Familie, allen voran meiner Tine und Wolfgang möchte ich herzlichst für all die grandiose Unterstützung und das unglaubliche Verständnis, wenn ich mal wieder keine Zeit hatte um z. B. nach Hause zu kommen, danken. Für die Korrekturen, die finanzielle Unterstützung und unser besonderes Verhältnis. Danke auch für die tollen Reisen und dass es immer schön ist nach Hause zu kommen! Ernie, danke für den Bully.

Zu guter Letzt möchte ich mich bei Nils herzlichst bedanken. Angefangen bei der Hilfe der Formatierung dieser Arbeit, dem Überwinden der kleinen und großen Tiefpunkte (mit „the help“) bis hin zu den großartigen gemeinsamen Erlebnissen wie an einem Nachmittag im November 2011 vor dem GEOMAR oder Hawaii und insgesamt den tollen letzten sieben Jahren in Kiel. Die großen Tugenden machen einen Menschen bewundernswert, die kleinen Fehler machen ihn liebenswert. Der Sommer mit Bully kann jetzt kommen und ich freue mich!

Diese Arbeit wurde finanziert durch den DFG (CR145/17-1) und im Rahmen dieses Projektes durchgeführt. Zusätzliche Finanzierung wurde durch das BMBF Verbundprojekt SOPRAN (FKZ 03F0462A und 03F0611A) bereitgestellt. Die Fahrten wurden im Rahmen des SFB754 und das Mesokosmen-Projekt im Rahmen von ANRDUNE (ANR-07-BLAN-0126-01) durchgeführt.



## CURRICULUM VITAE

Kathrin Wuttig

---

Address: Franckestr. 14  
24118 Kiel

Date of birth: 03/03/1983

Place of birth: Emmendingen, Germany

Nationality: German

E-mail: kwuttig@geomar.de

### Tertiary education

---

- 11/09 – 03/13 PhD-Thesis with Prof. Dr. P. L. Croot and Prof. Dr. A. Körtzinger in the department of marine biogeochemistry at the GEOMAR, Helmholtz Centre for Ocean Research Kiel at the Christian-Albrechts-Universität, Kiel, Germany  
Topic: „Manganese biogeochemistry in the sunlit ocean”
- 03/09 – 10/09 Research associate in the department of marine biogeochemistry at the IFM-GEOMAR to investigate the speciation of inorganic iodine species ( $I^-$ ,  $IO_3^-$ ,  $MeI$ ), its redoxchemistry and the relation to the marine picoplankton *Prochlorococcus*.
- 11/08 – 02/09 Student research assistant to investigate the photoreduction of Fe-complexes and ROS (reactive oxygen species) and to measure Al. Working area focused on the deposition of dust to surface waters of the Equatorial Oceans, the upwelling areas and the influence of the dust and sediments on trace metal biogeochemical cycles (Meteor cruise M77/4)
- 05/08 – 11/08 Diploma thesis with Dr. P. L. Croot and Prof. Dr. D. Wallace in the department of marine biogeochemistry at the IFM-GEOMAR, Leibniz-Institute for marine sciences at the Christian-Albrechts-Universität, Kiel, Germany.  
Topic: „Electrochemical and spectrochemical investigations into the determination of Niobium and Zirconium complexes in seawater”
- 10/05 – 11/08 Diplom Study Course in chemistry with the main subject marine chemistry at the Christian-Albrechts-Universität, Kiel, Germany
- 02/05 – 07/05 ERASMUS-scholarship in chemistry at the Universidad de Alicante, Spain with an internship in the department of air chemistry (with Dr. A. Carratalá )and marine biology  
Topic: Análisis de nitrógeno en vertidos de plantas depuradoras de agua al mar y en material sedimentado en el entorno de granjas de cría de dorada.
- 10/02 – 09/05 Diplom Study Course in chemistry at the Albert-Ludwigs-Universität, Freiburg (im Breisgau), Germany

## Education

---

- 09/93 – 06/02      Albert-Schweitzer-Gymnasium in Gundelfingen (high school)  
Graduation: Allgemeine Hochschulreife (A-Levels)
- 08/89 – 07/93      Johann-Peter-Hebel-Schule, primary school in Gundelfingen

### School attendance in foreign countries:

- 08/02 – 09/02      Internship at the marine biological institute of the university of Dunedin,  
New Zealand
- 07/00 – 10/00      Colegio Alemán de Valparaíso, Viña del Mar, Chile
- 09/98 – 10/98      Coláiste Muire, Cork, Ireland

## Publications

---

Bluhm, K., Croot, P. L., **Wuttig, K.** and Lochte, K. (2010), "Transformation of iodate to iodide in marine phytoplankton driven by cell senescence." *Aquatic Biology* 11(1): 1-15.

Croot, P. L., Heller, M. I., Schlosser, C. and **Wuttig, K.** (2011), "Utilizing Radioisotopes for Trace Metal Speciation Measurements in Seawater." *Radioisotopes - Applications in Physical Sciences*. N. Singh, InTech: 247-278.

**Wuttig, K.**, Wagener, T., Dammshäuser, A., Bressac, M., Streu, P., Guieu, C. and Croot, P. L. (2013), "Impacts of dust deposition on dissolved trace metal concentrations (Mn, Al and Fe) during a mesocosm experiment." *Biogeosciences*, 10: 2583-2600.

**Wuttig, K.**, Heller, M. I. and Croot, P. L., "Pathways of  $O_2^-$  decay in the Tropical Atlantic." *Environmental Science and Technology*, submitted, 2013.

**Wuttig, K.**, Heller, M. I. and Croot, P. L., "Reactivity of inorganic Mn and Mn Desferrioxamine B with  $O_2$ ,  $O_2^-$  and  $H_2O_2$  in seawater." *Environmental Science and Technology*, submitted, 2013.

## Conference Presentations

---

**Wuttig, K.** (2012) *Manganese biogeochemistry in the sunlit ocean*, Dissertations Symposium on Chemical Oceanography XXIII, 07.-11.10.2012, Lihue, Hawaii, USA.

**Wuttig, K.**, Heller, M. und Croot, P. (2012) *Examination of the Biogeochemical processes of the trace metals Mn and Cu and reactive oxygen species in the Tropical North Atlantic*, Goldschmidt Conference 2012, 24.-29.06.2012, Montreal, Canada.



**Wuttig, K.**, Heller, M., Guieu, C. and Croot, P. (2011) *Uncovering the key processes involved in manganese biogeochemical cycling in the Ocean*, Goldschmidt Conference 2011, 14.-19.08.2011, Prague, Czech Republic.

**Wuttig, K.**, Wagener, T., Dammshäuser, A., Bressac, M., Heller, M., Streu, P., Guieu, C. and Croot, P. (2011) *Temporal changes in the biogeochemistry of Mn, Fe and Al after an artificial dust deposition to large mesocosms (DUNE project)*, GEOTRACES-Conference, 02.-06.05.2011, Liège, Belgium.

**Wuttig, K.**, Wagener, T., Dammshäuser, A., Bressac, M., Streu, P., Guieu, C. and Croot, P. (2011) *Dissolution of trace metals following an artificial dust deposition*, DUNE Workshop, 03.-04.10.2011, Villefranche-sur-Mer, France.

**Wuttig, K.**, Wagener, T., Dammshäuser, A., Bressac, M., Heller, M., Streu, P., Guieu, C. and Croot, P. (2011) *Temporal changes in the biogeochemistry of Mn, Fe and Al after an artificial dust deposition to large mesocosms (DUNE project)*, ASLO Aquatic Sciences Meeting 2011, 13.-18.02.2011, San Juan, Puerto Rico, USA.

## Oceanographic cruises

---

### Atlantic Ocean

- **M80/1** – R.V. Meteor (Oct 26 – Nov 23, 2009, Mindelo to Mindelo) SFB754.
- **M83/1** – R.V. Meteor (Oct 14 – Nov 13, 2010, Las Palmas to Mindelo) SFB754.
- **MSM17/4** – R.V. Maria S. Merian (Mar 10 – Apr 12, 2011, Dakar to Las Palmas) SFB754.

### Pacific Ocean:

- **M77/4** – R.V. Meteor (Jan 27 – Feb 18, 2009, Callao to Balboa) SFB754.
- **M90** – R.V. Meteor (Oct 28 - Nov 28, Christobal to Callao) SFB754.

### Mediterranean/Mesocosm Project:

- DUNE2: a DUSt experiment in a low Nutrient, low chlorophyll Ecosystem (Jun 20 – Jul 15, 2010, on Corsica in the Marine Conservation area of Scandola) ANR-Blanc Project.



## EIDESSTATTLICHE ERKLÄRUNG

Hiermit erkläre ich, dass ich die von mir vorgelegte Dissertation – abgesehen von der Beratung durch meinen Betreuer – selbstständig und ohne Zuhilfenahme unerlaubte Hilfsmittel angefertigt habe. Alle benutzten Quellen und Hilfsmittel habe ich vollständig angegeben und die Zusammenarbeit mit anderen Wissenschaftlern habe ich kenntlich gemacht. Zudem versichere ich, dass diese Arbeit unter Einhaltung der Regeln guter wissenschaftlicher Praxis der Deutschen Forschungsgesellschaft verfasst wurde, und dass sie nach Form und Inhalt meine eigene Arbeit ist. Weder diese noch eine ähnliche Arbeit wurden an einer anderen Abteilung oder Hochschule im Rahmen eines Prüfungsverfahrens vorgelegt, veröffentlicht oder zur Veröffentlichung vorgelegt. Dies ist mein erstes und einziges Promotionsverfahren.

Kiel, den 17. April 2013

\_\_\_\_\_  
(Kathrin Wuttig)